TESIS DOCTORAL

Photovoltaic self-consumption heating system: analytical model, experimental results and autonomy prospects

Autor:

Pablo de Agustín Camacho

Director/es:

Dr. Marcelo Izquierdo Millán

Dr. Néstor García Hernando

Tutor:

Marcelo Izquierdo Millán

Departamento de Ingeniería Térmica y de Fluidos

Unidad Asociada de Ingeniería de Sistemas Energéticos UC3M-CSIC

Leganés, septiembre 2015

TESIS DOCTORAL

Photovoltaic self-consumption heating system: analytical model, experimental results and autonomy prospects

Autor: *Pablo de Agustín Camacho*

Director/es: **Dr. Marcelo Izquierdo Millán**
                Dr. Néstor García Hernando

Firma del Tribunal Calificador:

                                                            Firma

Presidente: Dr. Francisco Javier Rey Martínez

Vocal: Dr. Rafael Antonio Salgado Mangual

Secretario: Dr. María del Carmen Venegas Bernal

Suplente: Dr. José Antonio Almendros Ibáñez

Calificación:

Leganés,   11 de septiembre de 2015

A mi ama y mi aita,

por todo.

Resumen

Actualmente, en la Unión Europea los edificios demandan un 40% del consumo total de energía y son responsables del 36% de emisiones de gases de efecto invernadero, contribuyendo significativamente al calentamiento global antropogénico. Dado que la calefacción supone la principal porción del consumo energético en los edificios en España, los sistemas de calefacción renovable surgen como una alternativa para mitigar dicha problemática.

Esta tesis plantea un sistema de calefacción fotovoltaica en el que la producción eléctrica es auto-consumida por una bomba de calor. Para ello se ha diseñado y construido un sistema fotovoltaico sin inyección a red para alimentar una bomba de calor aire-agua que calienta un pequeño edificio mediante suelo radiante. El edificio, tendente a la autonomía, incluye conexión a red, por lo que el suministro a la bomba de calor puede permutarse entre la micro-red fotovoltaica y la red convencional. El campo fotovoltaico, con un área total de 15,7m^2 y útil de 14m^2, está compuesto de 12 paneles, de 180W de potencia nominal cada uno. La potencia térmica nominal de la bomba de calor es de 6kW, al igual que la carga térmica máxima del edificio.

Para dimensionar adecuadamente un sistema fotovoltaico de estas características es necesario simular realísticamente la producción fotovoltaica a lo largo del tiempo. En esta tesis, se ha abordado la producción desde un punto de vista físico, haciendo hincapié en la influencia de la temperatura de las celdas solares en su eficiencia. Se ha desarrollado un modelo de transferencia de calor que permite determinar con exactitud la temperatura de celda para condiciones meteorológicas cambiantes y, a partir de ahí, la producción fotovoltaica en cada momento, basándose en especificaciones comunmente suministradas por los fabricantes de módulos. La validación experimental del modelo, tanto para la predicción de la temperatura de celda como para la producción fotovoltaica, es incluida en la presente tesis. La eficiencia de los módulos utilizados, respecto a su área total, es de 13.73% a 25°C, 12.08% a 50°C y 10.76% a 70°C.

El método planteado es fácilmente adaptable a cualquier tipo de módulo fotovoltaico a partir de los materiales que lo componen, y su producción simulable para cualquier ángulo de inclinación y localización, para la que se disponga de datos meteorológicos. Dependiendo de las temperaturas de trabajo obtenidas, la utilización de paneles híbridos fotovoltaicos/térmicos puede ser planteada.

En concreto, el modelo de producción fotovoltaico fue simulado para el periodo de calefacción entre el 4/12/2012 y el 30/04/2013, prediciendo una producción fotovoltaica alcanzable de 1.265,8kWh y una temperatura media de trabajo de celda de 21,3°C, que alcanza una máxima diaria media de 47,5°C. La energía solar interceptada durante ese periodo fue de 8.869,4kWh, por lo que la eficiencia del campo considerando su área útil sería del 14,3%, frente al 15,4% nominal.

El sistema de calefacción fotovoltaica fue estudiado experimentalmente durante el mismo periodo de calefacción. El campo produjo 820,8kWh de electricidad, por lo que la eficiencia fotovoltaica estacional fue del 9,26%. La producción obtenida fue inferior a la potencialmente alcanzable, de acuerdo con la simulación.

La bomba de calor fue alimentada con 723,9kWh de electricidad, de los cuales 501,4kWh provenían de la fuente fotovoltaica: eficiencia útil del sistema del 5,7%. Multiples factores provocaron dicha eficiencia, tales como las pérdidas eléctricas en las diferentes conversiones, limitaciones del sistema de control, capacidad del sistema de almacenamiento y ajuste de la producción a la demanda.

El calor suministrado al suelo radiante fue 2.321,9kWh. El COP estacional de la bomba de

calor fue de 3,2 y el rendimiento global del sistema del 18,2%. El sistema operó autónomo de la red a un 69,3%.

Las emisiones de gases de efecto invernadero ahorradas fueron de 170,5kg$_{CO_2}$ respecto a alimentar la bomba de calor con electricidad convencional (para un factor de emisión de 0,34kg$_{CO_2}$/kWh); de 835,9kg$_{CO_2}$ respecto a suministrar el mismo calor a partir de gas-oil C; de 573,6 kg$_{CO_2}$ respecto al uso de gas natural. Por otra parte, las fugas de refrigerante equivalieron a 132,1 kg$_{CO_2}$.

Abstract

In the European Union, buildings are responsible for 40% of energy consumption and 36% of CO_2 emissions, which contribute significantly to anthropogenic climate change. Since heating represents the major portion of energy consumption in buildings in Spain, renewable heating systems emerge as an alternative to mitigate this problem.

This thesis proposes a heating system in which the PV production is self-consumed by a heat pump. For this purpose, a photovoltaic off-grid system that feeds an air-water heat pump to heat a small building through radiant floor has been designed and built. The building, despite the aim of being independent, incudes connection to the grid, so the heat pump supply can be switched between the photovoltaic microgrid and the conventional grid. The photovoltaic array, with a total area of 15.7m^2 and useful area of 14m^2, is composed by 12 modules, nominal power of 180W each. Heat pump's nominal heating power is 6kW, which is in line with building's maximum thermal load.

To size properly this type of photovoltaic system, it is necessary to go beyond peak sun hours term commonly used by installers and to simulate realistically photovoltaic production over time. The method known as five-parameter model, details the working curve of a module for a given cell temperature. In this thesis, production has been addressed from a physical point of view, emphasizing the influence of solar cells' temperature on their efficiency. A heat transfer model has been developed, which allows to determine accurately cell temperature under changing meteorological conditions, and then to calculate the photovoltaic production in each moment, basing on technical specifications commonly provided by the modules' manufacturers. This dissertation includes the experimental validation of both cell temperature and photovoltaic production models. The efficiency of the used modules, according to their total area, is 13.73% at 25°C, 12.08% at 50°C and 10.76% at 70°C.

The proposed method is easily adaptable to any type of photovoltaic module, once its material composition is known, and its output can be simulated for any tilt angle and location, for where meteorological data are available. Depending on obtained working temperatures, the use of hybrid photovoltaic/thermal modules can be considered.

The photovoltaic production model was simulated for the heating period from 4/12/2012 to 30/04/2013, predicting an achievable production of 1265.8kWh and an average cell temperature of 21.3°C, which reaches an average daily maximum value of 47.5°C. The intercepted solar energy during that period was 8869.4kWh, so the efficiency of the array according to its useful area would be 14.3%, instead of the nominal value of 15.4%.

The photovoltaic heating system was experimentally tested during the same heating period. The array produced 820.8kWh of electricity. The seasonal photovoltaic efficiency was 9.26%. The achieved production was significantly lower than the achievable one, according to the simulation.

The heat pump was fed with 723.9kWh of electricity, 501.4kWh of which came from photovoltaic source: useful efficiency of the system 5.7%. Several factors caused that efficiency, such as electrical losses in diverse conversions, control system's limitations, storage system's capacity and fit of the production to the demand.

The ammount of heat supplied to the radiant floor was 2321.9kWh. The seasonal COP was 3.2 and system's global efficiency was 18.2%. The system was isolated from the grid at 69.3%.

Greenhouse gases emissions saved were 170.5kg$_{CO_2}$ comparing to feeding the theat pump with

conventional electricity (for an emission factor of $0{,}34\mathrm{kg}_{\mathrm{CO_2}}/\mathrm{kWh}$); 835.9 $\mathrm{kg}_{\mathrm{CO_2}}$ comparing to supplying the same heat ammount through a gas-oil C boiler; 573.6 $\mathrm{kg}_{\mathrm{CO_2}}$ comparing to a natural gas boiler. On the other hand, refrigerant leaks were equivalent to 132.1 $\mathrm{kg}_{\mathrm{CO_2}}$.

Agradecimientos

Quiero reconocer al *Consejo Superior de Investigaciones Científicas* y al *Instituto de Ciencias de la Construcción Eduardo Torroja* (IETcc-CSIC) la formación y los medios que han puesto a mi alcance para la realización de esta tesis. Agradezco a los compañeros del instituto su ayuda profesional y su amistad. La *Universidad Carlos III de Madrid*, que me aceptó en su programa de doctorado, y los miembros de la *Unidad Asociada de Ingeniería de Sistemas Energéticos UC3M-CSIC* se han involucrado en la buena evolución de este trabajo.

Agradezco profundamente a Marcelo Izquierdo Millán, su empeño, exhortación y dirección de esta tesis doctoral, asi como que me haya hecho partícipe de todos los avances del grupo de *Ahorro de energia y reducción de emisiones en los edificios*. A Néstor García Hernando agradezco su confianza en esta tesis y sus consejos.

El trabajo en la *Planta Experimental de Energía Solar* del *IETcc-CSIC* requería de un doctorando experimental. Emilio Martín se implicó en mi formación práctica, tan necesaria en una tesis como esta. Por ello y su amistad, gracias. Quiero recordar a quienes han pasado por el laboratorio estos años, en especial a Ana, Víctor y Daniel.

El *Ministerio de Economía y Competitividad* financió la Estancia Breve (EEBB-I-13-06021) en la Universidad de Wisconsin-Madison. Agradezco a los profesores Sanford A. Klein y Douglas T. Reindl su implicación y supervisión durante tan provechosa estancia. Multitud de colegas y amigos hicieron de este intenso periodo profesional una grata experiencia intercultural. Gracias en especial a Erin, por hacerme sentir como en casa, y a Jean, por su complicidad.

Quiero agradecer a mis compañeros de clase y de piso, amigos de Bilbao y Madrid, que me han acompañado en diferentes etapas de mi formación y de la vida, su camaradería y confianza en mi en todas las aventuras.

Nunca hubiera llegado hasta aquí sin mi familia. Con su cariño incesante y respaldo en la distancia, me han alentado siempre, haciéndome creer que querer es poder.

Finalizo agradeciendo infinitamente a mi compañera en la vida, Patriπ, por su amor, inteligencia y apoyo constante en todos los retos a los que nos hemos enfrentado.

Acknowledgment

Nomenclature

Latin Symbols

$\dot{m}$ mass flow, kg/s.

$\dot{Q}$ heat power, W.

$\dot{q}_{cond}$ conduction heat flux, W/m^2

$\dot{q}_{conv}$ convection heat flux, W/m^2

$\dot{q}_{rad}$ radiation heat flux, W/m^2

$\dot{W}$ electrical power, W.

$\triangle x$ thickness, m.

C_p specific heat, kJ/kg·K.

G_{0n} extraterrestial solar radiation on the normal plane, W/m^2.

G_0 extraterrestial solar radiation on horizontal plane, W/m^2.

G_b solar beam radiation, W/m^2.

G_d solar diffuse radiation, W/m^2.

G_{sc} solar constant: 1367 W/m^2.

G_T solar radiation indicent on tilted surface, W/m^2.

H_T solar daily insolation indicent on tilted surface, kWh/m^2.

I_0 equivalent circuit's diode's reverse saturation current, A.

I_L equivalent circuit's lightcurrent, A.

L_c characteristic length, m.

R_{sh} equivalent circuit's shunt resistance,

R_s equivalent circuit's series resistance,

TH_D building's thermal demand, Wh.

w_s wind speed, m/s.

A area, m^2.

E energy, kWh.

FF fill factor of a photovoltaic module.

G solar radiation on horizontal plane, W/m^2.

Gr Grashof number.

I current intensity, A.

I electrical current, A.

IN energy inflow into the PV/T module, W.

ISE intecepted solar energy by the modules, kWh.

m mass, kg.

Nu Nusselt number.

OUT energy outlfow from the PV/T module, W.

P produced electrical power, W.

Per perimeter, m.

Pr Prandtl number.

Q quantity of energy transferred as heat, kWh.

R thermal resistance, m$^2 \cdot$K/W.

Ra Rayleigh number.

Re Reynolds number.

T temperature, ^{o}C.

U conductance or heat transfer coefficient, W/m$^2 \cdot$K.

V voltage, V.

W quantity of energy transferred as electricity, kWh.

Greek Symbols

α thermal diffusivity.

β tilted angle

δ declination

ϵ emissivity

η efficiency

κ conductivity

λ wavelength

μ dynamic viscosity.

$\mu_{I_{SC}}$ short-circuit current temperature coefficient, A/°C.

$\mu_{P_{max}}$ maximum power point temperature coefficient,

$\mu_{V_{OC}}$ open circuit voltage temperature coefficient, V/°C.

ν kinematic viscosity.

ω solar hour angle

ϕ latitude

ρ density

τ transmitance coefficient

θ incidence angle

ξ thermal expansion coefficient.

Subscripts

back   relative to a layer's rear surface.

cell   relative to a solar cell.

cond   relative to heat pump's condenser.

dp   relative to dew point temperature.

evap   relative to heat pump's evaporator.

film   relative to film temperature, the fluid layer above a solid surface.

front   relative to a layer's frontal surface.

ge   relative to conventional grid electricity.

hp   relative to the heat pump.

ind   relative to indoor temperature.

lam   relative to laminar flow.

mod   relative to a PV-T module.

mp   maximum power point.

OC   open circuit voltage.

odb   relative to outdoor dry bulb temperature.

PV   relative to photovoltaic.

PVMA relative to photovoltaic modules' array.

ref   reference conditions, usually Standard Test Conditions.

rfs   relative to radiant floor's surface.

SC   short-circuit current.

surf   relative to a surface.

turb   relative to turbulent flow.

Acronyms

COP   Coefficient of Perfomance.

EVA   Ethylene Vinyl Acetate.

GWP   Global Warming Potential.

IPCC   Intergovernmental Panel on Climate Change.

IR   Isolation Ratio

ITH   Integration Time Horizon.

MPPT Maximum Power Point Tracking.

NOCT Normal Operation Cell Temperature.

ODP   Ozone depletion potential.

PSH   Peak Sun Hours.

PV   Photovoltaic.

PV-T Photovoltaic-thermal hybrid.

SF   Solar Fraction

STC Standard Test Conditions.

STF Secondary Thermal Fluid.

TEWI Total Equivalent Warming Impact.

Contents

List of Figures

Chapter 1

Introduction

In the present, the growth in energy demand and uncertainty about future availability of fossil primary energy sources, along with global warming related to the emission of greenhouse gases represent a global problem of first magnitude. Different European and Spanish directives have been promoting renewable energy and its integration into buildings as a way to mitigate this problem. Solar heating systems could contribute to reduce the European and Spanish consumption of imported fossil primary energy and the emission of greenhouse gases. In addition, they might entail economic savings in homes against the increase in energy costs.

In this chapter the environmental, energy and regulatory issues that motivate this work are introduced, before outlining the scope of this study.

1.1 Motivation of the study

1.1.1 Enviromental problems

In recent decades, diverse global enviromental or climatic problems directly related with human activity have been detected. The ozone depletion phenomena was observed since the late 1970s and its relation with chlorofluoroncarbon gases (CFC) emissions was pointed out by Molina and Rowland [1974]. In addition, the detection of larger ozone decreases in Earth's polar regions [Farman et al., 1985], forced the international community to agree their production reduction in an international treaty, known as Montreal Protocol [U.N., 1987]. Since then, the CFCs have been replaced by alternative substances, such as hydrofluorocarbons (HFC) and perfluorocarbons (PFC) which present a low or null ozone depletion potential (ODP) but a global warming potential (GWP) up to thousand times higher than CO_2.

In the 1990s, the main global concern in environmental terms became the so-called climate change due to Earth's greenhouse effect increase. In 1988 the Intergovernmental Panel on Climate Change was established in order to assess scientific information on human contribution to Earth's greenhouse effect. Since then, through several reports, the IPCC has claimed that warming of the climate system is unequivocal, and since the 1950s, many of the observed changes are unprecedented over decades to millennia [IPCC, 2013]. In its fifth report, the IPCC states that it is extremely likely (95-100% probability) that human influence has been the dominant cause of the observed warming since the mid-20$^{\text{th}}$ century. It remarks that continued emissions of

greenhouse gases (GHG) will cause further warming and climate changes, so substantial and sustained reductions of GHGs will be required to limit climate change.

Based on that premises, the Kyoto Protocol [U.N., 1997] was elaborated, which commited the States Parties to reduce greenhouse gases emissions, in particular CO_2, CH_4, N_2O, HFC, PFC and SF_6. The signing countries agreed to implement and/or further elaborate policies and measures such as enhancement of energy efficiency, promotion of sustainable forms of agriculture, research and promotion of new and renewable forms of energy, progressive reduction of fiscal incentives and subsidies in all GHGs emitting sectors.

As it is well known, a large portion of anthropogenic GHGs emissions stem from energy exploitation of fossil fuels, so the promotion of renewable energies has been considered of great potential for climate change mitigation. According to IPCC [2011], solar energy offers significant near-term (2020) and long-term (2050) potential for this mitigation, producing photovoltaic electricity or through active solar heating and cooling of buildings.

1.1.2 European energy context

European Union's commitment with climate change mitigation, the aim of improving its energy security and the necessity to reduce energy costs in order to increase competitiveness, have motivated the 20-20-20 targets [E.U., 2009]. They consist of three key objectives for 2020:

- a 20% reduction in EU greenhouse gas emissions from 1990 levels.

- a 20% share of EU total energy consumption from renewables sources.

- a 20% improvement in energy efficiency.

Energy security in the EU can be improved if the heavy dependence on external fossil fuels and primary energy imports are mitigated. According to Eurostat, in 2012 EU imported 53.4% of its primary energy consumption, being Russia its main supplier for solid fuels, crude oil and natural gas. In Spain this energy dependence problem is intensified and a 73.3% rate was reached the same year. Indeed, the energy dependence rate surpassed 80% during the 2005-2008 period, when energy consumption was higher (fig. 1.1).
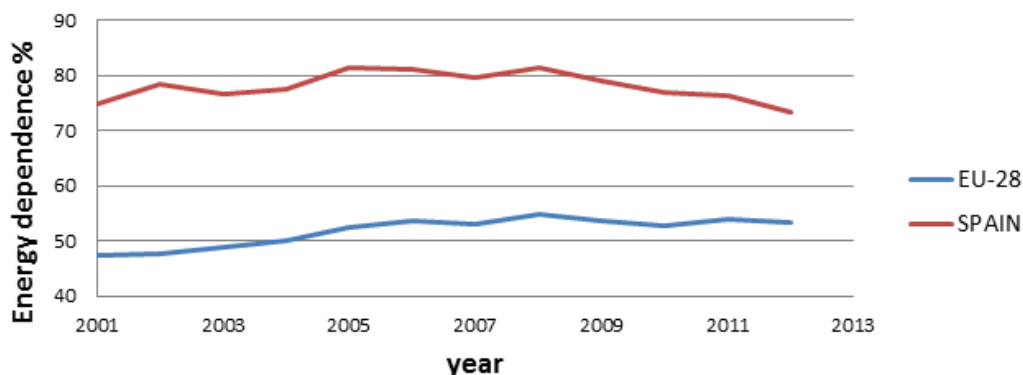
Figure 1.1: Energy dependence rate for Spain and EU [Eurostat].

The lack of fossil sources in the majority of EU member countries suggests the potential of renewable energies to alleviate the mentioned dependence on fuel from non-member countries, which in addition would reduce the GHGs emissions from fossil fuels combustion and decouple energy costs from oil prices. In fact, among primary energy production (the not imported share), the nuclear and renewable energies play the main roles. In particular, the share of renewables in gross inland energy consumption came to a 11.0% rate in EU and 12.6% in Spain.

Focusing on electricity generation, the renewable share rises up to 23.5% in EU and 33.5% in Spain in 2012, according to Eurostat.

1.1.3   Energy consumption in buildings

The residential and commercial buildings represents 40% of the European Union's total energy consumption and are responsible of 36% of the CO_2 emissions according to the directive published in the Official Journal of the EU about energy perfomance in buildings [E.U., 2010]. This directive aims at improving efficiency and reducing energy consumption and emissions in buildings. In particular, it requires all new buildings to be nearly zero-energy (NZEB) by the end of 2020, which are defined as very high energy performance buildings, where the nearly zero or very low amount of energy required should be covered to a very significant extent by energy from renewable sources, including energy from renewable sources produced on-site or nearby.

Consistently, in Spain the Technical Building Code regulates since 2006 certain mandatory minimum commitments for energy saving, setting a minimum contribution of solar energy for domestic hot water (DHW). Regarding solar photovoltaics, a minimum contribution to electrical consumption of the building is mandatory for commercial buildings and certain public spaces larger than 5000 m², avoiding any specification for residential buildings[CTE, 2013].

In Spain, according to IDAE [2011], residential sector requires 17% of spanish final energy consumption and 25% of electrical demand. This consumption is broken down in figure 1.2, where domestic heating represents 47.0% and air conditioning 1.1%. The domestic space cooling has grown the last years and, according to Izquierdo et al. [2011], in Madrid's region, during summer months represents up to 6.7% of domestic consumption and contribute to a 33% to summer peak demands.
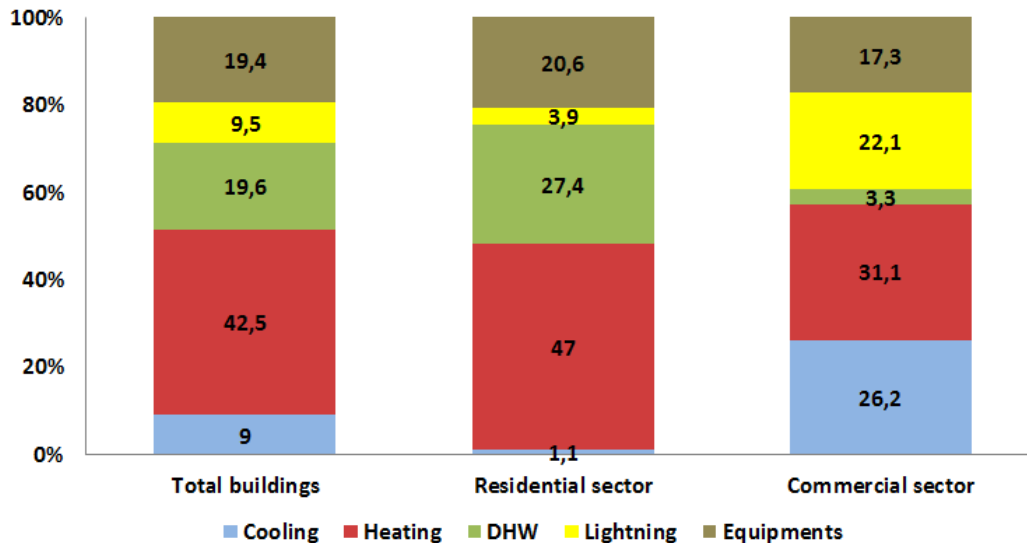
Figure 1.2: Distribution of energy consumption in buildings [IDAE, 2011]

According to SECH-SPAHOUSEC report[IDAE, 2011], 49% of spanish houses are equiped with some type of air-conditioning system, among which 84% are reversible vapor-compression machines that could be used for heating. However, just 22% of heating in spanish houses comes from the use of heat pumps.

In the whole EU, where Spain is the biggest market, there are 25 million of residential air conditioning machines, which represent about 37% of the total units in buildings, according to Bertoldi et al. [2012]. The same report states that air-conditioning for both the residential and tertiary sector demands yearly 17 TWh.

1.1.4 Enviromental impact of heat pumps

Heat pumps have been referenced in the mentioned diverse european directives as high-efficiency alternative systems to be considered for energy savings. In such directives, heat pumps are defined as machines that transfer heat from natural surroundings such as air, ground or water to buildings or industrial applications by reversing the natural flow of heat such that it flows from a lower to a higher temperature. Therefore, that aerothermal, geothermal or hydrothermal renewable heat is used for indoor heating, requiring an external work. The common domestic heat pumps are electrically driven.

However, heat pumps based on vapor-compression cycle entail an enviromental double impact that must be remarked. On the one hand, these machines contain greenhouse gases as refrigerant, which present a high global warming potential, and on the other, they are fed with grid electricity which equivalent CO_2 emissions must be taken into account. The sum of these direct and indirect emissions define the total equivalent warming impact (TEWI) of a heat pump. The GWP of each type of refrigerant can be consulted in the work by IPCC [2013].

For the existing heat pumps the TEWI can be reduced by minimizing the indirect emissions. This is where photovoltaic generation of electricity can contribute to reduce heat pumps' enviromental impact, forming a solar photovoltaic heating system.

1.1.5 Subsidies and moratoriums to photovoltaics

In the last decade, the EU member countries have promoted diverse public policies to encourage the growth of renewable energies in order to meet the energy and environmental goals. For photovoltaics, in particular, most of them have opted for economic premiums for production as feed-in-tariff (guaranteed access to the network, long-term contracts and higher market prices purchase based on the largest cost of photovoltaic generation) or installation (tax benefits).

However, in the recent years this regulatory context is abruptly changing in Spain and other europeans countries. At the present moment, in Spain the domestic PV systems cannot be beneficted of any premiums as the feed-in-tariffs (FIT) for injecting PV production into the national grid. In addition to this FIT moratorium, there is a legal uncertainty about the future of self-consumption domestic PV systems that are on-grid connected. The legislative evolution and present context is detailed in the next chapter.

In conclusion, the PV premiums moratorium and the prospect of possible taxes applied to domestic on-grid PV systems provide a new and full interest in the study and analysis of off-grid systems for PV solar heating.

1.2 Objectives to study

The main objective of this work is the study of a photovoltaic heating system as much isolated from the grid as possible. For this purpose an off-grid photovoltaic system has been designed and installed in the *Solar Energy Experimental Plant* of the *Eduardo Torroja Institute for Construction Science* (IETcc-CSIC), which feeds a reversible air-water heat pump to heat a small building through radiant floor. The heat pump can be fed by this off-grid PV system or by the conventional grid. In this way, the potential application of PV heating systems as much autonomous as possible will be concluded for both developed countries where PV surplus grid injection is not an option or is penalized, and off-grid remote areas.

Nowadays, diverse solar heating and cooling systems have attracted the interest of scientific community. Although heat pump and photovoltaic technology have been studied separately for long time, the perfomance of experimental PV heating facilities are very scarce in the scientific literature. Therefore, this work aims to provide detailed results to support positive or negative arguments in the solar heating debate.

This work, on one hand, pretends to provide a sharp PV model that allows to predict precisely the production of a PV array for a given location and meteorological database, which would provide a proper tool for sizing PV systems. In particular, this model should emphasize on the cell temperature dependence of the PV efficiency and include a heat transfer model to calculate it dynamically. With this tool, the real achievable PV production could be determined. The proposed model is pretended to be validated through experimental measurements.

The experimental facility is composed of PV/T modules. The heat transfer model should allow to discuss their applicability.

On the other hand, the PV heating system is detailed, with a full description of its components and characteristics. This facility has been tested for a whole heating season and its performance studied. The heat pumps' working characteristics are theoretically introduced to be able to analyze its daily and seasonal perfomance.

The proposed solar heating system presents a double enviromental benefict: the heat pump gains aerothermal heat from the low temperature outdoor air and its TEWI is reduced thanks to the PV source used for feeding it.

1.3   Summary of chapters

After this introduction to the dissertation, on the following lines abstracts of each chapter are outlined:

In *chapter 2* the historical development of photovoltaics and their implementation in on-grid and off-grid systems are narrated. After that, solar space heating and cooling systems are widely reviewed, concluding the novelty of the present study.

Chapter 3 describes the physics behind photovoltaic technology, the operating principles of PV modules and the diverse type of PV systems, in order to state a theoretical background that allows to understand the results of this study. In particular, the proposed PV heating system and its components are presented on *chapter 4*. In the same chapter, the measurement equipment and uncertainty propagation analysis method are described.

In the following part of the work a PV production predicting model for a given meteorological database is developed.

Chapter 5 explains some photovoltaic models and proposes an eased method basing on manufacturer's common technical specifications. Precise PV models require as inputs the daily evolution of solar radiation and cell temperature. Therefore, in that same chapter, a method for calculating solar radiation over tilted surfaces at any angle from measured horizontal one is explained. After it, cell temperature determination is studied in *chapter 6*. For this purpose, a specific heat transfer model has been developed, which is experimentally validated for the specific modules employed in the designed PV heating system.

In *chapter 7* the PV production predicting model is experimentally validated and a simulation is run for a whole heating season. The seasonal PV production and average cell temperature are calculated. The potential use of PV/T modules is discussed.

Chapter 8 presents the experimental perfomance of the PV heating system. Its working characteristic along diverse days and seasonal results are shown. The enviromental impact reduction is studied, quantifying the CO_2 emmisions saved. In its last section, the experimentally obtained PV production and the simulated one are compared.

Finally, in *chapter 9* the conclusions of the study are discussed.

At the end, an appendix includes theoretical and experimental results of the PV-heat pump system in summer.

Chapter 2

State of the art

In this chapter the state-of-the-art of photovoltaics and their application for buildings is discussed. In particular the solar heating and cooling systems that have attracted the attention of scientific community are reviewed, pointing out the lack of simulation and/or experimental studies about solar off-grid PV heating systems.

2.1 Historical development of photovoltaics

2.1.1 Origins

The physical phenomenon in which part of the solar radiation incident on a semiconductor device produces electrical energy, the photoelectric effect, became known in the nineteenth century. Experimenting with electrolytic cells in 1839, Becquerel observed that electricity generation increased upon exposure to light. Thereafter, different inventors and scientists experimentally moved forward, but without getting a theory to explain this phenomenon. The various advances made thereon during the nineteenth century were summarized by Wolf [1981].

It was after the quantum conception of light by Planck, that during his annus mirabilis Albert Einstein published his explanatory theory of the photoelectric effect [Einstein, 1905], which was subsequently validated experimentally by Millikan. This is why they were recognized with the Nobel Prize in Physics in 1921 and 1923 respectively.

2.1.2 First applications

The first patents related to photovoltaic cells were registered in the late 1920s. However, it was not until 1955 when the company Bell developed a small panel that fed telephone equipment and its reduced battery in Georgia, USA. Nominal efficiency of the first devices was about 6%. It was the space race of the years 50-70 the true driving force behind the development of the photovoltaic sector and improving efficiency. The Vanguard I satellite, launched in 1958 and still in orbit [NASA], was the first to include six photovoltaic cells, with a nominal power around 1W, which fed a transmitter which signals were received until 1964. The success of the experiment made that in the following decades more than a thousand spatial devices were sent equipped with photovoltaic systems.

Following the oil crisis of the 1970s and the need for alternative energy sources, it began to raise the application of photovoltaic energy for terrestrial applications. The first research centers for the promotion of photovoltaic technology were established , the process began being industrialized, aiming for cheaper manufacturing costs, diversification in their applications, increasing efficiency and finding alternative materials .

Since then, photovoltaic technology has come to play a primarily terrestrial use (although still used in space facilities); at the same time the price has dropped over 100 times: now solar cells' price is below 0.5$/$W_{peak}$, where in 1977, adjusted to the inflation, still had a cost of 76.67 $/$W_{peak}$ [Bloomberg, 2012], according to figure 2.1.
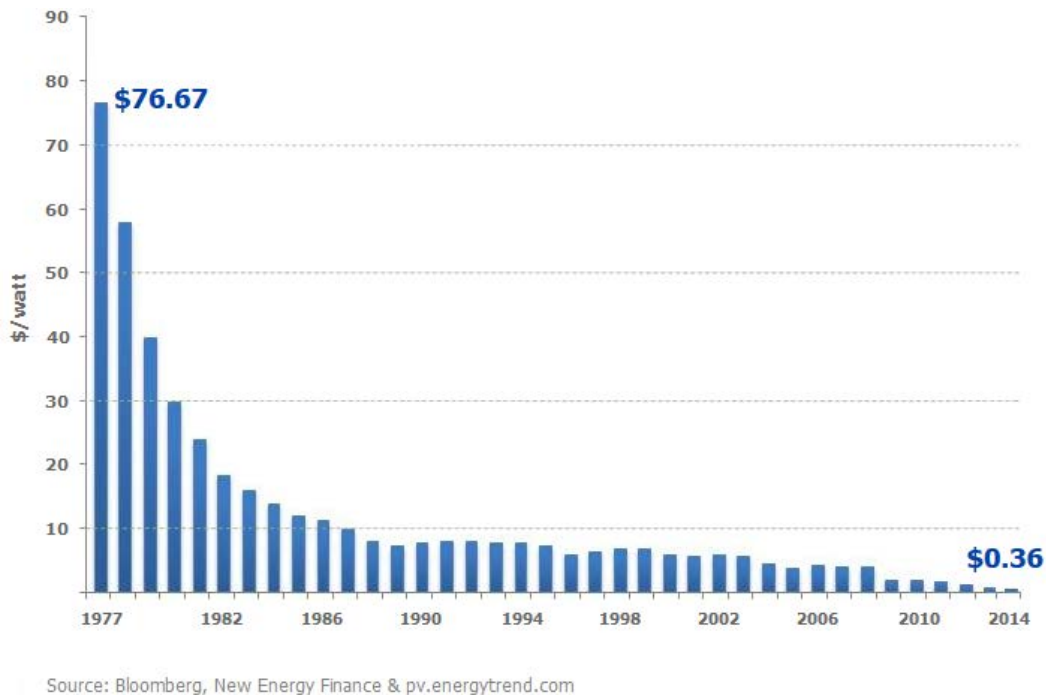
Figure 2.1: Evolution of the average PV cells' price.

2.1.3   Development of standalone applications

Initially, terrestrial applications of photovoltaics were designed to power small mobile devices or electrical consumption isolated systems, wherever national grids could not reach (isolated, off-grid), usually with some type of electrical storage battery that would meet demand when there was not generation.

A widespread application of photovoltaics was feeding the growing sector of telecommunication ground stations. Despite its high cost, photovoltaics appeared as one of the few alternative to power stations in remote areas or where to deploy the electrical network could have a cost of up to 6000 $/ km [Kelly, 1979].

Being able to actually generate electricity in places away from the conventional grid showed the potential of photovoltaics to power electrical components or small towns in remote rural areas, reserves or underdeveloped countries. The photovoltaic electrification (3.5 kW) of Schuchuli, a

village on an Indian reservation in Arizona, USA, in 1978, or the power of a system of a small grain mill and water supply (1.8 kW) in Tangaye , Burkina Faso, in 1979, were some of the first examples [Rosenblum et al., 1979]. Both with electric Pb-acid batteries.

Special mention deserves the use of photovoltaics to directly power DC motors [Bany, 1978], without losses of electric storage components or inverters, and that are instantly activated whenever there is photovoltaic generation. Due to their intermittent operation, greater application has been found in pumping water for drinking and irrigation in agriculture [Matlin et al., 1978], especially in underdeveloped regions [Malhotra, 1984].

2.2   Grid connection

According to the photovoltaic technology being matured, production costs decreased and more powerful photovoltaic systems were installed. In the 1980s it began the consideration of the installation of photovoltaic plants connected to the grid, contributing to the electricity mix, as an alternative to conventional electricity generation plants.

The first installations were practically demonstrative and testimonial compared to whole national power grids. However, with increasing awareness of environmental issues such as CO_2 emissions, various public policies promoted the installation of new renewable electrical production sources.

In the early 1990s the vast majority of PV installed capacity in the world , about 43MW, was as isolated systems. In 2000, the installed capacity on-grid surpassed isolated or off-grid as shown in figure 2.2.
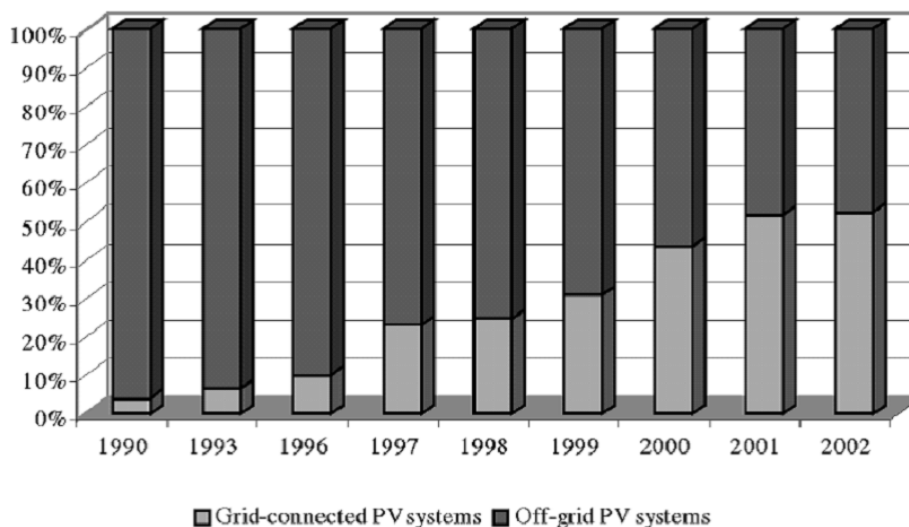
Figure 2.2: Global evolution of the ratio between autonomous and grid connected PV systems[Goetzberger and Hoffmann, 2005].

Since then the PV installed capacity worldwide has grown at an unprecedented rate, from 1 GW to 102GW, according to EPIA [2013]. As shown in figure 2.3, the main role has been played by Europe, with more than 70% of the installed capacity in the world.

	2000	2001	2002	2003	2004	2005	2006	2007	2008	2009	2010	2011	2012
ROW	751	807	887	964	993	1,003	1,108	1,150	1,226	1,306	1,590	2,098	2,098
MEA	n/a	n/a	n/a	n/a	1	1	1	2	3	25	71	192	601
China	19	24	42	52	62	70	80	100	140	300	800	3,300	8,300
Americas	146	178	225	290	394	501	650	863	1,209	1,752	2,780	4,959	8,717
APAC	355	495	686	916	1,198	1,500	1,825	2,096	2,631	3,373	4,956	7,628	12,397
Europe	129	262	396	598	1,305	2,289	3,281	5,310	11,020	16,850	30,472	52,884	70,043
Total	1,400	1,765	2,235	2,820	3,952	5,364	6,946	9,521	16,229	23,605	40,670	71,061	102,156

ROW: Rest of the World. MEA: Middle East and Africa. APAC: Asia Pacific.

Figure 2.3: Evolution of global PV cumulative installed capacity (MW) [EPIA, 2013].

2.2.1 Development in Europe

It is worth mentioning that different incentive public policies have encouraged the on-grid PV connection, where all production is supplied to the grid. Meanwhile, the off- grid installations in Europe have been set aside to their initial functions: small remote power systems, mountain shelters, rural electrification, ... representing 2% of the installed power on the continent and 0.24% in EU [EurObserv'ER, 2013]. At the same time, the industry has reduced the costs of PV modules in Europe more than 70 % compared to 2000 [EPIA, 2011a]. Assembled in modules, the price per watt is slightly higher than the one shown in figure 2.1; in January 2015 the price is about 0.5€/W_{peak}, which evolution can be consulted on pvXchange.

EU countries that have promoted solar photovoltaics have done it through tax incentives in the installation or fixing purchase prices, known as feed-in-tariffs (FIT). The conditions for such premiums vary in each country and may include items such as guaranteed access to the network, long-term contracts and higher market prices for purchase based on the higher cost of photovoltaic generation.

The different economic incentives have been key factor in the PV development in Europe, led by Germany since the beginning of the 2000s , in both manufacturing industries and installed PV power. In the German case, technological advances were both a result and engine of successive promotion policies [Hoppmann et al., 2014], where staggered FIT reduced the remuneration

according to the growth of the installed PV power. However, in other countries the FIT were introduced later and less gradually, inducing *PV booms*. One can observe in figure 2.4 a sharp increase in countries like Spain in 2008, Italy between 2010 and 2011, and France in 2011.
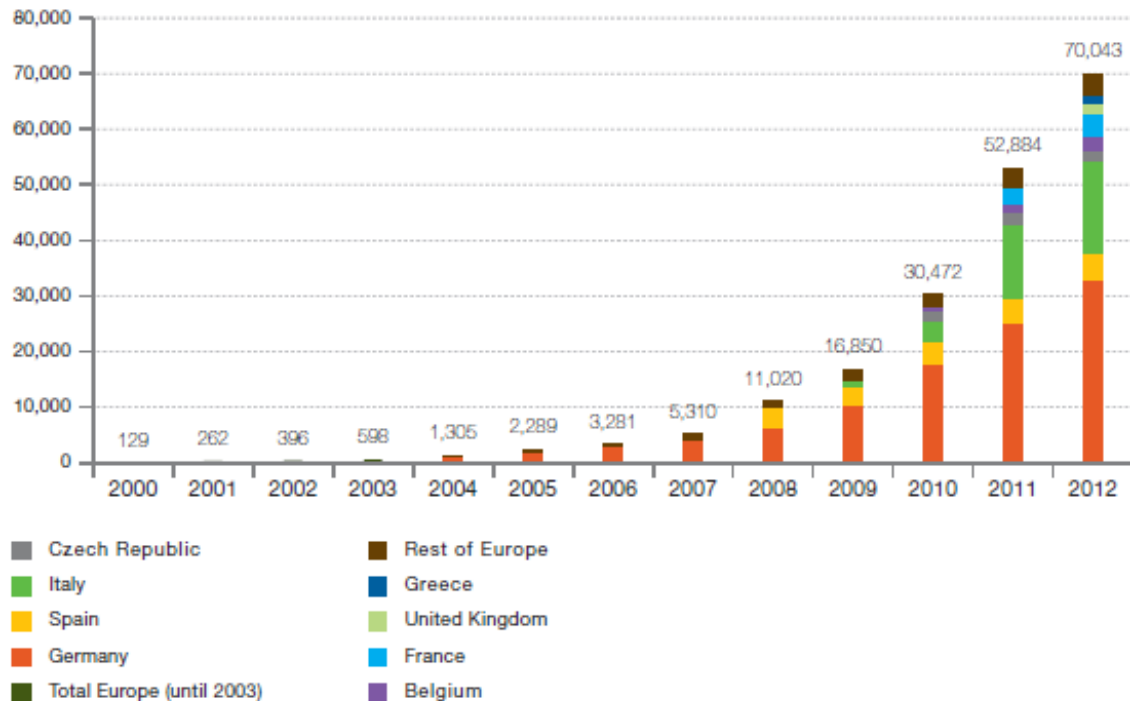
Figure 2.4: Evolution of european PV cumulative installed capacity (MW) [EPIA, 2013].

There is some controversy about the FIT: considered necessary to protect the photovoltaic industry from the competition with conventional electricity production technologies, all mature [Garcia-Alvarez and Mariz-Perez, 2012] and the launch of the photovoltaic sector in new scenarios, such as the UK [Cherrington et al., 2013], however lax regulation and erroneous planning can lead to uncontrolled growth that alters excessively market prices, as in Italy, triggering the FIT to be abruptly interrumpted [Antonelli and Desideri, 2014]. The different photovoltaic regulations for each country are listed in the report Global Status Report [REN21, 2013].

2.2.2   Development in Spain

2.2.2.1   Legislative and installation evolution

As shown in figure 2.4, a considerable part of the growth of PV in Europe has taken place in Spain during the last decade. Currently, it is the third European country with the largest installed on-grid photovoltaic power (4438 MW), after Germany and Italy.

This installed capacity, represents the 4.3% of the whole national grid's power and during 2013 has produced an annual output of 7900 GWh, 3% of the annual electrical demand in Spain

[REE, 2013]. However, development has not been linear (fig. 2.5, logarithmic scale) and has been clearly determined by the different public policies.
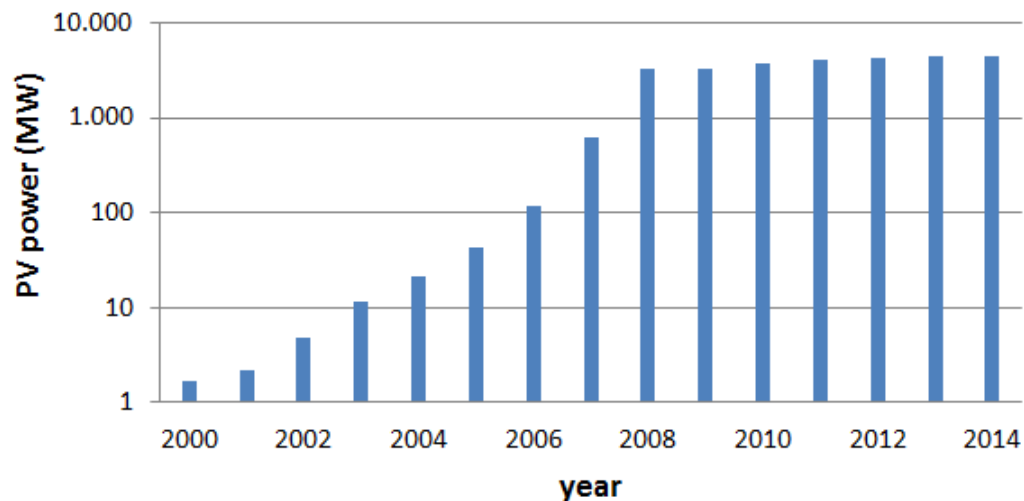
Figure 2.5: Evolution of PV cumulative installed capacity in mainland Spain [REE, 2013].

Photovoltaic technology already attracted some interest for the Spanish research since the late 1970s [Luque, 1989]. In 1984 the first on-grid photovoltaic array was installed in San Agustín de Guadalix, Madrid, with 100kW of nominal power. At the end of the next decade, they had only been connected to the network a few experimental or demonstration systems; photovoltaic power accumulated in the peninsular network barely exceeded 1 MW and there was no regulation governing such facilities.

In the late twentieth century, consistent with the renewable energies support policies implanted by other EU partners, the government of Spain approved the decrees RD 2818/1998 (on "Production of electricity by facilities supplied by resources or sources of renewable energy, waste and cogeneration", BOE, 1998) and RD 1663/2000 (on 'Connection of photovoltaic installations to the Low Voltage Grid", BOE, 2000). Thus, the technical and administrative conditions for regulating photovoltaic systems were established and the first premiums were assigned.

Still, the real takeoff of photovoltaics occurred since the RD 436/2004 [BOE, 2004], simultaneously with neighboring countries in Europe, coinciding with the decline in prices in photovoltaic modules and more advantageous premiums. The publication of RD 661/2007 [BOE, 2007] sought to encourage the installation of 400MW by 2010 as planned by the National Renewable Energy Plan [IDAE, 2005]. But it established such an attractive premium that it attracted an unexpected investment, resulting in 2008 PV boom: new 2595MW connected to Spanish National Grid, mainly in large PV arrays of tens of MW, including which was then the world's largest facility (Olmedilla de Alarcón, 60 MW). To correct excessive remuneration and adapting to the new economic situation, successive regulations have reduced premiums (RD 1578/2008, RD 1565/2010, RD 14/2010), while installation of new photovoltaic arrays were sharply decelerated, reaching the suspension of pre-allocation procedures and the removal of economic incentives for future installations (RD 1/2012).

Parallel to this on-grid boom, over the past three decades in Spain autonomous photovoltaic

systems have been installed, for small devices, electrification of agricultural structures and remote rural or mountain buildings, road signs, etc. At present , according to the EurObserv'ER [2013] project, in Spain there are 25 MW of off-grid PV systems, 0.6% of the total.

2.2.2.2   Future prospects without FIT

Already in the early development of photovoltaic technology the potential to supply to devices both grid and photovoltaic electricity was discussed [Barker, 1979], so that the grid supplemented the PV modules when there was shortfall in production. This concept is the basis of self-consumption for houses: the partial supply of domestic electrical demand through photovoltaics and consumption through the conventional grid when there is no PV production or it is insufficient. Currently this mixed system arises as an alternative to FIT for PV integration in housing [Poullikkas, 2013], starting from the premise that occasional excess or surplus of PV electricity can be injected to the grid for later consumption (net-balance).

Figure 2.6 shows that in a house that produces and consumes photovoltaic electricity, production and demand can be decoupled: in a net balance system, it would use the conventional grid as electrical storage. There are different ways to adjust the balance between consumer and electrical company, between production and demand [Yamamoto, 2012].
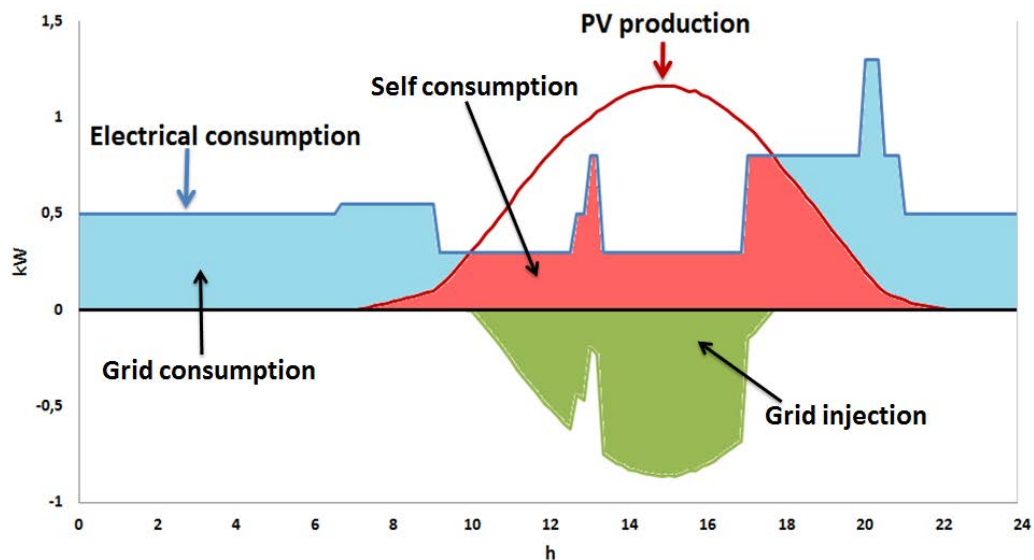
Figure 2.6: Example of a domestic self-consumption PV system daily operation.

However a self-consumption system does not strictly contemplate the drawn of PV surplus to the grid, or financial reward for it, or any right for deferred consumption, so it should be studied in different manner from a net-balance system.

In Spain, following the PV modules' prices drop, the growing price of electricity and despite of the moratorium on feed-in-tariffs, the self-consumptions emerges as a possibility for saving in domestic finances.

Contrary to the European trend, in Spain the vast majority of PV power has been installed in ground (over 80%), mainly in large photovoltaic fields, and not on the roofs [EPIA, 2013],

so a hypothetical expansion of self-consumption systems would require new installed power. A step towards normalization of self-consumption was led by the publication of RD 1699/2011, regulating technical and application conditions for grid connection of facilities of small power producing electricity (up to 100kW), keeping the economical conditions unregulated. "The future and forthcoming regulation of supply of electric energy produced within the grid of a consumer for his own consumption that will encourage self-consumption" was also anticipated.

Since then, various drafts and legislative proposals have been written. The first draft of Royal Decree [MINETUR, 2011] considered the net-balance and articulated the right of delayed consumption of photovoltaic energy previously injected to the grid. This project was dropped and now the proposed Royal Decree "on the regulation of the administrative, technical and economical modes of supply of electric power to self consumption and production to self consumption is established " [MINETUR, 2013], in its Article 9 does not consider the net-balance and introduces the concept of backup toll, tax payment for the supply function that conventional grid provides self-consumption facility when there is lack of production.

This new regulatory framework could drastically delay the payback periods [Talavera et al., 2014] of small domestic PV systems in Spain and even discourage the on-grid connections. The autonomous systems would not be subject to those tolls and legislative uncertainties so they arise as a possible alternative for building integration of photovoltaics and energy saving. If these new policies are extended, research in off-grid applications would be of big interest for the residential sector in developed countries.

2.3 Solar heating and cooling

The use of active solar energy as a renewable source for heating and cooling spaces has attracted attention for decades. Diverse solar heating and cooling systems are based both in solar thermal collectors or in photovoltaic electricity.

The most widespread application of solar heating is uptake of thermal energy through solar collectors of various kinds for later use, which has been the subject of theoretical and experimental research since the beginning of the domestic application of solar energy. Some of the first solar heating systems were based on plate solar air collectors like the ones on Colorado Solar House built in 1957 and tested for 18 years [Ward and Löf, 1976]. The air was substituted by water as thermal fluid in the solar collectors for heating as the technology advanced [Löf and Tybout, 1973]. The evolution of solar thermal flat collectors, storage and control systems allow to heat water to higher temperatures, to reduce losses and to improve system's efficiency [Brandemuehl and Beckman, 1979]. The seasonal performance of a recent solar space heating system based on flat-plate vacuum collectors was studied by de Agustin et al. [2013].

Besides space heating, solar thermal collectors are commonly applied for obtaining domestic hot water (DHW). This function is now a mature technology growing at a rate of about 16% per year and employed in most countries of the world [IPCC, 2013].

Solar thermal cooling, more complex, can be subdivided in open cycles, such as desiccant wheels, and closed cycles as $LiBr/H_2O$ absorption machines.

On the other hand, solar photovoltaic electricity can be used for feeding a mechanical compression heat-pump for heating, or cooling if equipped with a reversible machine.

For decades solar cooling research has been focused in thermal technology, as shown in the state

of the art in Europe review conducted by Balaras et al. [2007], where only solar thermal cooling of closed or open cycles were mentioned. Regarding solar electric cooling, although it is considered since the 1980s as a future alternative to absorption machines [Ayyash and Sartawi, 1983], the degree of technological maturity of its two main components: vapor-compression machine and the PV modules was uneven. Indeed, in the state of the art review developed by Kim and Ferreira [2008] it was underlined that, to be marketed, electrical systems faced two challenges: meeting the demand regardless of production either by electrical batteries, combinging conventional grid and PV electricity or by compressors with variable capacity, and a reduction in costs of photovoltaic modules.

When the PV grid connection and feed-in-tariffs were popularized in Europe, electrical solar heating and cooling seemed to overcome its biggest obstacle: the difficulties and need of electrical storage. Actually, the entire PV production was injected to the grid, with a financial reward, and the vapor-compression machines could operate fed by the grid, without interruption in the supply. Authors like Henning [2007], stood out that the study and research of a solar photovoltaic vapor-compression system as a whole seemed to present no great interest for industrialized countries, since, in fact, photovoltaic generation and operation of vapor-compression machine behaved like two independent systems. Assuming the conventional grid as an external energy accumulator, the challenge of storage was avoided, postponing the study of solar PV heating and cooling in isolated systems.

In the most recent scientific literature, theoretical studies and simulations comparing solar thermal and photovoltaic systems can be found. The vast majority of these publications consider electrical solar heating and cooling systems connected to the grid, so they assume independent behavior between electricity generation and demand, injection of PV surplus in the grid, and even complete injection thanks to the premiums. Hartmann et al. [2011] compared solar heating and cooling technologies both of photovoltaic and thermal base and they simulated annual performance in Freiburg and Madrid, considering an on-grid photovoltaic scenario in which the grid is equivalent to an ideal zero cost accumulator and including FIT existing at that time in Germany and Spain. Under these premises they concluded that solar photovoltaic cooling was a better present and future solution than solar thermal cooling, both from the primary energy and economic point of views. However, they did not considere photovoltaic source for heating, but they propose to heat the building with a gas fired condensed boiler. They highlighted the larger industrial development of mechanical compression machines over the absorption ones and the challenge for solar thermal storage systems when production exceeds demand or during the months when there is no heating no cooling demand. It is necessary to reiterate that this challenge is common to photovoltaic heating and cooling for off-grid systems or under a legislative scenario without premiums or where on-grid self-consumption is penalized.

In a similar vein, Eicker et al. [2014] performed an evaluation of thermal and photovoltaic solar cooling systems for Madrid, Stuttgart and Palermo. They considered a PV cooling system which would use the grid as backup and storage, and simulated three different scenarios of power regulation policies: high bonus, low bonus and no financial reward at all. The results obtained seemed to favored photovoltaic solar cooling. Currently, however, considered premiums have suffered a government moratorium in Spain and Italy, as mentioned previously, so that conclusions could be modified in this new scenario. On the other hand, the heating demand was simulated but how it would be satisfied was not faced, considering the PV production of a whole year for

satisfying just the cooling demand.

The application of photovoltaic electricity for feeding a vapor-compression heat-pump and heating spaces has not been as well studied as the photovoltaic cooling systems, obviating the fact that reversible heat-pumps connected to a PV system can provide heating and cooling along the diverse seasons of a year. Moldovan et al. [2014], motivated by the Nearly Zero Energy Buildings target of the EU, simulated a heating, cooling and DHW system along a year based on reversible heat pump with ground heat exchanger fed with PV electricity. Simulation resulted that heat pump's yearly electrical demand would be covered at 100% by the PV on-grid system, as whole electrical production would be injected in the grid along the year in a net-balance context. In a similar way, Kazanci et al. [2014] proposed a house prototype at Solar Decathlon that covered the heating demand with a ground source heat pump and employed the ground as heat sink in summer for free-cooling. The house included an on-grid PV array that, according to the authors, would inject into the grid more electricity in a year than the demanded one, claiming the building as a plus-energy house.

All mentioned PV heating or cooling works assume an on-grid scenario where the PV surplus is injected in the grid for future consumption, using the grid as storage system even for whole seasons, for which they have not considered any economic penalty. However, in order to compare them with solar thermal heating and cooling systems strictly in energy terms, they should be studied facing the storage issue.

As it said, solar thermal systems' perfomance is related to their storage system which is a real component of the system. Consequently, in these systems the thermal storage is usually sized for few hours or days and solar thermal heating and cooling systems are required to be properly designed for both winter and summer. In the last years, diverse solar thermal heating and cooling systems have been simulated and/or built. Fong and Lee [2015] proposed a system for subtropical climates composed of solar thermal collectors for heating and DHW and a water cooled single effect absorption machine for cooling. Marcos et al. [2011] studied the potential energy savings and emissions reduction of flat-plate vacuum solar collectors array for heating and for feeding an air cooled single effect $LiBr/H_2O$ absorption machine. An air cooled single-double effect absorption prototype is presented by Izquierdo et al. [2014b], which single effect would be solar thermal powered and could be assembled in a solar heating and cooling system [Izquierdo and de Agustin, 2014], feeding the double effect and, partially, the heating power through a burner. Calise [2012] proposes a high temperature heating and cooling system where solar thermal energy is obtained by parabolic trough collectors for heating and for feeding a water cooled double effect absorption machine for cooling.

The author studied the experimental perfomance of a PV off-grid cooling system through cooled floor [Izquierdo, de Agustin, and Martin, 2013]. This work, complementary to this dissertation, is attached on appendix A.

2.3.1   Photovoltaic/Thermal hybrid modules

The facts that PV modules exposed to solar radiation transform just a share in electricity and that PV efficiency decreases with temperature increase, motivated the idea of gaining heat and improving electrical production in a single hybrid module. Photovoltaic/Thermal (PV/T) solar modules have attracted attention of some researchers in the last years and wide reviews have

been published [Charalambous et al., 2007, Zondag, 2008, Ibrahim et al., 2011, Aste et al., 2014]. Some authors like Naveed et al. [2006] proposed the combination of air heating and electrical production with air cooled PV/T modules. On the other hand, recent works have been focused on water based PV/T modules.

The applicability of PV/T modules for efficient hot water and electrical production is issue of debate. Indeed, the thermal gain is useful above certain temperatures at which the PV efficiency decreases. Fortuin et al. [2014] point out the fact that low thermally insulated PV/T modules present an improved PV perfomance and low thermal perfomance. Matuska [2014] simulates the perfomance of PV/T modules in a building and compares them with PV and thermal modules, concluding that available PV/T collectors on the market are not competitive with separated thermal collectors for water heating and PV modules for electricity supply for the building.

Therefore, it seems that a PV/T system will not perform optimally for both heating and electrical production. Fraisse et al. [2007] propose a PV/T system for radiant floor heating with a burner backup, where electrical production, significantly smaller than the achievable one by regular PV modules, is sold to the grid. They conclude that the oversize of collectors during the summer when the heating needs are null, requires a thermal sink as a swimming pool or high temperatures would be reached with strong risks of degradation for modules' internal resin layers. Calise et al. [2012] design and simulate a heating and cooling system that employs PV/T modules which are estimated to operate at 55°C in winter and 80°C in summer, and that feed a single effect absorption machine for cooling. This is a mainly thermal system, so the heat gain is potentianted, obtaning a low PV production for lightning, equipments and parasitic loads of the building. Beyond flat PV/T collectors, concentrating PV/T collectors can be considered for reaching even higher temperatures (about 170°C) and feeding double effect absorption machines [Calise et al., 2013], which would require advanced PV materials like triple-junction.

On the other hand, if PV/T modules are efficiently cooled, the gained heat would be at low temperatures, pre-heating slightly water, before coupling it to a heater or heat pump. In this sense, Entchev et al. [2013] propose and simulate a heating system equipped with a ground source heat pump coupled to a tank for heating and DHW which is partially pre-heated with PV/T modules, where the use of electrical production is not detailed. Other authors [Jie et al., 2008, Keliang et al., 2009] were interested on the use of PV/T modules as low temperature heat source of a heat pump working as its evaporator, but assuming separately the PV production and the electrical consumption of the heat pump.

Recently, Li et al. [2015] have desinged and simulated a heating system with model-predictive control algorithms, in which an air-water heat pump pumps water through a radiant floor. A PV/T modules' array is presented as air pre-heater for increasing heat pump's efficiency; the PV production coupled with grid electricity feeds the heat pump in a on-grid scenario where all surplus is sold to the grid.

In conclusion, solar PV heating system are mainly approached in scientific literature as on-grid scenarios where the electrical production and the operation of vapor-compression heat pump actually behave as two independent systems. In addition, among this type of works the PV production is not usually simulated for real working conditions, but to nominal values. Therefore, it can be claimed that there is a lack of research in systems where the PV production is locally consumed for driving a heat pump. Moreover, available experimental studies in photovoltaic heating systems without surplus grid injection are certainly scarce [Izquierdo, de Agustín, and

Martín, 2014a].

2.4   Challenges for off-grid systems

The legislative changes about the the photovoltaic grid connection in European countries, as already mentioned, provide a force for research in isolated solar systems even for urban areas. Of course, to this must be added the constant interest which represents progress in off- grid systems for use in remote areas and underdeveloped countries.

Under the theme 'Sustainable Energy for All' United Nations has set the goal of promoting universal access to electricity by 2030. In a report together with the International Energy Agency [IEA, 2010], it was estimated that additional 952TWh would be required in 2030 to ensure that electrical access in underdeveloped countries. Given the sparse population and abundance of remote areas far from national grids, 42% of this energy must be provided by mini-grids and 18% by off-grid systems. In this scenario, renewables are called upon to play the leading role in the generation, especially solar technologies for Sub-Saharan Africa and India.

Currently the photovoltaic mini-grids and solar systems that are being designed for homes in underdeveloped countries aspire to provide them with electrification for lighting and small power consumption devices such as radios or mobile phones, supplying each household 50-100W [Breyer et al., 2009]. However, when these regions achieve greater level of development, domestic electricity consumption will increase. In fact, devices that require more electrical power have been needed for decades in these communities, such as refrigerators, for preservation of vaccines, based on photovoltaic energy [ElTom et al., 1991]. Several authors have explored the combination of small household refrigerators and photovoltaic panels for food and vaccines preservation in isolated systems [Kattakayam and Srinivasan, 2000], noting the need to evaluate experimentally, during seasonal periods, such systems for a correct sizing of electricity production and storage, given the temporal variability in electricity demand [Tina and Grasso, 2014]. The photovoltaic solar heat-pumps and air-condition for hospitals and other buildings will be an even greater challenge to be addressed in the future.

In developed countries, the study of off-grid photovoltaic systems for districts or individual households has been addressed primarily from the point of view of electricity generation and considering an average value for consumption. [Domenech et al., 2013] projected two PV mini-grids for Spanish communities in remote rural areas, but they considered a maximum electrical load of 1.5 kW per house and a daily consumption of 5 kWh/house, significantly lower than the average demand in urban areas connected to the grid. Such a system would not allow the operation of heat-pumps or reversible mechanical vapour compression machines at homes.

Recently, Ma et al. [2013] evaluated the annual yield of an isolated PV system for homes on an island in Hong Kong, which were equipped with mechanical vapour compression machines for food preservation and air-conditioning, so the average consumption per household was higher. The authors highlight inefficiencies in the system as energy losses due to the DC-AC and AC-DC inversion, battery charging cycles, and especially the temporal decoupling between photovoltaic production and demand. In fact, they underline that when the battery pack is fully charged, if the consumption is low, PV production decays until being almost canceled. As it is an annual balance, that publication does not detail the operation along one day of the photovoltaic solar vapor-compression system and how it can affect the variable load in the storage batteries; it does

mention, however, that the demand for daily and monthly cooling varies throughout the year, being this a determining factor in sizing the PV system. Due to Hong Kong's climate, the paper is focused on cooling mode of vapor-compression machines, but some of the pointed difficulties and aspects to improve are common to PV heating systems.

2.4.1 Energy storage systems

Since the very beginning of the autonomous PV applications, the energy storage has been an issue to be considered. The longest employed recheargable electrical storage system are the lead-acid batteries, although in the last decades new technologies have arised in the market or in research stage. Parallel to the autonomous renewable systems, the promise of electric vehicle has been a driving force behind development of new type of batteries. McGeehin [1980] carried out a review of batteries suitable for power storage and electric vehicles, wheter in existence or under development. Lead-acid was the most common type in that time, but future alternatives were pointed out: nickel, zinc or lithium based batteries, hydrogen storage, thermal (steam or oil) storage, flywheel, and hydro-pumped storage. Since then, diverse batteries have emerged in the market and are used on off-grid power systems [Duraman et al., 2015], which will be choosen based on diverse factors like cost, ease of maintenance, product longevity and storage capability. Lifecycle costs for various type of batteries are analyzed by Battke et al. [2013].

Diouf and Pode [2015] show how the lithium based batteries present a higher gravimetric energy density (150-190 Wh/kg) than the classical lead-acid batteries (30-50 Wh/kg). In fact, this type of Li-ion batteries are widely installed nowadays in electronic devices such as laptops and cellulars. A challenge to face is to improve not only their gravimentric energy density, Wh/kg, but their volumetric energy density, Wh/l, what would reduce their size. Scaling up this batteries for medium-big renewable energy systems is still problematic due to safety, costs, operational temperatures and material availability issues [Scrosati and Garche, 2010]. On the other hand, Capasso and Veneri [2014] remark that actual capacity of lithium technologies keep close to their nominal capacity also for high discharging currents. This is a promising fact for solar photovoltaic heating systems, that demand abruptly high currents in transient mode. Others authors like Cho et al. [2014] have studied through simulation the use of fuel cells for driving ground source heat pumps, passing over fuel generation. Finally, some authors skip the use of electrochemical storage for off-grid PV systems, replacing it with hydro-pumped storage systems [Ma et al., 2015].

2.5 Validity of this thesis

Following the state of the art presented various difficulties or challenges arise, not only about photovoltaic power generation, but also about its application for feeding vapour-compression heat pumps. In Spain and in other developed countries, after the photovoltaic boom experienced in recent years, there is a discouragement of photovoltaic grid connection and some legislative uncertainty about the PV on-grid self-consumption or net-balance. In this scenario, the PV isolated systems emerge as an uncertain alternative for energy saving in households. It requires a more detailed analysis of the advantages and practical drawbacks that could arise.

In particular, it should be emphasized that the annual energy production is intertwined with the demand and storage system, for a photovoltaic driven heat pump when PV surplus is not

stored by the grid. The decoupling between PV production and demand, both at different times of day and at long seasonal periods when demand is lower than production or even zero, appears to decrease the overall system performance.

It requires therefore a theoretical-experimental study in which the energy and environmental aspects are analyzed for a coupled PV array and heat pump system. It is expected to contribute to scientific literature with a more detailed analysis of the actual working characteristics of such systems so that they can be compared in depth with other existing alternatives such as solar thermal heating.

Chapter 3

Solar cells and photovoltaic systems

This chapter provides a brief compendium of the physical basis of solar photovoltaic electrical production (section 3.1). Solar cells are assembled to compose photovoltaic modules which operating curves, equivalent circuit and temperature dependence are pointed out on sections 3.2 and 3.3.

The latest PV modules efficiency achievements are listed on section 3.4. And finally, secondary components of PV systems and several conexion type diagrams are described on sections 3.5 and 3.6.

3.1 Physical fundamentals of photovoltaic effect

The mechanism of a photovoltaic module is explained basing on Planck's light conception. Due to wave-particle duality, incident solar radiation can be considered as quantized energy packets (photons). Each photon's energy is directly proportional to the frequency ν of this radiation (and inversely proportional to wave length λ), as it shows equation 3.1, where h represents Planck's constant and c is the speed of light.

$$E = h.\nu = h.\frac{c}{\lambda} \tag{3.1}$$

Consequently, most energetic photons are the ones with highest frequency, which is the same as saying lowest wave lenght. However, on the following lines it will be shown that each type of photovoltaic device "accepts" only photons within a range of whole solar spectrum.

Silicon is the most used element on solar cells, so the following theoretical explanations will be based on it. In addition, the solar modules experimentally used during this research are composed of polycrystalline silicon cells.

Materials can be clasified into insulators, conductors and semiconductors. All solid materials present a last band filled by electrons with highest range of energy (valence band) and over it an empty level (conduction band). Both bands are separated by certain "energetic distance" or forbidden gap, known as energy gap. If an electron absorbs enough energy to jump from valence band to conduction band, electrical conduction begins. On insulators the energy gap is very big; on the other hand, on conductors it is very small (almost spontaneous jump). However, semiconductors present a certain forbidden gap, characteristic of each material (for silicon, $E_{gap}=1.12eV$)

, so if a photon transmits to an electron on valence band higher energy than energy gap, this will jump into conduction band.

Energy of an incident photon causes gap jump (required energy or work function depends on a minimum or threshold frequency ν_0) and its surplus will transmit kinetic energy to the electron (equation 3.2).

$$h.\nu = h.\nu_0 + \frac{1}{2}m.v^2 \leftrightarrow E_{photon} = h.\nu_0 + E_{kinetic} \tag{3.2}$$

It must be underlined that intensity of incident radiation (photons per second) determines the ammount of freed electrons, but the fact that this liberation occurs is independent of intensity: it is determined by photons energy.

When a silicon cell is illuminated, silicon atoms in crystal lattice absorb photons from incident radiation. As explained above, if electron's energy is high enough (higher than silicon's energy gap), an electron from most external level of the atom will be freed. In this way, an electron-hole pair will be generated: a freed electron on crystal lattice's conduction band and, consequently, a hole due to lack of electrons on valence band. This pair would spontaneously disappear because of a recombination effect between holes and electrons. In order to reduce this unwanted process, a potential barrier, thin film or junction, is introduced in solar cells, doping silicon (group IV) with elements from groups III and V. One of silicon's sides is doped with boron, around one part per million, to form p-silicon, which has lack of electrons on its outer level. On the other side, phosphorous is used to dope silicon, forming n-silicon, which presents excess of electrons on its outer level. Free migration of electrons between both sides is inhibited by the barrier. If this sides are externally connected, as it is shown on figure 3.1, an electron current will flow through the circuit. Therefore, absorbed photons energy will liberate an excess of electrons on layer n, which will flow through the external cirtuit to layer p. Metallic electrical contacts are attached on the back of the solar cell and in a grid pattern in the front (to not obstruct photons penetration). A deeper description of semiconductors theory can be consulted on Goetzberger and Hoffmann [2005].
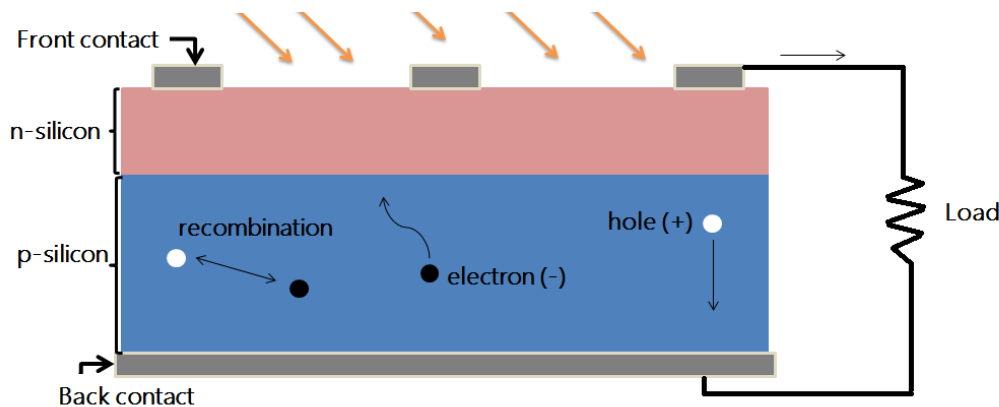
Figure 3.1: Silicon solar cell with p-n junction.

Electrical production on solar cells is limited by several factors. As it has been explained, each

material has a minimum energetic level, so only a fraction of solar spectrum would free electrons. In the case of silicon, solar radiation with a wave length bigger than 1.15 μm will not produce any photovoltaic effect and, however, it will heat the solar cell. Once electrons are freed, photons' extra energy will heat the solar cell too ($E_{photon} - E_{gap} > 0$). Even part of spontaneous hole-electron recombination will not be prevented by junction barrier and heat would be generated due to this process. Just under these assumptions, predicted maximum theoretical efficiency of silicon is 27% [Duffie and Beckman, 2013].

Additional external limitations are related with solar reflection on cells' surface, reduction of useful area as it is partially covered by metallic contacts, electrical resistances on junctions and contacts,... which all of them contribute to reducing cells and whole PV modules' efficiency.

3.2 Operating curves for photovoltaic modules

In the previous section the solar cells and their intrinsic losses have been introduced. However, solar cells are connected between them, in series or parallel, compounding PV modules, which are covered by diverse layers to protect the cells from external inclemencies like moisture. PV modules are composed by several solar cells and can reach dozens or thousands watts of electrical power. In turn, modules can be also connected between them in arrays or larger PV generation systems.

Electrical properties and external conditions determine a characteristic intensity-voltage curve for each type of photovoltaic module. Manufacturers usually provide modules' main characteristic under Standard Test Conditions (STC, solar irradiance on tilted module,G_T: 1000W/m², cell temperature, T_{cell}: 25°C, normal incidence angle, air mass: 1,5).

Every module presents an Intensity-Voltage curve under STC similar to the one shown on figure 3.2. Intensity of produced current will be related with working voltage and load, obtaining an electrical power for these conditions (eq. 3.3).

$$P = I \cdot V \tag{3.3}$$

Every I-V curve is delimited by a maximum intensity and null voltage point, known as short-circuit current I_{SC}, and a maximum voltage and zero current point, known as open circuit voltage V_{OC}. There will be an I-V point where electrical production is maximum, according to equation 3.4. All these characteristical points of I-V curve on STC, define fill factor (eq. 3.5) as indicator of PV module's quality: the higher FF the higher quality.

$$P_{max} = V_{mp} \cdot I_{mp} \tag{3.4}$$

$$FF = \frac{V_{mp} \cdot I_{mp}}{V_{OC} \cdot I_{SC}} \tag{3.5}$$

Starting from shortcircuit current point, I_{SC}, along I-V curve, as voltage increases, achieved power increases too, until the knee of the curve is reached around maximum power point. Once V_{mp} is exceeded, power drops sharply, as it it shown on figure 3.3.

Maximum power under STC is denominated as peak power or nominal power of the PV module, which nominal efficiency is defined as the quotient between obtained electrical power and incident solar radiation over module's area (eq. 3.6).
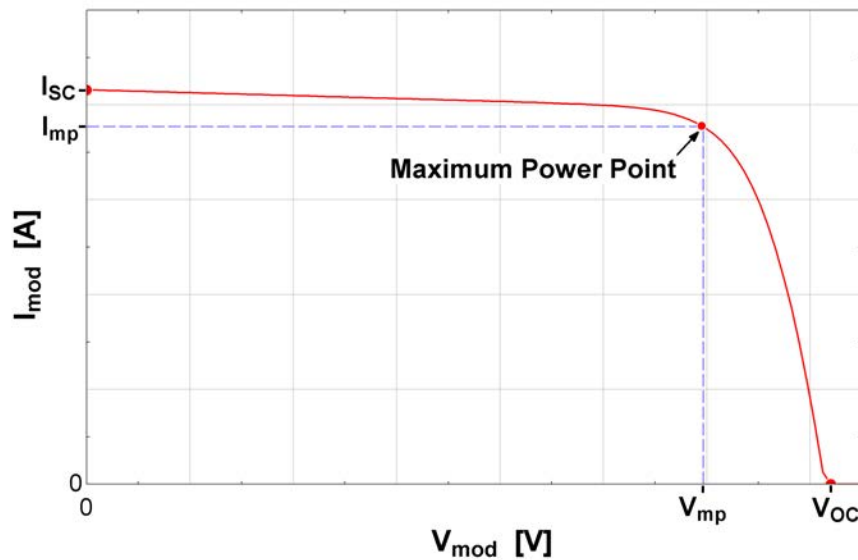
Figure 3.2: Generic I-V curve of a PV module.

$$\eta_{peak} = \frac{P_{max}}{G_T \cdot A_{mod}} \tag{3.6}$$

Nominal efficiency can be defined basing just on the useful area of the module (the solar cells) or considering module's total surface, including frame, contacts and gaps between cells, which is the most common definition among manufacturers.

According to the I-V and P-V curves under STC shown above, it may come up the idea of designing a system which operating constant voltage would be V_{mp} to obtain maximum power, or even a system with electrical storage which batteries nominal voltage would be V_{mp}. In this second case, while battery gets charged, system's voltage increases too, decreasing electrical power, until interrupting production when V_{OC} is reached, protecting storage system from overcharge.

However, I-V curve of a PV module varies with incident solar radiation and cell temperature, so for each conditon the maximum power point will be obtained at different V_{mp} and I_{mp}. In addition, it must be remarked that under real working conditions, solar cells' temperature can be much higher than the one defined on STC, which modifies significantly I-V curve and reduces achievable maximum power. In particular, cell temperature affects mainly to V_{OC} and solar radiation to I_{SC}, as figure 3.4 shows. Unfortunately, efficiency will drop under high temperature and solar radiation conditions.
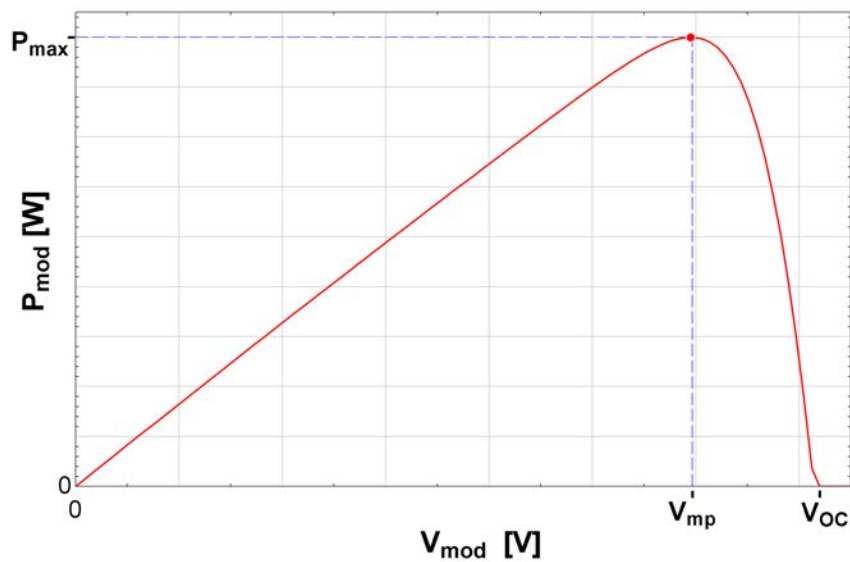
Figure 3.3: Generic P-V curve of a PV module.
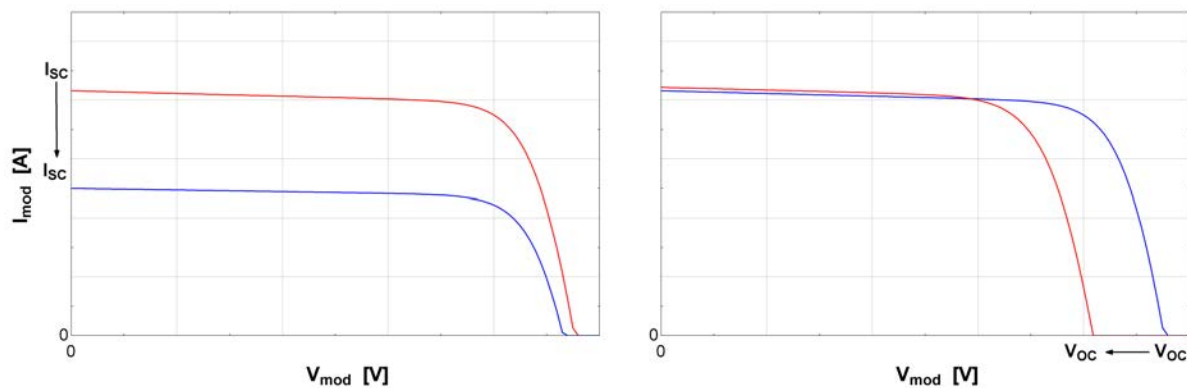
Figure 3.4: I-V curve variation at different solar radiation (left) and cell temperature (right).

For all those reasons, if you intend to obtain maximum power for every I-V curve, an electronic device for adapting working voltage to changing radiation and temperature conditions is required. This regulator is known as MPPT (Maximum Power Point Tracker), which maximizes dynamically PV system's power.

For isolated systems, a PV array has to adapt its electrical production to the demand. If load is interrupted or there is more production than consumption, electrical storage system will start to get charged. As it has been mentioned, to avoid overcharges, charging current must decrease progessively until practically cancel PV production when batteries are fully charged. This process is carried out by the controller, which varies load voltage between maximum power voltage V_{mp} and open circuit voltage V_{OC}, adjusting power to batteries' charge state.

3.3 Photovoltaic equivalent circuit

As it has been mentioned, the shape of a PV module's I-V curve will be determined by its intrinsic characteristics and given solar radiation level and cell temperature. An approach to obtain this curve is through the study of the equivalent circuit of a solar cell (figure 3.5), which is widely described on scientific literature (LoBrano and Ciulla, 2013, Duffie and Beckman, 2013), according to equation 3.7.
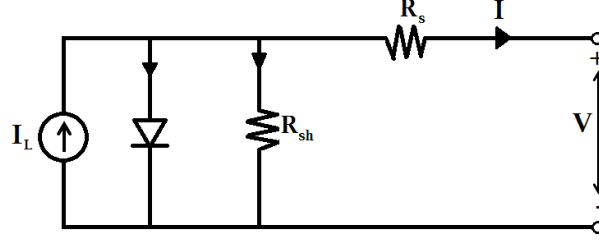
Figure 3.5: Equivalent circuit of a PV module.

$$I = I_L - I_0.[exp(\frac{V + I.R_s}{a}) - 1] - \frac{V + I.R_s}{R_{sh}} \tag{3.7}$$

where,

$$a = \frac{n.k_B.N_S.T_{cell}}{e} \tag{3.8}$$

In order to determine I-V curve, the mentioned circuit presents five characteristic parameters of the module: I_L, I_0, R_{sh}, R_s , a. First of them, I_L, represents photocurrent and depends on solar radiation; I_0 is diode's reverse saturation current and it is affected by silicon's temperature; a factor (eq. 3.8) is related to physical variables like Boltzmann constant k_B, electron charge e, number of cells connected in series N_S, an ideality coefficient n and cell temperature in Kelvin. Equation 3.7 includes two resistances, R_{sh} and R_s, which modify I-V curve's shape. Shunt resistance, R_{sh}, which represents current leaks at cells' borders, metallic shortcuts and hole-electron recombination, will reduce FF and V_{OC}. On the other hand, series resistance, R_s, is related to electrical contacts among semiconductors and electrical grid, which reduces FF too and, slightly, I_{SC} [Lamigueiro, 2013].

Therefore, it is necessary to know these five parameters in order to establish I-V curve for a given PV module under certain solar radiation and cell temperature. As these parameters are rarely provided by the manufacturers, on literature diverse theoretical and experimental models are available for obtaining the parameters under STC, and then, under any radiation and cell temperature conditions. de Soto et al. [2006, 2007] propose a non linear equations system, which is solved through discretization and approximations until clearing the parameters. On the other hand, LoBrano and Ciulla [2013] propose an analytical method to guess them. On both methods some characteristics provided by module's manufacturer are assumed, such as V_{OC}, I_{SC}, V_{mp} and I_{mp} under STC, and temperature dependance coefficient for I_{SC} and V_{OC}.

In conclusion, operating curves of a PV module under real working conditions must be established through a method that determines equation 3.7. This curve would be of special interest for cases when operating point is different to maximum power one, due to MPPT controller's inaccuracy or because of decoupling between demand and production. It should be noted that previously cell temperature and solar radiation need to be obtained through theoretical models and/or experimental data.

3.4 Advances in photovoltaic technology

Improving solar cells' efficiency arises as the main challenge for photovoltaic technology. Nowadays, cells built with diverse materials, doping type, design and manufacturing method can be found. Since mid-XX century, photovoltaic industry has developed solar cells based on diverse semiconductor materials, such as polycrystalline or amorphous silicon, cadmium sulfide (CdS), gallium arsenide (GaAs),... Advances have been done combinating different semiconductor materials in the same cell, using concentrated photovoltaics (CPV), thin-films technology, etc. On figure 3.6 efficiency records achieved in research laboratories are shown.
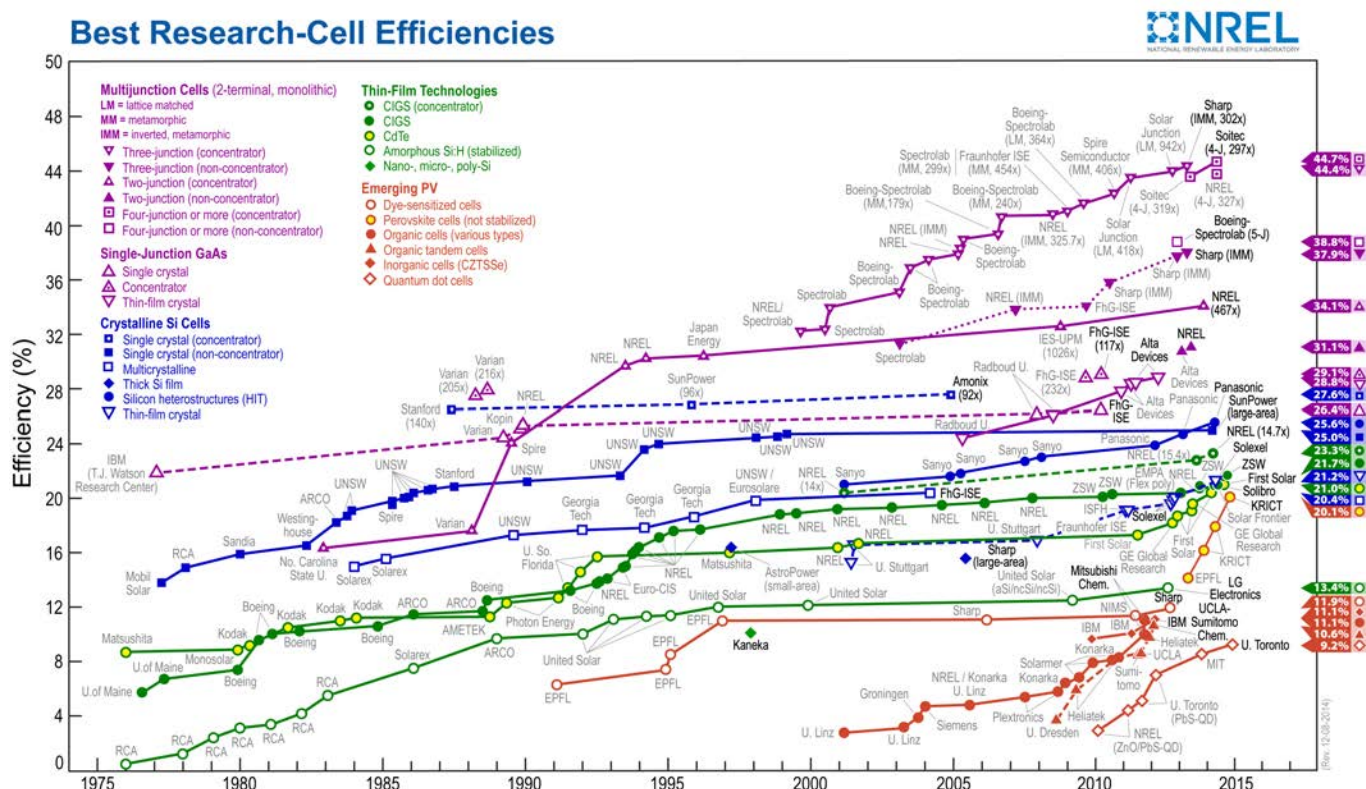
Figure 3.6: Research cell effiency records [NREL].

As it can be observed in figure 3.6, research efficiencies of 38.8% have been recently reached on multijunction solar cells, and up to 44.7% using concentrating photovoltaics. However, in the case of silicon (80% of nowadays global market), best achieved efficiencies are around 25% and have

not been improved in the last decade. It should be pointed out that these solar cell efficiencies decrease once assembled on modules and under outdoor operating conditions. The vast majority of installed silicon PV modules present under STC efficiencies between 11-15% for polycrystalline ones and 13-19% for monocrystalline ones [EPIA, 2011b].

A thermodynamical approach to ideal achievable efficiency for each type of cells is developed by Landsberg and Markvart [2012].

3.5   Additional components of a photovoltaic system

Once solar cells are enssambled in modules, the rest of electrical and electronic devices which are added to the PV system, depend on what is its purpose. The most common components, which have been previously mentioned, are the following:

- *Electrical storage system*: most of isolated PV systems include batteries to satisfy consumption also when there is no production. It is one of the aspects that should be improved for off-grid systems. Most used and economic type of battery is the well known Pb-acid one, although diverse types have been developed in last years (NiCd, NiMh, Li-Ion, Li-Polymerer) and even long term electrical storage (H_2). These other options present better perfomances like higher energetic density (more compact), higher efficiency, or higher resistance to deep dischages and intense charges. However, due to their cost, they are uncommon on storage systems over dozens of Ah.

- *Controller*: electronic device coupled between PV module or array and load, to regulate production. It can include the following functions:

  - To interrumpt production to protect batteries of overcharge.
  - To interrupt feeding consumption to avoid batteries deep discharge.
  - To transform electrical power from modules' voltage to batteries' voltage.
  - To maximize modules power (MPPT) and to adapt production to batteries' charge state..

- *Inverter*: device that transforms produced direct current to alternating current, to feed A.C. domestic loads or to supply photovoltaic electricity to public grid. In the market square or sine wave inverters can be found.

3.6   Typical schemes for diverse PV systems

In this last section, how diverse components are coupled depending on the aim of a PV system are explained schematically.

The simplest off-grid PV system constists of a PV module directly coupled to a D.C. load, such as D.C. water pumps (fig. 3.7).

Isolated PV systems, which feed single devices such as road signals and telecommunications or multiple consumption D.C. loads in remote buildings, just require a controller and batteries between PV modules and D.C. load (fig. 3.8).
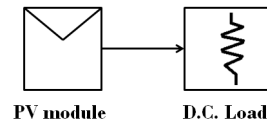
Figure 3.7: D.C. consumption system without storage.
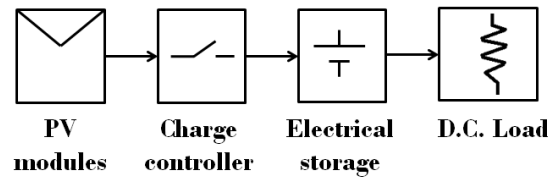
Figure 3.8: D.C. consumption system with electrical storage.

In the case that load operates on a different voltage to the batteries' one, a D.C./D.C. transformer will be intercalated (fig. 3.9).
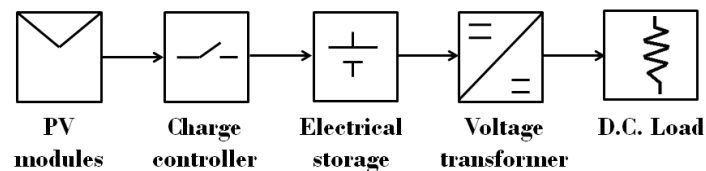
Figure 3.9: D.C. consumption system with storage and transformer.

However, if the purpose of the system is to feed a building which includes A.C. loads like domestic appliances, a D.C./A.C. inverter will be required (fig. 3.10).
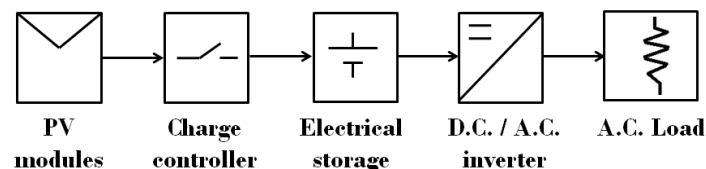
Figure 3.10: A.C. consumption system with storage and inverter.

On-grid systems that supply whole electrical production to public grid, it is necessary to transform photovoltaic electricity to grid's conditions through a D.C./A.C. inverter which includes maximization function (fig. 3.11).

Other on-grid PV systems, specially domestic rooftop modules, work on diverse self-consumption modes, where the aim is to produce and consume simultaneously photovoltaic electricity, using conventional grid to supplement energy deficit on certain moments (back-up) or to supply energy surplus on the grid (fig. 3.12).
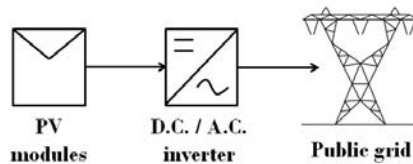
Figure 3.11: On-grid system for supplying electricity to public grid.
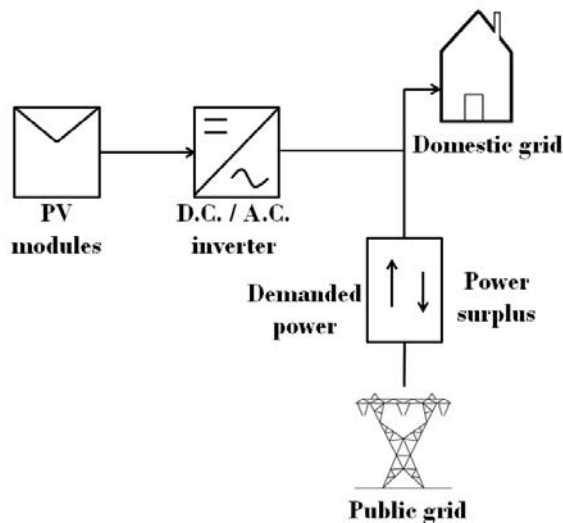
Figure 3.12: Net-balance on-grid PV system.

Chapter 4

Description of the PV heating system

In the present research, a solar photovoltaic heating system has been tested during whole seasons under real meteorological conditions. Before advancing the theoretical model and experimental results, in the following lines, the employed experimental system is described. This summary of the components will provide the readers an overview of the whole system (section 4.1). On the following sections, the different parts of the system are detailed, paying special attention to the key elements of the photovoltaic production: the PV/T modules (section 4.3) and the MPPT controller (section 4.4). The additional components: the building, the electrical storage system, the heat pump and the radiant floor are described in sections 4.2, 4.5, 4.6 and 4.7, respectively.

The diverse experimental parameters, digitally recorded for their representation, interpretation and later calculus, are measured through equipment which specifications and accuracy are included on section .

4.1   Overview of the system

The facility is composed by a photovoltaic array which feeds a reversible air-water mechanical compression heat pump in order to heat a building through radiant floor. This PV heating facility is part of the Solar Energy Experimental Plant owned by Eduardo Torroja Institute of Construction Sciences (IETcc) from the Spanish National Research Council (CSIC) and located in Arganda del Rey (40.3° N, 3.4° W), 20km east from Madrid (fig. 4.1).

This heating system was built as part of project ENE2010-20650-C02-01, supported by the Spanish Ministry of Science and Innovation and titled *Design, construction and experimental evaluation of a solar cooling and trigeneration high efficiency system for buildings and greenhouses.*

There has been a meteorological station at the plant for the last 20 years, where weather variables such as solar radiation on horizontal and tilted surface, outdoor dry bulb and dew point temperatures, wind speed and relative humidity are measured each 2 seconds and recorded in 10 minutes average values. Its measurement accuracy is detailed on section 4.8.
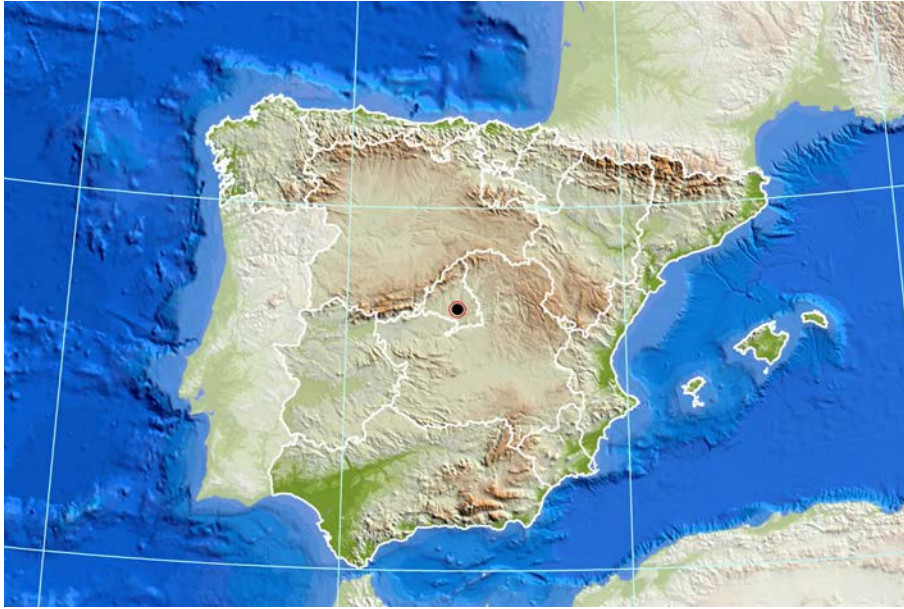
Figure 4.1: Solar Energy Experimental Plant's location in the Iberian Pensinsula [IGN].

Figure 4.2 details the system. The photovoltaic electricity is regulated by the MPPT controller, which transforms the output power to storage system's voltage. From the storage system, electricity could be consumed in D.C., but as the load works in A.C., a 3kW inverter is required to feed the mechanical compression heat pump. This conventional air-water heat pump, heats a secondary thermal fluid (STF) and pumps it through the building's radiant floor.
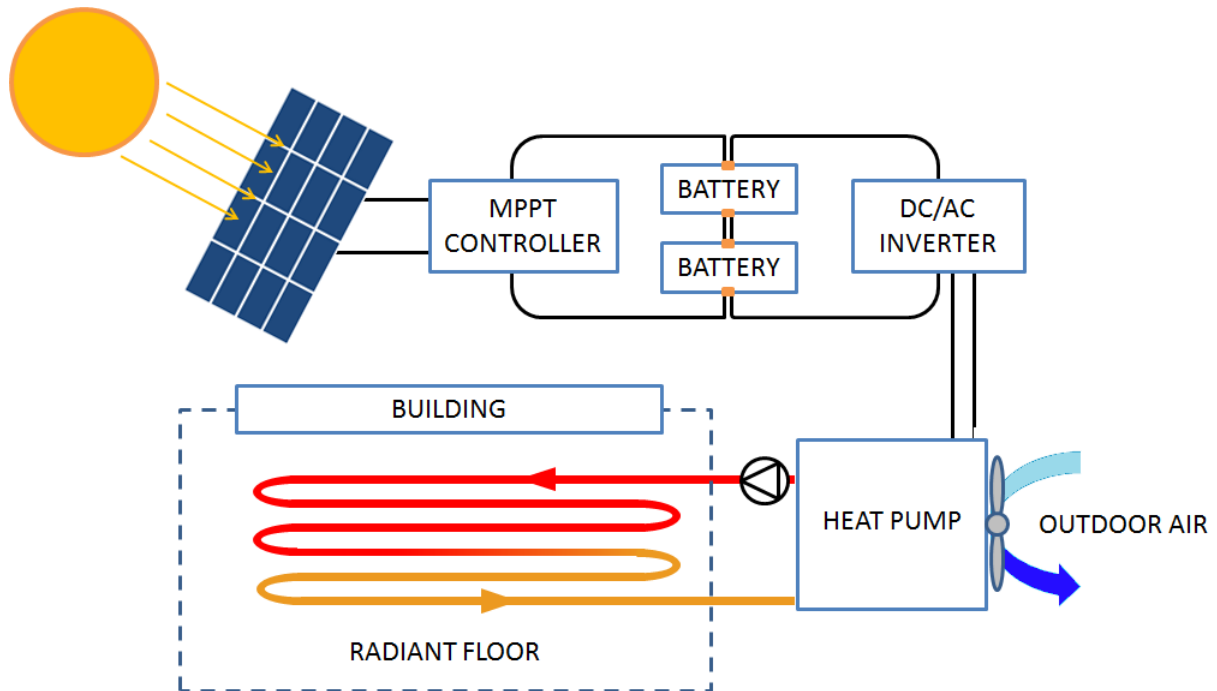
Figure 4.2: Solar photovoltaic assisted air-water heat pump on heating mode.

4.2   The building

The building to be acclimatized (fig. 4.3) is a thermal laboratory that is used as a prototype for the study of heating/cooling systems with photovoltaic electricity as the main energy source. The building has a 35 m^2 surface divided into two internal rooms: one of them housing the storage system, the inverter, the MPPT controller and the recording and control devices (fig. 4.4). The laboratory is usually occupied by three people, working in the other room.

Figure 4.3: Laboratory building and PV/T array.

Figure 4.4: MPPT controller, inverter, storage system and registering equipment.

The building has been built in accordance with Spain's Technical Bulding Code [CTE, 2009] and its update [CTE, 2013]. Its main thermal characteristic, in stationary regime, is UA = 125 W/°C. The maximum thermal heating load, in stationary regime, is about 3.0 kW, although it can reach a peak about 6.0 kW at the beginning of the heating process, when the thermal mass of the building plays a stronger role.

4.3   The PV/T modules

The photovoltaic array is composed by commercial photovoltaic-thermal modules, which electrical parameters are listed on table 4.1. The total receptive surface of a module is 1.31m^2 and its useful area is 1.17 m^2, as it is composed by 48 solar cells in series of 156x156 mm each (so the efficiency related to the useful area is 15.43%). There are 16 PV/T modules available at the plant. The tilt angle of the modules measured from the horizontal is 40°, close to location's latitude for better fit to solar radiation angle along the year.

These type of hybrid PV/T modules consist on a photovoltaic module which lays over a steel structure for a water thermal circuit (fig. 4.5). The function of this circuit is to pump water through it, cooling the solar cells to avoid photovoltaic efficiency losses and gaining thermal energy for domestic hot water or heating. Thermal circuit's capacity is 3.88 l and it allows a maximum operating pressure of 1.5 bar. In addition to the solar cells and the steel structure, there are other protective layers in between, which will be detailed on chapter 6.

P_{max}	180	W
V_{mp}	23.80	V
I_{mp}	7.56	A
V_{OC}	28.56	V
I_{SC}	8.32	A
η_{mp}	13.73	%
$\mu_{I_{SC}}$	0.0033	A/°C
$\mu_{V_{OC}}$	-0.0996	V/°C
$\mu_{P_{max}}$	-0.48	%/°C

Table 4.1: Electrical data of a PV/T module for *STC*.
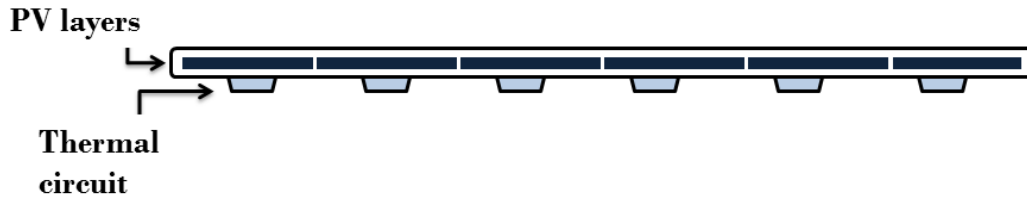
Figure 4.5: PV/T modules' structure.

Each two paralell are connected in series, making a couple with $V_{mp} = 47.6$V and $I_{mp} = 7.56$A. The heating system was fed with 12 PV/T modules connected as 6 pairs in parallel, so array's maximum power point will be $V_{mp} = 47.6$V, $I_{mp} = 45.36$A and $P_{max} = 2160$W.

4.4 The MPPT controller

As it was advanced on previous chapter, controller's main function will be to regulate photovoltaic production to batteries' charge state. As it is a MPPT regulator, it will try to adapt dynamically its operating voltage to match it with the maximum power voltage under changing conditions. However, once batteries get charged, the production will decrease to avoid overcharges, as it is detailed on this section.

The charging algorithm of the storage system depends on the controller, type of batteries and capacity, and the user is usually not able to change its parameters. The controller used on this work presents a charging steps like the one shown on figure 4.6 (adapted from manufacturer's instruction manual). When there is null photovoltaic production, the controller stays on *night* mode, which avoids return current from batteries to the PV module or array. Once the photovoltaic production starts, the controller works on its *MPPT* mode, producing as much electricity as possible and charging the storage system, while its voltage increases. For each type of batteries and nominal voltage, which is set on the controller, there is an *absorption* voltage, where controller keeps that voltage for a certain time, decreasing the electrical production until the batteries are completely full. The last step is the *float* phase, where batteries' voltage is slightly decreased, there is no more charging reactions into the batteries and the electrical production is minimum.

In case the batteries are fully charged and a load is connected, the controller will adjust the PV production to the consumption, keeping the batteries on float mode, while production can satisfy consumption.
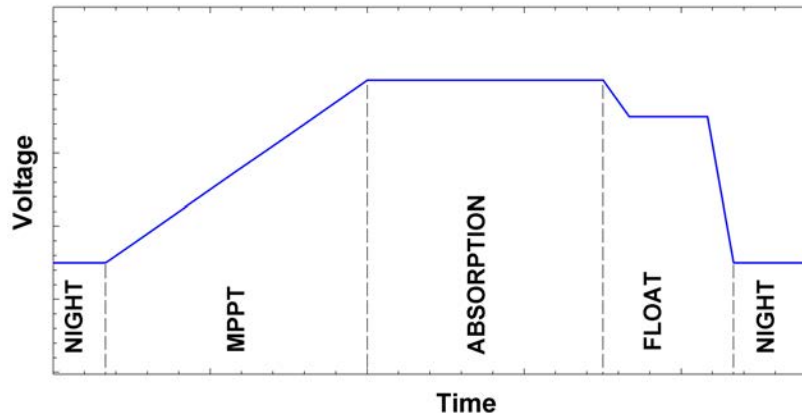
Figure 4.6: MPPT controller's charging phases.

For example, for a single 180 W PV/T module under STC, while the batteries are discharged, the controller will try to find the maximum power point, consequently keeping the voltage at 23.8 V, to obtain 7.56 A and 180 W. Once the batteries reach the absorption voltage, the controller scrolls the voltage to higher values, decreasing the obtained power, as it is shown on the black spots on figure 4.7, which values are listed on table 4.2.
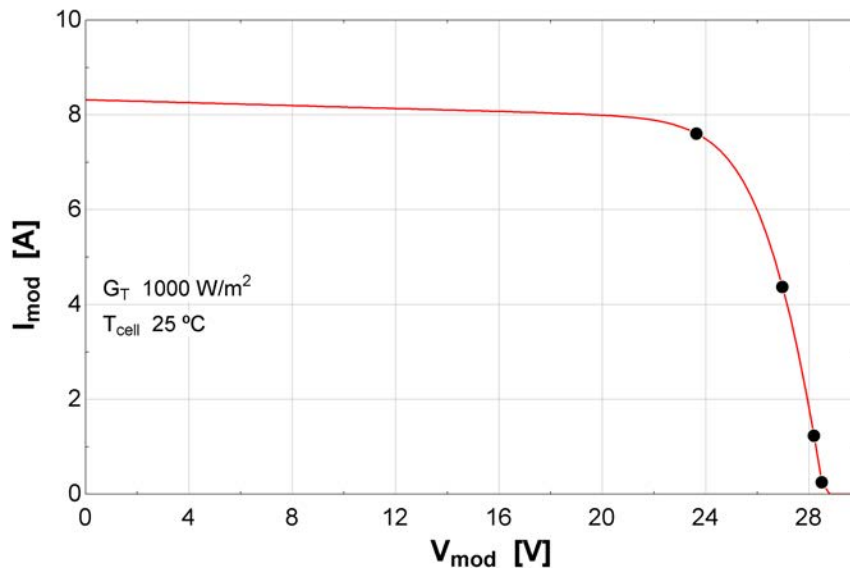
Figure 4.7: MPPT controller's adaption to batteries' charge state.

V_{mod}	I_{mod}	P_{mod}
23.8	7.56	180
26.97	4.38	118
28.18	1.24	35
28.48	0.25	7

Table 4.2: PV module's intensity and power output for a given voltage.

The controller used in this work, can manage a single module or an array, which operating voltage can be up to 150 V. It also transforms array's voltage to storage system's voltage, adjusting consequently the charging current, as it is expressed on equation 4.1. In fact, in the transformation process there can be some losses, although the observed daily losses are smaller than 1%.

$$P_{input} = P_{output} \leftrightarrow V_{array}{\cdot}I_{array} = V_{batt}{\cdot}I_{batt} \tag{4.1}$$

Charging process on 19/02/2015   Finally, a daily charging process for a clear winter day (fig. 4.8) is shown as example. At the beggining of the morning, storage system was deeply discharged (blue line on fig. 4.9). At sunrise, the PV production started and, consequently batteries began to get charged. During the morning, the controller made the array operate on maximum power, as the battery voltage was increasing. At 11.20 hours, the storage system reached 28V, stepping into the absorption phase. Since that moment, the electrical production reduced gradually, as it is shown on figure 4.9, keeping the batteries on absorption mode until 17.78 hours, when solar radiation was too low to maintain the charging process on that phase. It can be noticed, how at central hours of the day, some passing clouds decreased the incident solar radiation, and consequently perturbated slightly the charging process at 13.50 and 13.92 hours.
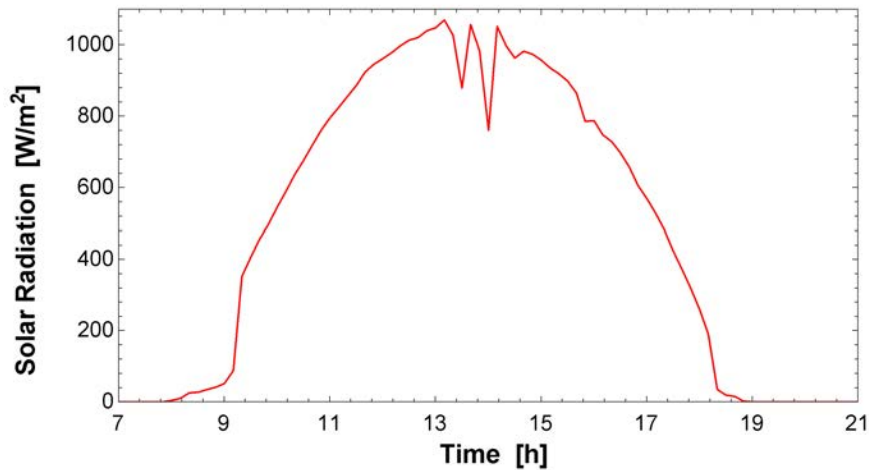
Figure 4.8: Solar radiation on 19/02/2015.
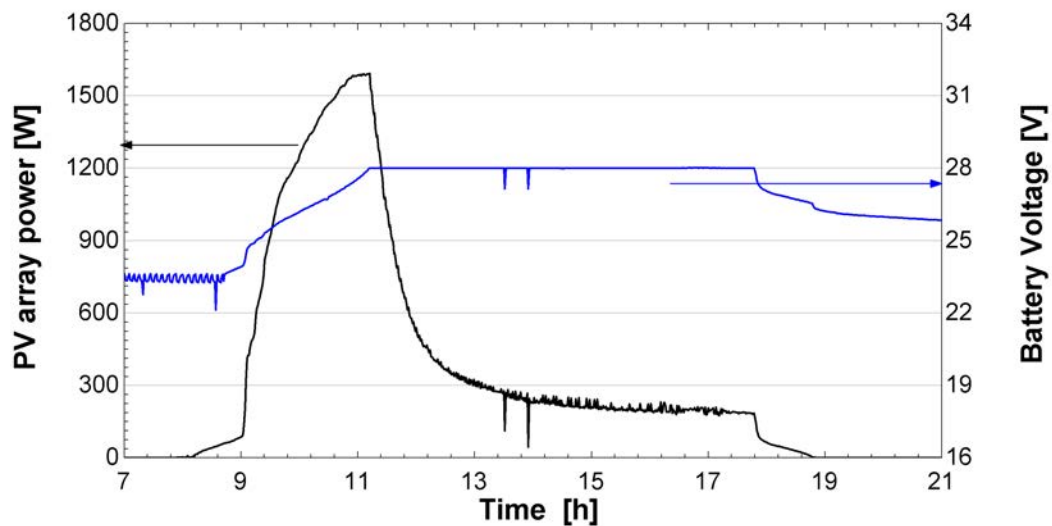
Figure 4.9: PV array's power and battery voltage on 19/02/2015.

As there was no load connected to the batteries during this day, the photovoltaic production was adjusted to the batteries capacity and charging phases, so during the central hours of the day array's power was far away from maximum achievable power. Therefore, the daily efficiency was just 4.0%.

The adjustment between production and consumption, and how the controller adapts the PV performance, are key factors to understand the global efficiency of an isolated system like the one proposed on this work.

4.5   The electrical storage system and inverter

The storage system is composed by two lead-acid batteries of 12V, 250 Ah and C120 each. Therefore the nominal feature of the storage system is 250Ah at 24V. However, it must be remarked that C120 means that this capacity can be capitalised if they are discharged in 120 hours, at 2.1A discharge current, thus at a 50 W rate. As the current demanded by the inverter in order to feed the heat pump can be 60 times bigger, this useful capacity will dramatically drop by a discharge rate factor which is characteristical of each battery. In addition, this capacity is also decreased by non constant currents [de Agustin, 2009], like heat-pump's operating mode.

The characteristics of each battery are 518x291x242mm, 60kg, and life >400 cycles. Their energy densities are 50Wh/kg and 82.2Wh/l. In this type of facility, the batteries are continously partially charged and discharged, so after two years of use, they had to be replaced, as shown on figure 4.4.

The D.C./A.C. inverter works with 24V as input voltage and provides up to 3.0kW of A.C. current at 230V. In case of batteries' voltage is too low, the inverter interrupts its demand in order to avoid overdischarges.

4.6   The heat pump

Once electricity is converted from D.C. to A.C. at 230V by the inverter, it is utilized to feed a reversible air-water mechanical compression, 5-6 kW cooling-heating capacity, heat pump (fig. 4.10).

Figure 4.10: The heat pump out of the building.

Heating capacity	6.02	kW
Power input	1.65	kW
COP	3.65	-
DB/WB 7°C-LWC 35°C (DT=5°C)		

Table 4.3: Heat pump's specifications.

This heat pump works as an indirect system, pumping a secondary thermal fluid (STF), at 840 l/h flow, into radiant floor's closed loop under the building. In this case, this fluid is a water/glycol mixture, in order to avoid freezing issues. Manufacturer's specifications for heating mode are listed on table 4.3.

In both applications, the STF circulates into a closed loop situated under the radiant floor (RF). In winter, the STF transports the heat from the condenser (hotter unit) to the rooms, where it is delivered. The colder unit (evaporator) transfer renewable heat from the outdoor air at low temperature (between -10°C and 14°C), to the indoor unit as consequence of the PV electricity supplied to the compressor and the ancillary equipment. The heat pump can be also driven by the electrical grid, in case of need. It must be remarked that the proposed PV microgrid and the conventional grid compound two independent circuits to feed the machine.

The heat pump uses R410A as refrigerant, containing 1.7 kg of it, which, according to the last review by IPCC [2013], does not present ozone deplecting potential, but it has a GWP equivalent to 4260 kg of CO_2 at an Integration Time Horizon (ITH) of 20 years and 1923 kg at an ITH of 100 years.

4.7   The radiant floor

The radiant floor (RF) has an area of 28 m^2 and a heat transfer coefficient of 7.5 W/°C·m^2, and is divided into two circuits in order to supply heat or cold to each of the two rooms. The system comprises a plate of expanded polystyrene with low thermal conductivity that insulates the radiant floor from the ground (fig. 4.11). Over this layer there is another one made of flexible plastic in which a number of spacers are distributed in order to facilitate the pipe installation. The setup is covered by an additional layer of HIPS (High Impact Polystyrene).
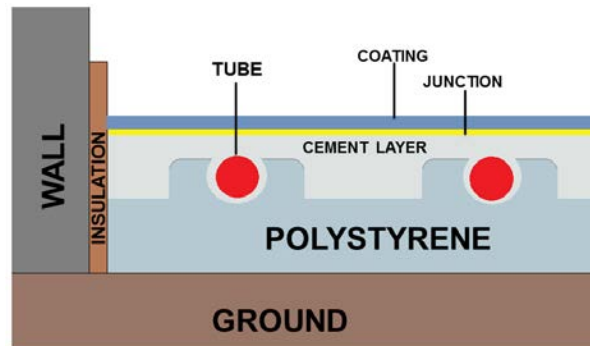
Figure 4.11: Radiant floor's scheme.

The distribution pipe for the thermal fluid is made of High-Density Polyethylene (HDPE) with an external/internal diameter of 0.020/0.016 m respectively. In order to optimize the heat pump efficiency and to obtain the optimum heat transfer coefficient, the tubes were separated 0.15 m, according to the standard UNE [2013]. The whole radiant system is covered by a layer of concrete of 0.05 m thickness and a tile of 0.02 m thickness installed over a thick layer of glue that attach it with the concrete. In order to isolate the foundation, an insulation layer of 0.02 m thickness is located along the perimeter of the foundation. The junction between the insulation perimeter layer and the baseboard is made with an elastic gasket.

4.8   The measuring equipment

In this section the measuring equipment are described and its accuracy detailed. From now on, the error in the measured variables plotted in the following chapters can be consulted in this section.

4.8.1   Meteorological variables

As it mentioned, to measure the meteorological variables an automatic weather station was used. The model is METEODATA 3008 CM.

It consists of a remote automatic data acquisition and transmission unit, teleprogrammable and compact mounted in a heavy duty metallic housing. It includes 8 analog input channels, 2 microrelay digital inputs, 2 microrelay digital outputs, 4 digital counters for pluviometers, anemometers and other similar sensors with impulse/frequency output, and 4 programmable serial ports RS232/422/485.

METEODATA 3008 CM and its sensors.

The following detectors were connected to the weather station:

Pyranometer

An SR11 pyranometer, whose main specifications are:

- sensitivity: 10 μV/W·m^{-2}.

- impedance: 350 Ω.

- temperature dependency: $\pm$1.5% constancy from 20°C to 40°C.

- linearity: $\pm$1% for 0 to 1400 W/m^2.

- mean minute accuracy: 4.7%.

Anemometer

Wind monitor model 05103 with the following specifications:

- 4-20 mA output.

- measurement range from 0 to 100 m/s.

- threshold sensitivity: 1 m/s.

- accuracy: $\pm$0.3 m/s.

Temperature and Relative Humidity sensor

Temperature and RH probe, STH/5031 model, has the following specifications:

- -30°C to 70°C temperature range.

- accuracy for dry bulb T: ±0.1°C.

- RH accuracy:

  - 3%, for 0-90% RH range.
  - 5%, for 90-98% RH range.

- The dew point temperature is registered as function of RH.

- Dew point T mean accuracy: ±0.6°C.

4.8.2   Photovoltaic variables

The produced electricity is measured along all the steps, from PV array to the final step of feeding the heat pump:

MPPT controller

The controller, TS-MPPT model, is connected to a computer through a RS232 port, registering array's output and its input on battery system, once voltage transformation has occured.

- voltage accuracy: 2%.

- intensity accuracy: 2%.

MPPT controller.

D.C. meter

The direct current electrical output from the batteries to the inverter is registered by a high precision battery monitor, BMV-600S model, which is connected to the computer through a RS232 port.

- voltage accuracy: 0.3%.

- intensity accuracy: 0.4%.

Battery monitor and its shunt meter.

D.C./A.C. inverter

A 24/3000 Phoenix inverter is used for transforming the direct current on alternating current. Its main specifications are:

- Input voltage range: 19-33 V.

- Output voltage: 230 V ±2%.

- Frequency: 50 Hz ±0.1%.

- Output power at 25°C: 3000 VA.

- Output power at 25°C for a non linear load: 2500 W.

- Output power at 40°C: 2000 W.

- Peak power: 6000 W.

- Maximum efficiency: 94%.

- Zero-load power: 15 W.

The A.C. current is measured through a ammeter clamp, which is connected to the computher through a USB port.

- Intensity accuracy: 2%.

D.C./A.C. inverter.

4.8.3 Fluid variables

In order to quantify the heat produced by the heat pump, secondary fluid's inlet and outlet temperatures and flow rates were registered using an ultrasonic flow meter, FleximFluxus AMD 6725 model. This type of flow meters perform non-invasive measurements, thus, there is no direct contact between sensors and fluid, which avoids fluid's leaks, pressure drops and sensor's corrosion. Their main characteristics are:

- Measuring principle: transit-time difference correlation.

- Flow velocity range from 0.01 to 25 m/s.

- Resolution: 0.025 cm/s.

- Accuracy: ±0.01m/s or 1.6% .

- Measurable fluids: all acoustically conductive fluids with <10% gaseous or solid content in volume.

The temperatures are measured through four-wire PT100 sensors:

- Temperature range: -50°C to 400°C.

- Resolution: 0.1K.

- Accuracy: ±0.2K or 0.1%.

The equipment can be placed wherever as it includes a battery and internal memory.

- Data memory capacity: 100,000 measured values.

- RS232 connection to computer.

The PV/T modules surface, building's indoor and radiant floor surface temperatures were registered using these devices too.

Flow meter and its sensor clamps on a tube.

4.9   Uncertainty propagation

In the experimental work, many parameters are obtained through mathematical calculation from measured variables (e.g., the heating power is calculated from measured inlet and outlet fluid temperature and flow). Directly measured variables' uncertainty or standard deviation is usually known or provided by measuring equipment's manufacturer, as listed on the previous section. However, when searched parameter is function of diverse measured variables its uncertainty will depend on the latter's ones [Kline and McClintock, 1953].

For a given function dependant on N measured variables $f(X_1, \ldots, X_N)$, according to , its propagated uncertainty will be related with measured variables as:

$$\delta f^2 = (\frac{\partial f}{\partial X_1})^2 \cdot \delta X_1^2 + (\frac{\partial f}{\partial X_2})^2 \cdot \delta X_2^2 + \ldots + (\frac{\partial f}{\partial X_1}) \cdot (\frac{\partial f}{\partial X_2}) \cdot \delta X_{12}^2 + \ldots$$

where,

δX_1 is the standard deviation of the X_1 measured variable

δX_2 is the standard deviation of the X_2 measured variable

$\frac{\partial f}{\partial X}$ is the partial derivative of the function f with respect to a given X

δX_{12} is the estimated covariance between the measured variables X_1 and X_2

Covariance terms can be difficult to estimate if measurements are not made in pairs. In fact, if the measurements of X_1, X_2, ... are independent, the associated covariance term is null [Ku, 1966].

So, f function's absolute uncertainty will be:

$$\delta f = \sqrt{(\frac{\partial f}{\partial X_1})^2 \cdot \delta X_1^2 + (\frac{\partial f}{\partial X_2})^2 \cdot \delta X_2^2 + \ldots + (\frac{\partial f}{\partial X_N})^2 \cdot \delta X_N^2}$$

If it is wanted to express it as a relative error, the expression will be:

$$\frac{\delta f}{f} = \sqrt{(\frac{\partial f}{\partial X_1})^2 \cdot \delta X_1^2 + (\frac{\partial f}{\partial X_2})^2 \cdot \delta X_2^2 + \ldots + (\frac{\partial f}{\partial X_N})^2 \cdot \delta X_N^2}$$

This method for guessing uncertainty propagation will be applied in the next chapters, for both simulations and experimental results.

Chapter 5

Photovoltaic production model

A precise model for predicting photovoltaic production, of a single module or a small array, must adjust itself to changing meterological conditions along a day. Some of the first models that could be found on scientific literature were based on average daily or monthly values of parameters like solar intercepted energy or outdoor temperature, providing a statistical approach [Evans, 1981, Clark et al., 1984] which did not predict photovoltaic production along diverse instants of a day. Nowadays, available detailed meteorological data have been improved significantly and yearly evolution of outdoor temperature, wind speed or solar radiation on horizontal surface can be obtained from public databases or meteorological institutions. Measurements' frequencies vary from hourly average to minutal values.

For the present research, detailed meteorological data were available, as mentioned on chapter 4, including detailed evolution of solar radiation on horizontal surface, so a precise PV production model can be developed.

In this chapter, the simplest PV array sizing method commonly used is shown (section 5.1). After it, two advanced PV production predicting models are explained. The first of them determines the five parameters of the equivalent circuit solving a non linear equations system (section 5.2). In the other method, developed in section 5.3, a simpler calculus is proposed, based on PV efficiency's temperature dependence. In both sections, after the equations' development, the methods are applied to the specific modules used in this research basing on manufacturer's electrical parameters.

In any case, the PV production methods present two variables that must be introduced: solar radiation and cell temperature. In section 5.4, how to calculate solar radiation on PV/T modules' tilted surface from horizontal radiation measured data is explained.

On the other hand, the cell temperature obtaining method has been considered a topic deep enough to be developed separately on chapter 6.

5.1 Sun Peak Hours concept

The simplest calculus method to estimate daily electrical production of a PV module is based on peak sun hours (PSH) concept [Castañer et al., 2012]. It refers to the daily solar insolation which a surface would receive if the sun was shining at 1000 W/m^2 during certain number of hours. For example, a clear february day in Madrid, as the one shown on figure 5.1, along 10.8 hours

of sunlight, daily insolation of 6.2 kWh/m² is received (graph on the left). From energy point of view, it is equivalent to 6.2 h of 1000 W/m²radiation (graph on the right). Consequently, basing on manufacturers nominal power under STC, daily photovoltaic production will be proportional to peak power during a certain number of PSH (eq. 5.1).
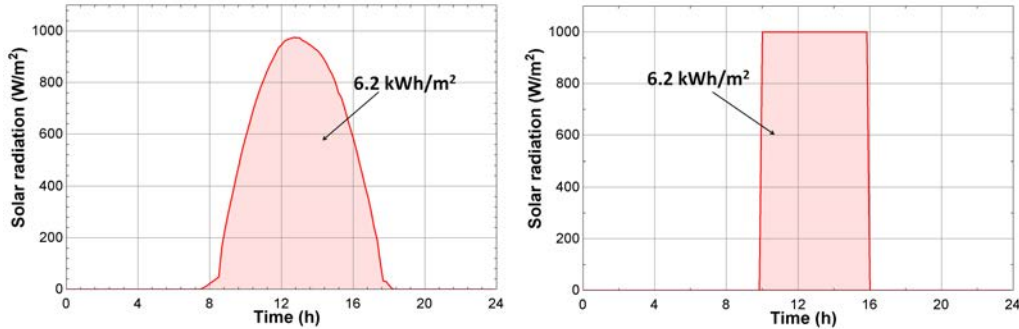
Figure 5.1: Solar radiation curve on a clear day (left) and its equivalent in PSH (right).

$$E_{PV} = PSH{\cdot}P_{peak} \tag{5.1}$$

Therefore, during this example day, a 180 W PV module, would produce 1.12 kWh. It is based on operation under STC, so no efficiency losses that appear under real working conditions are introduced. It must be remarked that this estimated electrical production will always be considerably higher than real production. However, even though its lack of precision, the mentioned method it is widely spread among installing companies to size PV arrays[Alonso, 2013].

For a detailed study of PV modules' perfomance, this method should be neglected as the PV power along a day present a shape wide different from a rectangle and, as it will be explained, real working conditions depend strongly on cell temperature and changing solar radiation.

5.2   Determining five parameters of the I-V curve

As it was mentioned on section 3.3, for a given radiation and cell temperature, each type of module presents a working I-V curve. This curve is described by equation 3.7, which is reminded now:

$$I = I_L - I_0{\cdot}[exp(\frac{V + I{\cdot}R_s}{a}) - 1] - \frac{V + I{\cdot}R_s}{R_{sh}} \tag{5.2}$$

Assuming that variables I_L, I_0, R_{sh}, R_s and a are not provided by the manufacturer, which depend on solar radiation on tilted surface, G_T, and cell temperature, T_c, a five equations system, based on available specifications, will be stated in order to obtain these five parameters.

In particular, the method proposed by de Soto et al. [2006, 2007] states the five equations system from data provided by the manufacturer such as V_{OC}, I_{SC}, V_{mp}, I_{mp}, temperature depending coefficientes of I_{SC} and V_{OC}, and relation between different points of the I-V curve, as the ones shown on figure 3.2.

At the short-circuit point, V=0 and I= I_{SC}, so:

$$I_{SC} = I_L - I_0 \cdot [exp(\frac{I_{SC} \cdot R_s}{a}) - 1] - \frac{I_{SC} \cdot R_s}{R_{sh}} \tag{5.3}$$

At the open-circuit point, V=V_{OC} and I=0, so:

$$0 = I_L - I_0 \cdot [exp(\frac{V_{OC}}{a}) - 1] - \frac{V_{OC}}{R_{sh}} \tag{5.4}$$

At the maximum power point, V=V_{mp} and I=I_{mp}, so:

$$I_{mp} = I_L - I_0 \cdot [exp(\frac{V_{mp} + I_{mp} \cdot R_s}{a}) - 1] - \frac{V_{mp} + I_{mp} \cdot R_s}{R_{sh}} \tag{5.5}$$

Power's derivative with respect to voltage, at the maximum power point, must be zero:

$$\frac{d(IV)}{dV}|_{mp} = I_{mp} + V_{mp} \cdot \frac{dI}{dV}|_{mp} = 0 \tag{5.6}$$

Finally,temperature coefficient of open-circuit voltage, defined as voltage derivative with respect to temperature evaluated for I=0, can be approximated as:

$$\mu_{V_{OC}} = \frac{dV}{dT}|_{I=0} \approx \frac{V_{OC} - V_{OC,T_{cell}}}{T_{STC} - T_{cell}} \tag{5.7}$$

Equations 5.3, 5.4, 5.5, 5.6 and 5.7, summed the five desired equations. As it is a non-linear equation system, it should be solved using specific software like *EES* or implementing numerical methods. Once five parameters are obtained, I-V curve for given radiation and cell temperature can be represented. If the precise maximum power point of that curve is required, I-V curve's equation must be maximized, as the equation 5.6 states, or through an specific software.

Application to the 180W PV/T modules Basing on manufacturer's parameters listed on table 4.1, the I-V curve (fig. 5.2) and, consequently, the P-V curve (fig. 5.3) of the PV/T modules used in this research can be plotted under STC.
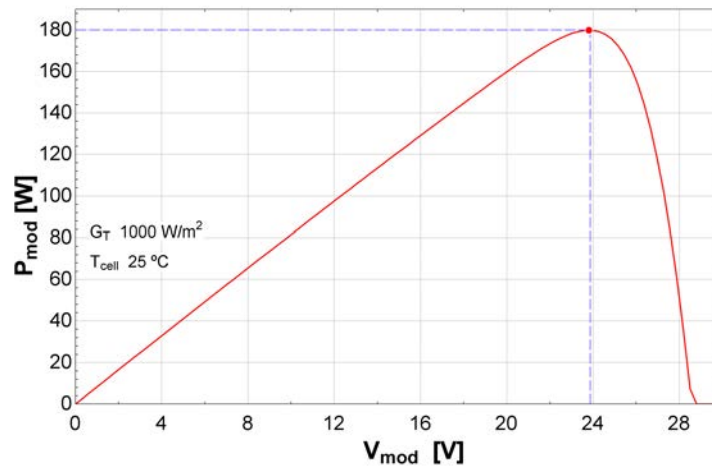
Figure 5.3: P-V curve for used PV/T modules at STC.
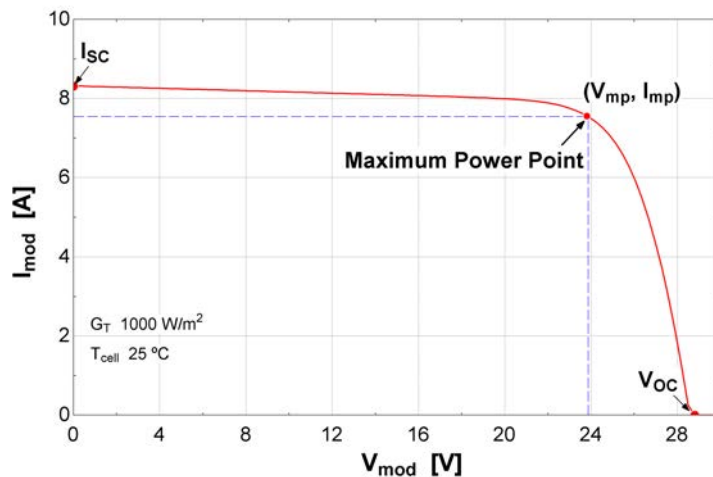
Figure 5.2: I-V curve for the PV/T modules at STC.

Figure 5.2 finds that maximum power point at STC will be for $I_{mp} = 7.54$A and $V_{mp} = 23.87$V, where achievable power will be 180W, where the manufacturer indicates almost the same values ($I_{mp} = 7.56$A and $V_{mp} = 23.80$V). The precision of the plotted curve will be related with the number of values asigned to V for obtaining I. In this section the curves have been plotted solving the equation system for 100 points.

Once the curves at STC are obtained, for any given cell temperature and solar radiation level specific curves can be plotted too. For example, for a constant cell temperature of 25 °C, the I-V curve varies with incident solar radiation, as figure 5.4 shows. As it was previously mentioned on section 3.2, the short-circuit current, I_{SC}, in each curve is proportional to solar radiation, but the open-circuit voltage, V_{OC}, is also horizontally displaced.
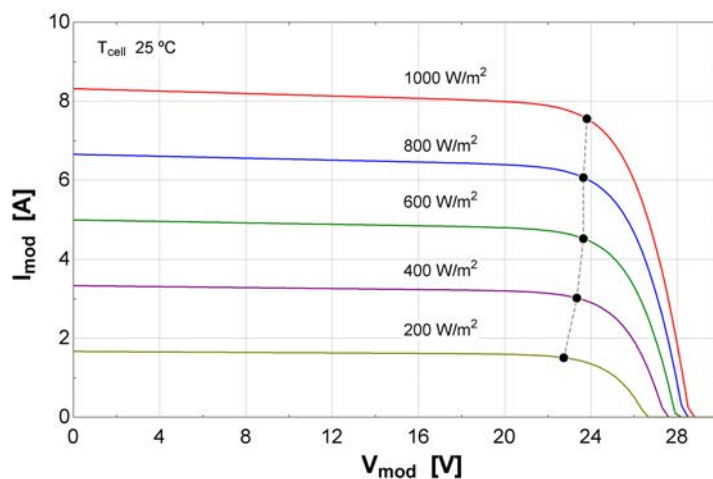
Figure 5.4: I-V curves for a PV module under different solar radiation.

On the other hand, assuming a constant solar radiation of 1000 W/m^2 the I-V curve for different cell temperatures are plotted on figure 5.5. In this case, the maximum power voltage

and open-circuit voltage are significantly displaced between the two cell temperatures, reducing in this case the maximum achievable power from the nominal value of 180W to 158.3W.
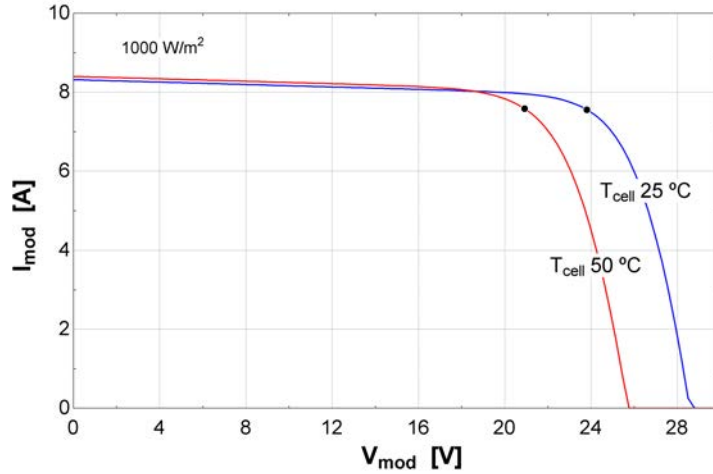
Figure 5.5: I-V curves for a PV module under different cell temperature.

It can be observed how maximum power points in each curve are horizontally and vertically displaced: V_{mp} and I_{mp} are different for each curve. A precise MPPT controller is thus of crucial importance.

5.3   Simplified method for maximum efficiency

The previous method reveals a strong calculus to obtain an I-V curve of a PV module for a given cell temperature and solar radiation. Thus, these two variables must be known or obtained through additional models. In addition, to get numerically the maximum power value, the obtained equation for I-V curve needs to be maximized.

In short, without denying the sharpness and robustness of the five-paramenter model, if just the maximum power point is searched for a given conditions, a simpler method can be proposed. This simplified model does not require numerical methods and its results are very similar to the ones obtained from five parameters model [Duffie and Beckman, 2013].

In this case, I-V curve is not obtained, but it is based on efficiency's temperature dependance to predict maximum achievable power. From temperature coefficients provided by manufacturers and reference values under STC, the following equation for efficiency under any cell temperature, T_{cell}, can be stated:

$$\eta_{mp} = \frac{I_{mp}V_{mp}}{A_{mod}\cdot G_T} = \eta_{mp,ref} + \mu_{\eta,mp}\cdot(T_{cell} - T_{cell,ref}) \tag{5.8}$$

where $\mu_{\eta,mp}$ is a negative value and, consequently, comparing to nominal values, cell efficiency will decrease for cell temperature higher than 25°C and increase in the opposite case.

On equation 5.8, efficiency for any condition is expressed as function of nominal efficiency and an unknown coefficient, $\mu_{\eta,mp}$, which is efficiency's derivative with respect to temperature:

$$\mu_{\eta,mp} = \frac{d\eta_{mp}}{dT} = (I_{mp} \cdot \frac{dV_{mp}}{dT} + V_{mp} \cdot \frac{dI_{mp}}{dT}) \frac{1}{A_{mod} \cdot G_T} \tag{5.9}$$

On vast majority of PV modules, $\mu_{I_{SC}}$ is a small value, which implies a negligible $\frac{dI_{mp}}{dT}$ term comparing to the other addend in equation 5.9.

$$I_{mp} \cdot \frac{dV_{mp}}{dT} \gg V_{mp} \cdot \frac{dI_{mp}}{dT} \tag{5.10}$$

At the same time, in that equation $\frac{dV_{mp}}{dT}$ term can be approached to open-circuit voltage temperature coefficient, $\frac{dV_{OC}}{dT} = \mu_{V_{OC}}$. Consequently, equation 5.9 can be expressed as:

$$\mu_{\eta,mp} \approx I_{mp} \cdot \mu_{V_{OC}} \cdot \frac{1}{A_{mod} \cdot G_T} = \eta_{mp,ref} \cdot \frac{\mu_{V_{OC}}}{V_{mp}} \tag{5.11}$$

So efficiency's final expression for a given cell temperature is:

$$\eta_{mp} = \eta_{mp,ref} + \eta_{mp,ref} \cdot \frac{\mu_{V_{OC}}}{V_{mp}} \cdot (T_{cell} - T_{cell,ref}) \tag{5.12}$$

And therefore, maximum power obtained from a PV module is:

$$P_{PVMAX} = \eta_{mp} \cdot A_{mod} \cdot G_T \tag{5.13}$$

In the last times, some manufacturers provide a temperature coefficient for the maximum power point, $\mu_{P_{max}}$, so if that parameter is known, equation 5.12 can be rewritten as:

$$\eta_{mp} = \eta_{mp,ref} + \eta_{mp,ref} \cdot \mu_{P_{max}} \cdot (T_{cell} - T_{cell,ref}) \tag{5.14}$$

Whenever $\mu_{P_{max}}$ is provided by the manufacturer, equation 5.14 should be choosen over equation 5.12.

Application to the 180W PV/T modules Substituting the specific values of the parameters listed from table 4.1 on equation 5.14, the temperature dependence of the PV/T modules' efficiency is obtained. This effect is plotted on figure 5.6 .
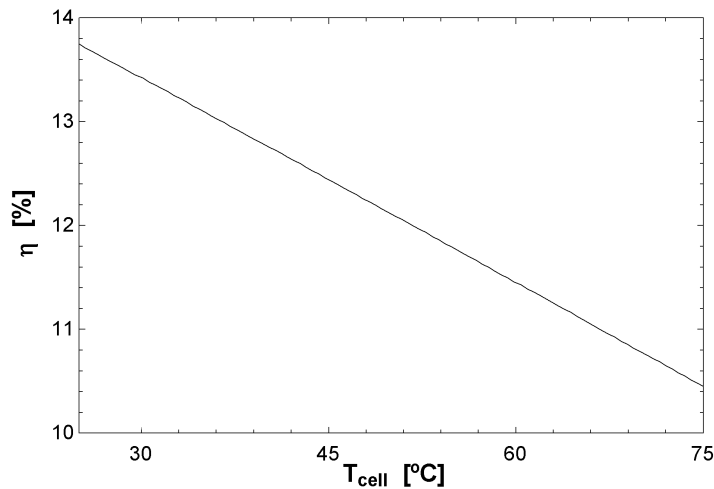
Figure 5.6: Maximum achievable efficiency at diverse cell temperatures.

Due to the quickness and simplicity of this second method (based in just eq. 5.12 and 5.13), it will be the applied one on this research when long time period PV perfomance is calculated. On the other hand, the De Soto model, as it said, requires specific non linear equations solving numerical methods or software like *EES* and, due to its complexity, longer calculation time or computing capacity. Therefore, it has been reserved for the cases when I-V curves need to be represented in detail or to understand the behavour of MPPT controller when it operates out of the maximum power point in batteries charging process like the example plotted on figure 4.7.

Now that the PV production predicting model has been choosen, the solar radiation over PV/T modules tilted surface and cell temperature need to be calculated.

5.4 Radiation on tilted surface

On literature different theoretical models can be found to calculate solar radiation over tilted surfaces once horizontal radiation is available from meteorological data bases. Certain models are based on daily insolation data to estimate hourly average values, which is a statistical approach to this issue. During this research, as it has been mentioned on chapter 4, precise meteorological data about daily evolution of solar radiation were available. Therefore, a model that allows to calculate solar radiation over tilted surfaces along the day has been choosen. After comparing classical model from Liu and Jordan [1960], which consideres an isotropic distribution of direct and diffuse radiation, and the HDKR anisotropic model, in which Reindl et al. [1990] updated previous work of Hay, Davies and Klucher, adding ground reflectance and tilted diffuse radiation terms, I chose the second one.

Applying HDKR model, for any instant of time, solar radiation over tilted surfaces can be calcuted from measured horizontal solar radiation. On the following lines, intermediate calculations and used equations are listed and detailed.

First of all, it will be necessary to obtain the geometric variables of Sun relative to Earth for a given julian day n, such as declination, δ (degrees), and the extraterrestial normal radiation,

G_{0n} (W/m^2), where G_{sc} represents solar constant (1367 W/m^2). From now on, all angles will be expressed in degrees and all radiation in W/m^2.

$$
\begin{aligned}
G_{0n} \quad = \quad & G_{sc} \cdot (1.000110 + 0.034221 \cdot cos(\Gamma) + 0.001280 \cdot sin(\Gamma) + \ldots \\
& + 0.000719 \cdot cos(2 \cdot \Gamma) + 0.000077 \cdot sin(2 \cdot \Gamma))
\end{aligned} \tag{5.15}
$$

$$
\begin{aligned}
\delta \quad = \quad & \frac{180}{\pi} \cdot (0.006918 - 0.399912 \cdot cos(\Gamma) + 0.070257 \cdot sin(\Gamma) - 0.006758 \cdot cos(2 \cdot \Gamma) + \ldots \\
& + 0.000907 \cdot sin(2 \cdot \Gamma) - 0.002697 \cdot cos(3 \cdot \Gamma) + 0.00148 \cdot sin(3 \cdot \Gamma))
\end{aligned} \tag{5.16}
$$

Where Γ:

$$
\Gamma = (n-1) \cdot \frac{360}{365} \tag{5.17}
$$

Equations 5.15 and 5.16 for extraterrestial normal radiation and declination are the ones proposed by Iqbal [1983]. The Spencer [1971] simpler equations are also commonly used in scientific literature.

Previous variables are calculated once per day, but the following ones are modified along the day, so they must be calculated in every time iteration of the model. On a latitude ϕ, to each instant of the day a solar angle ω corresponds, remembering that Sun sweeps out 15° per hour in the sky and solar angle is null at midday. Radiation incident angle on a tilted surface, θ, can be obtained from equation 5.18

$$
\begin{aligned}
cos(\theta) \quad = \quad & sin(\delta) \cdot sin(\phi) \cdot cos(\beta) - sin(\delta) \cdot cos(\phi) \cdot sin(\beta) \cdot cos(\gamma) + \ldots \\
& + cos(\delta) \cdot cos(\phi) \cdot cos(\beta) \cdot cos(\omega) + cos(\delta) \cdot sin(\phi) \cdot sin(\beta) \cdot cos(\gamma) \cdot cos(\omega) \ldots \\
& + cos(\delta) \cdot sin(\beta) \cdot sin(\gamma) \cdot sin(\omega)
\end{aligned} \tag{5.18}
$$

Where β is surface's inclination angle with respect to ground horizontal and γ represents surface azimuth angle, which is orientation angle with respect to the South.

If the tilted surface is south facing , $\gamma = 0$, as the PV modules on this research are, incident angle function can be simplified to:

$$
cos(\theta) = cos(\phi - \beta) \cdot cos(\delta) \cdot cos(\omega) + sin(\phi - \beta) \cdot sin(\delta) \tag{5.19}
$$

Where zenith angle, is obtained from:

$$
cos(\theta_z) = cos(\phi) \cdot cos(\delta) \cdot cos(\omega) + sin(\phi) \cdot sin(\delta) \tag{5.20}
$$

Sky clearness (eq. 5.22) is defined as the fraction between measured horizontal radiation,G, and extraterrestrial solar radiation on horizontal surface,G_0. Once k_T is known, through Erbs et al. [1982] correlation (eq. 5.23), the ratio between diffuse,G_d, and global radiation is given. And, consequently, beam radiation, G_b, is obtained (eq. 5.24).

$$
G_0 = G_{0n} \cdot cos(\theta_z) \tag{5.21}
$$

$$k_T = \frac{G}{G_0} \tag{5.22}$$

$$\frac{G_d}{G} = \begin{cases} 1.0 - 0.09{\cdot}k_T, & k_T \leq 0.22 \\ 0.9511 - 0.1604{\cdot}k_T + 4.388{\cdot}k_T^2 - 16.638{\cdot}k_T^3 + 12.336{\cdot}k_T^4, & 0.22 < k_T \leq 0.8 \\ 0.165, & k_T > 0.8 \end{cases} \tag{5.23}$$

$$G = G_b + G_d \tag{5.24}$$

HDKR method defined some extra coefficients, such as anisotropic index, A_i (function of beam radiation's atmospheric transmitance), fraction R_b(ratio between incidence angle on tilted surface and horizontal surface), and other factors like f .

$$A_i = \frac{G_b}{G_0} \tag{5.25}$$

$$R_b = \frac{cos(\theta)}{cos(\theta_z)} \tag{5.26}$$

$$f = \sqrt{\frac{G_b}{G}} \tag{5.27}$$

Once all these terms have been calculated, following the HDKR method [Reindl et al., 1990], terrestial solar radiation on tilted surface will be directly obtained from equation 5.28.

$$G_T = (G_b + G_d{\cdot}A_i){\cdot}R_b + G_d{\cdot}(1 - A_i){\cdot}(\frac{1 + cos(\beta)}{2})[1 + f{\cdot}sin^3(\frac{\beta}{2})] + G{\cdot}\rho_g{\cdot}(\frac{1 - cos(\beta)}{2}) \tag{5.28}$$

Through this method, for a certain instant of the day, which is to say for a given solar angle ω, solar radiation for a given β angle tilted surface will be obtained from horizontal radiation data.

Once solar radiation on tilted surface for a certain instant is obtained, the integral along the day will represent the daily solar energy per unit of area or daily insolation, H_T. If the solar radiation is obtained for equally time distant points, the integral can be approached to a summatory, as following:

$$H_T = \int G_T dt \simeq \sum G_T{\cdot}\triangle t \tag{5.29}$$

where $\triangle t$ represents measurements' time period.

Obviously this multiple equations' process must be implemented through computational functions in order to calculate solar radiation on tilted surface along a whole day, month or season.

Chapter 6

Photovoltaic cell temperature

As it has been mentioned previously, cell temperature is a key factor on PV modules efficiency. Therefore, in order to predict the electrical output of a PV module under certain meteorological conditions the evolution of its cells temperature must be calculated.

In the following chapter, the state-of-the-art in cell temperature models is reviewed (section 6.1) . After it, on section 6.2, composition of specific PV/T modules used on this research is detailed and a heat transfer model is proposed, which predicts their cell temperature based on available inputs like solar radiation, outdoor dry bulb temperature, dew point temperature and wind speed. This model is experimentally validated on section 6.3.

6.1   Existing correlations

Different authors have proposed semi-empirical expresions to guess how cells are heated under changing meteorological conditons. A simply polinomial function with ambient or outdoor dry bulb temperature (T_{odb}) and incident solar radiation (G_T) as variables (eq 6.1) was published by Ros [1976], where C is a semi-empirical constant.

$$T_{cell} = T_{odb} + C \cdot G_T \tag{6.1}$$

This model does not take into account wind speed or which materials compose each layer of the PV module.

A widely used method [Ros, 1980] is the one based on nominal operation cell temperature (NOCT) provided by the manufacturer. This technical information is usually provided for the following conditions: G_T: 800W/m^2, T_{odb}: 20°C and 1m/s wind speed, so eq. 6.2 estimates cell temperature at different conditions comparing with the nominal one.

$$T_{cell} = T_{odb} + (NOCT - 20) \cdot \frac{G_T}{800} \tag{6.2}$$

However, Alonso-Garcia and Balenzategui [2004] pointed that eq. 6.2 makes no distinction among modules mounting options and their convection heat losses, so guessed cell temperature may exceed 3°C to actual cell temperature on a well-ventilated module or underestimate on 20°C to a facade-integrated PV system.

King et al. [2004] expounded a quick model which introduces wind speed, w_s, as variable and semi-empirical constants a, b and $\triangle T$, related with mounting options (free standing, tilted open rack, closed roof,...), wind influence and temperature difference between front and rear surfaces of modules. For example, for a glass/cell/polymerer module on open rack the following values are proposed: a=-3.56, b=-0.075 y$\triangle T$=3°C, for equation 6.3.

$$T_{cell} = G_T \cdot e^{a+b \cdot w_S} + T_{odb} + \frac{G_T}{1000}\triangle T \qquad (6.3)$$

In a similar way, Skoplaki et al. [2008] proposed a correlation that includes convection losses due to wind speed, incident solar radiation and ambient temperature (eq. 6.4), where C is an empirical constant related with mounting option.

$$T_{cell} = T_{odb} + C \cdot \frac{0.32}{8.91 + 2 \cdot w_s} \cdot G_T \qquad (6.4)$$

As all the mentioned methods are based in different variables and semi-empirical constants the predicted cell temperature can be expected to not be equal under changing meteorological conditions. As example, cell temperature is predicted for a clear and mild day (27/10/2014), shown on 6.1, using diverse methods.
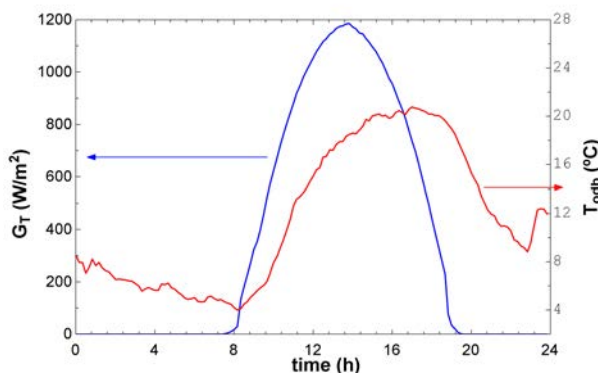
Figure 6.1: Solar radiation and ambient temperature on 27/10/2014.

Figure 6.3 shows evolution of cell temperature during sun hours according to equations 6.1, 6.2, 6.3 and 6.4, which reveals temperature differences among them up to 12°C. Even each model can change widely its prediction depending on the values asigned to the semi-empirical constants.

Others authors, like Koehl et al. [2011], propose to develop statistical models based on testing PV cells under certain meteorological conditions. As a survey, several cell temperature models are listed on the review published by Skoplaki and Palyvos [2009a] and even how they affect
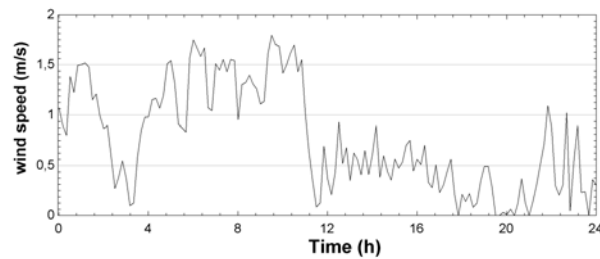
Figure 6.2: Wind speed on 27/10/2014.
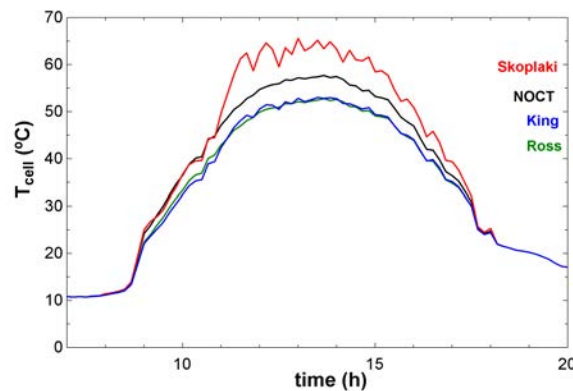
Figure 6.3: Cell temperature predicted by different methods.

to electrical efficiency of PV and Photovoltaic-Thermal (PV/T) modules [Skoplaki and Palyvos, 2009b]. In a similar way, Dubey et al. [2013] made a review of the cell temperature and PV efficiency semi-empirical correlations available in the literature, pointing out the influence of the outdoor temperature in the PV potential of the regions in the world.

However, it can be concluded that each semi-empirical model has been tested for certain types of modules and mounting options, so their results can not be extrapolated to any kind of module.

For PV cells assembled in multi-layer structures, like facade-intregated or hybrid PV/Thermal modules, cell temperature will be marked by layers thermal resistance and heat transfer processes, so they should be studied in detail.

PV/Thermal modules   As it was mentioned on *chapter 2*, the hybrid PV/T modules have become a topic of research. Oftenly, their operating temperatures are approached through empirical correlations or average values. For example, in order to obtain empirical constants, Kaya [2013] carried out an experimental characterization of some water PV/T modules. For each type of PV/T modules, parametric study and experimental validation of them can be carried out, as done by Tiwari and Sodha [2006, 2007].

However, in order to predict sharply cell and other inner layers' temperature, an analytical approach has been considered necessary for both PV or PV/T modules. In that way, some heat transfer models have been published in the last decadewhich are based on different assumptions, conditions and heat transfer correlations. Jones and Underwood [2001] proposed a transient

model with a differential equation of the variation of module temperature with time, arguing that for short time interval, in cloudy days the thermal mass would be significant. Their model is compared to experimental values just for short periods, without showing daily evolution of temperature. In addition, the transient model might require significant computational time when long periods are simulated. In a similar way, a transient model for specific PV/T modules was carried out by Chow [2003].

Jacques et al. [2013] proposed a 1-D steady-state thermal model and a validation by experimental data. However, in their model, heat exchange through radiation is omitted and the experimental validation is based on obtaining an empirical convection coefficient after testing the PV module inside a wind tunnel. It does not include daily evolution of cell temperature. Armstrong and Hurley [2010] argued that most of the available models had been tested under indoor artificial conditions of wind tunnels or darkness, and claim there is a need of experimental validation under real meteorological conditions. However, they did not include experimental and simulated cell temperature confrontation, but they focused on the influence of quick changing meteorological conditions in experimental cell temperature when some minutes intervals are studied.

Because of these reasons, in this work, a new model is developed and validated specifically for the used PV/T modules. This model, proposed on section 6.2, might be applied for different kind of modules if their composition is known.

Finally, it must be mentioned that most of cited models, for both PV or PV/T, do not include explicitly electrical production so the may fail to consider the possibility of partial load in isolated systems. What is more, when a PV module does not work on its maximum power point, the potential electrical energy not produced would count as thermal energy, increasing cell temperature.

6.2 Heat transfer model for predicting cell temperature under varying conditions

Due to the mentioned importance of knowing as sharp as possible the cell temperature of the PV/T modules used during research, the development of an specific heat transfer model has been assumed.

In a module exposed to solar radiation, different kind of energy transfer processes will occur in both external and internal layers. An scheme for this energy balance has been proposed as shown on figure 6.4, which is based on the layer composition of the used type of PV/T modules.

Intercepted solar radiation over tilted PV/T modules frontal glass surface, G_T, will be partially reflected or absorbed by the glass and front polymer of ethylene vinyl acetate (EVA). Therefore, the solar radiation that reachs the silicon cell to produce photovoltaic conversion will be determined by transmitivity property of both layers. Once part of transmitted solar energy is converted on photovoltaic electrical production, the rest of the energy is conducted through the layers of the module until reaching front and rear surfaces where it is dissipated by convection and radiation.
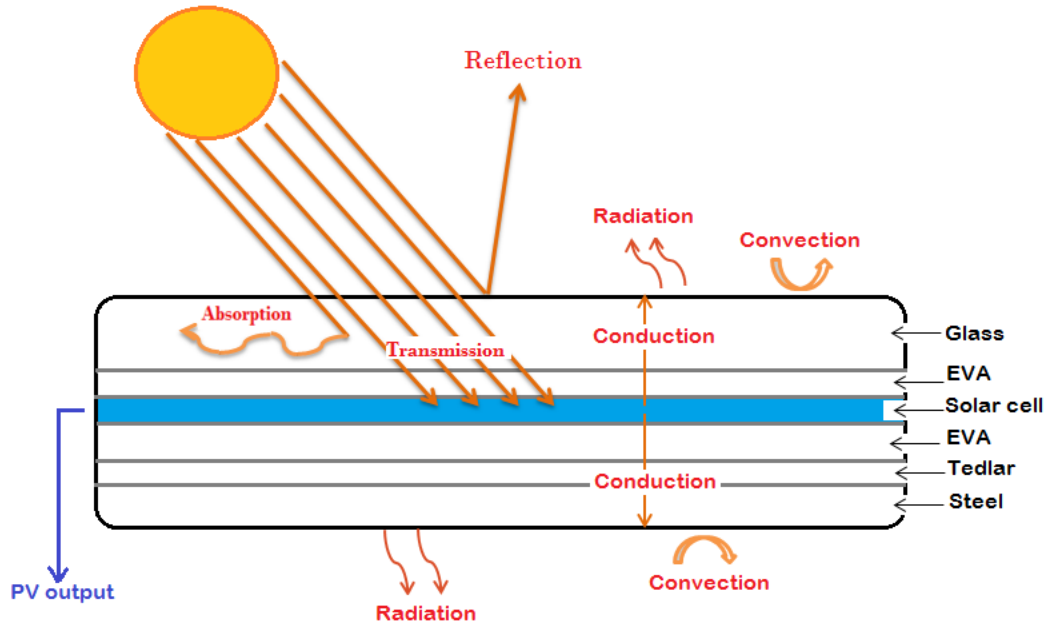
Figure 6.4: Energy balance diagram.

Layer	$\triangle x$[mm]	ρ[kg/m^3]	C_p[J/kg·K]	κ[W/m·K]	ε [-]	τ [-]
Glass	3.2	3000	500	1.8	0.9	0.915
EVA	0.5	960	2090	0.35	-	0.91
Silicon cell	0.2	2330	677	148	-	-
Tedlar	0.36	1200	1250	0.2	-	-
Steel	1.5	8100	500	16	0.8	-

Table 6.1: Physical properties of module layers.

Used hybrid modules include a thermal circuit gaps between some contact areas of Tedlar and stainless steel layers. However, thermal circuit was not used during this research and the measured surface temperature of steel on different points showed a temperature difference $< 0.5°C$. Consequently, the scheme shown of figure 6.4 is considered accurate enough for predicting layers temperature, when PV/T modules are used only for electricity production and no internal fluid is cooling them.

The thermal energy needed for temperature change of modules' materials depends on their thermal mass. Equation 6.5 expresses the thermal energy function for a layer, which is related to specific heat, mass and temperature gradient between two moments.

$$Q = m{\cdot}C_p{\cdot}\triangle T = \rho{\cdot}\triangle x{\cdot}A_{mod}{\cdot}C_p{\cdot}\triangle T \tag{6.5}$$

All the layers within a module, according to table 6.1, present a thermal mass per area which sum is:

$$\frac{Q}{A_{mod}{\cdot}\triangle T} = \sum \rho{\cdot}\triangle x \cdot C_p = 13,7\frac{kJ}{m^2{\cdot}K} \tag{6.6}$$

On a hot and clear day, like 15/7/2014 (plotted on appendix A), it took 3h 56m during the morning, to warm the module's glass 30°C, (from 35°C at 9.72h to 65°C at 13.63h). According to equation 6.5, for the all layers, 0.11 kWh/m²would be required due to the thermal mass. However, during that period of time, the intercepted solar insolation on modules' surface was 2.92 kWh/m². The thermal mass of the module is not significant on its thermal behavior under varying conditions .Therefore, it can be neglected in the energy balance of the proposed model, raising a non transient model.

If the attention is paid to the silicon cell surface of the scheme, under no transient mode assumption, the transmitted solar energy to the photovoltaic layer can be considered equal to the electrical production and heat conduction from the cell to the extenal surfaces of the PV/T module (eq. 6.7).

$$\tau_{glass} \cdot \tau_{EVA} \cdot G_T = \dot{q}_{cond_{front}} + \dot{q}_{cond_{back}} + \eta \cdot G_T \tag{6.7}$$

Once conducted heat reaches front and rear surfaces of PV/T module it is dissipated by radiation and convection processes. Therefore,

$$\dot{q}_{cond_{front}} = \dot{q}_{conv_{front}} + \dot{q}_{rad_{front}} \tag{6.8}$$

$$\dot{q}_{cond_{back}} = \dot{q}_{conv_{back}} + \dot{q}_{rad_{back}} \tag{6.9}$$

Solving this equation system for an instant, under certain meteorological conditions and PV production load, would determine cell temperature.

On the following subsections, selected heat transfer topics would be discussed, with the aim of determining conduction, convection and radiation flows and their relation with layers temperatures.

6.2.1 Conduction

Heat conduction is an energy transfer process based on microscopic vibration of particles due to temperature gradient within a material. The law of heat conduction, or Fourier's law, can be expressed in its integral form as:

$$\dot{Q} = -\kappa \oint_S \vec{\nabla} T \cdot \vec{dA} \tag{6.10}$$

Where,
$\dot{Q} = \frac{\partial Q}{\partial t}$ is the ammount of heat conducted in time, W
κ is thermal conductivity of the material, $\frac{W}{m \cdot K}$
∇T is the temperature gradient, $\frac{K}{m}$
dA is the oriented surface area, m^2
Its differential form is commonly expresed as function of flux, $\frac{W}{m^2}$, so $\dot{Q}$ is substituted by $\dot{q}$, according to:

$$\dot{q} = \frac{1}{A} \cdot \frac{\partial Q}{\partial t} \tag{6.11}$$

And consequently, differential form for Fourier's law will be:

$$\dot{q} = -\kappa \cdot \nabla T \tag{6.12}$$

6.2.1.1 Conduction within a flat wall

Solving conduction law for non homogeneous materials, function of three position coordinates and time can be quite complicated in some cases. However, an analytical solution can be found for a flat wall where temperature is only function of one direction, the width of the wall. In fact, flat PV/T modules can be simplified, in heat conduction terms, as multiple flat walls attached one to another.

As figure 6.5 shows, from a hot surface of a wall of width L to a colder surface a heat conduction flux would occur.
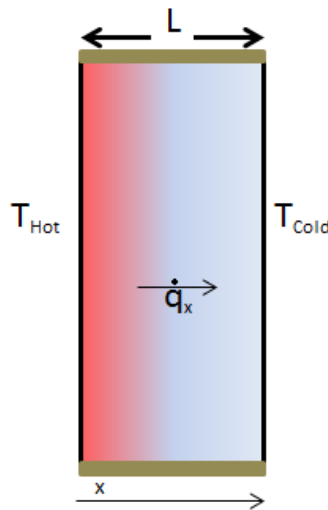
Figure 6.5: Conduction through a flat wall.

In that case, Fourier's law can be expressed only in function of x coordinate:

$$\frac{\partial Q}{\partial t} = -\kappa \cdot A \cdot \frac{\partial T}{\partial x} \tag{6.13}$$

Or, function of the flux:

$$\dot{q}_x = -\kappa \cdot \frac{dT}{dx} \tag{6.14}$$

As heat flux is assumed constant along wall's width:

$$\frac{d\dot{q}_x}{dx} = 0 \tag{6.15}$$

Combining equations 6.14 and 6.15, it leads to:

$$\frac{d}{dx}[-\kappa \cdot \frac{dT}{dx}] = 0 \tag{6.16}$$

If κ is constant through x :

$$\frac{d^2T}{dx} = 0 \tag{6.17}$$

Now, equation 6.17 is integrated:

$$\int \frac{d^2T}{dx}dx = \int 0 \cdot dx \rightarrow \frac{dT}{dx} = C_1 \tag{6.18}$$

And integrated again:

$$\int \frac{dT}{dx}dx = \int C_1 \cdot dx \rightarrow T = C_1 \cdot x + C_2 \tag{6.19}$$

The value of constants C_1 and C_2 must be determined applying boundary conditions:

$$\begin{array}{ll} x = 0, & T = T_{Hot} \\ x = L, & T = T_{Cold} \end{array} \tag{6.20}$$

What leads to a linear distribution of T through x :

$$T = \frac{(T_{Cold} - T_{Hot})}{L} \cdot x + T_{Hot} \tag{6.21}$$

The heat conduction flux at any location within the wall is obtained by substituting the temperature distribution (eq. 6.21) on equation 6.14, calculating derivative of T respect to x:

$$\dot{q} = \frac{\kappa}{L} \cdot (T_{Hot} - T_{Cold}) \tag{6.22}$$

In conclusion, for an ideal 1-D problem, the heat transferred during an amount of time within a material will be related with the temperature difference and distance between the ends:

$$\frac{1}{A} \cdot \frac{\triangle Q}{\triangle t} = -\kappa \cdot \frac{\triangle T}{\triangle x} \tag{6.23}$$

Therefore, solution 6.22 for heat flux through a plane wall suggests that, under some limiting conditions, conduction of heat through a solid can be thought of as a flow that is driven by a temperature difference and resisted by a thermal resistance, in the same way that electrical current is driven by a voltage difference and resisted by an electrical resistance. In this case, thermal resistance can be defined as:

$$R = \frac{\triangle x}{\kappa} \tag{6.24}$$

And consequently, the conductance, or heat transfer coefficient, of that material layer as:

$$U = \frac{1}{R} = \frac{\kappa}{\triangle x} \tag{6.25}$$

If multiple flat layers are attached, as it happens with electrical resistances combined in series, their resistances will be summed for obtaining equivalent resistance of the composition of n number of layers:

$$R_{equiv} = \sum_{i=1}^{n} \frac{\triangle x_i}{\kappa_i} \tag{6.26}$$

And composition's global conductance will be:

$$U_{equiv} = \frac{1}{R_{equiv}} = \frac{1}{\sum_{i=1}^{n} \frac{\triangle x_i}{\kappa_i}} \tag{6.27}$$

Therefore, the heat conduction flux through multiple flat layers, can be expressed as function of temperature difference between ends of whole composition and its equivalent conductance or resistance inverse:

$$\dot{q}_{cond} = U_{equiv} \cdot \triangle T = \frac{1}{R_{equiv}} \cdot \triangle T \tag{6.28}$$

Once the basis of Fourier's law has been discussed, the heat conduction within PV/T modules can be estimated.

6.2.1.2 Conduction within PV/T modules

Heat conduction equation should be specified for conduction processes within PV/T, as pointed on diagram 6.4. The first step to address this problem will be to know the composition of each layer of the PV/T module and their physical properties. Armstrong and Hurley [2010] summarized thermal conductivities, specific heats and thickness of most common layers. PV polycrystalline silicon cells used in this research are covered on the front by a glass layer and a polymer of ethylene vinyl acetate (EVA). These cells lie over another EVA layer, a Tedlar sheet to avoid moisture and, finally, an stainless steel holder. For each layer, table 6.1 shows thickness $\triangle x$ provided by the manufacturer, thermal conductivity κ, emissivity ε of the front and rear surfaces, and transmittance τ of the front layers.

The trasmitted solar energy, except the converted electricity, is conducted from silicon surface to front and rear surface of the PV/T module. This conduction flux will be characterized by the resistance offered by each layer and their interstitial resistance. When two solid surfaces are attached, depending on how flat they are, even at micro-scale considerations, some contact resistance between them appears. The thermal resistance between two layers contact is assumed [Nellis and Klein, 2009] as:

$$R_{contact} = \frac{1}{3000} \frac{m^2 \cdot K}{W} \tag{6.29}$$

In this way, from silicon front surface to the outdoor surface of the glass, the thermal resistances are shown on figure 6.6. In an analogous way, rear thermal resistances are described on figure 6.7. The numerical values of these thermal resistances and the equivalent frontal and back conduction resistances are listed on table .
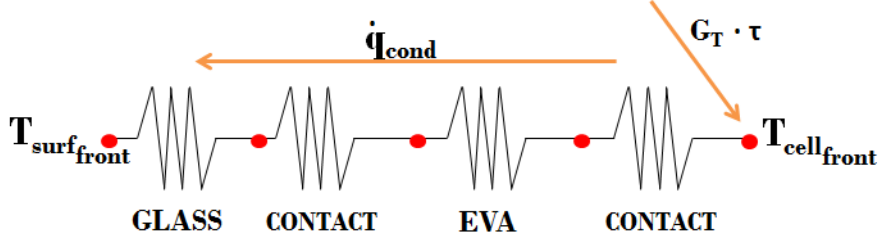
Figure 6.6: Front thermal resistances.
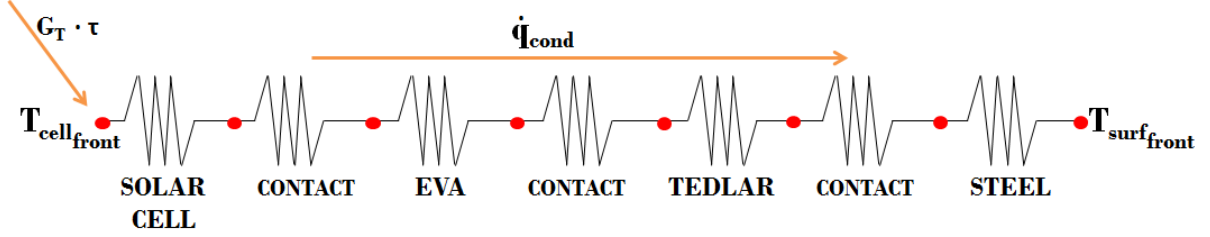
Figure 6.7: Rear thermal resistances

Conducted energy flux $\dot{q}$ (energy transfer per unit time and unit area) between silicon surface and glass frontal surface is determined by temperature difference between both points and combined thermal conductance of the layers, according to eq. 6.30. Overall heat transfer coefficient, U, is defined by equation 6.31. In analogous way, equations 6.32 and 6.33 describe rear conducted flux, from silicon surface to module's back surface.

$$\dot{q}_{cond_{front}} = \frac{1}{R_{front}} \cdot (T_{cell_{front}} - T_{surf_{front}}) \tag{6.30}$$

$$\frac{1}{R_{front}} = \frac{1}{R_{glass} + R_{EVA} + 2 \cdot R_{contact}} \tag{6.31}$$

$$\dot{q}_{cond_{back}} = \frac{1}{R_{back}} \cdot (T_{cell_{front}} - T_{surf_{back}}) \tag{6.32}$$

$$\frac{1}{R_{back}} = \frac{1}{R_{cell} + R_{EVA} + R_{Tedlar} + R_{Steel} + 3 \cdot R_{contact}} \tag{6.33}$$

Once $\dot{q}_{cond}$ are known, front and rear temperatures of any layer can be obtained. For example in the glass layer:

$$\dot{q}_{cond_{front}} = \frac{1}{R_{glass}} \cdot (T_{glass_{back}} - T_{glass_{front}}) \tag{6.34}$$

$$T_{glass} = \frac{T_{glass_{back}} + T_{glass_{front}}}{2} \tag{6.35}$$

In the case of silicon cells, the thermal resistance is so low that the temperature difference between front and rear surface of the silicon layer can be considered negligible and $T_{cell} \approx T_{cell_{front}}$.

Layers	R ($m^2 \cdot K/W$)
Glass	0.001778
EVA	0.001429
Solar cell	0.000001
Tedlar	0.001800
Steel	0.000094
Frontal R_{equiv}	0.003873
Back R_{equiv}	0.002895

Table 6.2: Thermal resistances of PV/T modules' layers.

Conducted energy flux that reach both external surfaces of the module is exchanged with the surroundings, as it has been mentioned, through radiative and convective fluxes. In the following lines, these both processes will be detailed.

6.2.2   Radiation

Radiation flux from a surface at a given temperature and its surroundings, is determined by Stefan-Boltzmann law. For the radiation exchange between the back surface of the module and the ground, the energy flux will be described by equation 6.36, where emissivity of the steel is ε_{steel} and σ is Stefan-Boltzmann's constant. The correlation between ground temperature and outdoor dry bulb temperature [IDAE, 2010] is described by equation 6.37.

$$\dot{q}_{rad_{back}} = \sigma \cdot \varepsilon_{steel} \cdot (T^4_{surf_{back}} - T^4_{ground}) \tag{6.36}$$

$$T_{ground} = 0.068 \cdot T^2_{odb} + 0.963 \cdot T_{odb} + 0.6865 \tag{6.37}$$

Front surface of the module, instead, will exchange radiation with the sky (eq. 6.38), which can be significantly lower than ambient temperature.

$$\dot{q}_{rad_{front}} = \sigma \cdot \varepsilon_{glass} \cdot (T^4_{surf_{front}} - T^4_{sky}) \tag{6.38}$$

In order to determine sky temperature, several empirical equations can be found on scientific literature. For the development of this work, complete meteorological data of the location were availabe, so equation 6.39, included on Duffie and Beckman [2013], is used. T_{odb} represents outdoor dry bulbtemperature expressed in Kelvin, T_{sky} is sky temperature in Kelvin, T_{dp} is the dew point temperature in degrees Celsius, and t the hours passed from midnight.

$$T_{sky} = T_{odb} \cdot [0.711 + 0.0056 \cdot T_{dp} + 0.000073 \cdot T^2_{dp} + 0.013 \cdot cos(15 \cdot t)]^{\frac{1}{4}} \tag{6.39}$$

In case of having no data about relative humidity or dew point, equation 6.40 is suggested.

$$T_{sky} = 0.0552 \cdot T^{\frac{3}{2}}_{odb} \tag{6.40}$$

It must be remarked than in both equations 6.36 and 6.38, temperature variables must be introduced in Kelvin.

6.2.3   Convection

Heat transfer between a solid surface and a moving fluid (in this case the surrounding air), can be simply explained by Newton's law of cooling. As it occurs on conduction, heat convection flux is proportional to temperature difference and an overall coefficient. Therefore, convection energy flux on external surfaces of the PV/T module is determined by equations 6.41 and 6.42. However, the main difficulty lies on guessing convection coefficients h_{conv}, which may have a forced component, related with wind speed, and a free convection component.

$$\dot{q}_{conv_{front}} = h_{conv_{front}} \cdot (T_{surf_{front}} - T_{odb}) \tag{6.41}$$

$$\dot{q}_{conv_{back}} = h_{conv_{back}} \cdot (T_{surf_{back}} - T_{odb}) \tag{6.42}$$

6.2.3.1   Forced convection

Many authors have proposed polynomial correlations to obtain forced convection coefficient from wind speed. One of the first proposal was done by McAdams [1954]:

$$h_{conv} = 5.7 + 3.8 \cdot w_s \tag{6.43}$$

That coefficient might include radiative losses, so Watmuff et al. [1977] proposed a new correlation:

$$h_{conv} = 2.8 + 3 \cdot w_s \tag{6.44}$$

After testing heated flat plates in a wind tunnel for different angles, Sparrow et al. [1979], proposed correlation 6.45.

$$Nu = 0.86 \cdot Re^{\frac{1}{2}} \cdot Pr^{\frac{1}{3}} \tag{6.45}$$

Where average Nusselt, Prandtl and Reynolds's dimensionless parameters for longitudinal flow are calculated from physical parameters of the air (density ρ, thermal conductivity κ, dynamic viscosity μ) for a given temperature, wind speed w_s (in m/s) and characteristic length L_c (function of module's area and perimeter), as described by equations 6.46, 6.47, 6.48 and 6.49.

$$Pr = \frac{\mu \cdot C_p}{\kappa} \tag{6.46}$$

$$Re = \frac{w_s \cdot L_c \cdot \rho}{\mu} \tag{6.47}$$

$$Nu = \frac{h_{conv,forced} \cdot L_c}{\kappa} \tag{6.48}$$

$$L_c = \frac{4 \cdot A_{mod}}{Per_{mod}} \tag{6.49}$$

Others authors, like Cengel [2003], reduced the multiplying factor, considering equation 6.50 for a laminar flow.

$$Nu = 0.664 \cdot Re^{\frac{1}{2}} \cdot Pr^{\frac{1}{3}} \tag{6.50}$$

A wider range of correlations were listed by Rabadiya and Kirar [2012].

6.2.3.2   Natural convection

Apart from wind effect, air surrounding a heated surface also moves due to density gradients induced as this fluid is heated and cooled. These heat losses are defined as natural or free convection.

As it happens with forced convection, different authors propose different correlations that relate free convection dimensionless parameters as Rayleigh number to Nusselt number and convection coefficient.

For a heated plate, authors like Nellis and Klein [2009], Cengel [2003], Incropera [1990] propose that Rayleigh number for longitudinal flow will be defined by equation 6.51 and average Nusselt number by equation 6.52.

$$Ra = \frac{g \cdot L^3 \cdot \xi \cdot (T_{surf} - T_{odb})}{\upsilon \cdot \alpha} \tag{6.51}$$

$$Nu = \frac{h_{conv,free} \cdot L}{\kappa} \tag{6.52}$$

Where ξ represents the thermal expansion coefficient, g the gravitational acceleration, α the kinematic viscosity and L is the characteristic lenght (defined in this case by eq. 6.53). Air properties are evaluated for the film temperature (eq. 6.54).

$$L = \frac{A_{mod}}{Per_{mod}} \tag{6.53}$$

$$T_{film} = \frac{T_{surf} + T_{odb}}{2} \tag{6.54}$$

However, mentioned authors differ in the correlations between average longitudinal Ra and Nu. Cengel [2003] uses a quite accurate expression (eq. 6.55) for vertical and tilted plates. However, on tilted plates it can be only applied for front surfaces colder than outdoor dry bulb temperature and hotter rear surfaces.

$$Nu = \{0.825 + \frac{0.387 \cdot Ra^{1/6}}{[1 + (\frac{0.492}{Pr})^{9/16}]^{8/27}}\}^2 \tag{6.55}$$

As Nellis and Klein [2009] proposed a method for obtaining convection coefficient for tilted plates heated on both sides (as our PV modules are), that will be the used method. It is based on obtaining the convection coeffient for heated vertical plate, horizontal heated upward facing plate, horizontal heated downward facing plate, and choosing the highest value obtained among the three of them. The following lines describe the calculus method for each of them.
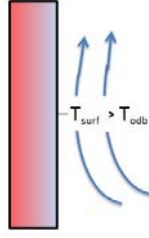
Figure 6.8: Vertical heated plate.

Heated vertical plate   Average longitudinal Nusselt number is defined as a combination of laminar and turbulent flow (eq. 6.56).

$$Nu = (Nu_{lam}^6 + Nu_{turb}^6)^{1/6} \tag{6.56}$$

Laminar Nusselt number will be:

$$Nu_{lam} = \frac{2}{ln(1 + \frac{2}{C_{lam} \cdot Ra^{0.25}})} \tag{6.57}$$

where,

$$C_{lam} = \frac{0.671}{[1 + (\frac{0.492}{Pr})^{9/16}]^{4/9}} \tag{6.58}$$

And turbulent Nusselt number will be:

$$Nu_{turb} = \frac{C_{turb} \cdot Ra^{1/3}}{1 + (1.4 \cdot 10^9) \cdot \frac{Pr}{Ra}} \tag{6.59}$$

where,

$$C_{turb} = \frac{0.13 \cdot Pr^{0.22}}{(1 + 0.61 \cdot Pr^{0.81})^{0.42}} \tag{6.60}$$

In this case, for Rayleigh expression 6.51, g will be substituted by $g \cdot sin(\beta)$, where β is surface's tilted angle.

Horizontal heated upward facing plate   For this case, shown on figure 6.9, an analogous method is proposed. An average longitudinal Nusselt number is obtained combining laminar and turbulent components:

$$Nu = (Nu_{lam}^{10} + Nu_{turb}^{10})^{1/10} \tag{6.61}$$

Where:

$$Nu_{lam} = \frac{1.4}{ln(1 + \frac{1.4}{0.835 \cdot C_{lam} \cdot Ra^{0.25}})} \tag{6.62}$$
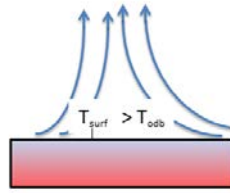
Figure 6.9: Horizontal heated upward facing plate.

$$C_{lam} = \frac{0.671}{[1 + (\frac{0.492}{Pr})^{9/16}]^{4/9}} \tag{6.63}$$

$$Nu_{turb} = C_{turb} \cdot Ra^{1/3} \tag{6.64}$$

$$C_{turb} = 0.14 \cdot (\frac{1 + 0.0107 \cdot Pr}{1 + 0.01 \cdot Pr}) \tag{6.65}$$

In this case, for Rayleigh expression 6.51, g will be substituted by $g \cdot max[0, cos(\beta)]$.

Horizontal heated downward facing flate On the case shown on fig. 6.10, a shorter correlation is proposed:

$$Nu = \frac{2.5}{ln\{1 + \frac{2.5}{0.527 \cdot Ra^{0.2}}[1 + (\frac{1.9}{Pr})^{0.9}]^{2/9}\}} \tag{6.66}$$
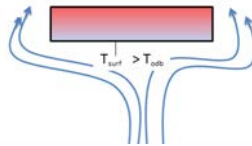
Figure 6.10: Horizontal heated downward facing plate.

In this last case, for Rayleigh expression 6.51, g will be substituted by $g \cdot max[0, -cos(\beta)]$.
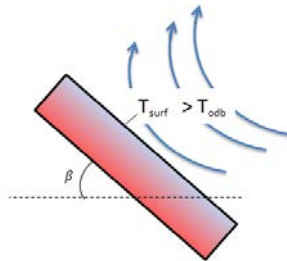
Figure 6.11: Tilted heated plate.

Tilted plate   Once correlations for three cases are known, natural convection coefficient for a heated tilted surface (fig. 6.11), will be the maximum h obtained by three mentioned methods [Nellis and Klein, 2009].

$$h_{conv,free} = Max(h_{vert}, h_{horiz,up}, h_{horiz,down}) \tag{6.67}$$

For the surface of the module that faces the ground (fig. 6.12), the back steel cover, the convection coefficient is calculated through the same method, subsituting β by $180^0 - \beta$.
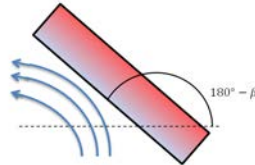
Figure 6.12: Tilted heated plate with downside convection.

6.2.3.3   Combining natural and forced convection

Therefore, if subsections 6.2.3.1 and 6.2.3.2 are followed, forced and natural convection coefficients can be obtained. However, they need to be combined for calculating the global heat losses due to convection on both front and back surfaces of the module.

Many authors [Nellis and Klein, 2009, Cengel, 2003], suggest that natural convection can be neglected comparing to forced convection or vice versa, under certain conditions. A criterion for guessing it would be based on a Richardson number (fraction between Grashof and Reynolds' numbers) as the following:

$Ri = \frac{Gr}{Re^2} \ll 1 \rightarrow$only forced convection is considered

$Ri = \frac{Gr}{Re^2} \gg 1 \rightarrow$only natural convection is considered

$Ri = \frac{Gr}{Re^2} \approx 1 \rightarrow$both natural and forced convection must be considered

In the experimental validation carried out on section 6.3, this fraction provide values around 10^{-3}. However as it will be shown, the heat transfer model matches when both kind of convection are taken into account. In fact, the wind speed over modules' surface averagely keeps around 1 m/s, it is commonly almost null and it rarely exceeds 5 m/s, so it seems reasonable to considerate both natural and forced convection under these conditions.

How both convections combine to obtain a global convection coefficient on a surface, depends on different considerations. In this work, two different assumptions are proposed:

Forced convection on front glass, natural on both external surfaces   It might be considered that wind only affects the front glass of the module, and natural convection occurs on both sides. In that hypothesis front and rear convection flux would be:

$$h_{conv_{front}} = h_{conv,forced} + h_{conv,free_{front}} \tag{6.68}$$

$$h_{conv_{back}} = h_{conv,free_{back}} \tag{6.69}$$

$$\dot{q}_{conv_{front}} = h_{conv_{front}} \cdot (T_{surf_{front}} - T_{odb}) \tag{6.70}$$

$$\dot{q}_{conv_{back}} = h_{conv_{back}} \cdot (T_{surf_{back}} - T_{odb}) \tag{6.71}$$

Natural and forced convection on both external surfaces   As the used PV modules are mounted on an open rack, it might also be considered that wind affects to both sides of the modules. In addition, authors like Cengel [2003], Nellis and Klein [2009] mention that forced and natural convection combine according to equation 6.72.

$$h_{conv_{front}} = \sqrt[3]{h_{conv,free_{front}}^3 + h_{conv,forced}^3} \tag{6.72}$$

$$h_{conv_{back}} = \sqrt[3]{h_{conv,free_{back}}^3 + h_{conv,forced}^3} \tag{6.73}$$

So,

$$\dot{q}_{conv_{front}} = h_{conv_{front}} \cdot (T_{surf_{front}} - T_{odb}) \tag{6.74}$$

$$\dot{q}_{conv_{back}} = h_{conv_{back}} \cdot (T_{surf_{back}} - T_{odb}) \tag{6.75}$$

Both calculus proposals are theoretically simulated for diverse conditions and compared with the experimentally measured values (section 6.3) in order to choose the most appropiate one for used PV/T modules.

6.2.4   Explicit energy balance and cell temperature determination

On the previous sections, equations for heat conduction, convection and radiation have been explicited for specificic PV/T modules. In this way, the energy balance system proposed on equations 6.7, 6.8 and 6.9 is explicitly rewritten as the following equation system:

$$
\begin{cases}
\tau_{glass} \cdot \tau_{EVA} \cdot G_T = \frac{1}{R_{front}} \cdot (T_{cell} - T_{surf_{front}}) + \frac{1}{R_{back}} \cdot (T_{cell} - T_{surf_{back}}) + \eta \cdot G_T \\[4ex]
\frac{1}{R_{front}} \cdot (T_{cell} - T_{surf_{front}}) = h_{conv_{front}} \cdot (T_{surf_{front}} - T_{odb}) + \sigma \cdot \varepsilon_{glass} \cdot (T_{surf_{front}}^4 - T_{sky}^4) \\[4ex]
\frac{1}{R_{back}} \cdot (T_{cell} - T_{surf_{back}}) = h_{conv_{back}} \cdot (T_{surf_{back}} - T_{odb}) + \sigma \cdot \varepsilon_{steel} \cdot (T_{surf_{back}}^4 - T_{ground}^4)
\end{cases}
$$

In conclusion, for any instant of a day, once meteorological conditions (G_T, T_{sky}, T_{ground}, T_{odb}, w_s) are known and conduction resistances, R, and forced/natural convection combined coefficients, h, for these PV/T modules are obtained, the 3 equation system, shown above, will solve 3 unknown variables: both external surface temperatures $T_{surf_{back}}$, $T_{surf_{front}}$ and, the main reason of this chapter, silicon cell's temperature, T_{cell}.

This proposed method could be easily extrapolated for other type of multi-layer PV modules if their construction and physical properties are known. In case of different mounting options of the modules, the convection correlations might change. For modules laying on roofs, there would not be forced convection by wind in their rear side and, even, the natural convection term could be neglected in case there is no air gap in between the roof surface and the module. Consequently, the energy balance equations system should be modified.

6.2.4.1 Example of temperature distribution within modules' layers

Before advancing into the experimental validation of the proposed heat tranfer model, it is solved for a certain instant and temperatures distribution are plotted on figure 6.13. The choosen instant is October 27th 2014 at 13.50 hours, when solar radiation was 1000 W/m^2, wind speed 1 m/s, outdoor dry bulb temperature 22.5°C, dew point temperature 7.4°C and PV efficiency 0.5% (as the batteries were full, on *float* mode).

The temperatures in each layer's surface have been marked with red points on the figure. The heat transfer method has been run under two different hypothesis for convection: forced and natural convection on both surfaces (diagram on the top) or forced and natural convection on front surface and natural convection on the back (diagram on the bottom). During this day, frontal and rear PV/T modules' surface temperatures were measured (blue point on the figure) in order to compare with the theoretically predicted values.

As it can be seen on figure 6.13, the frontal and rear surfaces of the silicon cell are at identical temperatures as it was previously guessed. Predicted cell temperatures are very similar under both convection hypothesis. If the calculated and measured external surface temperatures are compared, the first hypothesis provides a shorter difference between the frontal and back surface temperatures, as it happens with the experimentally measured temperatures.

Before making the choice between one of the two proposed correlations, between both methods is done along two days, which in addition should validate the heat transfer model.
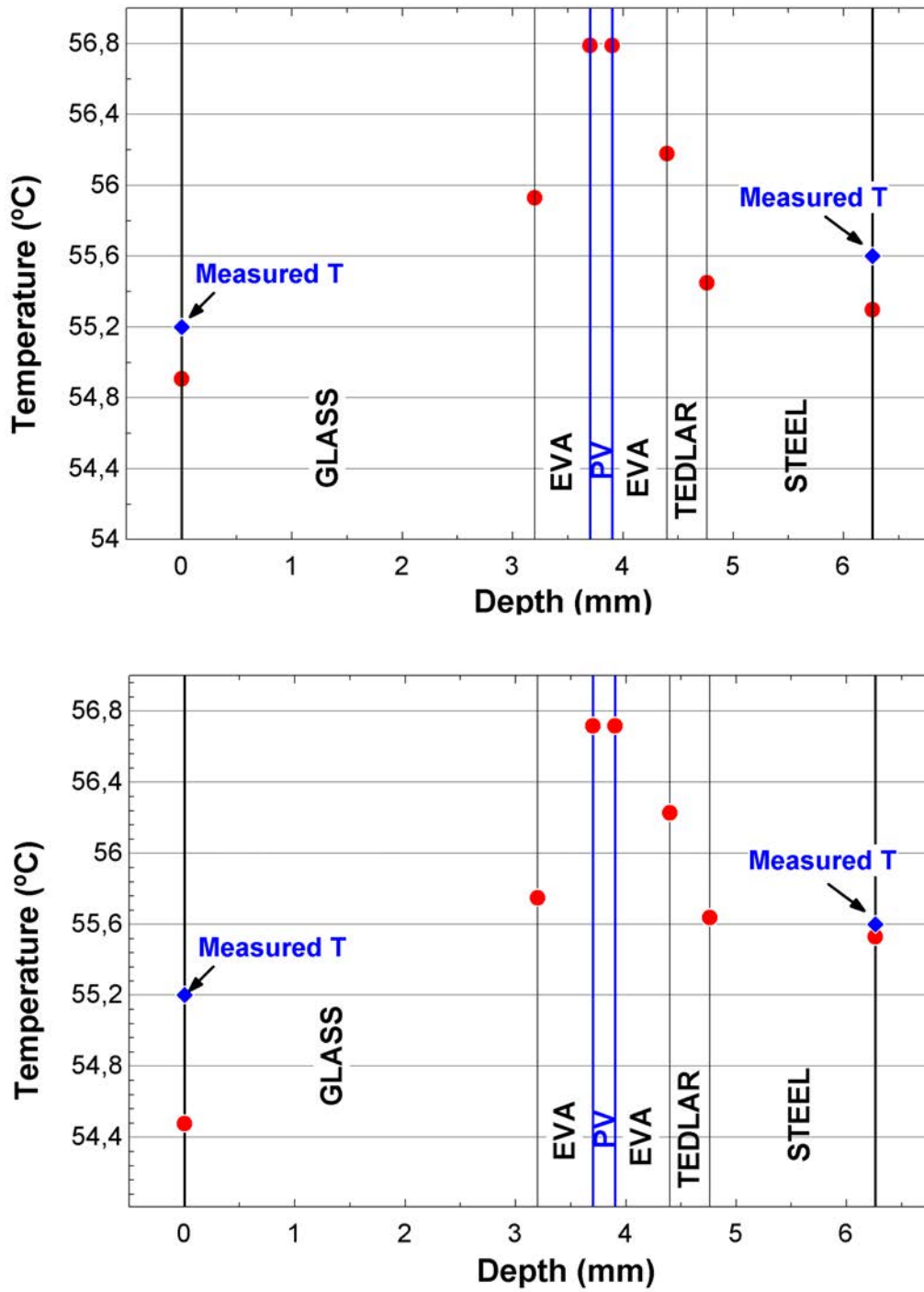
Figure 6.13: Temperature distribution example for both convection hypothesis.

6.3 Experimental validation of the proposed model

Proposed model is tested for some days when external surface temperatures were recorded. During these days, temperature sensors were attached to the frontal and back surface of the PV/T module. The one in the back was attached to the steel surface were it is direct contact with the tedlar layer.

In order to check if the proposed energy balance would match, energy inflow and outflow were calculated independently and compared. So the first equation of the proposed equation system, will be splitted in two no related equations:

$$IN = \tau_{glass} \cdot \tau_{EVA} \cdot G_T \tag{6.76}$$

$$OUT = \dot{q}_{conv_{front}} + \dot{q}_{rad_{front}} + \dot{q}_{conv_{back}} + \dot{q}_{rad_{back}} + P_{PV} \tag{6.77}$$

As one equation is addes to the energy balance equation system one more input is required, that is why, besides mentioned material properties and regular inputs G_T, T_{dp}, T_{odb}, P_{PV} and w_s, measured $T_{surf_{back}}$ is introduced as an input to determine OUT components. If the proposed energy balance along section 6.2 and its assumptions are correct, IN and OUT should be approximately equal.

As it was mentioned on subsection 6.2.3.3, forced and natural convection can be combined under two different assumptions. The experimental validation of the model has been done under both different hyphotesis:

1. forced convection on front glass, natural on both external surfaces. Applying equations: 6.50, 6.68 and 6.69.

2. forced and natural convection on both external surfaces. Applying equations: 6.45, 6.72 and 6.73.

On the following lines, energy balance is calculated for diverse days when surface temperature, electrical production and meteorological conditions were measured. Both IN and OUT terms are calculated independtly and faced one to another.

6.3.1 October 27$^{\text{th}}$ 2014

This clear and mild day is the one represented on figures 6.1 and 6.2. The equations system is solved for both convection hyphotesis.

Summands of energy outflow (PV production and radiative and convective flux) are shown on 6.14, where the difference between both hypothesis can be noticed. As it is shown, during this day, PV production was very low because there was no consumption and batteries were on *float* mode. In both cases, the radiative components behave equally, but in first of them front convection weight much more than rear convection. On the other hand, if forced and natural convection is considered for both surfaces, the front and rear dissipated flux get closer.
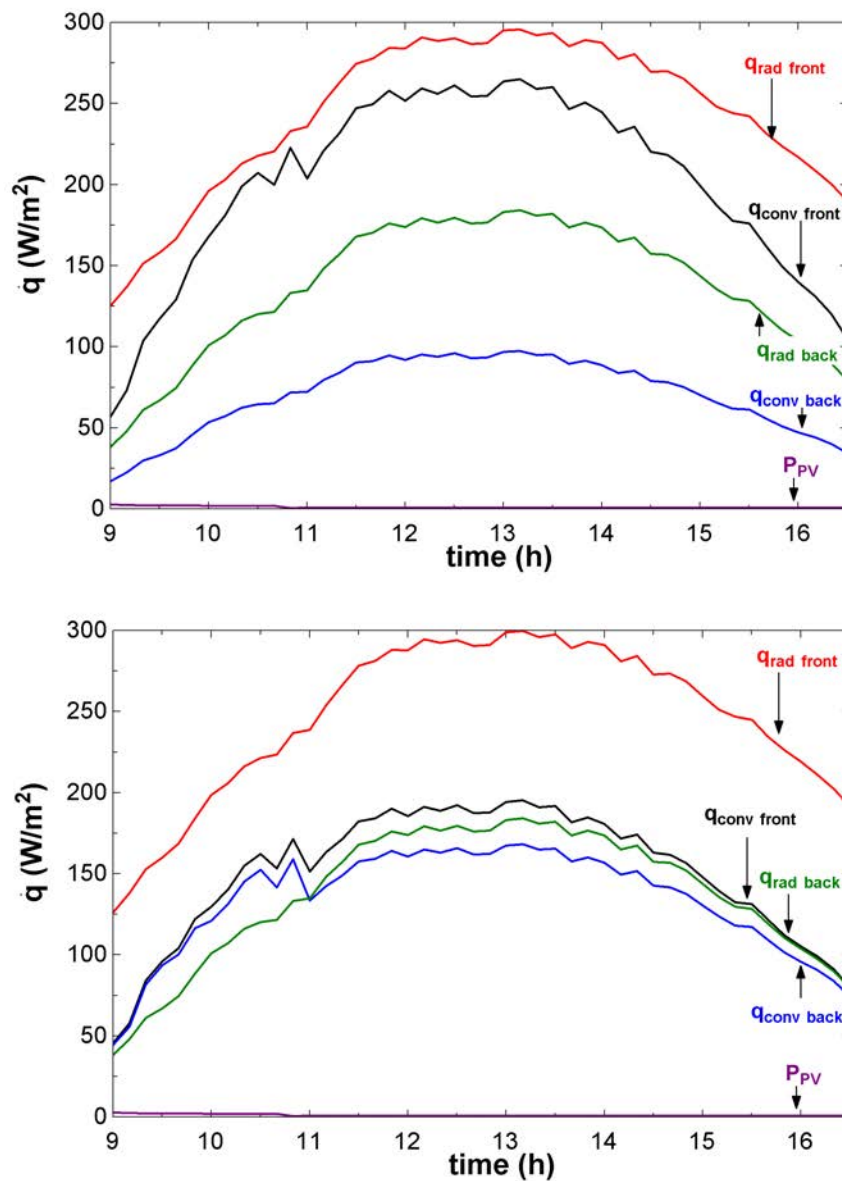
Figure 6.14: Summands of outflow for hypothesis 1 (top) and hypothesis 2 (bottom) for 27/10/2014.

Figure 6.15 shows the energy inflow and outflow for both hyphotesis. As it can be seen, both of them match very similary the IN and OUT balance.
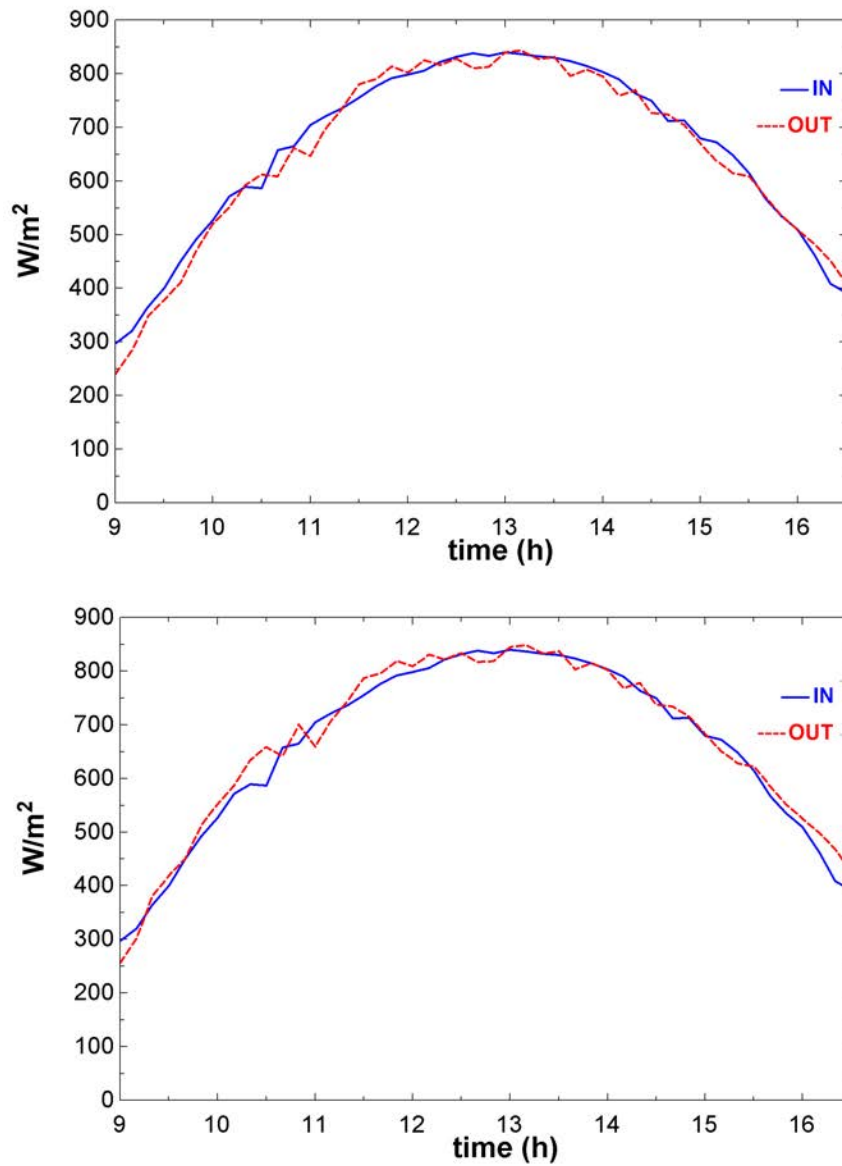
Figure 6.15: Energy IN and OUT for hypothesis 1 (top) and hypothesis 2 (bottom) for 27/10/2014.

As it can be expected, in the second hypothesis, there will be lower temperature gap between front glass surface and back steel surface, as it can be seen on figure 6.16.
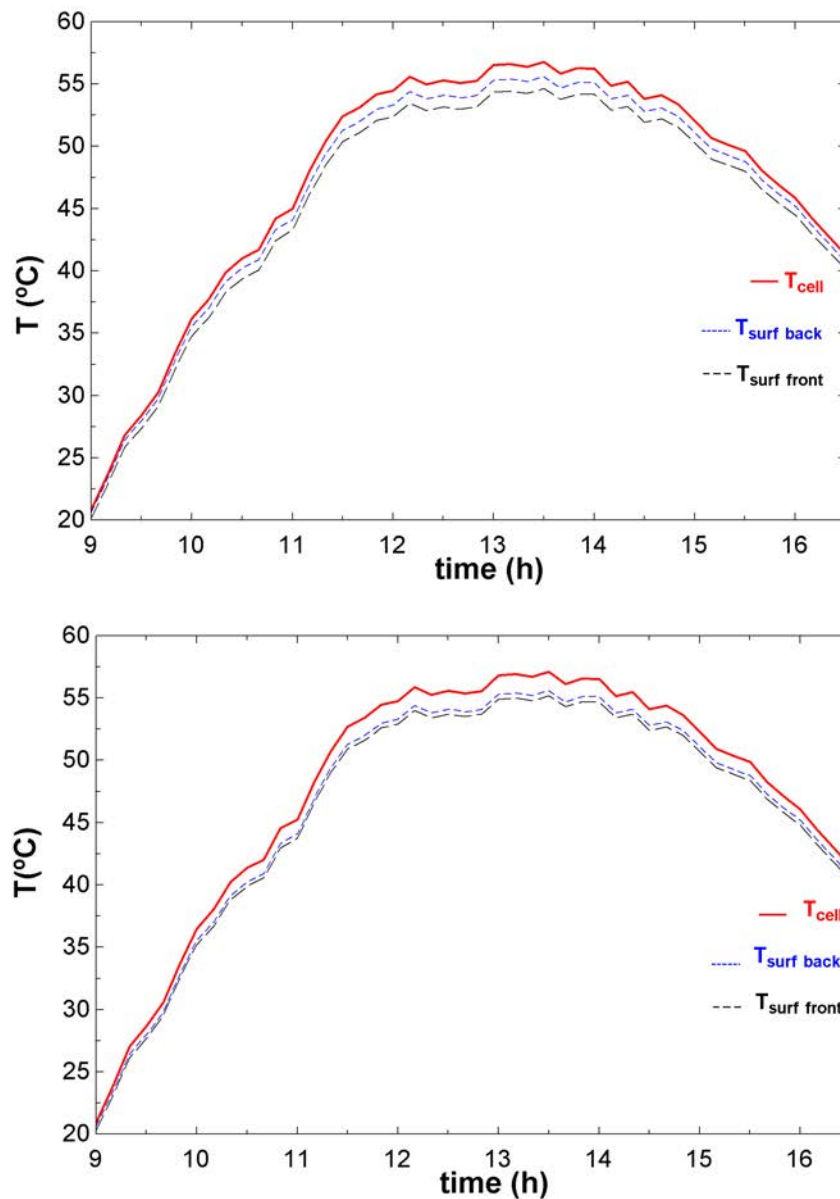
Figure 6.16: Cell and surfaces temperatures for hypothesis 1 (top) and hypothesis 2 (bottom) for 27/10/2014.

During this day, both external surfaces were measured and recorded. Front surface is is not recommended as a measuring point, because it can undermine thermorresistance's measurement accuracy (as it is harder to isolate it from external gain such as solar radiation) and can damage PV production. However, figure 6.17 shows how during central hours of the day, measured front and rear surface temperature lines were very close (see: Error propagation Appendix at the end of this work). If this fact is compared with figure 6.16, it suggests that hypothesis number 2 provides a more realistic solution for external surfaces. On the other hand, predicted cell temperature behaves similarly under both hypothesis.
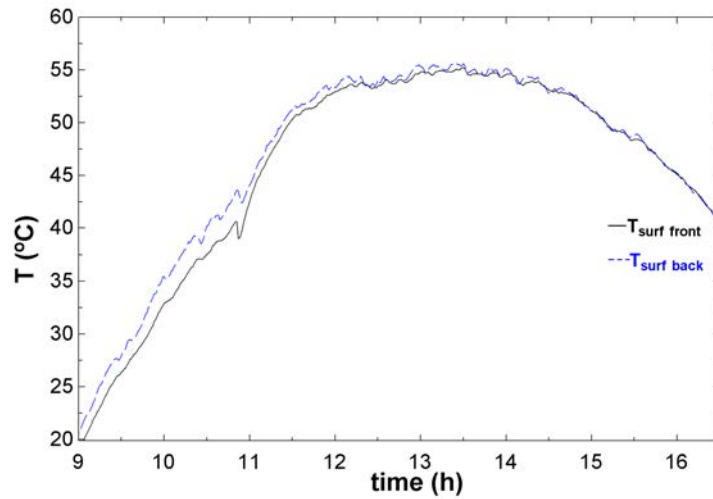
Figure 6.17: Measured front and back surface temperatures for 27/10/2014.

6.3.2 October 30th 2014

An analogous test is carried out for another autumn day, october 30th, which meteorological conditions are shown on figures 6.18 and 6.19. As on previous example, energy balance and temperatures are calculated for two cases: forced convection on front glass, natural on both external surfaces (hypothesis no.1), and forced and natural convection on both external surfaces (hypothesis no.2).
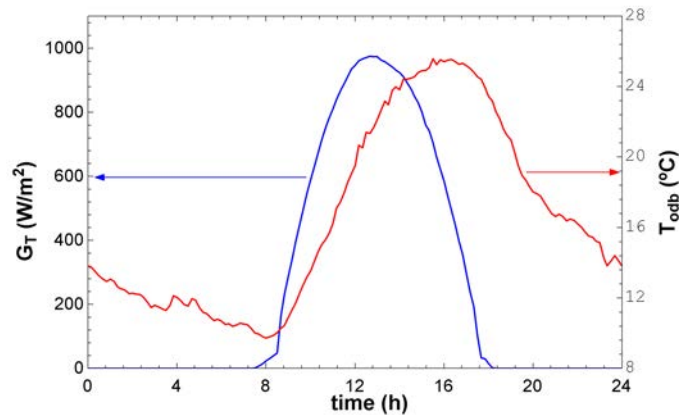
Figure 6.18: Solar radiation on tilted surface and ambient temperature on 30/10/2014.
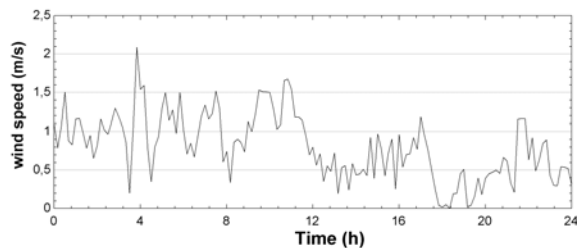
Figure 6.19: Wind speed on 30/10/2014.

Energy outflow summands are descomposed on graph 6.20; total outflow is faced to energy inflow on graph 6.21. IN and OUT fit considering instrument error ranges (see: Error propagation Appendix at the end of this work), as it happened on the previous example. Convective and radiative summands behave in a similar way too: closer front and rear convective flux imply lower temperature difference between front glass and back steels surfaces, as show on fig 6.22.
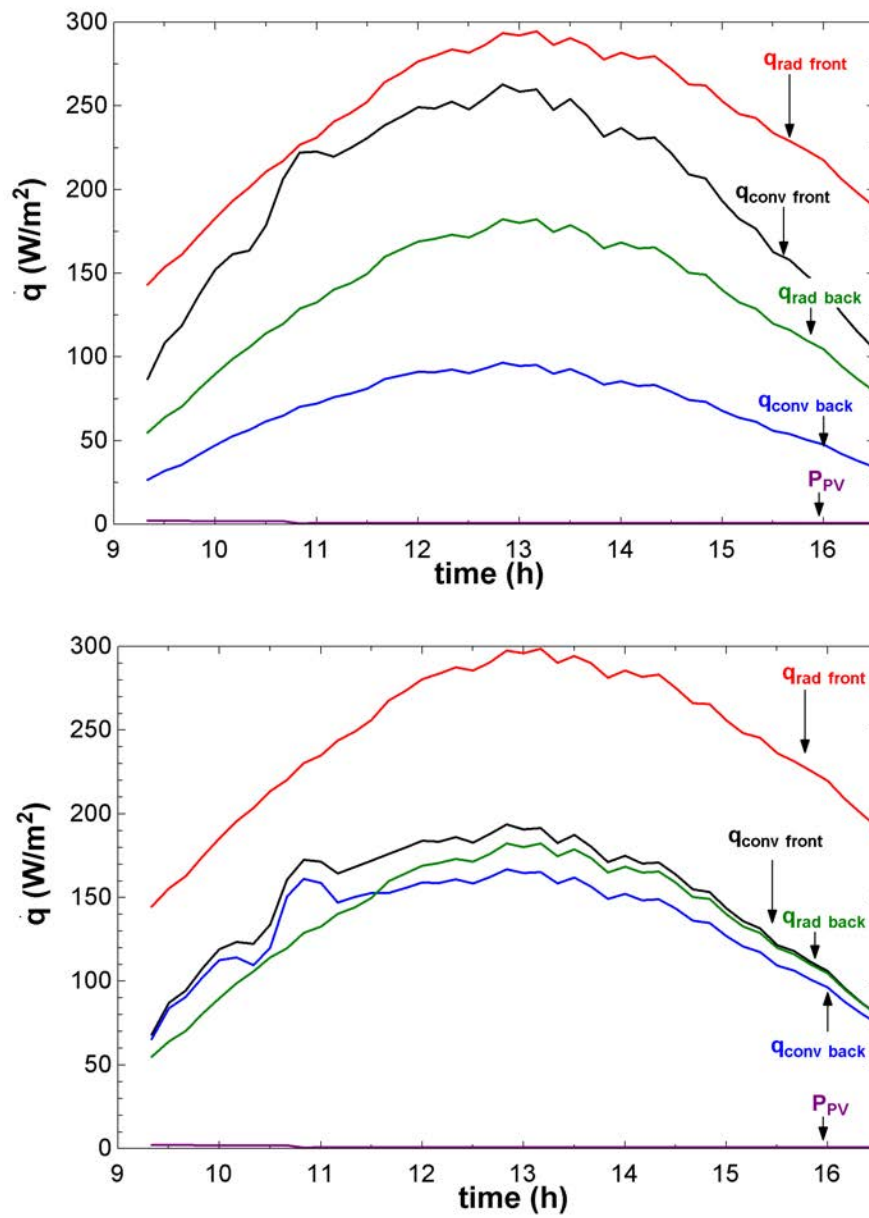
Figure 6.20: Summands of outflow for hypothesis 1 (top) and hypothesis 2 (bottom) for 30/10/2014.
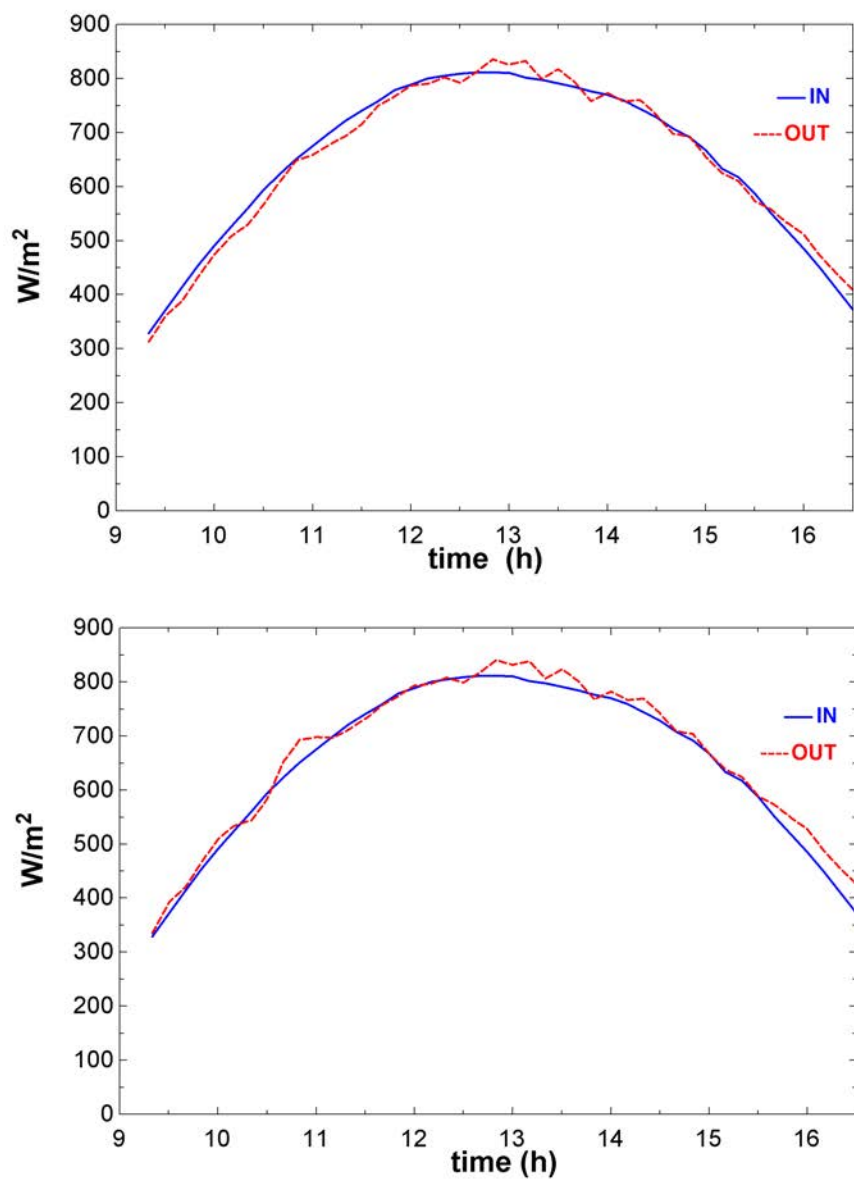
Figure 6.21: Energy IN and OUT for hypothesis 1 (top) and hypothesis 2 (bottom) for 30/10/2014.
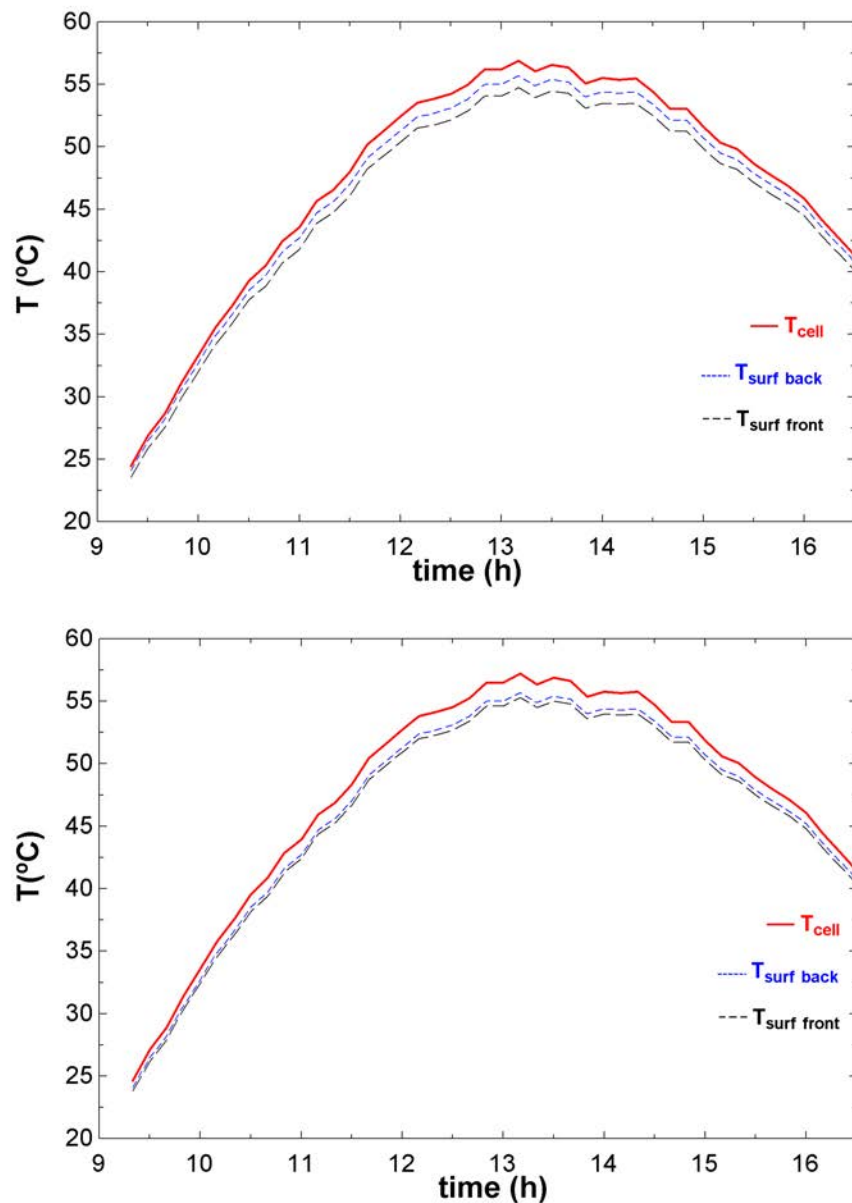
Figure 6.22: Cell and surfaces temperatures for hypothesis 1 (top) and hypothesis 2 (bottom) for 30/10/2014.

6.3.3 Conclusion of the experimental validation

According to the experimental tests exposed above, the heat transfer model along this chapter can be considered sharp enough for obtaining the operating temperature of the silicon cells of specific PV/T modules. In regards to which natural and forced convection combining equations must be used, it can be concluded that both hypothesis are adjusted to the state-of-the-art, providing a similar cell temperature and matching properly the energy inflow and outlflow balances.

From now on, during computational simulation of this research, wind convection will be considered on both external surfaces of the PV/T modules as they are mounted on open-rack, applying equations of hypothesis no. 2. As it has been mentioned, open-rack mounting option exploites the wind effect that cools the modules.

On the following section, this heat transfer model will be run for diverse days, when meteorological conditions and the obtained photovoltaic production were registered, which will predict the temperature evolution for each layer of the PV/T module. The predicted temperature for the external surfaces will be compared with the experimentally measured ones.

6.4 Daily test of heat transfer model for diverse days

Once the heat transfer model has been validated and the convection correlation has been choosen, the model is tested for diverse days, when the surface temperatures were measured. On the following lines, three different winter days are shown, plotting the predicted cell and surface temperatures to compare them with the measured temperature on module's external surface. Additional validation for spring and summer days is shown on appendix A.

6.4.1 January 17th 2015

This cold winter day, the minimum outdoor dry bulb temperature just before sunshine was -2.8 °C and the maximum reached 9.7 °C (fig. 6.23). Wind blew under 1m/s most of the day (fig. 6.24). At sunshine the modules were covered by a frost layer, which last during the first hours of the morning (fig. 6.25).

Figure 6.23: Solar radiation and outdoor dry bulb temperature (17/01/2015).
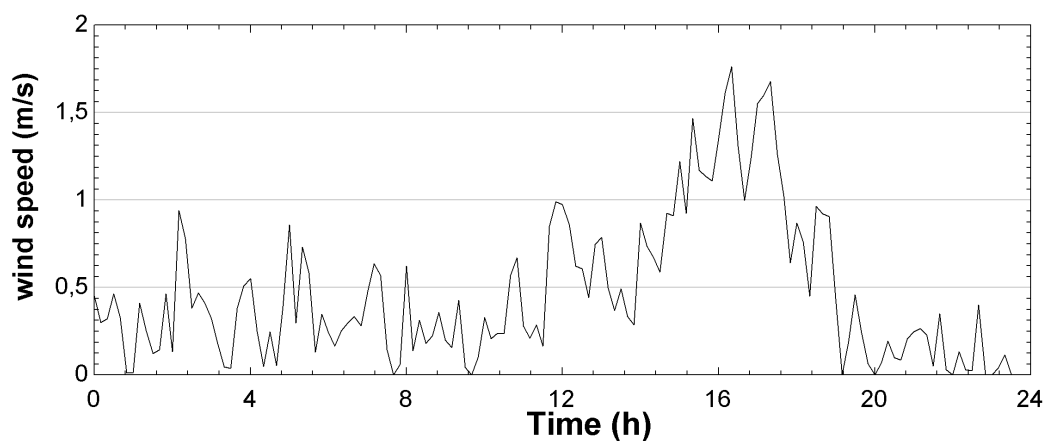
Figure 6.24: Wind speed (17/01/2015).

Figure 6.25: Morning frost over modules' frontal surface.

This day, 10 PV/T modules were connected to charge the batteries and to feed the heat pump. The electrical production of the array, which was adapted to batteries' charge state, is plotted on figure 6.26. On the other hand, 6 modules were left on open-circuit. The rear surface temperature on both type of modules was measured and, as it could be expected, the disconnected ones reached higher temperatures.
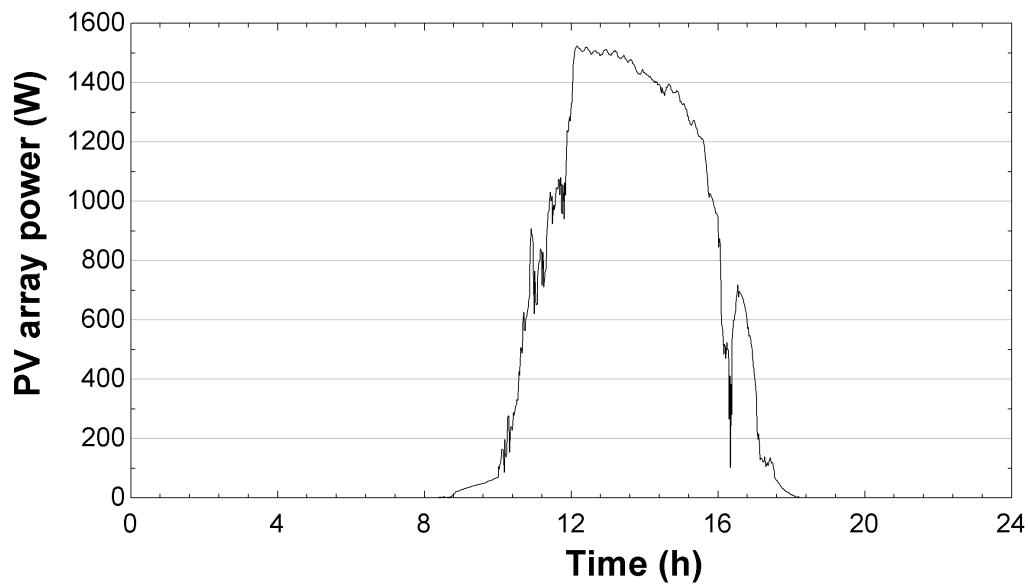
Figure 6.26: PV array's electrical production (17/01/2015).
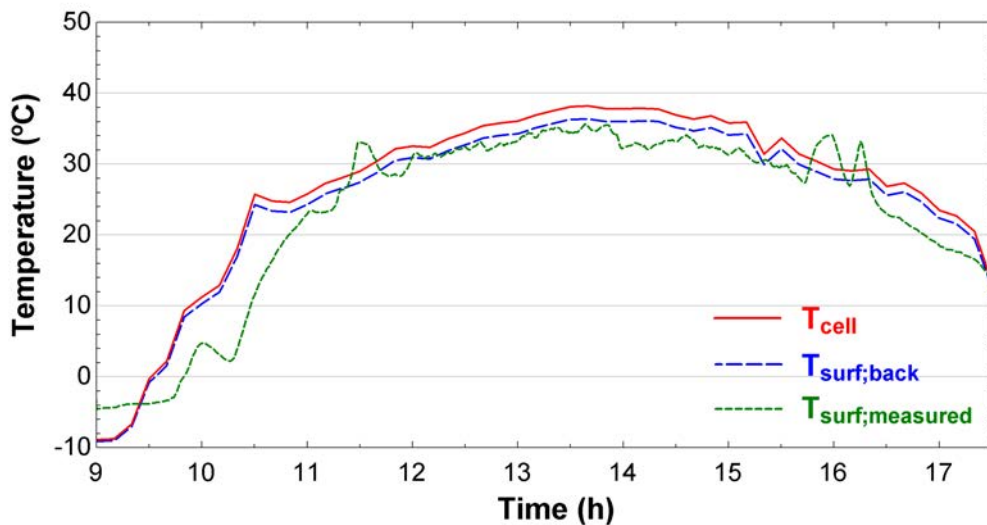
Figure 6.27: Predicted and measured layers' temperatures for a connected module (17/01/2015).

Figure 6.27 shows the thermal behavour of the connected modules. In this case predicted and measured temperatures match during the central hours of the day, but differ on other moments of the day. The main mismatch between predicted and measured surface temperature appears during the first hours of sun, until 11.00 h. The presence of morning frost is not included on the heat transfer model, so this fact may explain why the predicted temperature is higher during that hours. Actually, that day, part of the thermal gain melted the frost layer instead of heating the

module. However, this phenomenon rarely last later than mid-morning, so it doesn't affect to the PV production when solar radiation is higher at central hours of the day.

In any case, the measured back surface temperature did not exceed 34 °C and the predicted cell temperature reached a maximum of 38.2 °C.

On the other hand, figure 6.28 shows the temperature evolution of an open circuit module. As it was expected, the measured temperature was higher, reaching a maximum of 42.1 °C. The maximum predicted cell temperature for these conditions is 44.6 °C. As it occured in the connected case, the heat transfer model predicts a higher surface temperature than the measured one, specially during the early morning hours.
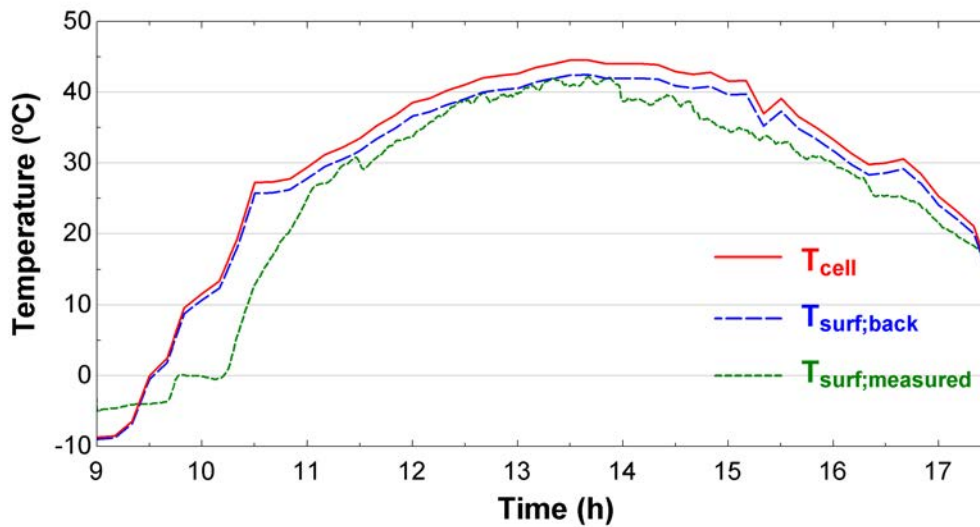
Figure 6.28: Predicted and measured layers' temperatures on a disconnected module (17/01/2015).

6.4.2   January 19th 2015

This cold winter day, the minimum outdoor dry bulb temperature before sunshine was 1.0 °C and the maximum reached 7.0 °C, decreasing to -0.2 °C at midnight (fig. 6.29). The modules were free of frost in the morning and the temperature gradient was lower than January 17th, as it was clouded until around 11 hours. In addition this was a windy day (fig. 6.30) that around midday blew at 5 m/s, so the thermal losses due to forced convection were higher than January 17th.
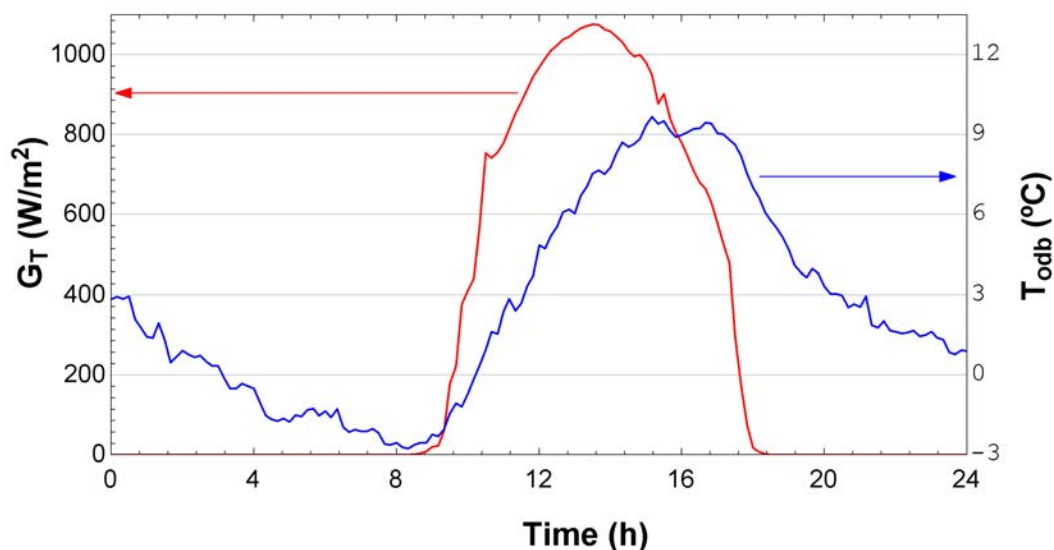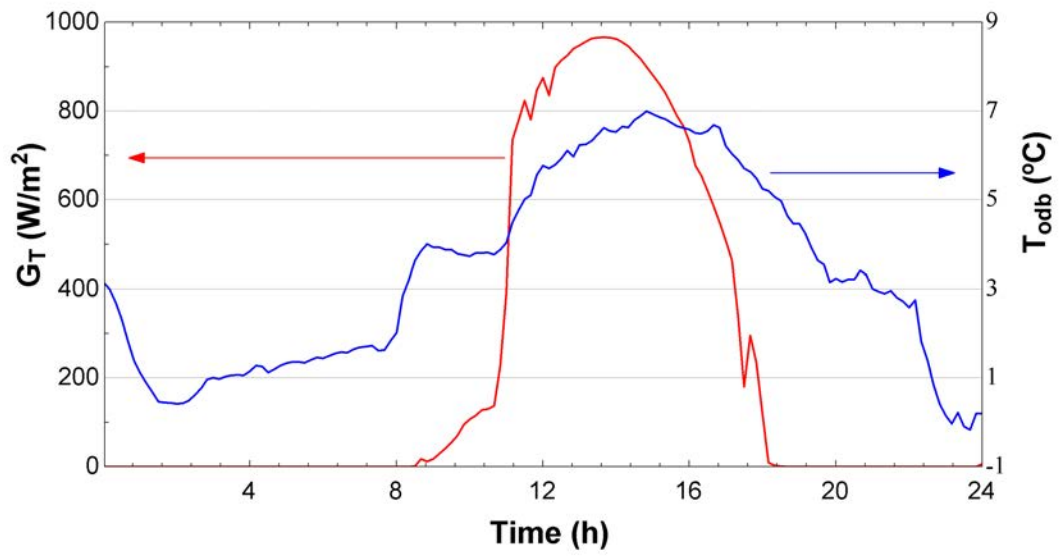
Figure 6.29: Solar radiation and outdoor dry bulb temperature (19/01/2015).
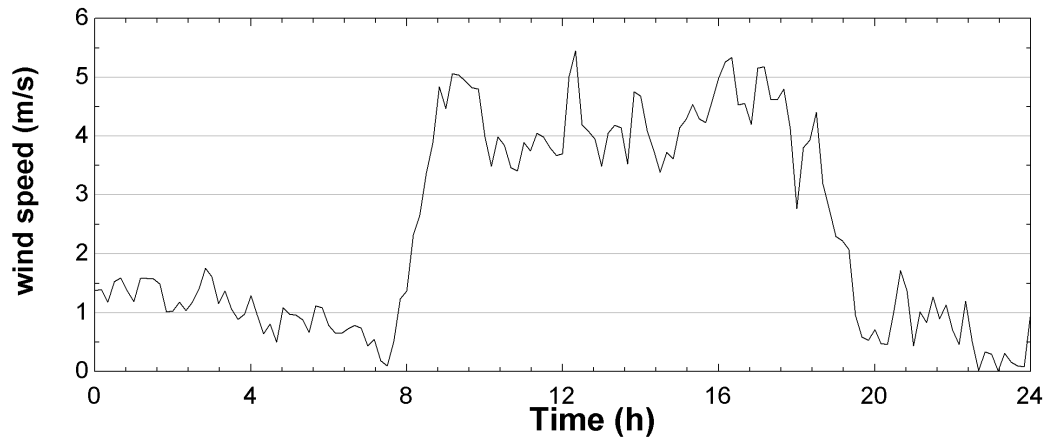
Figure 6.30: Wind speed (19/01/2015).
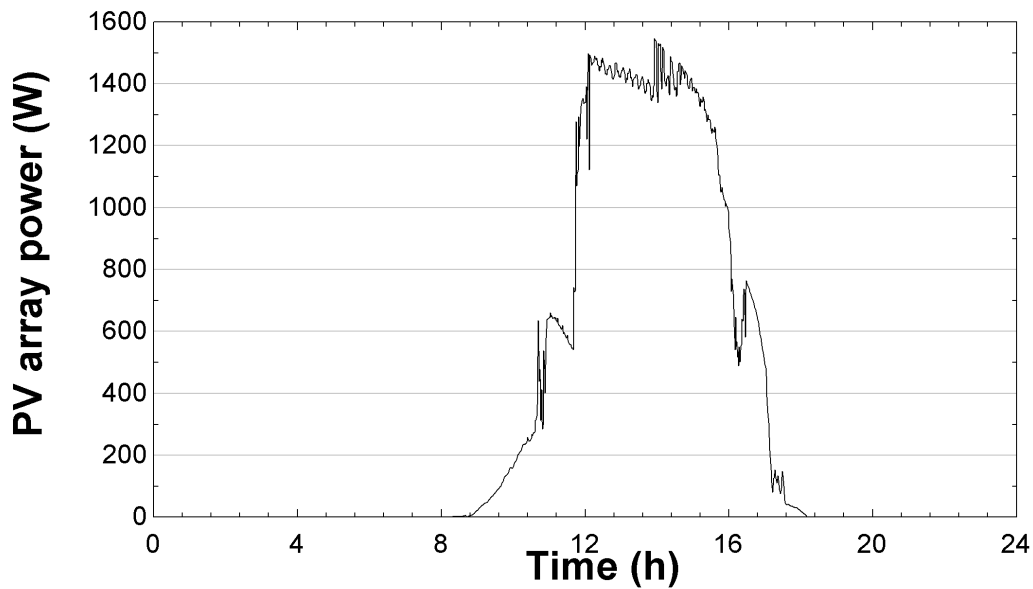
Figure 6.31: PV array's electrical production (19/01/2015).

As it was done on January 17$^{\text{th}}$, 10 PV/T modules were connected to charge the batteries and to feed the heat pump and another 6 modules were left disconnected. The electrical production of the array, which was adapted to batteries' charge state, is plotted on figure 6.31.

Figure 6.32 shows temperatures' evolution along the day on a connected module. Besides some peaks, the predicted and measured surface temperatures match within the accuracy and uncertainty limits. Both measured and predicted temperatures kept below 30 °C. In fact, the maximum predicted temperature for the silicon cells' layer was 28.4 °C.
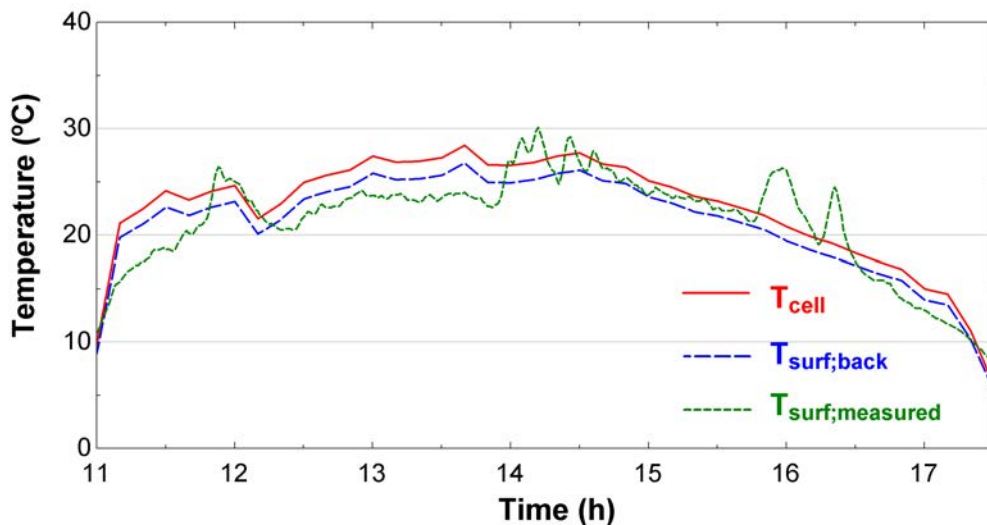
Figure 6.32: Predicted and measured layers' temperatures for a connected module (19/01/2015).

On the other hand, figure 6.33 shows the temperature evolution of an open circuit module. Even in this case, both predicted and measured rear surface temperatures kept under 30 °C. The maximum predicted cell temperature for these conditions was 32.2 °C. In this case, the predicted temperature match even better with the measured temperature's line.
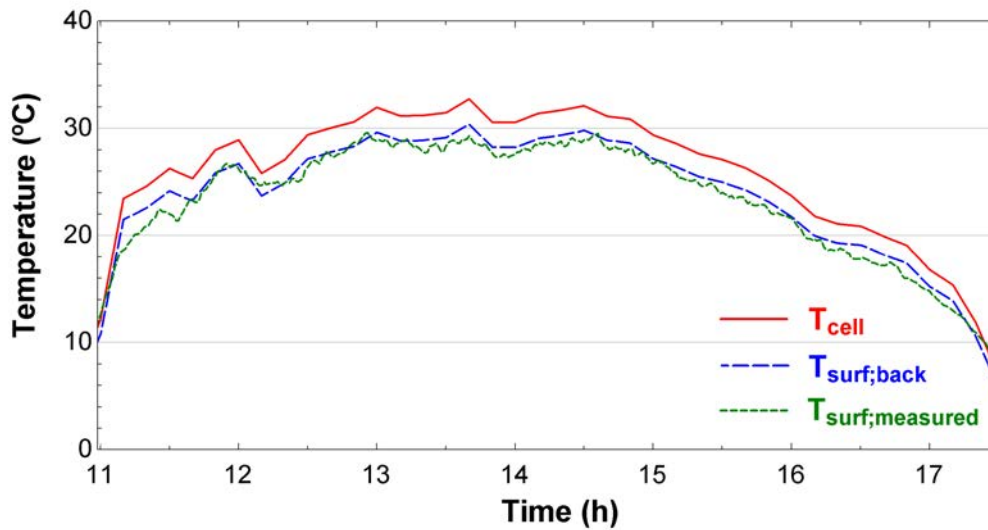
Figure 6.33: Predicted and measured layers' temperatures on a disconnected module (19/01/2015).

6.4.3   February 5$^{\text{th}}$ 2015

This cold winter day, the minimum outdoor dry bulb temperature before sunshine was 1.6 °C and the maximum reached 5.4 °C (fig. 6.34). This was a very windy day that around midday blew over 10 m/s (fig. 6.35), so the thermal losses due to forced convection were very high.
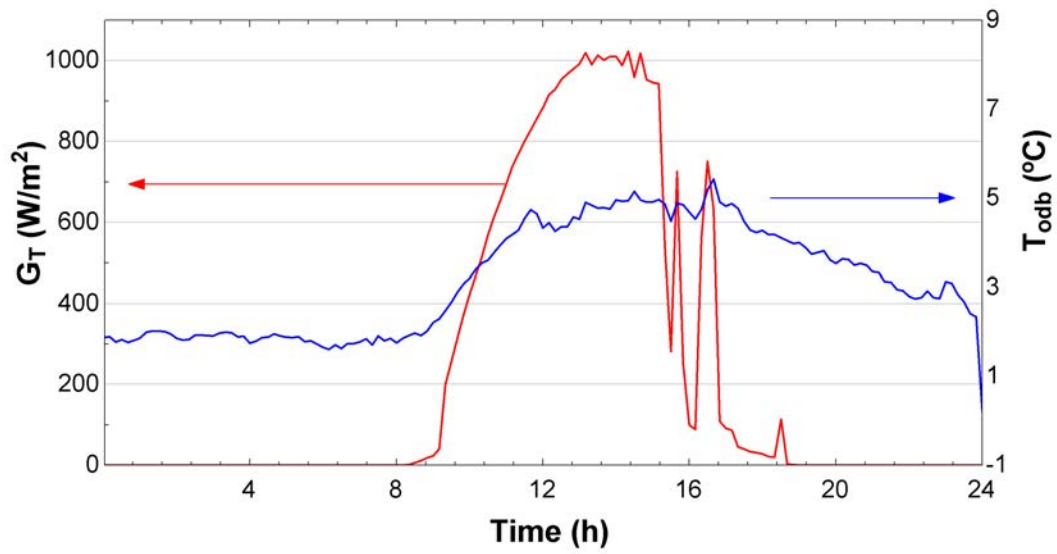
Figure 6.34: Solar radiation and outdoor dry bulb temperature (5/02/2015).
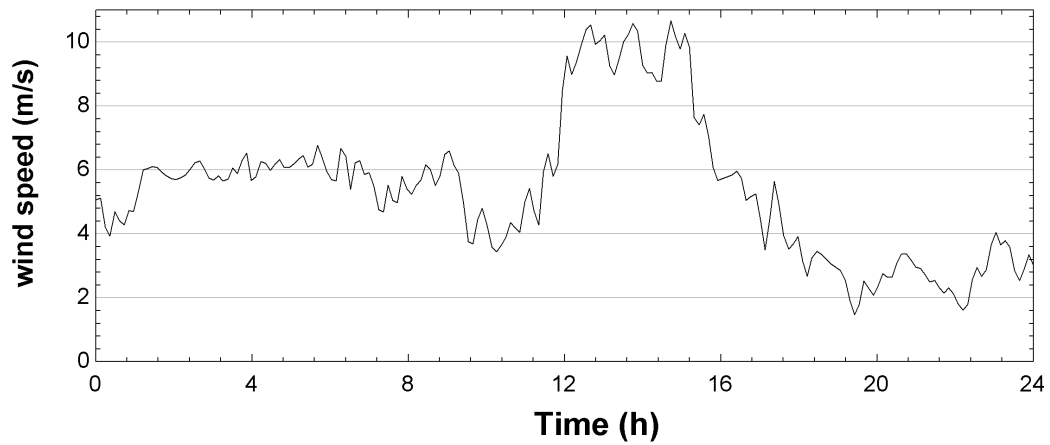
Figure 6.35: Wind speed (5/02/2015).
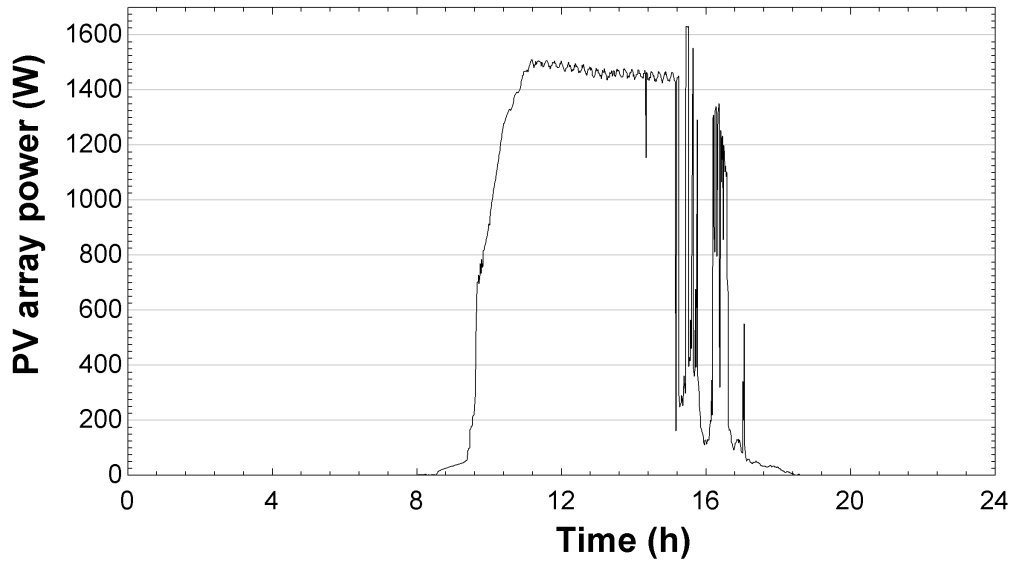
Figure 6.36: PV array's electrical production (5/02/2015).

As it was done on previous examples, 10 PV/T modules were connected to charge the batteries and to feed the heat pump and another 6 modules were left disconnected. The electrical production of the array, which was adapted to batteries' charge state, is plotted on figure 6.36.

Figure 6.37 shows temperatures' evolution along the day on a connected module. Besides some peaks, the predicted and measured surface temperatures match within the accuracy and uncertainty limits. Both measured and predicted temperatures kept below 22 °C.
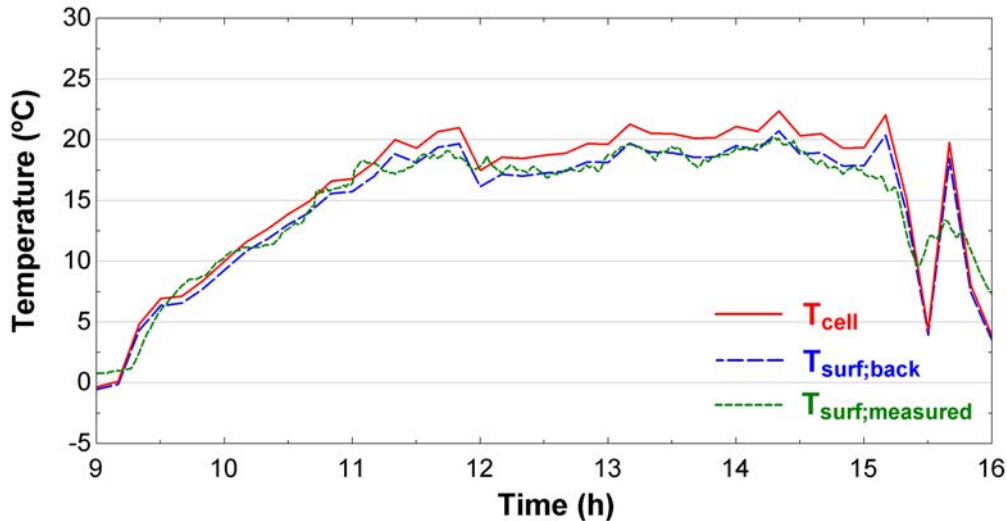
Figure 6.37: Predicted and measured layers' temperatures for a connected module (5/02/2015).

On the other hand, figure 6.38 shows the temperature evolution of an open circuit module.

Both predicted and measured rear surface temperatures kept under 24.5 °C. The maximum predicted cell temperature for these conditions was 25.5 °C. In this case, the simulated temperatures and the measured ones match precisely.
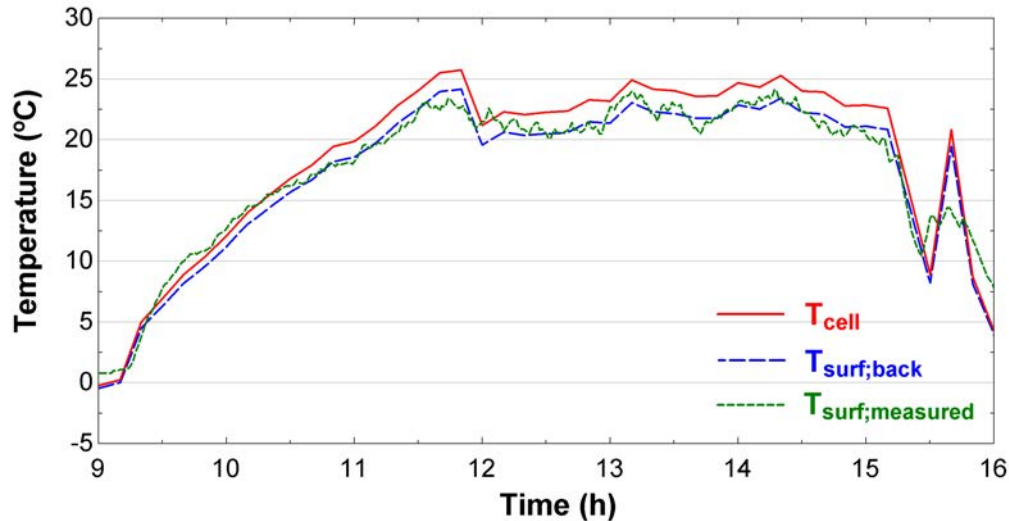
Figure 6.38: Predicted and measured layers' temperatures on a disconnected module (5/02/2015).

6.4.4   Conclusions of the comparation

On these last two sections a wide range of days has been analyzed, including experimental measurements for autumn and winter days and their comparation with the predicted temperatures by the proposed heat transfer model. According to these results, the proposed model can be claimed as accurate enough for cell temperature prediction.

The important role of wind in the cell temperature has been revealed. Contrary to solar thermal collectors, photovoltaic perfomance is benefitted by high wind speeds. Thus, in order to improve the electrical efficiency of a PV or PV/T system, mounting options that take advantage of wind incidence should be considered. As it said, in this work the PV array was mounted on an open-rack, that benefits this natural cooling effect on the solar cells.

The author would like to remark that this model add to the scientific literature a sharp cell temperature prediction for any type of PV or PV/T modules, once their composition and layers thickness are known. In the case of rooftop or facade integrated PV systems, the heat exchange on the back surface of the modules could decrease. The heat transfer model could be easily adapted, neglecting the forced convection losses on the back surface or adding a facade heat conduction term in each case.

The proposed heat transfer model consideres explicitly the PV production and, once implemented, is quick, it does not require large computing capacity.

Chapter 7

PV production model simulation

Once the heat transfer model has been validated, it can be assembled with the PV production predicting model in order to simulate daily and seasonal performance of a PV array. After discussing some computational issues of the model (section 7.1) and possible losses within arrays (section 7.2), PV production model is simulated for certain days and its results compared with experimentally achieved ones (section 7.3). After precising the accuracy of the proposed model, it is simulated for a whole heating season in section 7.5. Finally, after guessing the operating cell temperatures, the potential use of PV/T modules is discussed in section 7.6.

7.1   Cell temperature - efficiency iteration

Probably the reader has noticed that the heat transfer model equation system proposed on section 6.2.4 includes photovoltaic efficiency, η, as an input in order to determine cell temperature, T_{cell}. However, this is an implicit equation system, as the efficiency depends on cell temperature too. Therefore, this is a trial and error case. The first step is to obtain cell temperature through the heat transfer model, using as guess value for η : the value for STC. Once the cell temperature is obtained, cell efficiency is calculated through the simplified method expressed by equation 5.12. Obtained efficiency is compared with the previous guess value, until the process converges, which will occur rapidly as efficiency is not an strong variable on the heat transfer model. An example of this iteration is shown now.

Example: For a given PV/T module, with the electrical parameters listed on table 4.1, in a sunny spring day, at midday, solar radiation over a tilted module is 1000 W/m^2, wind speed 1 m/s, $T_{odb} = 25$ °C and $T_{dp} = 8$ °C. The initial guess value for efficiency is the nominal one, $\eta = 0.1373$. The simplified method (eq. 5.12) is applied for obtaining the efficiency. The iteration process provides the following:

$$\eta = 0.1373 \rightarrow T_{cell} = 58.69 \rightarrow \eta = 0.1151 \rightarrow T_{cell} = 58.76 \rightarrow \eta = 0.1151 \rightarrow T_{cell} = 58.76$$

So, after 3 iterations, the final solution is obtained. Under that meteorological conditions, cell temperature will be 58.76 °C and maximum achievable efficiency 11.51%.

Instead of applying the simplified method, if the five parameter equation is solved as explained on section 5.2, for a 58.69 °C cell temperature, the maximum achievable efficiency would be

11.54%. So, apparently, both methods calculate a similar efficiency at the maximum power point, being the simplified method quicker.

7.2   Energy output of a PV array

The electrical nominal output of a PV array composed of N numbers of modules would be equivalent to that number multiplied to the predicted PV power for a single module:

$$P_{PVMA} = N_{mod} \cdot P_{PV} = N_{mod} \cdot \eta \cdot G_T \cdot A_{mod} \tag{7.1}$$

However the conditions on all the modules of the array can be not exactly identical due to partial shading or diverse wind incident angle that can vary slightly each module's maximum power point for a certain instant. Therefore, the MPPT controller will adapt the array's global voltage to maximize the production, however the chosen voltage might not be the the maximum power point voltage for every module if their I-V curves are not identical for given solar radiation and cell temperature conditions. For standard test conditions, array's voltage at maximum power point, as it has been explained, will be 47.6 V, that entails 23.8 V at each module. However, if one module is partially shaded by a cloud or voltage has decreased due to cables' resistance, operating at that voltage will not provide the maximum power, reducing whole array's output. This unwanted effect is known as mismatch and has been studied by diverse authors, although their conclusions differ.

Losses due to partial shading can be up to 7% in a series-parallel connected array according to Picault et al. [2010]. However, others authors like Wurster and Schubert [2014] considere that the mismatch losses do not worth the installation of multiple MPPT controller for an array.

An experimental work comparing type of connections among silicon cells and its influence on mismatch losses can by consulted on the work of Forniés et al. [2013].

In addition, the PV power that reaches the controller might be slightly lower to the real produced electricity, due to electrical losses in the transport process from the modules to the controller and the rest of consumption components. In particular, the electrical power disipated by Joule's effect due to cable's electrical resistance will be defined, according to Ohm's law, by :

$$P_{Joule} = V \cdot I = \rho \cdot \frac{L}{\phi} \cdot I^2 \tag{7.2}$$

In the case that maximum power is produced at the array, as it said on section 4.3, a current of 45.36A will pass through 16m of cable (cross section, ϕ, of 16 mm^2) from the array to inside of the building and 7.56A will pass among the modules' connection 20m of cable (cross section of 4 mm^2). Copper's resistivity is 16.78 nΩ·m, so the power losses in this case would be 27.6W out of 2160W, which is a 1.3%.

In the present model validation, equation 7.1 will be assumed, bearing in mind that the real obtained PV production (measured at the controller) can be affected by explained mismatch and conduction losses.

7.3   Daily tests of the PV production model

To test the proposed PV production model, it will be compared with experimental results obtained in maximum PV production days. To ensure that the controller stayed in maximum power production mode, these days the PV system did not feed the heat pump, but a load of diverse resistances were connected to the batteries, trying to adapt the consumption to the PV production. On the following lines two winter days are used as validating examples. In appendix A a warm day example for different number of modules is attached too.

7.3.1   February 19th 2014

During this clear and cold day (fig. 7.1), 8 PV/T modules were connected to the controller. The wind blew at an average speed of 0.4m/s (fig. 7.2)
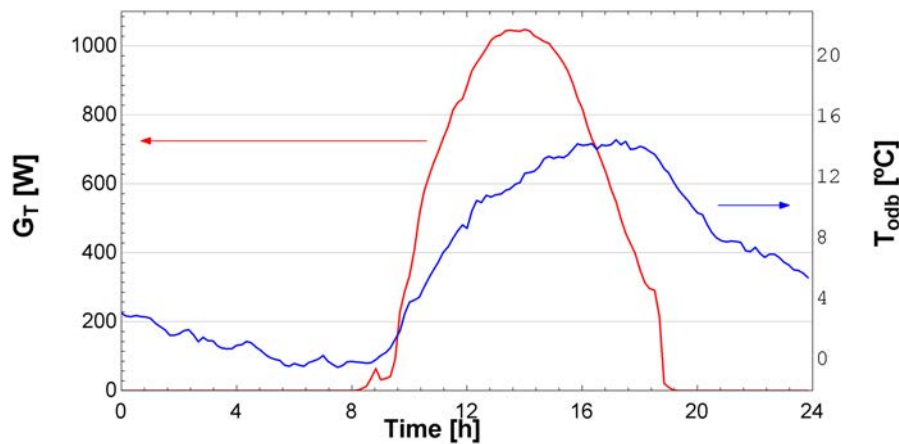
Figure 7.1: Solar radiation and outdoor dry bulb temperature (19/02/2014).
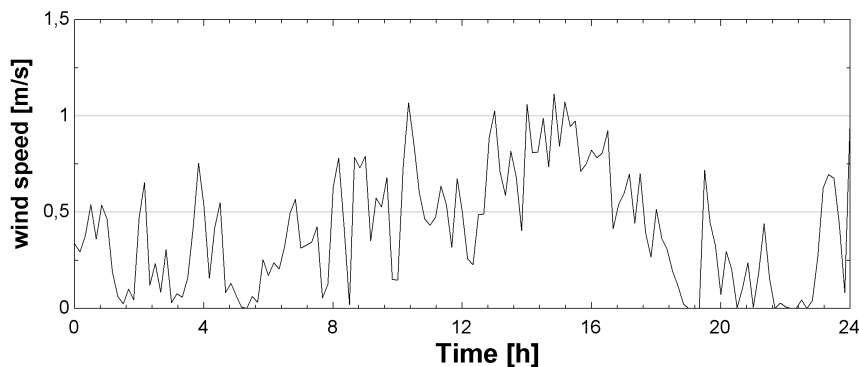
Figure 7.2: Wind speed (19/02/2014).

7.3.1.1   Experimental result

Figure 7.3 shows the PV production measured by the controller and the load of diverse resistances, $\dot{W}_{batt}$, that kept the controller in $MPPT$ mode. The total electricity extracted from the batteries for this purpose was 7.99 kWh.

Along the day, the intercepted solar energy by array's total surface (10.5 m^2) was 72.12 kWh and array's whole electrical production was 8.65 kWh. The maximum array output was 1283.9W (160.5 kW per module).
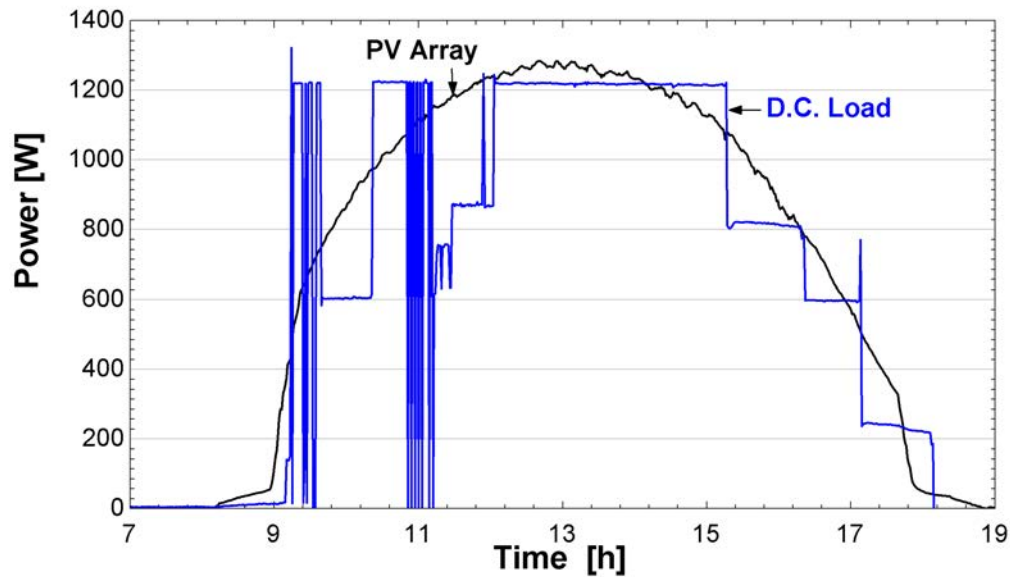
Figure 7.3: Experimental PV array's output and consumption from the batteries (19/02/2014).

7.3.1.2   Simulation result

For the given meteorological conditions, photovoltaic prediction model is run. According to the model, the maximum cell temperature was 52.2°C and its average temperature during the sunshine hours was 31.8°C. These temperatures are higher than other winter days due to the low wind speed, high solar radiation and outdoor dry bulb temperature over 10°C at central hours of the day. Therefore, the efficiency decreased as the cell temperature increased. The efficiency curve according to the model simulation is plotted on figure 7.4. As it can be observed, the achieved efficiency was over nominal one (13.73% refered to total area) at early morning and afternoon, and below it at central hours of the day.

Figure 7.4: Simulated photovoltaic efficiency (19/02/2014).

The predicted array's production by the proposed model is shown on figure 7.5. The predicted daily electrical production would be 8.94 kWh, which is higher than the experimentally obtained electricity.
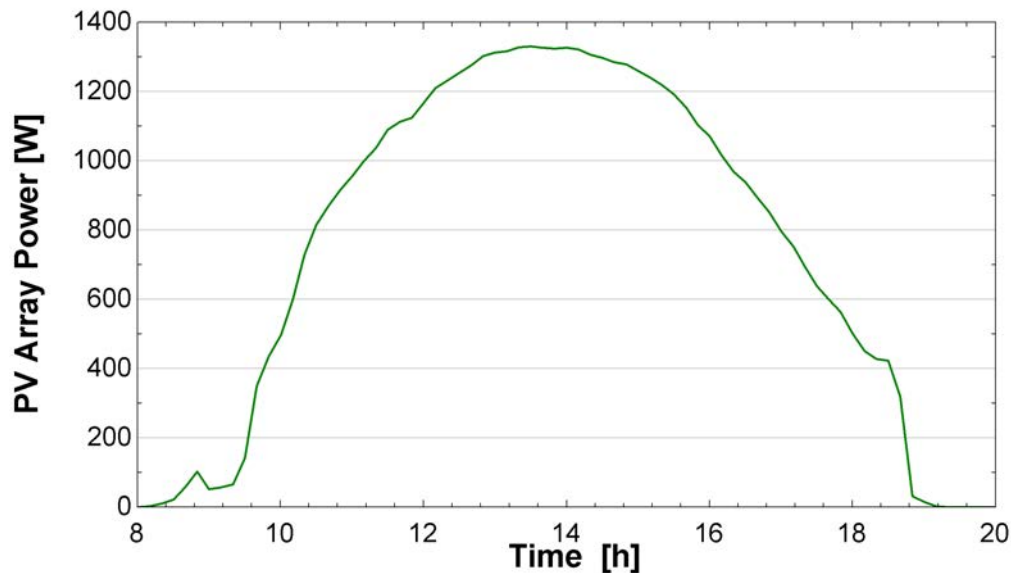
Figure 7.5: Simulated PV array production (19/02/2014).

The simulation predicted 0.29kWh extra of photovoltaic production that were not registered at the controller. As it was explained on section 7.2, Joule effect conduction losses are calculated taking into account the changing value of intensity along the day and 0.08kWh of losses are quantified. The other 0.21kWh would be related to mismatch and/or additional losses.

7.3.2   January 28$^{\text{th}}$ 2015

During this clear and cold day winter (fig. 7.6), again 8 PV/T modules were connected to the controller. Wind blew over 2m/s at night, decreasing during sun hours (fig. 7.2). The daily average wind speed was 0.8m/s.
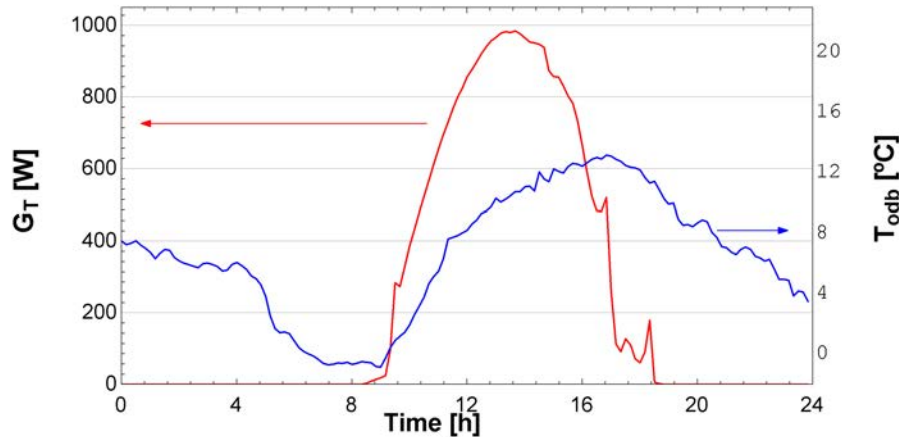
Figure 7.6: Solar radiation and outdoor dry bulb temperature (28/01/2015).
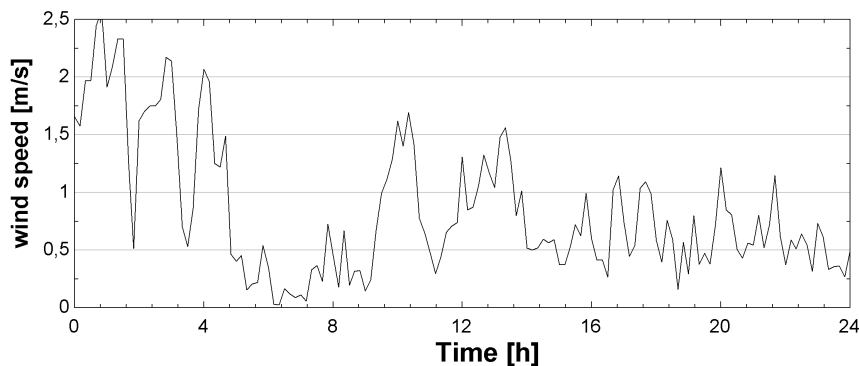
Figure 7.7: Wind speed (28/01/2015).

7.3.2.1   Experimental result

Figure 7.8 shows the PV production measured by the controller and the load of diverse resistances, $\dot{W}_{batt}$, that kept the controller in $MPPT$ mode. The total electricity extracted from the batteries for this purpose was 6.10 kWh.

Along the day, the intercepted solar energy by array's total surface (10.5 m^2) was 60.60 kWh and array's whole electrical production was 7.18 kWh. The maximum array output was 1276.7W (159.6 kW per module).
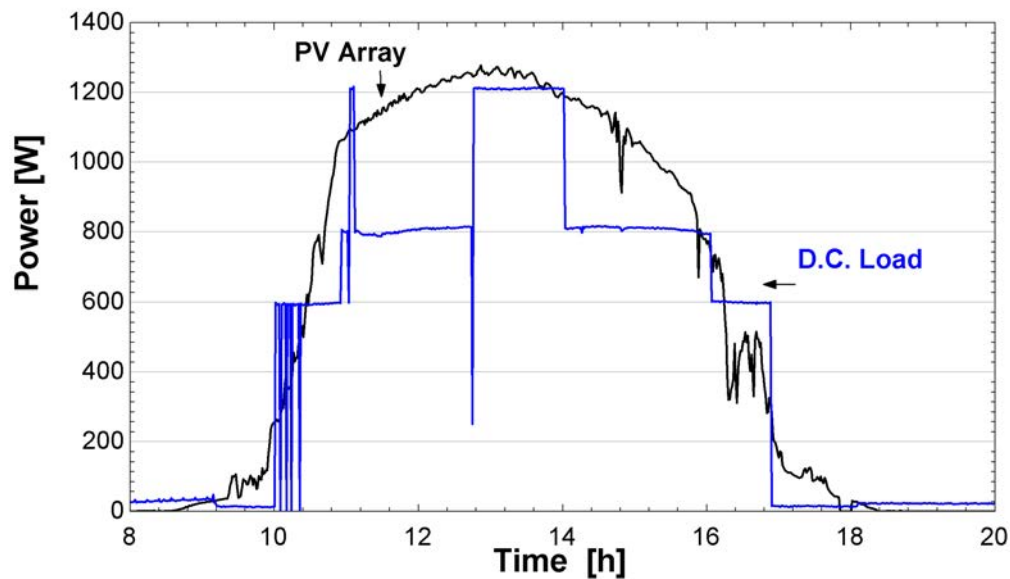
Figure 7.8: Experimental PV array's output and consumption from the batteries (28/01/2015).

7.3.2.2 Simulation result

For the given meteorological conditions, photovoltaic prediction model is run. According to the model, the maximum cell temperature was 48.1°C and its average temperature during the sunshine hours was 28.8°C.

The efficiency curve according to the model simulation is plotted on figure 7.9, which behaves in a similar way to the one in the previous example. As it can be observed, the achieved efficiency was over nominal one (13.73% refered to total area) at early morning and afternoon, and below it at central hours of the day.
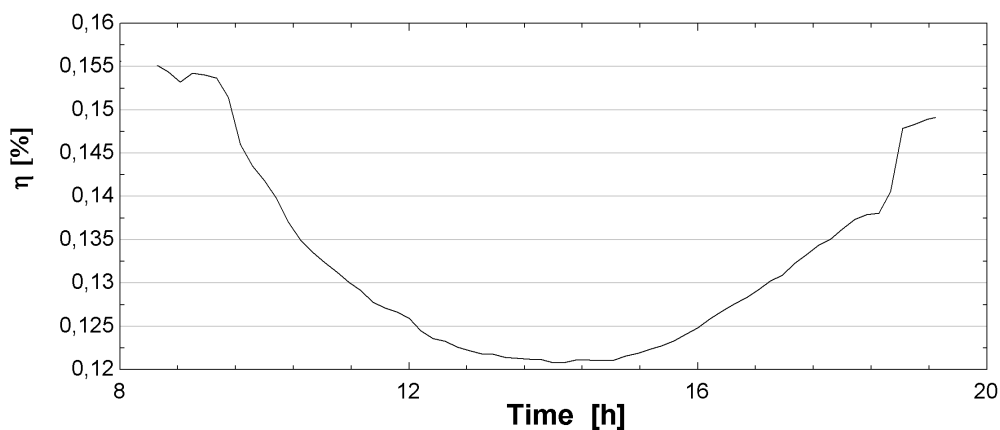
Figure 7.9: Photovoltaic efficiency (28/01/2015).
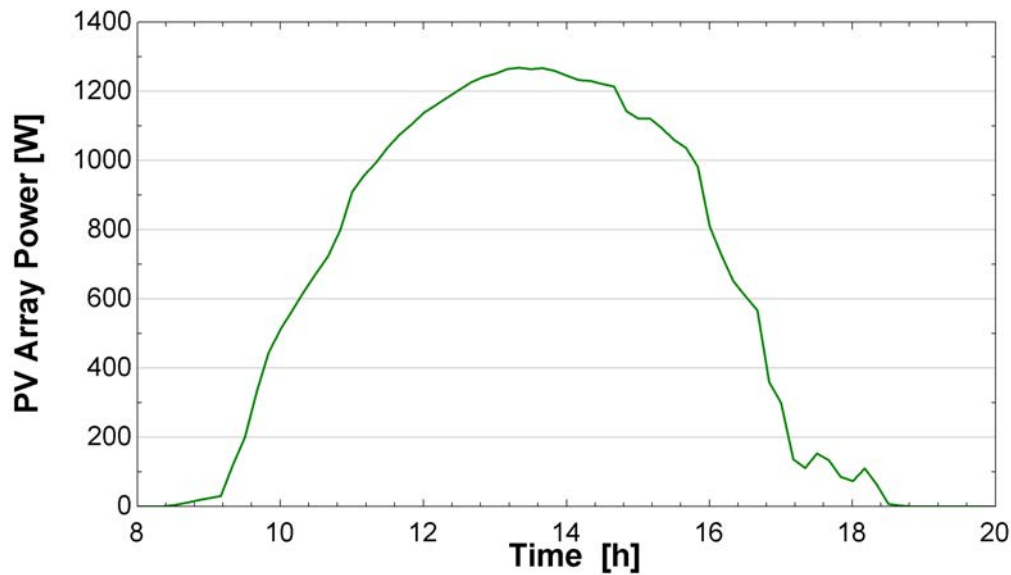
Figure 7.10: Simulated PV array production (28/01/2015).

The predicted array's production by the proposed model is shown on figure 7.10. The predicted daily electrical production would be 7.68kWh, which is higher also than the experimentally obtained electricity.

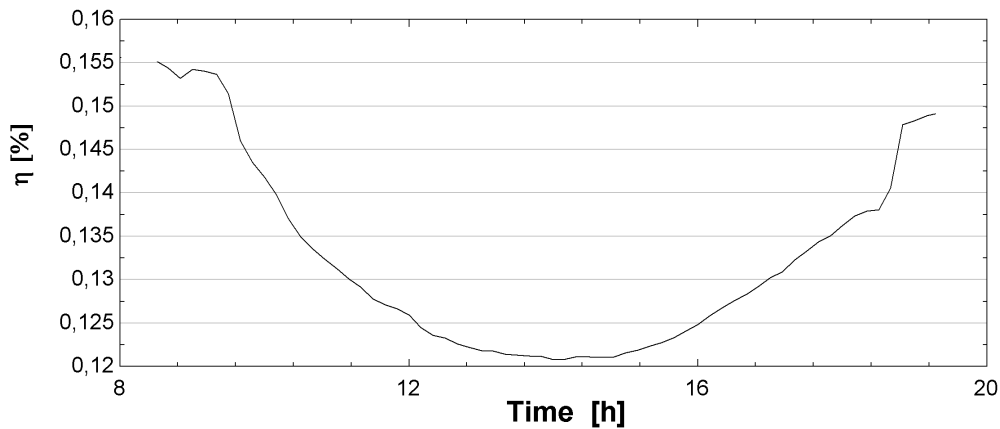The simulation predicted 0.50kWh extra of photovoltaic production that were not registered at the controller. The losses due Joule effect in conduction were 0.06kWh. The rest of the losses would be related to mismatch and/or additional effects.

7.3.3 Conclusions of the test

In both examples, the predicted PV production through simulation exceeds the experimentally obtained production. As it was mentioned on section 7.2, equation 7.1 was applied on simulation without considering any conduction or mismatch losses. However, the experimentally PV production is measured at the controller, so the value has been reduced by those losses between each module and the controller. Considering both examples (and the summer one added in appendix A), it can be concluded that losses cannot be neglected in the simulation model. As it was explained on 7.2, conduction losses along the cables due to Joule effect can be quantified and, from now on, will be included in the simulations. Additional losses related with mismatch effects, degradation and/or dust deposition on modules' surface are hard to quantify and will not be included.

On the other hand, the deviation between measured and simulated production is within margins of uncertainty, as indicated in the next section.

7.4 Uncertainty analysis

The proposed model, as it is based on measured meteorological variables, will provide cell temperature and, consequently, photovoltaic power with certain uncertainty. The measured or calculated variables plotted on the previous daily tests present an uncertainty propagation that has been calculated as indicated on section 4.9.

The mean values of uncertainty on the electrical output from the batteries, $\dot{W}_{batt}$, obtained cell temperature, the measured PV power and the calculated one through the proposed model are listed on table 7.1.

Represented function	Uncertainty [%]
Measured W_{batt}	0.5
Measured P_{PVMA}	2.8
Calculated T_{cell}	2.7
Calculated P_{PVMA}	4.0

Table 7.1: Uncertainty on represented variables.

7.5 Seasonal simulation for the 2012-13 heating period

During the 2012-13 heating period, 12 PV/T modules were used for feeding the heat pump facility previously explained. In the following chapter the experimental results of this photovoltaic heating facility are detailed and its performance as isolated system.

In order to compare the obtained photovoltaic production, which as isolated system was conditioned by production-demand mismatch, and the maximum achievable photovoltaic production if the array had been constantly kept on it maximum power point, the proposed cell temperature-PV production model has been run.

The photovoltaic electricity produced each month of the period is shown on figure 7.11, where the total electricity was 1265.8 kWh. During this period, as it has been explained, the thermal hydraulic circuit of the PV/T modules was kept empty. The cell temperature usually reached its instant maximum value around solar midday, this maximum value's monthly average is plotted in red on figure 7.12. Although the maximum instant values reached over 50 °C in february, due to high insolation, and in april, when the outdoor mean temperatures were higher and days longer, along the sunshine hours, the average cell temperature was quite lower, keeping below 28 °C even in april.

7.6 Potential use of PV/T modules

As it said, during this work the use of the thermal component of the PV/T modules was rejected The hypothesis was that the reachable temperatures would not considered high enough for a thermal application of them. Once heat transfer model has been developed and experimentally validated, some conclusions about the application of PV/T modules arise.

For central Spain climate, this type of PV/T modules' thermal performance seems to be neglectible on winter. Around solar midday on sunny winter days, the solar cells' temperature
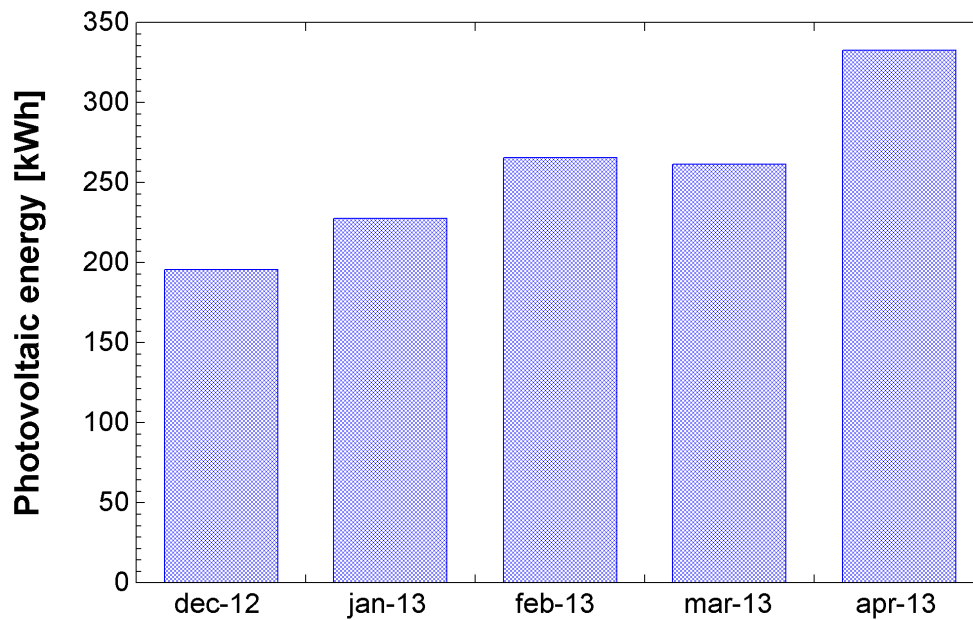
Figure 7.11: Calculated PV array production along the heating period.

reach peak values up to 45 °C, but during most of sunshine hours PV/T modules' temperatures are lower. In fact, these temperatures keep frequently below the STC temperature, 25 °C, reaching photovoltaic efficiency higher than the nominal one. As it has been plotted in this chapter. Therefore, pumping water through the PV/T modules' thermal circuit would provide low thermal gain and the electrical efficiency would be just slightly higher than the achievable one by regular PV modules.

On the other hand, the authors have observed that on summer, the PV/T modules reached temperature peaks of 65-70 °C (Appendix A). In this case, the use of PV/T modules would provide a significant thermal gain, according to manufacturer's specifications, and at the same time, as heat is partially removed from the solar cells, the electrical efficiency would be improved. However, the thermal demand of a Spanish home of 3 people on summer would be about 4 kWh [IDAE, 2011], which according to manufacturer's datasheet, would be satisfied by just 3-4 PV/T modules. It must be remarked that 14 m2 of PV cells were required for a 35 m2 house heat pump. For a regular home of 70 m2 , the photovoltaic production of 24 of these modules would be required. As the domestic hot water demand would be satisfied with 4 modules, an application for the rest of 20 modules' thermal production should be found on a system like the proposed on this research. Combining different PV and PV/T modules in the same off-grid array would be counterproductive from the electrical production point of view, as the maximum power points could be different in both type of modules arising significant mismatch losses.
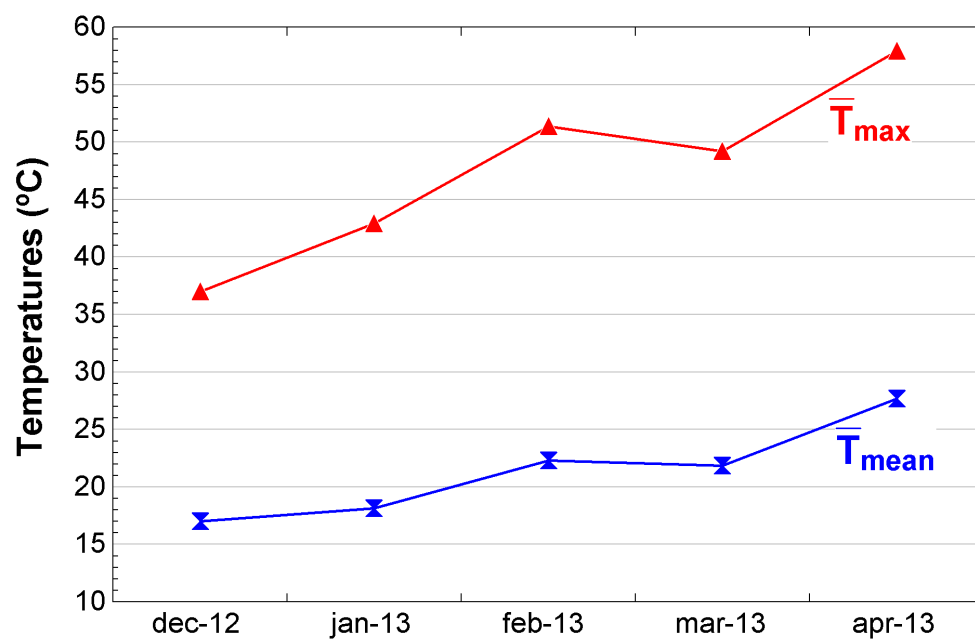
Figure 7.12: Average maximum cell temperature and daily mean cell temperature.

Chapter 8

PV heating experimental results

The photovoltaic system described on chapter 4, which combines solar electricity and a heat pump, was assembled with 12 modules and utilized during the 2012-13 heating season, from november 2012 to april 2013. The building to be heated is the laboratory previously described, which was heated up to 8 hours a day, whenever there was electricity available.

November and first three days of december were used as a test month in order to adjust all the operating and recording devices, therefore, and due to its weak relevance, it will not be presented on this chapter. In fact, that first weeks the array was composed by 16 modules, as it was used in summer (appendix A), but it was revealed to be oversized for winter season and it was adjusted to 12 modules.

This season's meteorological characteristics and building's thermal demand are presented on sections 8.1 and 8.2. After them, system's performance equation are listed and the seasonal results are presented, detailing the experimental behavour for three days. In addition, CO_2 emission reduction and the potential influence of heat pump's refrigerant R410A emission are discussed.

In the last section, the experimentally obtained PV production is compared to the one theoretically predicted through model simulation on section 7.5.

The experimental results shown in this chapter have been recently published by the author [Izquierdo and de Agustín-Camacho, 2015].

8.1 Seasonal meteorological characteristics

The average minimum and maximum daily temperatures along the season's months are plotted on figure 8.1, where it can be observed that during the winter months, the monthly outdoor dry bulb temperatures were below 3℃ for the minimums and 12℃ for the maximums.

The system was benefited by a considerably high solar insolation also during january and december (fig. 8.2).
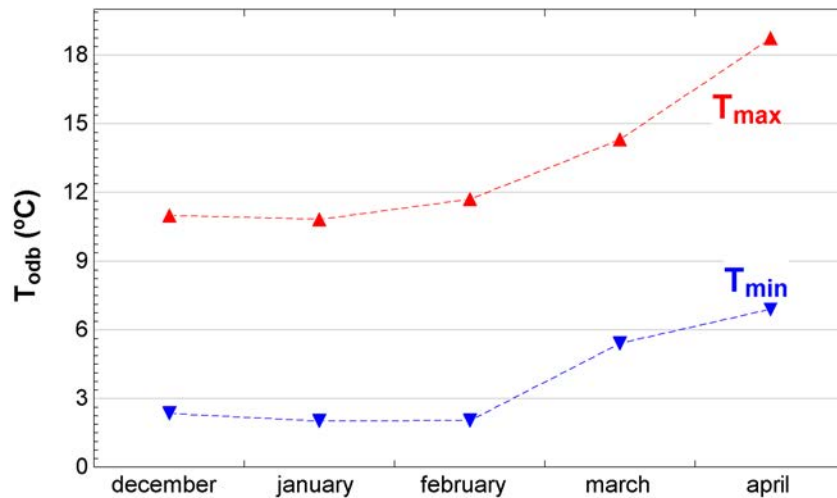
Figure 8.1: Monthly average minimum and maximum daily temperatures.
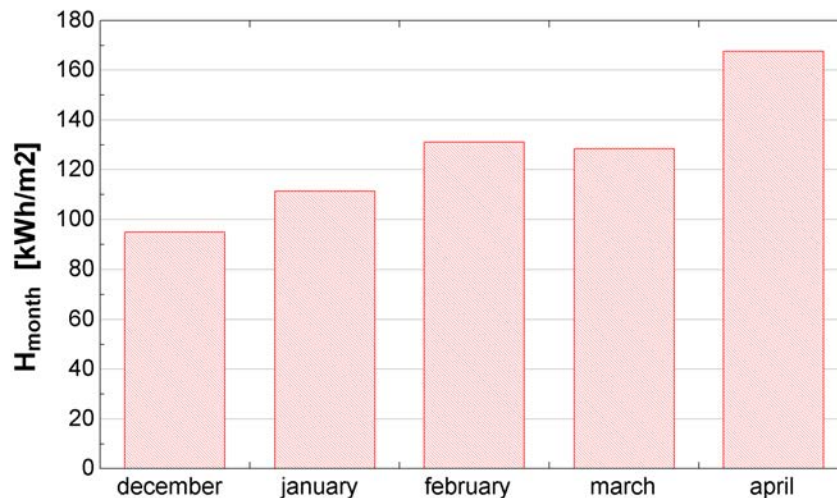
Figure 8.2: Monthly solar insolation.

8.2   Building's thermal demand

Heat transfer (U) and thermal load, TH_{LOAD}, through building's envelope (walls, ceilings and floors, etc.), ventilation, infiltration etc., was calculated applying the method given by Izquierdo et al. [2011] and España-Diaz [2014]. Figure 8.3 shows the evolution of thermal demand, during the heating period. It is plotted as a negative value to mean the heat leaving the building. This amount includes the thermal load in stationary regime, calculated in accordance with Izquierdo

et al. [2011], and building's thermal inertia (dynamic load), calculated in accordance with España-Diaz [2014].

It shows a notorious variable behaviour, with minimum values at the beginning of November and mid-April, and a maximum values 07/01/2013, when daily thermal demand (TH_D) was about 35.6 kWh. The whole seasonal thermal demand, from december 4th to april 30th was 3325 kWh, being 3825 kWh if november is also taken into account.
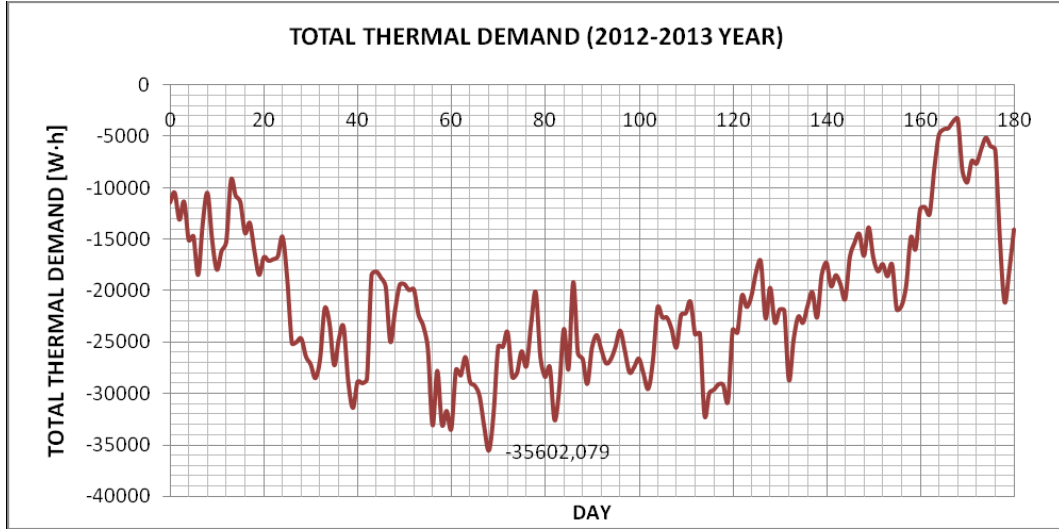
Figure 8.3: Building's thermal demand during the 2012-13 heating season.

8.3 Heat pump equations

Before presenting the experimental results, some equations are described here which will allow to analyze heat-pump and global PV system's performance.

As it is known, a heat-pump takes renewable thermal energy from the outdoor air and thanks to supplied electricity, it produces heat. This process is shown on the following balance:

$$\dot{Q}_{evap} + \dot{W}_{hp} = \dot{Q}_{cond} \qquad (8.1)$$

where $\dot{Q}_{evap}$ and $\dot{Q}_{cond}$ represent evaporator and condenser's calorific powers, respectively.

The heat power can be measured through the secondary fluid's behaviour in the radiant floor's circuit:

$$\dot{Q}_{cond} = \dot{m}_{stf} \cdot C_{p,stf} \cdot \triangle T_{stf} \qquad (8.2)$$

where,

$\dot{m}_{stf}$ is the seconday thermal fluid's flow (kg/s)

$C_{p,stf}$ is the secondary thermal fluid's specific heat (kJ/kg·°C)

$\triangle T_{stf}$ is the difference between inlet and outlet fluid temperature (°C)

The renewable power transferred from the outdoor air to heat-pump's circulating refrigerant (R410A) can be obtained from the following equation:

$$\dot{Q}_{evap} = \dot{m}_{oa} \cdot C_{p,oa} \cdot \triangle T_{oa} \tag{8.3}$$

where,

$\dot{m}_{oa}$ is outdoor air's flow through the evaporator (kg/s)

$C_{p,oa}$ is outdoor air's specific heat (kJ/kg·°C)

$\triangle T_{oa}$ is the outdoor air's temperature difference through difference between inlet and outlet fluid temperature (°C)

The coefficient of performance of the heat-pump is defined as the ratio between the heat production and electrical consumption:

$$COP = \frac{\dot{Q}_{cond}}{\dot{W}_{hp}} \tag{8.4}$$

As it has been mentioned, the heat pump can be fed through PV electricity or grid electricity. Consequently, the powers and COP will be distinguished depending on its electrical source:

$$COP_{pv} = \frac{\dot{Q}_{cond,pv}}{\dot{W}_{hp,pv}} \tag{8.5}$$

$$COP_{ge} = \frac{\dot{Q}_{cond,ge}}{\dot{W}_{hp,ge}} \tag{8.6}$$

It must be remarked that the electrical power, $\dot{W}_{hp}$, feeds the main consumer unit, the compressor, and diverse ancillary devices such as evaporator's fan, control system and secondary fluid's pump.

The PV efficiency of the array is defined as the ratio between the production and the intercepted solar energy:

$$\eta_{pv} = \frac{P_{PVMA}}{ISE} \tag{8.7}$$

Remembering that:

$$ISE = G_T \cdot A_{mod} \cdot N_{mod} \tag{8.8}$$

Produced PV electricity is transformed, stored and inverted before feeding the heat pump. This process' electrical efficiency is defined according to:

$$\eta_{elect} = \frac{\dot{W}_{hp,pv}}{P_{PVMA}} \tag{8.9}$$

So the useful efficiency is defined by:

$$\eta_{usefulpv} = \frac{\dot{W}_{hp,pv}}{ISE} \tag{8.10}$$

The aim of the system is to generate heat, so its global efficiency is defined by:

$$\eta_{globalpv} = \frac{\dot{Q}_{cond,pv}}{ISE} \tag{8.11}$$

Which can be also defined as:

$$\eta_{globalpv} = COP_{pv} \cdot \eta_{usefulpv} \tag{8.12}$$

Both COP and efficiencies can be also obtained for daily energies instead of power as:

$$COP = \frac{\int \dot{Q}_{cond} dt}{\int \dot{W}_{hp} dt} \simeq \frac{\sum \dot{Q}_{cond} \triangle t}{\sum \dot{W}_{hp} \triangle t} = \frac{Q_{cond}}{W_{hp}} \tag{8.13}$$

Daily system's COP is defined as:

$$COP_{sys} = \frac{Q_{cond,pv} + Q_{cond,ge}}{W_{hp,pv} + W_{hp,ge}} \tag{8.14}$$

Building's isolation ratio from the grid, IR, can be defined as:

$$IR = \frac{W_{hp,pv}}{W_{hp,pv} + W_{hp,ge}} \tag{8.15}$$

And the solar fraction, considering the renewable power used to heat the building over its total thermal demand and when that energy was able to maintain $T_{ind} > 18°C$, is defined as:

$$SF = \frac{Q_{cond,pv} + (Q_{cond,ge} - W_{hp,ge})}{TH_D} \tag{8.16}$$

Where $Q_{cond,ge} - W_{hp,ge} = Q_{evap,ge}$ and TH_D is represented on figure 8.3.

When the heat pump is fed by PV electricity, the facility works as a total renewable energy system: photovoltaic + heat transferred from the outdoor air to evaporator.

When the heat pump is driven by grid's conventional electricity, then, the facility works as a partial renewable system, being the heat transferred from the outdoor air (Q_{evap}) the renewable energy share.

8.4   Experimental daily results

Before describing the seasonal results of the PV system, the behavour of its components along a day needs to be understood. In this section, three different clear and cold winter days are choosen to explain the working details of the system:

- 28/12/2012 - Heat pump fed with PV electricity..

- 21/01/2013 - Heat pump fed with grid and PV electricity.

- 21/01/2013 - Heat pump fed with PV electricity.

8.4.1   December 28$^{\text{th}}$ 2012

During this day, the heating experiment was carried out using only PV electricity as energy source.

8.4.1.1   Meteorological conditions

It was a clear and cold day, as it can be seen on figure 8.4. Maximum solar radiation reached above 1050 W/m^2 at solar midday, with a short fall due to afternoon clouds. The daily insolation on tilted surface, H_T, was 5.4 kWh/m^2, so the intercepted solar energy, *ISE*, by the 12 modules (14 m^2 useful area) was 75.6 kWh. Minimum and maximum outdoor dry bulb temperatures were -1.1 °C and 13 °C, respectively.
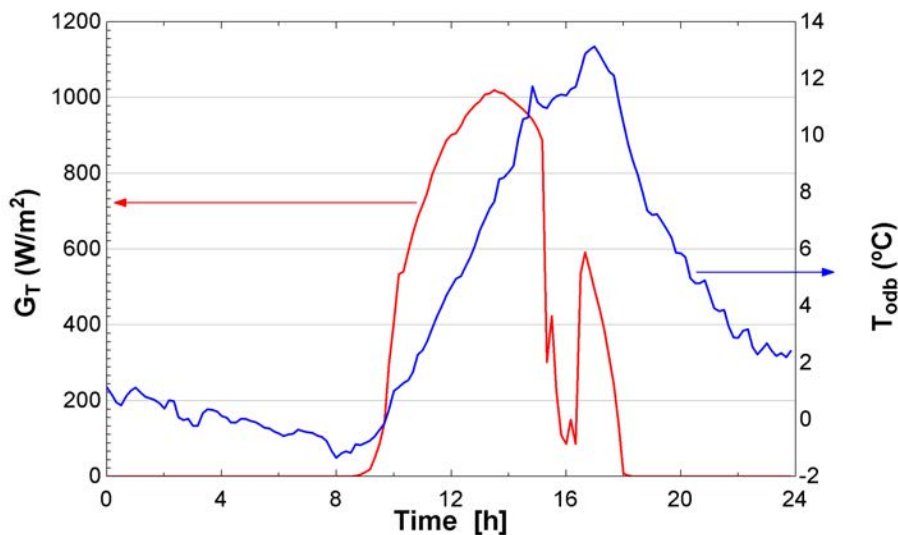
Figure 8.4: Solar radiation and outdoor dry bulb temperature (28/12/2012).

8.4.1.2   Energy balance

As it was introduced on chapter 4, the array's photovoltaic production (fig. 8.5) is related to batteries' charge state or battery voltage (fig. 8.6). During this day, under *ISE*, the electricity generated by the modules array, E_{PVMA}, was 7.6 kWh, so the daily efficiency of the array was 10.1%.

Figure 8.5 shows how the photovoltaic production started at 8.38 hours, reaching 400 W at 10.45 hours, 1400W at 11.73 and 1600 W at 14.40 hours declining to 1500 W at 15.41, 352 W at 16.21 until zero at 18.00 sunset hour. During the central hours of the day, the energy flow fluctuated due to the MPPT controller-batteries interaction. These fluctuating peaks can be explained through the batteries' voltage along the day.

During the night, batteries got slightly discharged due to system's stand-by losses, so the voltage of the battery system decreased down to 22 V before the sunrise (fig. 8.6). Once the PV production began, the batteries started to get charged and, consequently, their voltage increased. It must be reminded now that this battery system's maximum operating voltage is 28V, so whenever this value was reached, the PV production was reduced by the MPPT controller, in order to avoid overcharges. That is how the PV production and voltage fluctuation peaks that appear during the central hours of the day are related. The voltage in the batteries was maintained between 26 V and 28 V from 10.31 until 17.23 hours; it varied in that range because their were

being simultaneously partially discharged by the load during that period. The charging operation finalized when the voltage was 25 V at 18.00 hours.
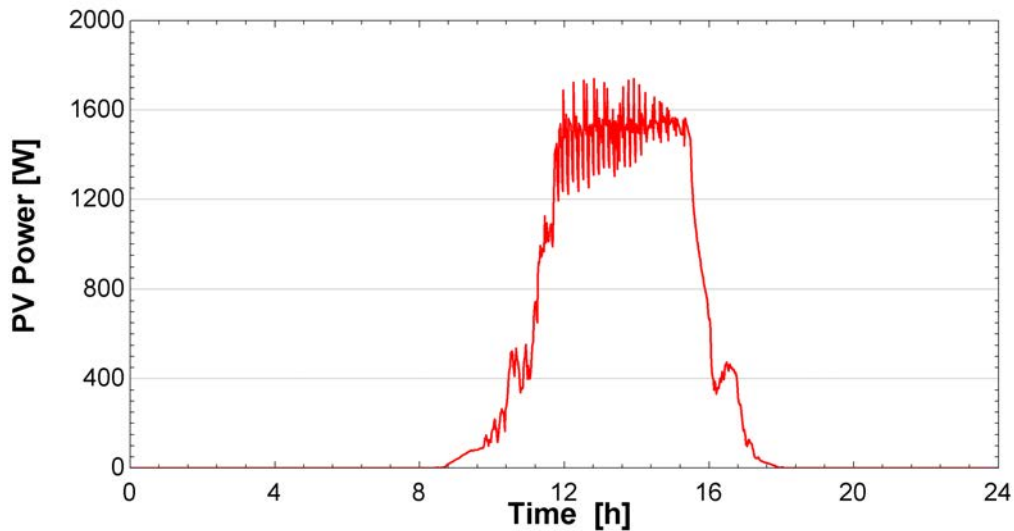
Figure 8.5: Electrical output of the PV array (28/12/2012).
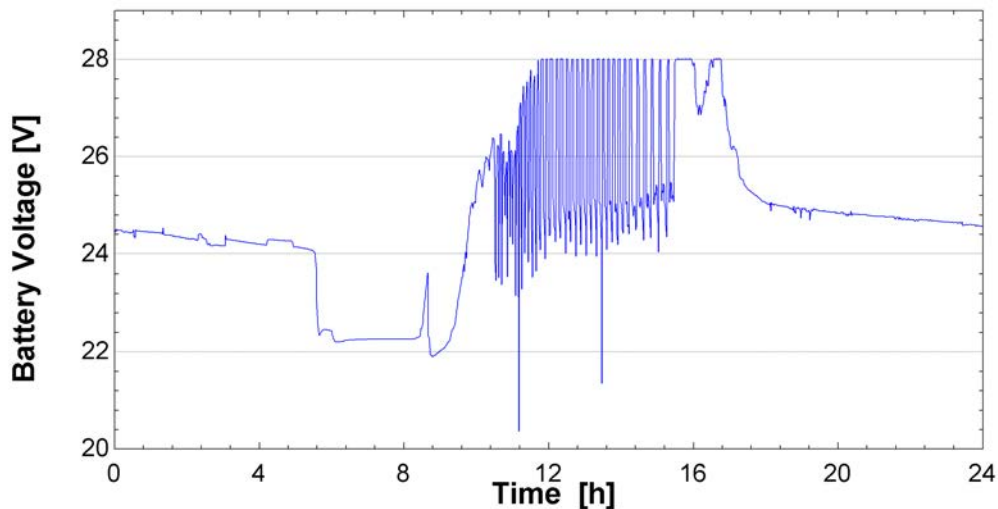
Figure 8.6: Battery system's voltage (28/12/2012).

As it is described on the following lines, load was interrupted at 15.51 hours and the batteries' voltage was kept at 28 V, until the PV production decreased. The PV electricity stored from 15.51 hour to 18.00 hours was about 0.9 kWh and the useful PV electricity driven to the Inverter, 6.7 kWh.

This day, the heat pump was running between the 10.53 and 15.51 hours (fig. 8.7). As the batteries had been partially charged the day before and also during this day until 10.53 hours, so it was able to suply 1.33 kW to the heat pump, $\dot{W}_{hp,pv}$, declining to 0.25 kW at 11.10 hours when the batteries were discharged. At 11.20 hours, as consequence of the PV electricity generated, 1.0 kW were supplied, increasing to 1.7 kW at 11.48 hours.
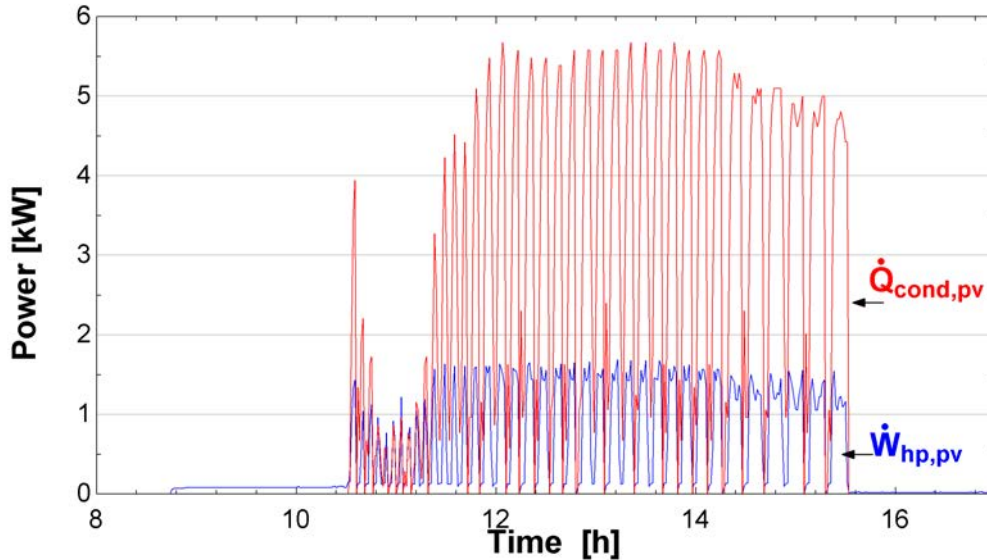
Figure 8.7: Heat pump's electrical consumption and heat production (28/12/2012).
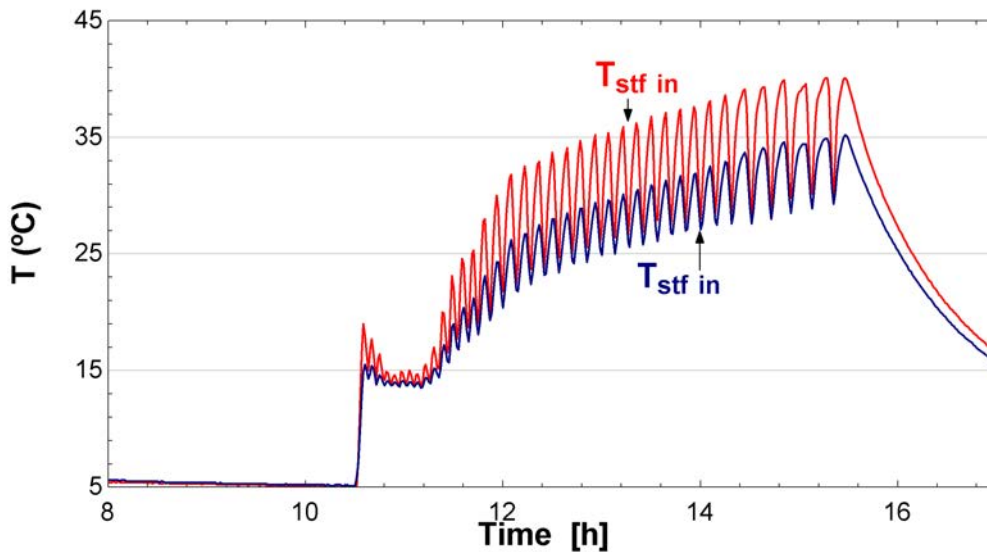
Figure 8.8: Secondary fluid's inlet and outlet temperatures (28/12/2012).

The available PV electricity (produced+stored) along this day was: 0.40 kWh stored before

10:53 hours; 6.54kWh generated by the PV field from which 1.09kWh were stored from 10:53 to 15:51 hours and 0.83kWh were stored from 15:51 to 18:10 hours. The electricity stored for next day was 1.92kWh.

The electrical energy, $W_{hp,pv}$, supplied to the heat pump along the day was 4.7 kWh: 0.40 kWh came from PV electricity stored the day before and 4.3 kWh was the PV electricity generated and supplied during that day.

The condenser's calorific power, $\dot{Q}_{cond,pv}$, initiated with a peak value of 3.94kW, declining rapidly until almost zero kW at 11.17 hours, and increasing up to 4.5 kW at 11.48 hours. The maximum $\dot{Q}_{cond,pv}$ produced was 5.67 kW at 12.06 hours. This value was maintained almost constant until 14:25, declining later to 4.7 kW, at 15:51 hour. The experiment finalized at 15.51 when the heat power dropped to zero.

The total daily heat produced by the heat pump and supplied to the radiant floor, $Q_{cond,pv}$, was 14.5 kWh: 0.9 kWh was produced driving the heat pump with the PV electricity stored the day before and 13.6 kWh was produced driving the heat pump with the PV electricity generated during that day.

Figure 8.8 shows the secondary fluid's inlet and outlet temperatures into the radiant floor's circuit. As the heat pump got periodically interrupted due to the lack of electricity, these temperatures fluctuated, instead of reaching the target temperature and keeping it constant.

The electrical efficiency, according to equation 8.9, from 10:53 hours to 15:51 hours was 4.7/(6.54-1.09) = 0.86. The electricity losses in the Inverter during the period were 14% of total supplied to the heat pump.

The daily losses are the sum of the losses in the MPPT regulator, in the batteries, in the Inverter and in the transport from the modules' field to the heat pump. These are obtained as the difference between the available PV electricity (((7.6+0.4)−1.92) = 6.1 kWh) and the electricity provided to the heat pump, 4.7 kWh. Therefore, the total losses were 6.1-4.7 = 1.4 kWh, 17.5% of total available. The main losses happened in the inverter (14%), being the rest of them, 3.5%, the ones happened in regulator, batteries and transport.
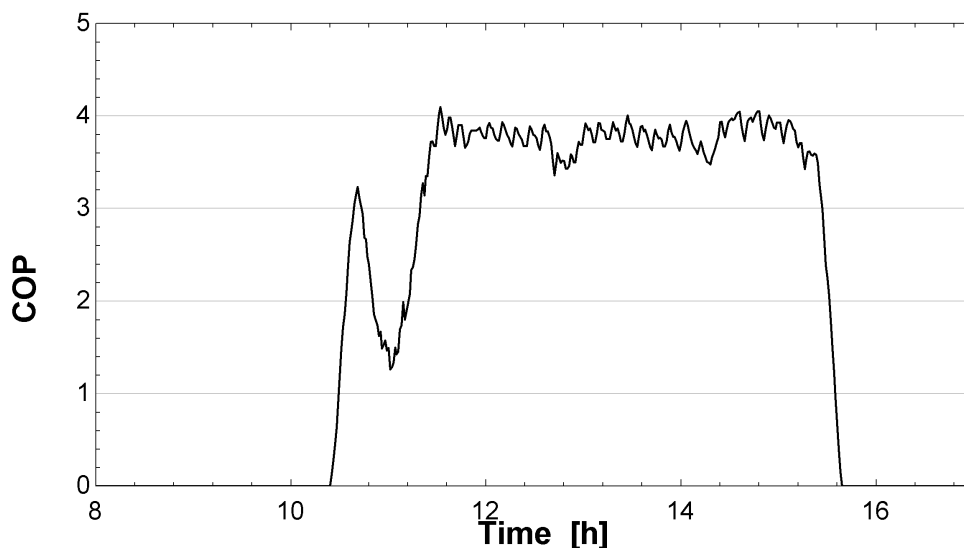
Figure 8.9: Heat pump's coefficient of perfomance (28/12/2012).

Figure 8.9 describes the daily distribution of the COP, obtained according to equation 8.13, starting with values of 3.3 and declining to 1.3 around 11:00 when the batteries were in discharge phase. From this moment the COP increased until a maximum value of 4.1 near 11:30 hours. From 12:00 to 15:47 hours, when the experiment finalized, the COP fluctuated between 3.5 and 4.0.

Daily COP was 3.5; the useful efficiency according to equation 8.10 was $4.7/69 = 0.068$ (6.8%), and the global efficiency (eq. 8.11) was about 23.8% if we take into account the stored electricity until 10.53 hours.

8.4.1.3 Temperatures
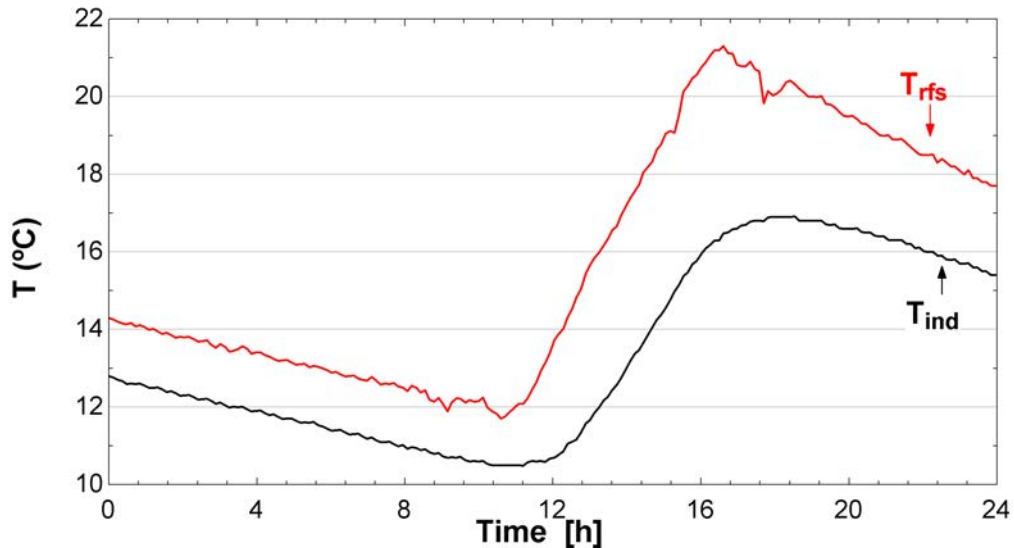
Figure 8.10: Radiant floor surface and indoor temperatures (28/12/2012).

The radiant floor surface temperature, T_{rfs}, was 12°C at 10.50 hours, which increased up to a maximum value of 21.2°C at 16.00 hours, declining to 17.7°C at 24.00 hours. At 10.50 hours the indoor temperature, T_{ind}, was about 10.5°C, increasing to 17.0 °C at around 19.00, and declining to 15.5°C at 24.00 (fig. 8.10).

Although along the day, the system was fed through PV source (IR=100%) and it was able to produce and supply 14.5 kWh to the radiant floor, this heat was not enough to reach the minimum comfort conditions (18 °C) because building's daily demand was around 32.5kWh (fig. 8.3). From this point of view, the solar fraction (eq. 8.16), was zero.

8.4.1.4 Environmental impact reduction

During this day, the whole electricity supplied to the heat pump was from photovoltaic source, so there were not CO_2 emissions related to it (if the energy used during modules manufacturing process is not considered). Comparing to supplying the heat pump through conventional grid electricity, the CO_2 emissions saved , in the case of Spain, were $0.34\frac{kg_{CO_2}}{kWh} \cdot 4.7kWh = 1.6kg_{CO_2}$, according to Izquierdo et al. [2011].

In addition, the renewable heat absorbed from outdoor air by the system, according to equation 8.1, was $Q_{evap} = 9.8kWh$.

If the whole facility, PV system+heat pump, was replaced by a boiler burning Gas-oil C or Natural Gas to produce the same ammount of heat ($Q_{cond,pv} = 14.5kWh$):

1. Gas-oil C, with a boiler efficiency 0.75 (combustion, generation, transport, etc.) and emission 0.27 kg_{CO_2}/kWh, the emitted CO_2 would be 5.2 kg_{CO_2}/day.

2. Natural gas, with a boiler efficiency 0.85 (combustion, generation, transport, etc.) and emission 0.21 kg_{CO_2}/kWh, the emitted CO_2 would be 3.6 kg_{CO_2}/day.

However, to complete the environment balance it is necessary to determine the emission of the refrigerant R410A to the atmosphere during this day. For such a short period of time, this operation could not be done.

8.4.2 January 21st 2013

On this day, heat pumps operated from 8.75 to 15.10 hours. Grid electricity was supplied to the heat pump at the beginning of the morning, switching to photovoltaic electricity at 10.8 hours.

8.4.2.1 Meteorological conditions

This was a clear day, with a narrower temperature range, as it can be seen on figure 8.11, and some crossing clouds. Measured solar radiation reached 1100 W/m^2 at solar midday. The daily insolation on tilted surface, H_T, was 6.29 kWh/m^2, so the intercepted solar energy, ISE, by the 12 modules (14 m^2 useful area) was 88.0 kWh. Minimum and maximum outdoor dry bulb temperatures were 2.6 °C and 9.6 °C, respectively.

Figure 8.11: Solar radiation and outdoor dry bulb temperature (21/01/2013).

8.4.2.2 Energy balance

Array's PV power (fig. 8.12), which started at 8.41 hours and lasted until 18.5, was determined by meteorological conditions an batteries charge state (fig. 8.13). During this day, the photovoltaic electricity generated, E_{PVMA}, was 8.4 kWh, so according to the ISE, the daily efficiency of the array was 9.6%.

If we focus on the interval from the sunrise to 15:10 hours when the module field finalized the supply of PV electricity to heat pump, the ISE was 78.6 kWh and the PV production was 7.2 kWh. The PV electricity stored from 15:10 hour to 18:10 hours was about 1.2 kWh.
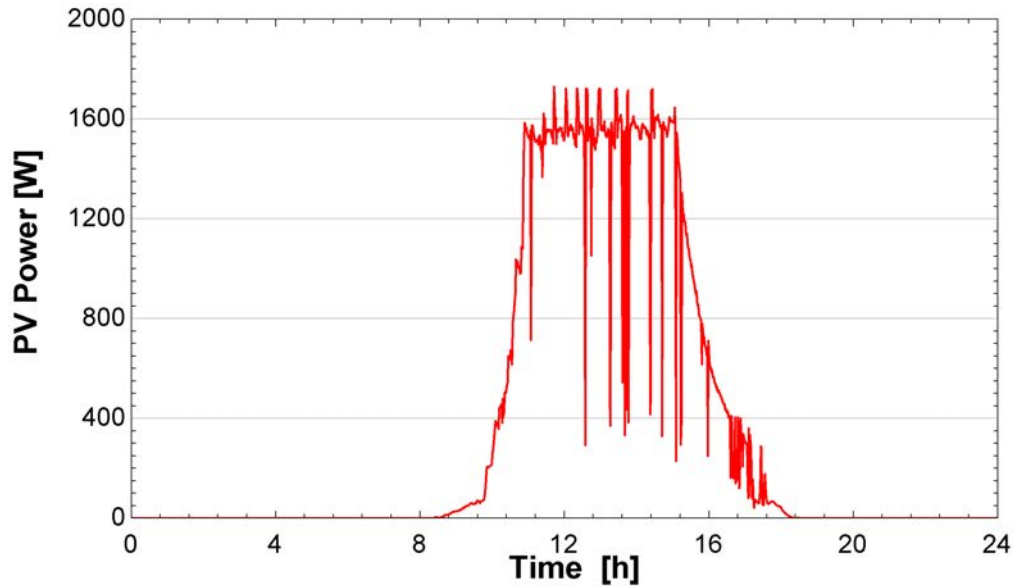
Figure 8.12: Electrical output of the PV array (21/01/2013).
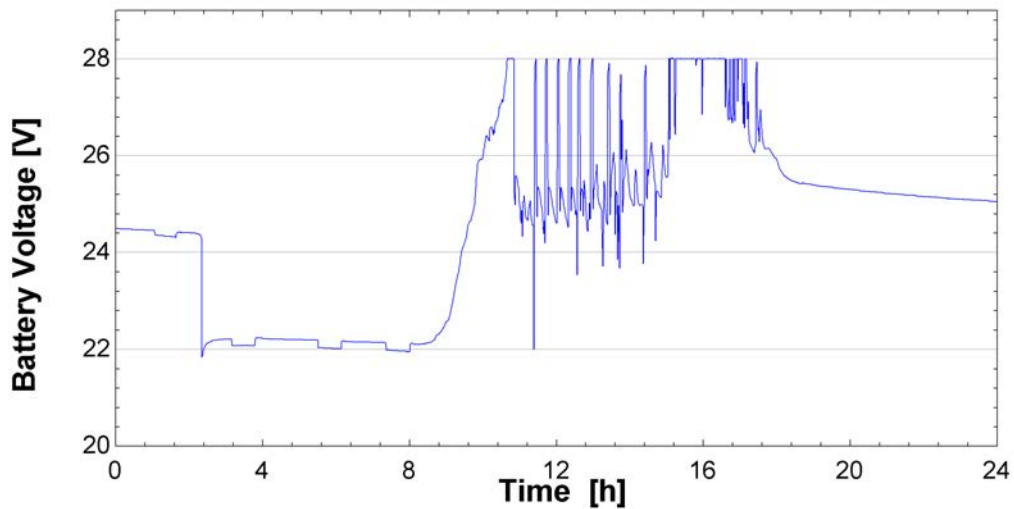
Figure 8.13: Battery system's voltage (21/01/2013).

As the batteries' voltage was low, according to figure 8.13, the heat pump was initially turned on plugin it to the grid.

From 8.75 hours to 10.8, the grid electricity supplied to the heat pump, $W_{hp,ge}$, was 1.8 kWh. During that time, condenser's heat production, $Q_{cond,ge}$, was 10.5 kWh, providing an average COP of 5.83. This high performance can be explained due to the wide initial temperature gap between radiant floor and inlet secondary fluid.

Once the electrical source was switched to PV electricity, the heat pump run until 15.10 hours. During that period, supplied $W_{hp,pv}$ was 3.9 kWh and produced heat, $Q_{cond,pv}$, was 14.2 kWh. The COP during that period decreased to an average coefficient of 3.6.

As it is shown on figures 8.14 and 8.15, the electrical supply was not as much interrupted as it was on December 28$^{\text{th}}$, and most of power drops on $\dot{W}_{hp,pv}$ curve were related to normal compressor interruptions controlled by heat-pump's SF thermostate. In fact, target temperature on SF was quickly approached, keeping inlet temperature above 40°C during the vast majority of time.
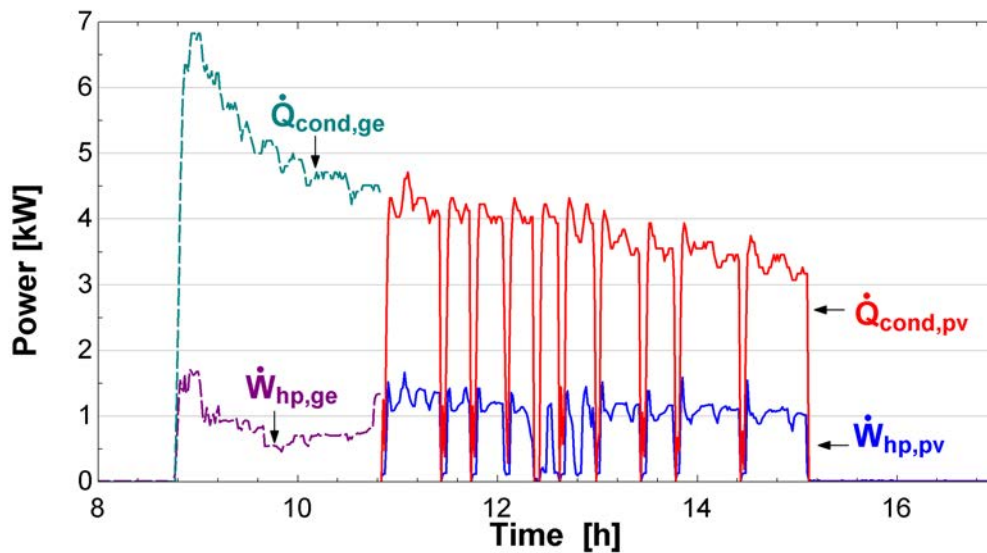
Figure 8.14: Heat pump's electrical consumption and heat production (21/01/2013).
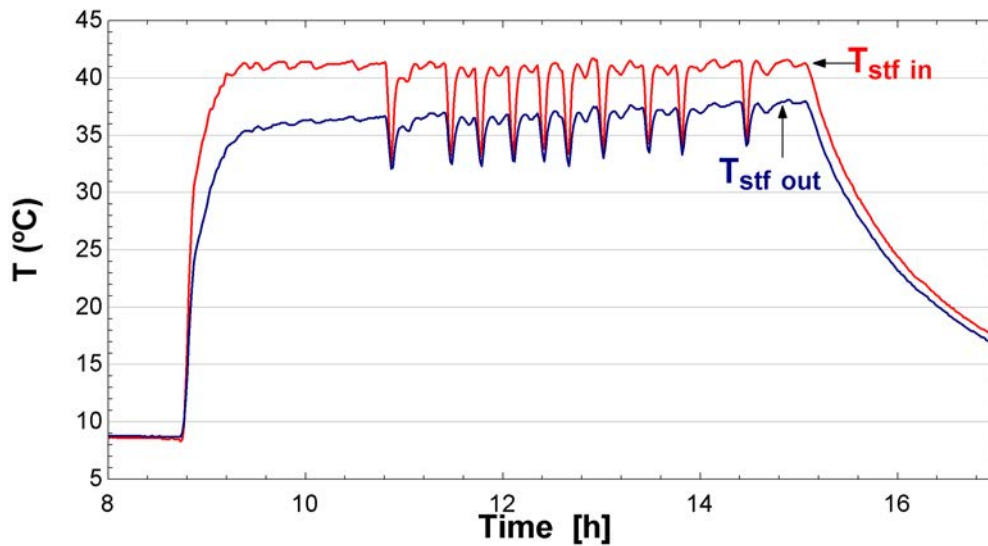
Figure 8.15: Secondary fluid's inlet and outlet temperatures (21/01/2013).

The global efficiency, Equations 7 and 8, taken into account only the PV electricity supplied until 15:10 hours, was 3.5·4.1/78.6= 0.182 (18.2%).

Out of the heating producing period,, heat pump still demanded 0.40 kWh due to its stand-by consumption and in order to prevent water freezing effect during the night. So during 24 hours (including the electricity provided to avoid freezing of SF and compressor sump's oil), the total W_{hp} was 6.09 kWh, being Q_{cond} 24.7 kWh the total heat generated.

The daily COP was about 4.0, according to figure 8.16. The ratio of isolation from the grid, IR, was 4.3/(4.3+1.8) =71.0%. As according to figure 8.3, the daily thermal demand was 33 kWh, the solar fraction was, 74.8%.

Figure 8.16: Heat pump's coefficient of perfomance (21/01/2013).

8.4.2.3   Temperatures
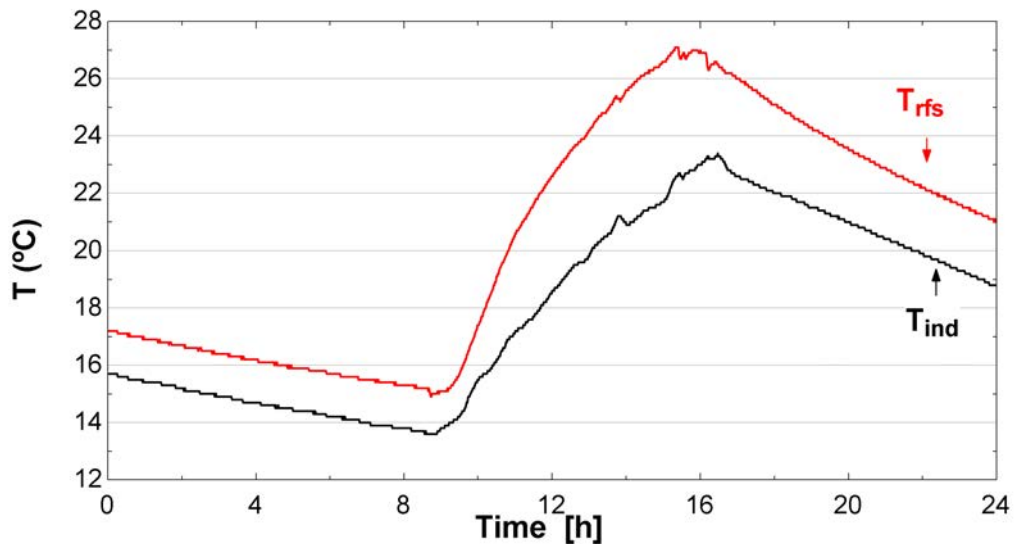
Figure 8.17: Radiant floor surface and indoor temperatures (21/01/2013)..

At 8.45 hours, T_{ind} was 13.7 °C, reaching the maximum of 23.3°C at 16.2h. On the other hand, radiant floor surface temperature grew quicker, being T_{rfs} 20.3°C at 10:55 and 27°C at 16:00 hours. As it is shown on figure 8.17, T_{ind} rose from 18°C to 23 °C, from 11:40 to 16:42 hours, declining to 18.8°C at 24:00. Thanks to this system's thermal mass, the indoor temperature was kept above 18°C nine hours after the heat pump was turned off.

8.4.2.4 Environmental impact reduction

As it said, during this day the facility operated during some hours with grid electicity, so the CO_2 emissions related to that electricity were: $0.34\frac{kg_{CO_2}}{kWh}\cdot 1.8kWh = 0.6kg_{CO_2}$, according to Izquierdo et al. [2011]. On the other hand, the rest of the day, even during the night and stand-by hours, the heat pump was fed through the PV system, so the CO_2 emissions saved were: $0.34\frac{kg_{CO_2}}{kWh}\cdot 4.3kWh = 1.5kg_{CO_2}$.

In addition, the renewable heat absorbed from outdoor air by the system (whenever fed by PV and grid), according to equation 8.1, was $Q_{evap} = 24.7 - (3.9 + 1.8) = 19.0kWh$.

If the whole facility, PV system+heat pump, was replaced by a boiler burning Gas-oil C or Natural Gas to produce the same ammount of heat ($Q_{cond} = 24.7kWh$):

1. Gas-oil C, with a boiler efficiency 0.75 (combustion, generation, transport, etc.) and emission 0.27 kg_{CO_2}/kWh, the emitted CO_2 would be 8.9 kg_{CO_2}/day.

2. Natural gas, with a boiler efficiency 0.85 (combustion, generation, transport, etc.) and emission 0.21 kg_{CO_2}/kWh, the emitted CO_2 would be 6.1 kg_{CO_2}/day.

8.4.3 February 23rd 2013

During this day, the heating experiment was carried out using only PV electricity as energy source. Heat-pump operated from 10.50 to 16.50 hours.

8.4.3.1 Meteorological conditions

This was a clear day and cold day, as it can be seen on figure 8.18. Measured solar radiation reached 1180 W/m^2 at solar midday. The daily insolation on tilted surface, H_T, was 8.10 kWh/m^2, so the intercepted solar energy, *ISE*, by the 12 modules (14 m^2 useful area) was 113.37 kWh. Minimum and maximum outdoor dry bulb temperatures were 0.7 °C and 6.2 °C, respectively.
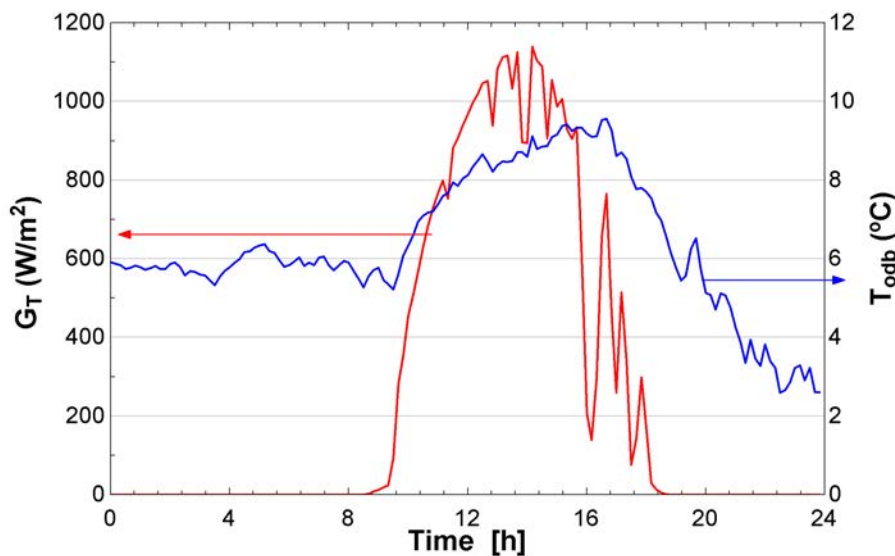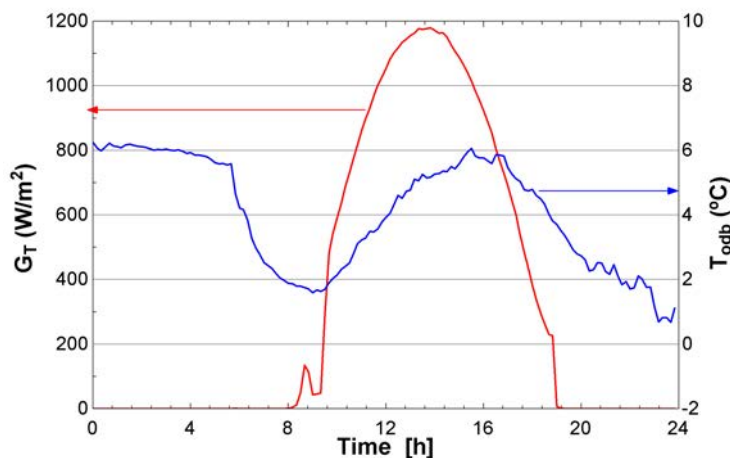

Figure 8.18: Solar radiation and outdoor dry bulb temperature (23/02/2013).

8.4.3.2 Energy balance

Array's PV power curve (fig. 8.19) was strongly sharped by batteries charge state (fig. 8.20). Initially the batteries were partially discharged and the controller operated on *MPPT* mode, from 7.75 to 9.53 hours, when batteries reached 28V and stepped into absorption phase, from that moment the production was gradually reduced until the heat-pump was turned on and consumption started at 10.50 hours. The daily generated PV electricity by the array, P_{PVMA}, was 10.2 kWh, so according to the ISE, the daily efficiency of the array was 9.0%.

Once the heat pump was interrupted, the PV array still produced 0.14 kWh that were delivered to the storage system.
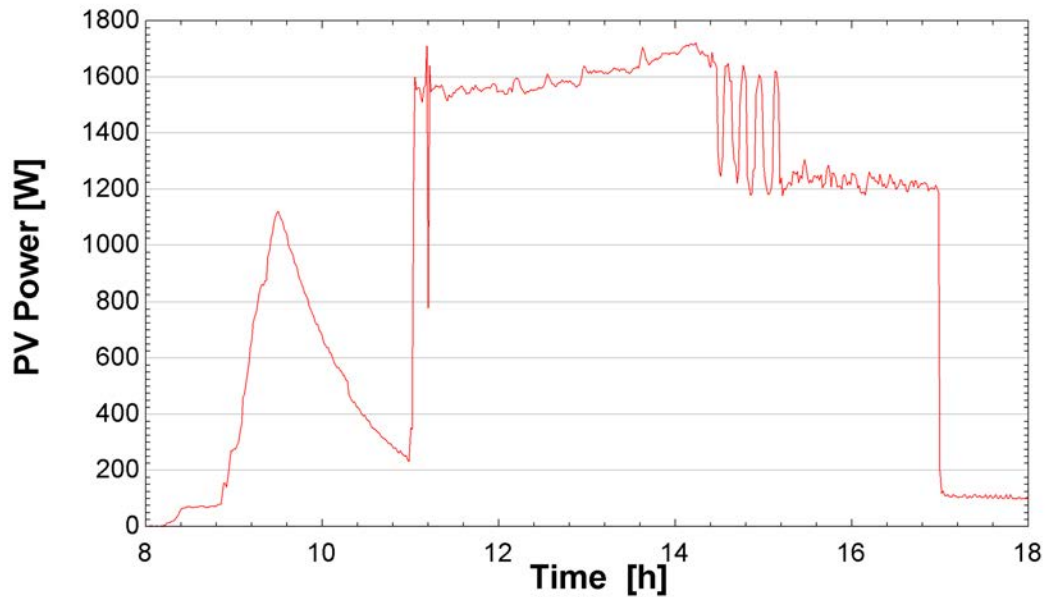
Figure 8.19: Electrical output of the PV array (23/02/2013).
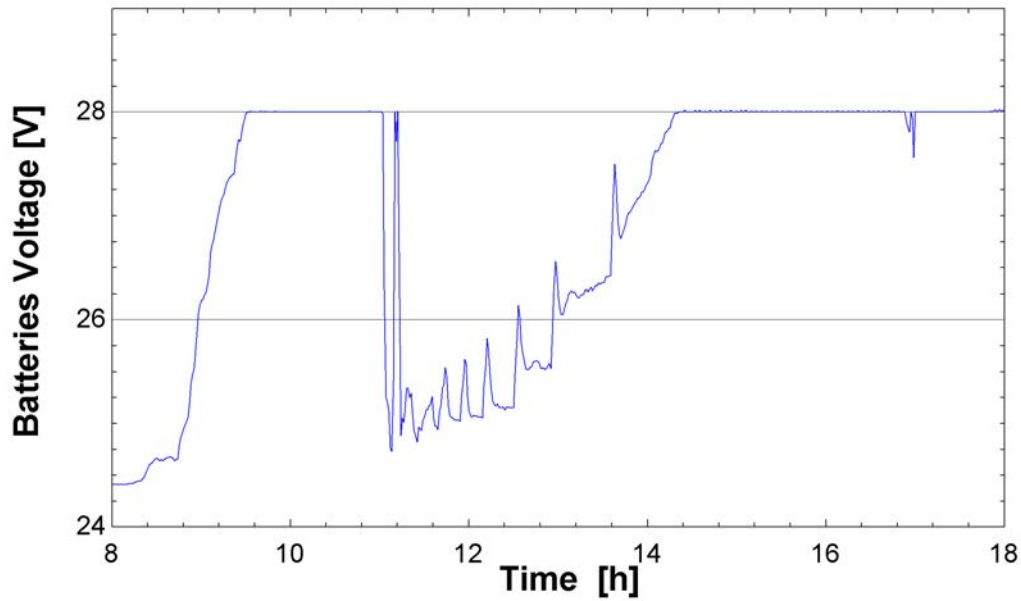
Figure 8.20: Battery system's voltage (23/02/2013).

During heat-pump's operating period, supplied $W_{hp,pv}$ was 5.8 kWh and produced heat, $Q_{cond,pv}$, was 19.3 kWh. The COP during its working time was 3.3.

As it is shown on figures 8.21 and 8.22, the electrical supply was not interrupted once permanent regime was reached. Target temperature on secondary thermal fluid was quickly approached, keeping inlet temperature around 37°C during working period.
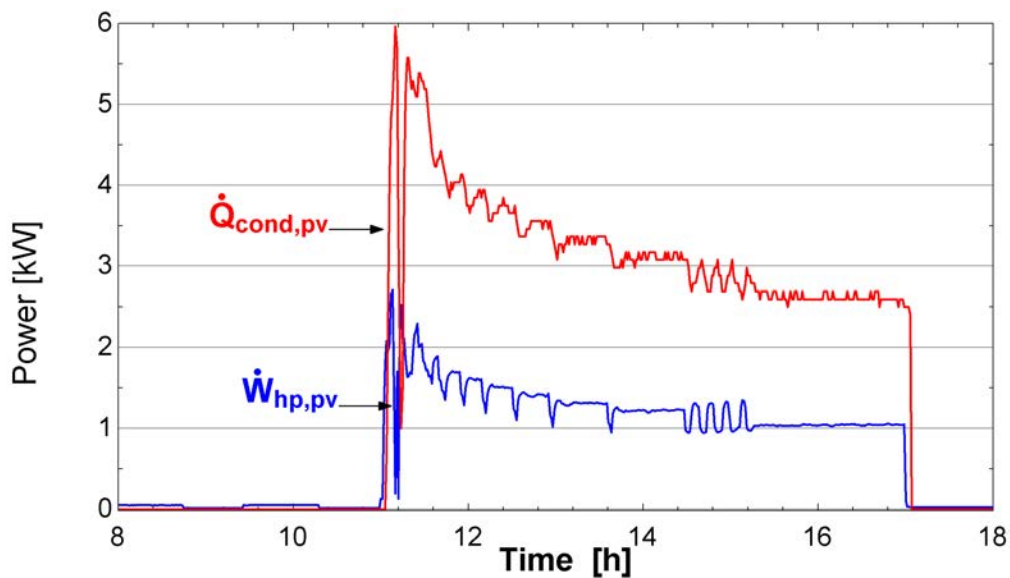
Figure 8.21: Heat pump's electrical consumption and heat production (23/02/2013).
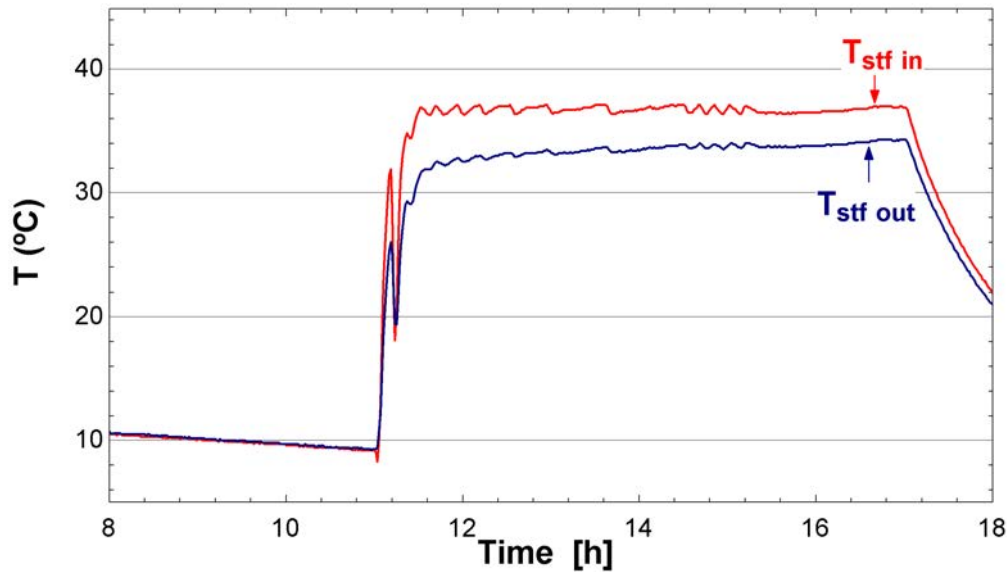
Figure 8.22: Secondary fluid's inlet and outlet temperatures (23/02/2013).

The global efficiency, during of the system was 17.0%.

Out of the heating producing period, heat pump still demanded 0.34 kWh due to its stand-by consumption and in order to prevent water freezing effect during the night. Therefore, the daily COP was 3.1, according to figure 8.23. According to figure 8.3, the daily thermal demand was 30 kWh, so the solar fraction was, 64.3%, and the isolation ratio 100%.
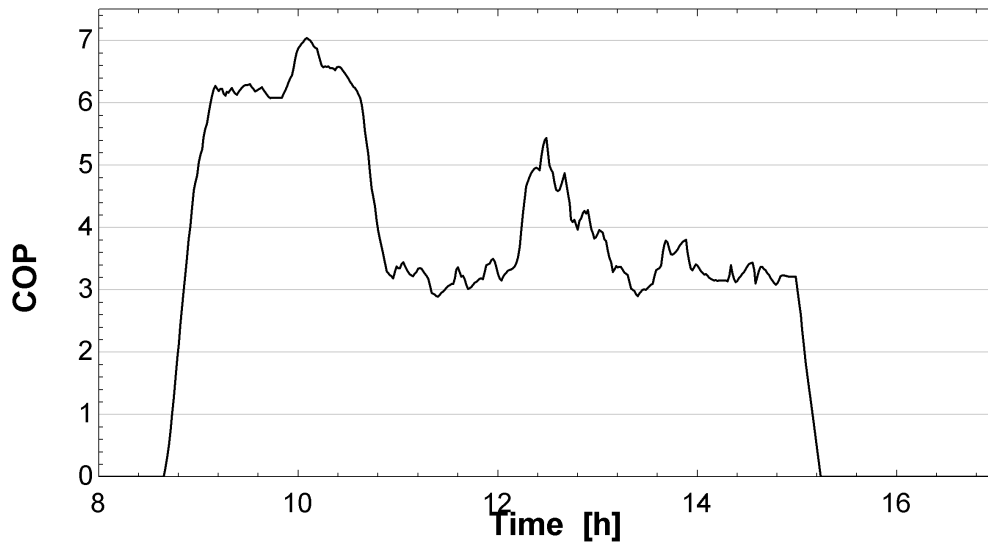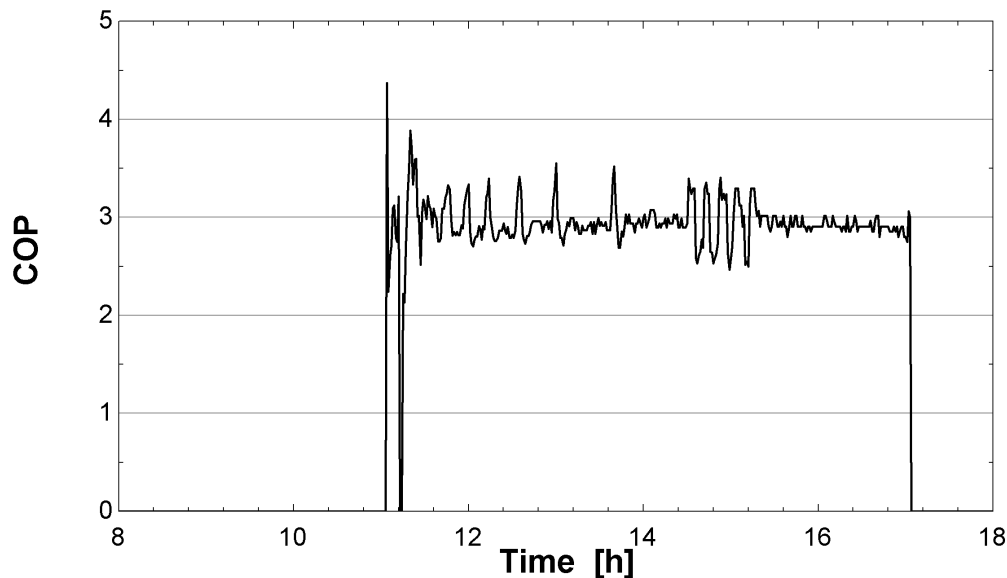

Figure 8.23: Heat pump's coefficient of perfomance (23/02/2013).

8.4.3.3   Temperatures
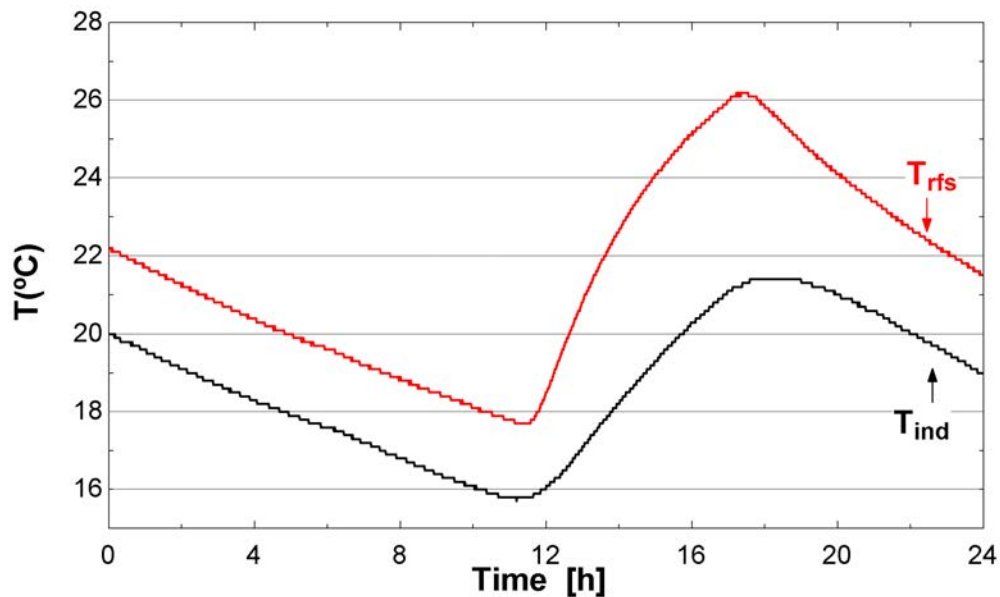
Figure 8.24: Radiant floor surface and indoor temperatures (23/02/2013).

Minimum indoor temperature was 15.8 °C at 11.0 hours, reaching the maximum of 21.4°C at 18.03h. On the other hand, radiant floor surface temperature grew quicker, being T_{rfs} 26.2°C at 17.03 hours. Indoor temperature was kept above 18°C from 13.75 hours to beyond midnight.

8.4.3.4   Environmental impact reduction

There were not CO_2 emissions related with total electricity supplied to the heat pump as it was fully from PV source, so it implied savings of $0.34\frac{kg_{CO_2}}{kWh} \cdot 6.1 kWh = 2.1 kg_{CO_2}$.

In addition, the renewable heat absorbed from outdoor air by the system, according to equation 8.1, was $Q_{evap} = 13.5 kWh$.

If the whole facility, PV system+heat pump, was replaced by a boiler burning Gas-oil C or Natural Gas to produce the same ammount of heat ($Q_{cond,pv} = 19.3 kWh$):

1. Gas-oil C, with a boiler efficiency 0.75 (combustion, generation, transport, etc.) and emission 0.27 kg_{CO_2}/kWh, the emitted CO_2 would be 6.9 kg_{CO_2}/day.

2. Natural gas, with a boiler efficiency 0.85 (combustion, generation, transport, etc.) and emission 0.21 kg_{CO_2}/kWh, the emitted CO_2 would be 4.8 kg_{CO_2}/day.

8.5   Uncertainty analysis

The daily evolution of diverse variables have been plotted on section 8.4. As they have been calculated from measured variables as mass flow, SF's inlet and outlet temperatures, current,

voltage,... , uncertainty propagation must be estimated as indicated on section 4.9.

The mean values of uncertainty on the electrical power supplied to the heat pump, $\dot{W}_{hp}$, its heat power generation, $\dot{Q}_{cond}$, and instant coefficient of performance, are listed on table 8.1.

Represented function	Uncertainty [%]
$\dot{W}_{hp}$	2.2
$\dot{Q}_{cond}$	7.3
COP	11.4

Table 8.1: Uncertainty on represented variables.

8.6   Seasonal results

As it has been mentioned, the heating experiment was carried out daily from December 4th 2012 to April 30th 2013, whenever there was energy available. Considering the total insolation, which has been monthly represented on figure 8.2, the modules array's useful area intercepted 8869kWh of solar energy along the whole period. The photovoltaic electricity generated by the array during the same time, due to the meteorological conditions and system's electrical demand, was 820 kWh, so array's seasonal efficiency (eq. 8.9) was 9.26%. Figures 8.25 and 8.26 show monthly values of ISE and E_{PVMA}, respectively. The monthly values of the different parameters plotted in this section are listed on table 8.2.
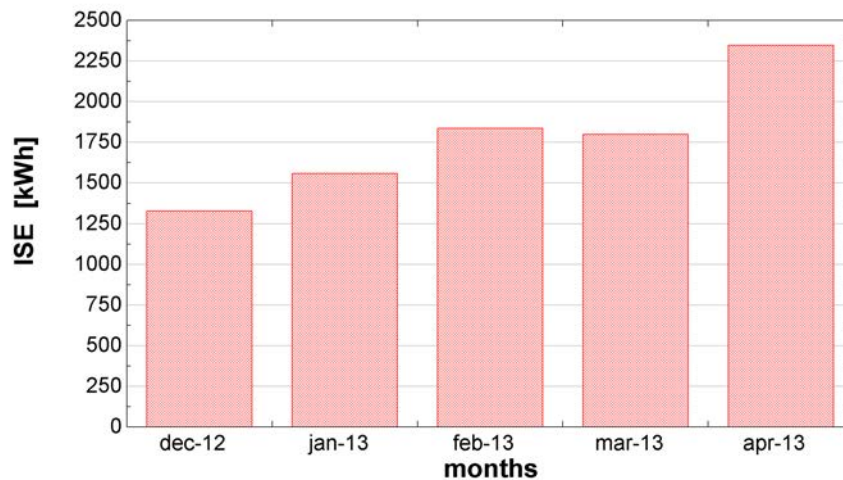
Figure 8.25: Monthly Intercepted Solar Energy during the heating period.
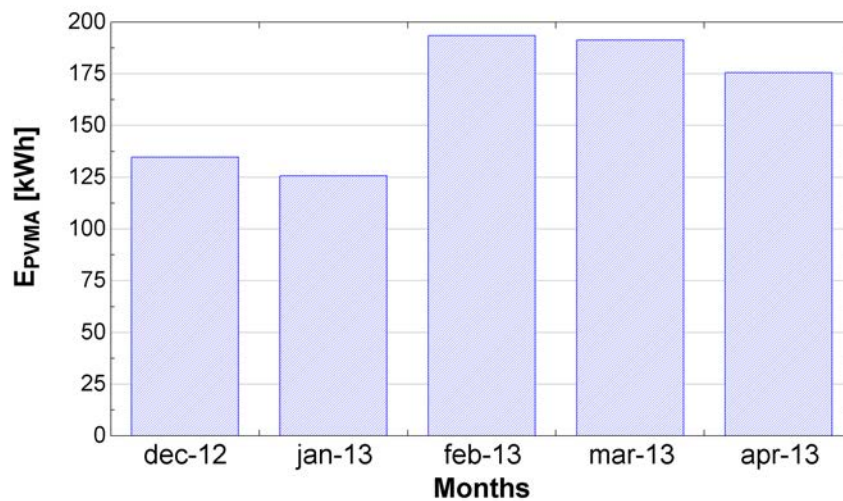
Figure 8.26: Monthly PV production during the heating period.

During the whole period, the heat produced at heat-pump's condenser, Q_{cond}, was 2322 kWh, and its electrical demand was 724 kWh, so the seasonal COP was 3.21 (13% smaller to the nominal one on table 4.3). This difference could be expected when seasonal COP is compared to the one provided by the manufacturer for given temperature conditions at permanent regime. If the supplied electricity is splitted depending on its source, the PV electricity supplied to the heat-pump, $W_{hp,pv}$, was 501 kWh, for producing a $Q_{cond,pv}$ of 1610 kWh. On the other hand, 223 kWh of grid electricity was supplied to generate 712 kWh. The monthly distribution of the demanded electricity and produced heat is represented on figure 8.27.
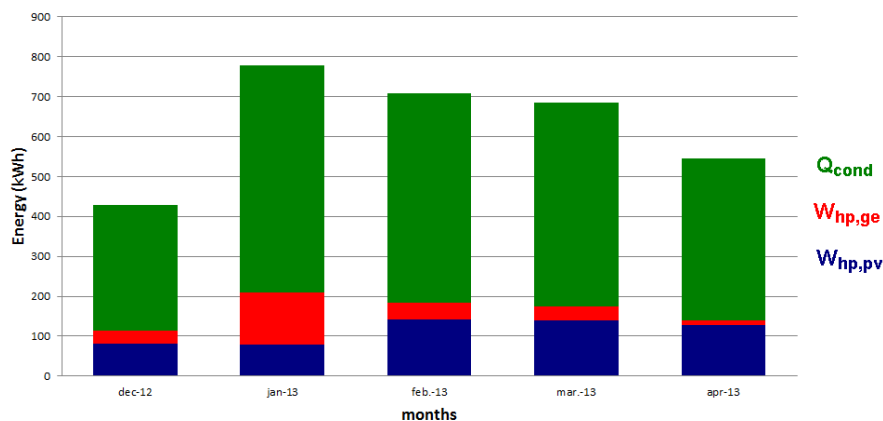
Figure 8.27: Monthly heat-pump's electrical demand and heat generation.

The overall electrical useful perfomance of the whole PV system, defined as the ratio between PV electricity supplied to the the heat-pump and intercepted solar energy (eq. 8.10), was 5.7%. The difference between the D.C. input measured at the controller and the useful A.C. electricity supplied to the heat pump is about 319kWh, this is a 38.9% of produced energy. That efficiencies can be understood through two steps: the electrical production at the array; the internal

transformation and consumption within the heating system.

Electrical production at the array, which is measured at the controller's input, could be reduced by different factors hard to quantify, as they were mentioned on subsection 7.3.3: time degradation, dust and frost deposition, mismatch effect among the modules and/or controller's uncertainty on tracking maximum power point. In addition there will be conduction losses, as it was explained, between the modules and the controller, about 1.3%. The production was also limited by controller's maximum output intensity during some very cold and high insolation days, when production at midday could exceed the controller's capacity, although most of the days this limitation was neglectible. The effect of building's thermal demand on production will be discussed in section 8.7, comparing with previously simulated production.

On the other hand, once electrical production, 820kWh, was delivered to the controller , in the subsequent steps, until the final supply into the heat pump, there were that 319kWh of losses, 38.9%, which will be detailed on the following lines. The controller adapts the electrical production from the array's voltage to batteries' voltage, and losses up to 2% of the production have been observed in this process (about 16kWh). After it, the production was delivered to the batteries for instant or deferred consumption, where some losses would arise related with continuous charging and discharging cycles at varying intensity, and night unintentional autodischarge (about 4%, 33kWh). As it has been shown in the daily results on section 8.4, the fluctuating behaviour of the system implied to operate frequently on transient mode (figs. 8.7, 8.14 and 8.21), causing about 16% of losses, 131kWh, due to peaks and interruptions.

The inverter itself is fed by the batteries and presents a zero-load power of 30W during stand-by hours, so along the season it consumed about 60kWh (7.3% of the production). During the heat-pump's operating hours 580.1kWh were delivered from the batteries to the inverter in D.C., to supply useful 501.4kWh in A.C. to the heat pump. Therefore 80kWh were lost on D.C./A.C. inversion (9.6%). Adding, all these terms, that 38.9% of losses, 319kWh, are explained.

The maximum efficiency of the inverter, according to the manufacturer, is 94%. However, the experimentally measured efficiency of the inverter was about 86.4%, probably due to partial loads, working temperature and/or transient modes.

All these factors made that the useful PV electricity supplied to the heat pump was that 501.4kWh

Once this electricity was used for heat generation, system's global efficiency (eq. 8.11) was 18.2%. Building's isolation from the grid ratio, according to equation 8.15, was 69.3% and the solar fraction, defined by equation 8.16 was 65.3%.

months	H_T [kWh/m^2]	ISE [kWh]	E_{PVMA} [kWh]	$W_{hp,pv}$ [kWh]	$W_{hp,ge}$ [kWh]	Q_{cond} [kWh]
dec-12	94.86	1328.04	134.83	72.14	28.56	314.52
jan-13	111.39	1559.46	125.67	69.51	114.05	569.43
feb-13	131.17	1836.38	193.39	124.56	37.47	523.21
mar-13	128.46	1798.44	191.36	123.56	30.39	509.18
apr-13	167.65	2347.1	175.58	111.63	12.06	405.56
TOTAL	633.53	8869.42	820.83	501.41	222.53	2321.90

Table 8.2: Monthly sums of the main variables during the heating season.

Thanks to the heat produced up to 8 hours a day, the building's indoor temperature was kept

at an average value of 19°C, 24 hours a day. The radiant floor's surface average temperature was 22°C. Figure 8.28 represents the monthly average temperatures obtained.
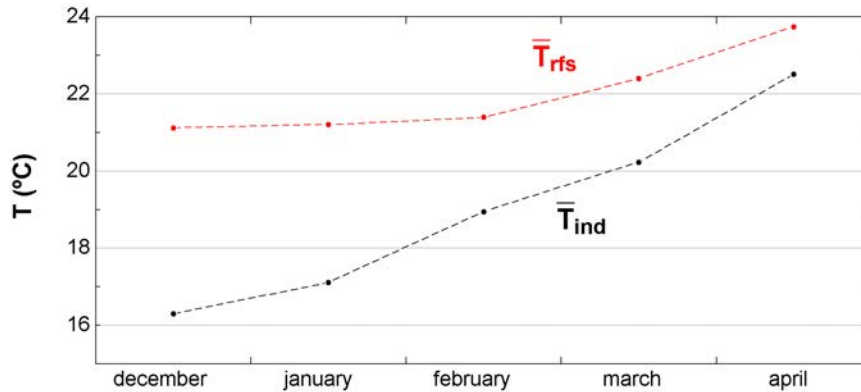
Figure 8.28: Monthly average radiant floor surface and indoor temperatures.

8.6.1   Enviromental impact reduction

The total useful PV electricity supplied to the heat pump, 501.4 kWh, did not generate CO_2 (nor others pollutants). The emission saving related would be $0.34\frac{kg_{CO_2}}{kWh}{\cdot}501.4kWH = 170.5kg_{CO_2}$.

In addition, the renewable heat gained from outdoor air along the whole season (eq. 8.1) was $Q_{evap} = 2321.9 - (501.4 + 222.5) = 1598.0kWh$.

If the whole facility, PV system+heat pump, was replaced by a boiler burning Gas-oil C or Natural Gas to produce the same ammount of heat $(Q_{cond} = 2321.9kWh)$:

1. Gas-oil C, with a boiler (combustion, generation, transport, etc.) efficiency 0.75 and emission 0.27 kg_{CO_2}/kWh, the emitted CO_2 would be 835.9 kg_{CO_2}.

2. Natural gas, with a boiler efficiency 0.85 (combustion, generation, transport, etc.) and emission 0.21 kg_{CO_2}/kWh, the emitted CO_2 would be 573.6 kg_{CO_2}.

To complete the environment balance a refill operation was done to determine the emission of the refrigerant R410A to the atmosphere during this period (fig. 8.29). The refrigerant charged to the heat pump is 1.7 kg. The mass of R410 emitted since the marketed data, March 2012, to April 2013 when finalised this investigation, was 0.031 kg, approximately, or 2% of the charge in 13 months. The emission of equivalent CO_2 was 132.1 kg at 20 years ITH.

Figure 8.29: Heat pump's refrigerant refill operation.

8.7 Comparison between simulation and experimental PV production

Finally, in this section, the experimentally achieved PV production (fig. 8.26) and the simulated achievable PV production (fig. 7.11) are compared. The numerical values plotted in those figures are listed on table 8.3. Along the five months, the 12 modules produced 820.8kWh. However, according to the simulation model proposed in this dissertation, the achievable PV production, once cell temperature and PV efficiency have been calculated every 10 minutes for the five months, would be 1265.8kWh. That means that not all the achievable PV production was achieved: 445.0kWh of PV electricity were not produced.

	Achievable PV production	Achieved PV production	Exploited
dec-12	193.2 kWh	134.8 kWh	69.8%
jan-13	224.5 kWh	125.7 kWh	56.0%
feb-13	261.9 kWh	193.4 kWh	73.8%
mar-13	258.0 kWh	191.4 kWh	74.2%
apr-13	328.2 kWh	175.6 kWh	53.5%
TOTAL	1265.8 kWh	820.8 kWh	64.8%

Table 8.3: Comparison between predicted and achieved PV production.

Table 8.3 compares the theoretically achievable PV production and the experimentally achieved production for each month, and, consequently, the explotation percentage. Along the five months, the PV array was exploited at different rates, which implied that production was not only related to the intercepted solar energy but to the following phenomena:

- In december and januray the PV array was exploited partially. As first months of the experiment, the system got interrupted unintentionally diverse days, achieving lower production than expected.

- As it has been explained on section 4.4, whenever the batteries were partially or full charged, the MPPT controller did not operate at maximum power point but at its *absorption* or *float* modes decreasing the PV production and consequently the photovoltaic efficiency. Even during the coldest months, in sunny days controller did not kept in *MPPT* mode at central hours of the day, when production could exceed the demand, switching to *absorption* mode those hours and also sometimes near sunshine and sunset (when heat pump was interrupted), as it has been plotted as example on figures 8.5, 8.12 and 8.19. An ideal storage system should be able to store that 445.0kWh surplus for satisfying future loads. However, storing all that energy is not feasible with the current available batteries without oversizing unreasonably the storage system. Due to their cost and enviromental impact, the capacity of the used lead-acid batteries was choosen just enough for supporting the system on the first hours of the morning and when PV power drops related with passing clouds. Adding more batteries to the system could allow to store sometimes extra energy on the coldest days, but would oversize the system from a seasonal point of view.

- In some very cold and high solar insolation days the production was limited by controller's maximum intensity capacity at midday. This reason, added to the one mentioned in the previous point, made the achievable PV production not be exploited at 100%, neither in winter coldest months (table 8.3). On the other hand, due to storage system's limitations, grid electricity was demanded along the season.

- During temperate months of the heating season, as it occurs with solar thermal systems, production can excess widely the demand. In the solar thermal heating systems, that heat has to be dissipated; in the photovoltaic heating system, the electricity production is adjusted by the controller. In fact, according to figure 8.25, the highest monthly intercepted solar energy was in april (2347.1kWh), but as the electrical demand of the heat pump was lower, just 175.6kWh of PV electricity were produced (PV efficiency of 7.5%). Thus, a high solar insolation does not necessarily imply a high PV production, specially when building's thermal demand decreases.

Chapter 9

Conclusions

Finally in this chapter, the main conclusions derived from the present research are summarized. In the first section, the scope of the work and the objectives stated in the first chapter are reminded and their achievement justified. After it, the main conclusions achieved in this work are remarked, specially for the developed cell temperature-PV production model simulation, the applicability of PV/T modules and the PV heating system's experimental results. To conclude, some future works that arise are listed.

9.1   Scope of the work

In this proposed research, the perfomance of a solar PV heating system was studied. After a review of the state-of-the-art and overview to PV technology (chapters 2 and 3, respectively), a microgeneration PV array which feeds a vapor-compression heat pump has been presented in chapter 4. The air-water heat pump heats a small building through a radiant floor circuit. The diverse components that are required to operate a PV heating system like this are detailed in chapter 4.

In order to size properly this type of arrays, a precise PV production model has been developed, which allows to predict the PV production of an array at any location basing in meteorological databases. The cell temperature has been remarked as a key factor on PV production and a detailed heat transfer model has been developed to determine this temperature under changing meteorological conditions (chapter 6).

The proposed cell temperature-PV production model has been run for a whole heating period predicting the maximum achievable PV generation and the working cell temperatures (chapter 7). In the same chapter, the potential application of PV/T modules in such systems has been discussed.

Finally, the experimental results of the whole PV heating facility have been described in chapter 8. In the following section the main conclusions of the analytical and experimental work are discussed and the differences articulated.

9.2 Main conclusions achieved

Diverse photovoltaic models can be found on scientific literature. Some of them are based on the determination of five parameters of the I-V curve of a PV module, which require complex equation systems and usually specific software or numerical methods to be solved. In order to simulate the real achievable PV energy of an array, an eased method is proposed which can be quickly implemented and simulated. This method requires solar radiation and cell temperature as inputs. In fact, due to PV efficiency's dependence on cell temperature, a precise PV production predicting model should face the determination of that temperature under changing meteorological conditions.

The proposed heat transfer model is easily suitable for any type of PV or PV/T modules once the internal layers' composition and thickness are known. In addition, the heat transfer model takes into account the PV production rate, predicting cell temperature for given meterological conditions and arrays' operation mode, showing how the temperature increase when there is not demand and PV production is decreased. The need of precise cell temperature determination has been inspired by experimental observations. The proposed heat transfer model is theoretically developed and experimentally compared. Simulations run for diverse autumn and winter days match with the experimentally measured values. Therefore, the cell temperature predicting model is claimed as valid.

Based on the cell temperature determination, the PV production model's simulation is run for diverse days and compared with experimentally obtained values. Both simulated and measured results match.

The cell temperature-PV production model is simulated for the heating period between 4/12/2012 and 30/4/2013. During that period, 12 PV/T modules of the array could produce 1265.8 kWh. During the sunshine hours, the average cell temperature would be 21.3℃. At midday, the seasonal average maximum cell temperature would be 47.5℃.

Basing on simulation results, the thermal application of PV/T modules for Madrid's winter climate is concluded to be negligible. The proposed model allows to evaluate the PV/T potential for diverse locations; their applicability might be different in warmer climates.

After developing and simulating the PV production model, the experimental perfomance of the PV self-consumption heating system has been presented.

12 PV modules with a total area of 15.7 m^2 (14 m^2 useful area) were employed for feeding a heat pump. The PV array was part of a self-consumption off-grid system, where the eventual PV surplus was not injected to the grid but adapted to the storage system capacity. The building to be heated includes a connection to the conventional grid so the heat pump's plug could be switched between both sources. Building's maximum thermal load is 6.0 kW, considering the load in stationary regime and building's thermal inertia. Each PV module presents a nominal peak power of 180 watts. Heat pump's nominal heating power is 6kW. During the coldest winter days, the PV system cannot supply heat enough to maintain the legal inner conditions: it would be necessary to feed partially the heat pump through grid electricity.

Period's thermal demand was 3325 kWh; the seasonal efficiency of the PV field was 9.26%. This means that the real efficiency of modules' field, functioning during a period of five months, is about 62% of the module efficiency obtained in Standard Test Conditions (STC) operating at maximum power point. The seasonal heat pump COP was 3.2 and the global conversion

from solar energy over PV modules to useful AC electricity was 5.7%. The losses from PV array's output to heat pump's input occured due to: mismatches in the array, MPPT regulator, storage in batteries, conversion from DC to AC electricity in the inverter and electricity transport through the circuits. Finally, the global efficiency from solar energy to heat produced in heat pump's condenser was 18.2%, and the solar fraction was about 65.3%.

An isolation ratio has been defined to discuss the autonomy prospects of the system. During this season, the heating system was at a 69.3% autonomous from the grid.

The heat delivered to the radiant floor was 2321.9kWh, for this purpose 723.9kWh of electricity was supplied to the heat pump. 501.4kWh of that electricity came from PV source, so the emissions of 170.5kg_{CO_2} were saved. Producing the same ammount of heat with a gas-oil C boiler would emit 835.9 kg_{CO_2}. In the case of natural gas boiler, 573.6 kg_{CO_2} would be emitted. During 13 months, since manufacturing date, an ammount of refrigerant leaked, equivalent to 132.1 kg_{CO_2}.

Finally, comparing the simulated PV production along the heating period, 1265.8kWh, and the experimental production, 820.8kWh, some conclusions for off-grid systems arise. As it has been explained, the experimental PV production was adjusted to the demand of the heat pump and batteries' charge state. Frequently when production was higher than the demand, the controller did not operate in *MPPT* mode, implying a significantly smaller PV production than the maximum achievable one predicted by the simulation. As heating season passes, the explotation of the PV system decreases adjusted to the demand. Due to storage system's limitations, 445.0kWh were not exploited.

In order to maximize the PV perfomance in an off-grid system, the consumption should be constantly adapted to the production. In the proposed PV heating system, as it aims to be integrated in buildings in the future, the electrochemical storage has been minimized. On the other hand, during operating hours, the heat pump produced as much heat as possible, using the building itself as thermal storage.

In conclusion, the developed PV production model is a precise tool for predicting the real achievable production of a PV array, but to ensure as much as possible that production the loads of an off-grid system have to be designed and dynamically adapted to it, increasing the explotation of the array.

9.3   Recommendation for future research

From the reached results of this dissertation some future works might arise. On the following lines, some of these researchs are proposed:

- The developed model could be run for a whole year, calculating the yearly achievable PV production, for heating and cooling, and operating average cell temperature for each month, discussing the potential use of PV/T modules in diverse seasons of the year.

- In central Spain's climate a PV heating system like the proposed one would be used at most during 7-8 months. In the aim of maximizing PV system's perfomance along the year, reversible heat pump's potential for air-conditioning should be studied through simulation and/or experimental test, expanding the experimental results attached on appendix A.

- The economical aspect could be added to the model in order to study the pay-back period of the facility.

- In case of designing an off-grid PV heating system for remote areas where there is not the possibility of eventually connecting the heat pump to the grid, the installation of a D.C. heat pump would offer a complementary research line.

- The design for future experimental facilities could be increased in complexity.

Bibliography

Interface design considerations for terrestrial solar cell modules, 1976.

Flat-Plate Photovoltaic Array Design Optimization, 1980.

Une-en-1264 water based surface embedded heating and cooling systems., 2013.

Alonso. Boletín solar fotovoltaica autónoma. Technical report, SunFields Europe, 2013.

M.C. Alonso-Garcia and J.L. Balenzategui. Estimation of photovoltaic module yearly temperature and performance based on nominal operation cell temperature calculations. *Renewable Energy*, 29(12):1997 – 2010, 2004. ISSN 0960-1481. doi: http://dx.doi.org/10.1016/j.renene.2004.03.010.

Marco Antonelli and Umberto Desideri. The doping effect of italian feed-in tariffs on the pv market. *Energy Policy*, 67(0):583 – 594, 2014. ISSN 0301-4215. doi: http://dx.doi.org/10.1016/j.enpol.2013.12.025.

S. Armstrong and W.G. Hurley. A thermal model for photovoltaic panels under varying atmospheric conditions. *Applied Thermal Engineering*, 30(11-12):1488 – 1495, 2010. ISSN 1359-4311. doi: http://dx.doi.org/10.1016/j.applthermaleng.2010.03.012.

Niccola Aste, Claudio del Pero, and Fabrizio Leonforte. Water flat plate pv-thermal collectors: A review. *Solar Energy*, 102(0):98 – 115, 2014. ISSN 0038-092X. doi: http://dx.doi.org/10.1016/j.solener.2014.01.025.

S. Ayyash and M. Sartawi. Economic comparison of solar absorption and photovoltaic-assisted vapour compression cooling systems (kuwait). *International Journal of Energy Research*, 7(3): 279–288, 1983.

Constantinos A. Balaras, Gershon Grossman, Hans-Martin Henning, Carlos A. Infante Ferreira, Erich Podesser, Lei Wang, and Edo Wiemken. Solar air conditioning in europe-an overview. *Renewable and Sustainable Energy Reviews*, 11(2):299 – 314, 2007. ISSN 1364-0321. doi: http://dx.doi.org/10.1016/j.rser.2005.02.003. URL http://www.sciencedirect.com/science/article/pii/S1364032105000456.

J. Bany. Analysis of a direct coupling d.c. motor and a photovoltaic converter. *Energy Conversion*, 18(2):73 – 79, 1978. ISSN 0013-7480. doi: http://dx.doi.org/10.1016/0013-7480(78)90075-X. URL http://www.sciencedirect.com/science/article/pii/001374807890075X.

A.S. Barker. Photovoltaic solar cell array used for supplemental power generation. *Solar Energy*, 23(5):427 – 434, 1979. ISSN 0038-092X. doi: http://dx.doi.org/10.1016/0038-092X(79)90151-8. URL http://www.sciencedirect.com/science/article/pii/0038092X79901518.

Benedikt Battke, Tobias S. Schmidt, David Grosspietsch, and Volker H. Hoffmann. A review and probabilistic model of lifecycle costs of stationary batteries in multiple applications. *Renewable and Sustainable Energy Reviews*, 25(0):240 – 250, 2013. ISSN 1364-0321. doi: http://dx.doi.org/10.1016/j.rser.2013.04.023. URL http://www.sciencedirect.com/science/article/pii/S136403211300275X.

Paolo Bertoldi, Bettina Hirl, and Nicola Labanca. Energy efficiency status report 2012. jrc scientific and policy reports. Technical report, European Commission, 2012.

Bloomberg. New energy finance. pv market outlook, 2012.

BOE. Real decreto 2818/1998, de 23 de diciembre, sobre producción de energía eléctrica por instalaciones abastecidas por recursos o fuentes de energía renovables, residuos y cogeneración., July 1998.

BOE. Real decreto 1663/2000, de 29 de septiembre, sobre conexión de instalaciones fotovoltaicas a la red de baja tensión., July 2000.

BOE. Real decreto 436/2004, de 12 de marzo, por el que se establece la metodología para la actualización y sistematización del régimen jurídico y económico de la actividad de producción de energía eléctrica en régimen especial., July 2004.

BOE. Real decreto 661/2007, de 25 de mayo, por el que se regula la actividad de producción de energía eléctrica en régimen especial., July 2007.

M.J. Brandemuehl and W.A. Beckman. Economic evaluation and optimization of solar heating systems. *Solar Energy*, 23(1):1 – 10, 1979. ISSN 0038-092X. doi: http://dx.doi.org/10.1016/0038-092X(79)90038-0.

C. Breyer, A. Gerlach, M. Hlusiak, C. Peters, P. Adelmann, J. Winiecki, H. Schützeichel, S. Tsegaye, and W. Gashie. Electrifying the poor: Highly economic off-grid pv systems in ethiopia - a basis for sustainable rural development. In *24th European Photovoltaic Solar Energy Conference, 21-25 September 2009, Hamburg, Germany*, 2009. doi: 10.4229/24thEUPVSEC2009-5EP.2.3.

Francesco Calise. High temperature solar heating and cooling systems for different mediterranean climates: Dynamic simulation and economic assessment. *Applied Thermal Engineering*, 32(0): 108 – 124, 2012. ISSN 1359-4311. doi: http://dx.doi.org/10.1016/j.applthermaleng.2011.08.037.

Francesco Calise, Massimo Dentice d'Accadia, and Laura Vanoli. Design and dynamic simulation of a novel solar trigeneration system based on hybrid photovoltaic/thermal collectors (pvt). *Energy Conversion and Management*, 60(0):214 – 225, 2012. ISSN 0196-8904. doi: http://dx.doi.org/10.1016/j.enconman.2012.01.025. URL http://www.sciencedirect.com/science/article/pii/S0196890412000787. Special issue

of Energy Conversion and Management dedicated to {ECOS} 2011 - the 24th International Conference on Efficiency, Costs, Optimization, Simulation and Environmental Impact of Energy Systems.

Francesco Calise, Massimo Dentice d'Accadia, Adolfo Palombo, and Laura Vanoli. Dynamic simulation of a novel high-temperature solar trigeneration system based on concentrating photovoltaic/thermal collectors. *Energy*, 61(0):72 – 86, 2013. ISSN 0360-5442. doi: http://dx.doi.org/10.1016/j.energy.2012.10.008. URL http://www.sciencedirect.com/science/article/pii/S0360544212007700.

Clemente Capasso and Ottorino Veneri. Experimental analysis on the performance of lithium based batteries for road full electric and hybrid vehicles. *Applied Energy*, 136(0):921 – 930, 2014. ISSN 0306-2619. doi: http://dx.doi.org/10.1016/j.apenergy.2014.04.013. URL http://www.sciencedirect.com/science/article/pii/S0306261914003560.

Luis Castañer, Sandra Bermejo, Tom Markvart, and Katerina Fragaki. Chapter iia-2 - energy production by a pv array. In Augustin McEvoy, Tom Markvart, and Luis Castañer, editors, *Practical Handbook of Photovoltaics (Second Edition)*, pages 645 – 658. Academic Press, Boston, second edition edition, 2012. ISBN 978-0-12-385934-1. doi: http://dx.doi.org/10.1016/B978-0-12-385934-1.00018-0. URL http://www.sciencedirect.com/science/article/pii/B9780123859341000180.

Yunus Cengel. *Heat Transfer: A Practical Approach*. 2003.

P.G. Charalambous, G.G. Maidment, S.A. Kalogirou, and K. Yiakoumetti. Photovoltaic thermal (pv/t) collectors: A review. *Applied Thermal Engineering*, 27(2-3):275 – 286, 2007. ISSN 1359-4311. doi: http://dx.doi.org/10.1016/j.applthermaleng.2006.06.007. URL http://www.sciencedirect.com/science/article/pii/S1359431106002316.

R. Cherrington, V. Goodship, A. Longfield, and K. Kirwan. The feed-in tariff in the uk: A case study focus on domestic photovoltaic systems. *Renewable Energy*, 50(0):421 – 426, 2013. ISSN 0960-1481. doi: http://dx.doi.org/10.1016/j.renene.2012.06.055. URL http://www.sciencedirect.com/science/article/pii/S0960148112004065.

Soolyeon Cho, Eun Chul Kang, and Euy Joon Lee. Energy savings analysis of fuel-cell microgeneration systems with ground source heat pumps in load-sharing buildings. *International Journal of Low-Carbon Technologies*, 2014. doi: 10.1093/ijlct/ctu009. URL http://ijlct.oxfordjournals.org/content/early/2014/03/04/ijlct.ctu009.abstract.

T.T. Chow. Performance analysis of photovoltaic-thermal collector by explicit dynamic model. *Solar Energy*, 75(2):143 – 152, 2003. ISSN 0038-092X. doi: http://dx.doi.org/10.1016/j.solener.2003.07.001. URL http://www.sciencedirect.com/science/article/pii/S0038092X03002512.

D.R. Clark, S.A. Klein, and W.A. Beckman. A method for estimating the performance of photovoltaic systems. *Solar Energy*, 33(6):551 – 555, 1984. ISSN 0038-092X. doi: http://dx.doi.org/10.1016/0038-092X(84)90010-0. URL http://www.sciencedirect.com/science/article/pii/0038092X84900100.

CTE. Codigo técnico de la edificación. Technical report, Ministerio de la Vivienda, 2009.

CTE. Actualización del codigo técnico de la edificación. Technical report, Ministerio de Fomento, 2013.

P. de Agustin, M. Izquierdo, and E. Martin. Solar heating system performance for the heating season 2011-12 in madrid. *Renewable Energy and Power Quality Journal*, (11), 2013.

Pablo de Agustin. Estudio del almacenamiento eléctrico en un sistema solar fotovoltaico con minipaneles para alimentación de un conjunto de magnetómetros. Master's thesis, Universidad Complutense de Madrid, 2009.

W. de Soto, S.A. Klein, and W.A. Beckman. Improvement and validation of a model for photovoltaic array performance. *Solar Energy*, 80(1):78 – 88, 2006. ISSN 0038-092X. doi: http://dx.doi.org/10.1016/j.solener.2005.06.010. URL http://www.sciencedirect.com/science/article/pii/S0038092X05002410.

W. de Soto, S.A. Klein, and W.A. Beckman. Erratum to "improvement and validation of a model for photovoltaic array performance"[solar energy 80 (2006) 78-88]. *Solar Energy*, 81 (1):150 –, 2007. ISSN 0038-092X. doi: http://dx.doi.org/10.1016/j.solener.2006.05.001. URL http://www.sciencedirect.com/science/article/pii/S0038092X06001691.

Boucar Diouf and Ramchandra Pode. Potential of lithium-ion batteries in renewable energy. *Renewable Energy*, 76(0):375 – 380, 2015. ISSN 0960-1481. doi: http://dx.doi.org/10.1016/j.renene.2014.11.058. URL http://www.sciencedirect.com/science/article/pii/S0960148114007885.

B. Domenech, M. Ranaboldo, L. Ferrer-Marti, A. García-Villoria, and R. Pastor. Design of autonomous rural electrification systems for isolated spanish communities. In *MicrogenIII: Proceedings of The 3rd edition of the International Conference on Microgeneration and Related Technologies (Naples, Italy, April 15-17, 2013)*, 2013.

Swapnil Dubey, Jatin Narotam Sarvaiya, and Bharath Seshadri. Temperature dependent photovoltaic (pv) efficiency and its effect on pv production in the world - a review. *Energy Procedia*, 33(0):311 – 321, 2013. ISSN 1876-6102. doi: http://dx.doi.org/10.1016/j.egypro.2013.05.072. URL http://www.sciencedirect.com/science/article/pii/S1876610213000829. {PV} Asia Pacific Conference 2012.

John A. Duffie and William A. Beckman. *Solar Engineering of Thermal Processes, 4th Edition*. 2013.

N.P.H. Duraman, K.L. Lim, and S.L.I. Chan. Chapter 16 - batteries for remote area power (rap) supply systems. In Chris MenictasMaria Skyllas-KazacosTuti Mariana Lim, editor, *Advances in Batteries for Medium and Large-Scale Energy Storage*, Woodhead Publishing Series in Energy, pages 563 – 586. Woodhead Publishing, 2015. ISBN 978-1-78242-013-2. doi: http://dx.doi.org/10.1016/B978-1-78242-013-2.00016-9. URL http://www.sciencedirect.com/science/article/pii/B9781782420132000169.

Ursula Eicker, Antonio Colmenar-Santos, Lya Teran, Mariela Cotrado, and David Borge-Diez. Economic evaluation of solar thermal and photovoltaic cooling systems through simulation in different climatic conditions: An analysis in three different cities in europe. *Energy and Buildings*, 70(0):207 – 223, 2014. ISSN 0378-7788. doi: http://dx.doi.org/10.1016/j.enbuild.2013.11.061. URL `http://www.sciencedirect.com/science/article/pii/S0378778813007688`.

A. Einstein. Über einen die erzeugung und verwandlung des lichtes betreffenden heuristischen gesichtspunkt. *Annalen der Physik*, 17(132), 1905.

O.M.M. ElTom, S.A. Omer, A.Z. Taha, and A.A.M. Sayigh. Performance of a photovoltaic solar refrigerator in tropical climate conditions. *Renewable Energy*, 1(2):199 – 205, 1991. ISSN 0960-1481. doi: http://dx.doi.org/10.1016/0960-1481(91)90075-Z. URL `http://www.sciencedirect.com/science/article/pii/096014819190075Z`.

E. Entchev, L. Yang, M. Ghorab, and E. J. Lee. Simulation of hybrid photovoltaic thermal-ground source heat pump microgeneration system in load sharing applications. In *MicrogenIII: Proceedings of The 3rd edition of the International Conference on Microgeneration and Related Technologies (Naples, Italy, April 15-17, 2013)*, 2013.

EPIA. Solar photovoltaics competing in the enegy sector: On the road to competitiveness, european photovoltaic industry association, September 2011a.

EPIA. Solar generation 6, european photovoltaic industry association, February 2011b.

EPIA. Global market outlook for photovoltaics 2013-2017, european photovoltaic industry association, May 2013.

D.G. Erbs, S.A. Klein, and J.A. Duffie. Estimation of the diffuse radiation fraction for hourly, daily and monthly-average global radiation. *Solar Energy*, 28(4):293 – 302, 1982. ISSN 0038-092X. doi: http://dx.doi.org/10.1016/0038-092X(82)90302-4. URL `http://www.sciencedirect.com/science/article/pii/0038092X82903024`.

Ana España-Diaz. Demanda de calefacción en régimen permanente y dinámico. especificación de la bomba de calor. Trabajo Fin de Grado, Universidad Carlos III de Madrid. Tutor: Marcelo Izquierdo Millan, 2014.

E.U. Directive 2009/28/ec of the european parliament and of the council of 23 april 2009 on the promotion of the use of energy from renewable sources and amending and subsequently repealing directives 2001/77/ec and 2003/30/ec. Official Journal of the European Union, 2009.

E.U. Directive 2010/31/eu of the european parliament and of the council of 19 may 2010 on the energy performance of buildings. Official Journal of the European Union, 2010.

EurObserv'ER. Photovoltaic barometer, April 2013.

Eurostat. Energy production and imports. URL `http://ec.europa.eu/eurostat/web/main` (last access: 20/02/2015).

D.L. Evans. Simplified method for predicting photovoltaic array output. *Solar Energy*, 27(6):
   555 – 560, 1981. ISSN 0038-092X. doi: http://dx.doi.org/10.1016/0038-092X(81)90051-7. URL
   `http://www.sciencedirect.com/science/article/pii/0038092X81900517`.

J. C. Farman, B. G. Gardiner, and J. D. Shanklin. Large losses of total ozone in antarctica reveal
   seasonal clox/nox interaction. *Nature*, 315:207–210, 1985.

K.F. Fong and C.K. Lee. Investigation of separate or integrated provision of solar cooling and heat-
   ing for use in typical low-rise residential building in subtropical hong kong. *Renewable Energy*,
   75(0):847 – 855, 2015. ISSN 0960-1481. doi: http://dx.doi.org/10.1016/j.renene.2014.10.069.
   URL `http://www.sciencedirect.com/science/article/pii/S0960148114007095`.

E. Forniés, F. Naranjo, M. Mazo, and F. Ruiz. The influence of mismatch of solar ccell on relative
   power loss of photovoltaic modules. *Solar Energy*, 97:39–47, 2013.

Stefan   Fortuin,   Michael   Hermann,   Gerhard   Stryi-Hipp,   Peter   Nitz,   and
   Werner   Platzer.   Hybrid   pv-thermal   collector   development: Concepts,   expe-
   riences,   results   and   research   needs.   *Energy   Procedia*,   48(0):37   –   47,   2014.
   ISSN   1876-6102.   doi: http://dx.doi.org/10.1016/j.egypro.2014.02.006.   URL
   `http://www.sciencedirect.com/science/article/pii/S1876610214002689`.   Proceed-
   ings of the 2nd International Conference on Solar Heating and Cooling for Buildings and
   Industry (SHC 2013).

G. Fraisse, C. Ménézo, and K. Johannes.   Energy performance of water hybrid pv/t col-
   lectors applied to combisystems of direct solar floor type.   *Solar Energy*, 81(11):1426 –
   1438, 2007.   ISSN 0038-092X.   doi: http://dx.doi.org/10.1016/j.solener.2006.11.017.   URL
   `http://www.sciencedirect.com/science/article/pii/S0038092X07000266`.

Maria Teresa Garcia-Alvarez and Rosa Maria Mariz-Perez.   Analysis of the success of
   feed-in tariff for renewable energy promotion mechanism in the eu: Lessons from
   germany and spain.   *Procedia - Social and Behavioral Sciences*, 65(0):52 – 57,
   2012.   ISSN 1877-0428.   doi: http://dx.doi.org/10.1016/j.sbspro.2012.11.090.   URL
   `http://www.sciencedirect.com/science/article/pii/S1877042812050756`. International
   Congress on Interdisciplinary Business and Social Sciences 2012 (ICIBSoS 2012).

A. Goetzberger and V.U. Hoffmann. *Photovoltaic Solar Energy Generation*. Springer, 2005.

N. Hartmann, C. Glueck, and F.P. Schmidt. Solar cooling for small office buildings: Comparison
   of solar thermal and photovoltaic options for two different european climates. *Renewable Energy*,
   36(5):1329 – 1338, 2011. ISSN 0960-1481. doi: http://dx.doi.org/10.1016/j.renene.2010.11.006.
   URL `http://www.sciencedirect.com/science/article/pii/S0960148110005082`.

Hans-Martin   Henning.   Solar   assisted   air   conditioning   of   buildings   -   an
   overview.   *Applied   Thermal   Engineering*,   27(10):1734   –   1749,   2007.   ISSN
   1359-4311.   doi: http://dx.doi.org/10.1016/j.applthermaleng.2006.07.021.   URL
   `http://www.sciencedirect.com/science/article/pii/S1359431106002547`. Heat transfer
   and sustainable energy technologies.

Joern Hoppmann, Joern Huenteler, and Bastien Girod. Compulsive policy-making–the evolution of the german feed-in tariff system for solar photovoltaic power. *Research Policy*, (0):–, 2014. ISSN 0048-7333. doi: http://dx.doi.org/10.1016/j.respol.2014.01.014. URL `http://www.sciencedirect.com/science/article/pii/S0048733314000249`.

Adnan Ibrahim, Mohd Yusof Othman, Mohd Hafidz Ruslan, Sohif Mat, and Kamaruzzaman Sopian. Recent advances in flat plate photovoltaic/thermal (pv/t) solar collectors. *Renewable and Sustainable Energy Reviews*, 15(1):352 – 365, 2011. ISSN 1364-0321. doi: http://dx.doi.org/10.1016/j.rser.2010.09.024. URL `http://www.sciencedirect.com/science/article/pii/S1364032110003114`.

IDAE. Plan nacional de energías renovables 2005-2010. Technical report, Instituto para la Diversificación y el Ahorro de Energía. Ministerio de Industria, Turismo y Comercio, 2005.

IDAE. Condiciones climáticas exteriores de proyecto: Guía técnica. Technical report, Instituto para la Diversificación y el Ahorro de Energía. Ministerio de Industria, Turismo y Comercio, 2010.

IDAE. Análisis del consumo energético del sector residencial en españa, proyecto sech-spahousec. Technical report, Instituto para la Diversificación y el Ahorro de Energía. Ministerio de Industria, Energía y Turismo, 2011.

IEA. Energy poverty - how to make modern energy access universal? special early excerpt of the world energy outlook 2010 for the un general assembly on the millenium devel goals. Technical report, OECD / IEA, 2010.

IGN. Instituto geográfico nacional. URL `http://www.ign.es (last access: 8/2/2015)`.

Franck Incropera. *Fundamentals of heat and mass transfer*. 1990.

IPCC. *Special Report on Renewable Energy Sources and Climate Change Mitigation*. Cambridge University Press, 2011.

IPCC. *Climate Change 2013: The Physical Science Basis. Contribution of Working group I to the Fifth Assesment Report of the Intergovernmental Panel on Climate Change*. Cambridge University Press, 2013.

M. Iqbal. *An introduction to Solar Radiation*. Academic Press, 1983.

M. Izquierdo and P. de Agustin. Sistema de calefacción y refrigeración solar integrado en el edificio. In *Jornadas internacionales conmemorativas del 80 aniversario del IETcc (12,13,14 noviembre 2014, Madrid)*, 2014.

M. Izquierdo and P. de Agustín-Camacho. Solar heating by radiant floor: Experimental results and emission reduction obtained with a micro photovoltaic-heat pump system. *Applied Energy*, 147(0):297 – 307, 2015. ISSN 0306-2619. doi: http://dx.doi.org/10.1016/j.apenergy.2015.03.007. URL `http://www.sciencedirect.com/science/article/pii/S0306261915002913`.

M. Izquierdo, A. Moreno-Rodriguez, A. Gonzalez-Gil, and N. Garcia-Hernando. Air conditioning in the region of madrid, spain: An approach to electricity consumption, economics and co2 emissions. *Energy*, 36:1630–1639, 2011.

M. Izquierdo, P. de Agustin, and E. Martin. Heat pump for radiant cooled and heated floor driven by a microphotovoltaic system. In *MicrogenIII: Proceedings of The 3rd edition of the International Conference on Microgeneration and Related Technologies (Naples, Italy, April 15-17, 2013)*, 2013.

M. Izquierdo, Pablo de Agustín, and E. Martín. A micro photovoltaic-heat pump system for house heating by radiant floor: Some experimental results. *Energy Procedia*, 48(0):865 – 875, 2014a. ISSN 1876-6102. doi: http://dx.doi.org/10.1016/j.egypro.2014.02.100. URL `http://www.sciencedirect.com/science/article/pii/S1876610214003622`. Proceedings of the 2nd International Conference on Solar Heating and Cooling for Buildings and Industry (SHC 2013).

M. Izquierdo, A. González-Gil, and E. Palacios. Solar-powered single-and double-effect directly air-cooled libr-h2o absorption prototype built as a single unit. *Applied Energy*, 130(0):7 – 19, 2014b. ISSN 0306-2619. doi: http://dx.doi.org/10.1016/j.apenergy.2014.05.028. URL `http://www.sciencedirect.com/science/article/pii/S0306261914005236`.

Marcelo Izquierdo. Diseño, construcción y evaluación experimental de un sistema de refrigeración solar y trigeneración de alta eficiencia para edificios e invernaderos (ene2010-20650-c02-01). Technical report, Ministerio de Ciencia e Innovación, 2010.

S. Jacques, A. Caldeira, Z. Ren, A. Schellmanns, and N. Batut. Impact of the cell temperature on the energy efficiency of a single glass pv module: thermal modeling in steady-state and validation by experimental data. *Renewable Energy and Power Quality Journal*, (11), 2013.

Ji Jie, Liu Keliang, Chow Tin-tai, Pei Gang, He Wei, and He Hanfeng. Performance analysis of a photovoltaic heat pump. *Applied Energy*, 85:680–693, 2008.

A.D. Jones and C.P. Underwood. A thermal model for photovoltaic systems. *Solar Energy*, 70 (4):349 – 359, 2001. ISSN 0038-092X. doi: http://dx.doi.org/10.1016/S0038-092X(00)00149-3. URL `http://www.sciencedirect.com/science/article/pii/S0038092X00001493`.

Thomachan A Kattakayam and K Srinivasan. Thermal performance characterization of a photovoltaic driven domestic refrigerator. *International Journal of Refrigeration*, 23(3):190 – 196, 2000. ISSN 0140-7007. doi: http://dx.doi.org/10.1016/S0140-7007(99)00049-3. URL `http://www.sciencedirect.com/science/article/pii/S0140700799000493`.

Mustafa Kaya. Thermal and electrical performance evaluation of pv/t collectors in uae. Master's thesis, KTH School of Industrial Engineering and Management, 2013.

Ongun B. Kazanci, Martynas Skrupskelis, Pavel Sevela, Georgi K. Pavlov, and Bjarne W. Olesen. Sustainable heating, cooling and ventilation of a plus-energy house via photovoltaic/thermal panels. *Energy and Buildings*, 83(0):122 – 129,

2014.   ISSN   0378-7788.   doi: http://dx.doi.org/10.1016/j.enbuild.2013.12.064.   URL
`http://www.sciencedirect.com/science/article/pii/S0378778814002308`.

Liu Keliang, Ji Jie, Chow Tin-tai, Pei Gang, He Hanfeng, Jiang Aiguo, and Yang Jichun. Performance study of a photovoltaic solar assisted heat pump with variable-frequency compressor - a case study in tibet. *Renewable Energy*, 2009.

Henry Kelly. Photovoltaic power for telecommunications. *Journal of Power Sources*, 4(4):337 – 347, 1979. ISSN 0378-7753. doi: http://dx.doi.org/10.1016/0378-7753(79)80008-7. URL `http://www.sciencedirect.com/science/article/pii/0378775379800087`.

D.S. Kim and C.A. Infante Ferreira. Solar refrigeration options – a state-of-the-art review. *International Journal of Refrigeration*, 31(1):3 – 15, 2008. ISSN 0140-7007. doi: http://dx.doi.org/10.1016/j.ijrefrig.2007.07.011. URL `http://www.sciencedirect.com/science/article/pii/S0140700707001478`.

King, Boyson, and Kratochvil. Photovoltaic array performance model. Technical report, Sandia National Laboratories, 2004.

S. J. Kline and F.A. McClintock. Describing uncertainties in single-sample experiments. *ASME Mechanical Engineering*, 3, 1953.

Michael Koehl, Markus Heck, Stefan Wiesmeier, and Jochen Wirth. Modeling of the nominal operating cell temperature based on outdoor weathering. *Solar Energy Materials and Solar Cells*, 95(7):1638 – 1646, 2011. ISSN 0927-0248. doi: http://dx.doi.org/10.1016/j.solmat.2011.01.020. URL `http://www.sciencedirect.com/science/article/pii/S0927024811000304`.

H.H. Ku. Notes on the use of propagation of error formulas. *Journal of Research on the National Bureau of Standars - C. Engineering and Instrumentation*, 70C(4), October-December 1966.

Oscar Perpiñán Lamigueiro. *Energía Solar Fotovoltaica*. Creative Commons ebook, 2013.

Peter T. Landsberg and Tom Markvart. Chapter ia-3 - ideal efficiencies. In Augustin McEvoy, Tom Markvart, and Luis Castañer, editors, *Practical Handbook of Photovoltaics (Second Edition)*, pages 63 – 75. Academic Press, Boston, second edition edition, 2012. ISBN 978-0-12-385934-1. doi: http://dx.doi.org/10.1016/B978-0-12-385934-1.00003-9. URL `http://www.sciencedirect.com/science/article/pii/B9780123859341000039`.

G.O.G. Löf and R.A. Tybout. Cost of house heating with solar energy. *Solar Energy*, 14(3):253 – 278, 1973. ISSN 0038-092X. doi: http://dx.doi.org/10.1016/0038-092X(73)90094-7. URL `http://www.sciencedirect.com/science/article/pii/0038092X73900947`.

Siwei Li, Jaewan Joe, Jianjun Hu, and Panagiota Karava. System identification and model-predictive control of office buildings with integrated photovoltaic-thermal collectors, radiant floor heating and active thermal storage. *Solar Energy*, 113(0):139 – 157, 2015. ISSN 0038-092X. doi: http://dx.doi.org/10.1016/j.solener.2014.11.024. URL `http://www.sciencedirect.com/science/article/pii/S0038092X14005684`.

Benjamin Y.H. Liu and Richard C. Jordan. The interrelationship and characteristic distribution of direct, diffuse and total solar radiation. *Solar Energy*, 4(3):1 – 19, 1960. ISSN 0038-092X. doi: http://dx.doi.org/10.1016/0038-092X(60)90062-1. URL `http://www.sciencedirect.com/science/article/pii/0038092X60900621`.

Valerio LoBrano and Giuseppina Ciulla. An efficient analytical approach for obtaining a five parameters model of photovoltaic modules using only reference data. *Applied Energy*, 111(0): 894 – 903, 2013. ISSN 0306-2619. doi: http://dx.doi.org/10.1016/j.apenergy.2013.06.046. URL `http://www.sciencedirect.com/science/article/pii/S0306261913005539`.

Antonio Luque. Photovoltaics and its research and development structure in spain: the situation in 1988. *Solar Cells*, 26:107 – 123, 1989. ISSN 0379-6787. doi: http://dx.doi.org/10.1016/0379-6787(89)90071-9. URL `http://www.sciencedirect.com/science/article/pii/0379678789900719`.

Tao Ma, Hongxing Yang, and Lin Lu. Performance evaluation of a stand-alone photovoltaic system on an isolated island in hong kong. *Applied Energy*, 112(0):663 – 672, 2013. ISSN 0306-2619. doi: http://dx.doi.org/10.1016/j.apenergy.2012.12.004. URL `http://www.sciencedirect.com/science/article/pii/S0306261912008811`.

Tao Ma, Hongxing Yang, Lin Lu, and Jinqing Peng. Pumped storage-based standalone photovoltaic power generation system: Modeling and techno-economic optimization. *Applied Energy*, 137(0):649 – 659, 2015. ISSN 0306-2619. doi: http://dx.doi.org/10.1016/j.apenergy.2014.06.005. URL `http://www.sciencedirect.com/science/article/pii/S0306261914005790`.

Kulbir Singh Malhotra. Potential for pumping irrigation water with renewable sources of energy in indian arid zone. *Energy in Agriculture*, 3(0):245 – 251, 1984. ISSN 0167-5826. doi: http://dx.doi.org/10.1016/0167-5826(84)90026-3. URL `http://www.sciencedirect.com/science/article/pii/0167582684900263`.

J.D. Marcos, M. Izquierdo, and D. Parra. Solar space heating and cooling for spanish housing: Potential energy savings and emissions reduction. *Solar Energy*, 85(11):2622 – 2641, 2011. ISSN 0038-092X. doi: http://dx.doi.org/10.1016/j.solener.2011.08.006. URL `http://www.sciencedirect.com/science/article/pii/S0038092X11002787`.

Ronald W. Matlin, William R. Romaine, and Paul E. Fischbach. 25 -kilowatt photovoltaic powered irrigation and grain drying experiment. In Francis de Winter and Michael Cox, editors, *Sun: Mankind's Future Source of Energy*, pages 1925 – 1929. Pergamon, 1978. ISBN 978-1-4832-8407-1. doi: http://dx.doi.org/10.1016/B978-1-4832-8407-1.50373-1. URL `http://www.sciencedirect.com/science/article/pii/B9781483284071503731`.

Tomas Matuska. Performance and economic analysis of hybrid pvt collectors in solar dhw system. *Energy Procedia*, 48(0):150 – 156, 2014. ISSN 1876-6102. doi: http://dx.doi.org/10.1016/j.egypro.2014.02.019. URL `http://www.sciencedirect.com/science/article/pii/S1876610214002811`. Proceedings of the 2nd International Conference on Solar Heating and Cooling for Buildings and Industry (SHC 2013).

W.H. McAdams. *Heat transmission*. 1954.

P. McGeehin. Energy storage by batteries. *Physics in Technology*, 11(1):8, 1980. URL `http://stacks.iop.org/0305-4624/11/i=1/a=I04`.

MINETUR. Proyecto de real decreto por el que se establece la regulación de las condiciones administrativas, técnicas y económicas de la modalidad de suministro de energía eléctrica con balance neto. Technical report, Ministerio de Industria, Turismo y Comercio, November 2011.

MINETUR. Propuesta de real decreto por el que se establece la regulación de las condiciones administrativas, técnicas y económicas de las modalidades de suministro de energía eléctrica con autoconsumo y de producción con autoconsumo. Technical report, Ministerio de Industria, Energía y Turismo, July 2013.

Macedon D. Moldovan, Ion Visa, Mircea Neagoe, and Bogdan G. Burduhos. Solar heating & cooling energy mixes to transform low energy buildings in nearly zero energy buildings. *Energy Procedia*, 48(0):924 – 937, 2014. ISSN 1876-6102. doi: http://dx.doi.org/10.1016/j.egypro.2014.02.106. Proceedings of the 2nd International Conference on Solar Heating and Cooling for Buildings and Industry (SHC 2013).

Mario J. Molina and F. S. Rowland. Stratospheric sink for chlorofluoromethanes: chlorine atomcatalysed destruction of ozone. *Nature*, 249(5460):810–812, June 1974.

NASA. National space science data center, vanguard 1, nssdc/cospar id: 1958-002b. URL `http://nssdc.gsfc.nasa.gov/nmc/spacecraftDisplay.do?id=1958-002B` (last access: 8/2/2015).

A.T. Naveed, E.J. Lee, and E.C. Kang. Operation of solar photovoltaic-thermal (pv/t) hybrid system in kier. *Renewable Energy Resources and a Greener Future*, VIII, 2006. Proceedings of the Sixth International Conference for Enhanced Building Operations, Shenzhen, China, November 6-9, 2006.

G. Nellis and S. Klein. *Heat Transfer*. 2009.

NREL. Research cell efficiency chart. URL `http://www.nrel.gov/ncpv/` (last rev: 12/08/2014).

D. Picault, B. Raison, S. Bacha, J. de la Casa, and J. Aguilera. Forecasting photovoltaic array power production subject to mismatch losses. *Solar Energy*, 84:1301–1309, 2010.

Andreas Poullikkas. A comparative assessment of net metering and feed in tariff schemes for residential {PV} systems. *Sustainable Energy Technologies and Assessments*, 3(0): 1 – 8, 2013. ISSN 2213-1388. doi: http://dx.doi.org/10.1016/j.seta.2013.04.001. URL `http://www.sciencedirect.com/science/article/pii/S2213138813000313`.

pvXchange. Price index. URL `http://www.pvxchange.com` (last access: 8/3/2015).

Rabadiya and Kirar. Comparative analysis of wind loss coefficiente (wind heat transfer coefficient) for solar flat plate collector. *International Journal of Emerging Technology and Advanced Engineering*, 2(9), 2012.

REE. Series estadísticas de red eléctrica de españa www.ree.es/es/publicaciones/indicadores-y-datos-estadisticos/series-estadisticas, 2013.

D.T. Reindl, W.A. Beckman, and J.A. Duffie. Evaluation of hourly tilted surface radiation models. *Solar Energy*, 45(1):9 – 17, 1990. ISSN 0038-092X. doi: http://dx.doi.org/10.1016/0038-092X(90)90061-G. URL http://www.sciencedirect.com/science/article/pii/0038092X9090061G.

REN21. Renewables 2013 global status report. Technical report, Renewable Energy Policy Network for the 21st Century, 2013.

Louis Rosenblum, William J. Bifano, Gerald F. Hein, and Anthony F. Ratajczak. Photovoltaic power systems for rural areas of developing countries. *Solar Cells*, 1(1):65 – 79, 1979. ISSN 0379-6787. doi: http://dx.doi.org/10.1016/0379-6787(79)90008-5. URL http://www.sciencedirect.com/science/article/pii/0379678779900085.

Bruno Scrosati and Jürgen Garche. Lithium batteries: Status, prospects and future. *Journal of Power Sources*, 195(9):2419 – 2430, 2010. ISSN 0378-7753. doi: http://dx.doi.org/10.1016/j.jpowsour.2009.11.048. URL http://www.sciencedirect.com/science/article/pii/S0378775309020564.

E. Skoplaki and J.A. Palyvos. Operating temperature of photovoltaic modules: A survey of pertinent correlations. *Renewable Energy*, 34(1):23 – 29, 2009a. ISSN 0960-1481. doi: http://dx.doi.org/10.1016/j.renene.2008.04.009. URL http://www.sciencedirect.com/science/article/pii/S0960148108001353.

E. Skoplaki and J.A. Palyvos. On the temperature dependence of photovoltaic module electrical performance: A review of efficiency/power correlations. *Solar Energy*, 83(5):614 – 624, 2009b. ISSN 0038-092X. doi: http://dx.doi.org/10.1016/j.solener.2008.10.008. URL http://www.sciencedirect.com/science/article/pii/S0038092X08002788.

E. Skoplaki, A.G. Boudouvis, and J.A. Palyvos. A simple correlation for the operating temperature of photovoltaic modules of arbitrary mounting. *Solar Energy Materials and Solar Cells*, 92 (11):1393 – 1402, 2008. ISSN 0927-0248. doi: http://dx.doi.org/10.1016/j.solmat.2008.05.016. URL http://www.sciencedirect.com/science/article/pii/S0927024808001918.

E.M. Sparrow, J.W. Ramsey, and E.A. Mass. Effect of finite width on heat transfer and fluid flow about an inclined rectangular plate. *ASME Journal of Heat Transfer*, 101(2), 1979.

J. W. Spencer. Fourier series representation of the position of the sun. *Search*, 2(5):172, 1971.

D.L. Talavera, J. de la Casa, E. Muñoz-Cerón, and G. Almonacid. Grid parity and self-consumption with photovoltaic systems under the present regulatory framework in spain: The case of the university of jaén campus. *Renewable and Sustainable Energy Reviews*, 33(0):

752 – 771, 2014. ISSN 1364-0321. doi: http://dx.doi.org/10.1016/j.rser.2014.02.023. URL `http://www.sciencedirect.com/science/article/pii/S1364032114001440`.

Giuseppe Marco Tina and Alfio Dario Grasso. Remote monitoring system for stand-alone photovoltaic power plants: The case study of a pv-powered out-door refrigerator. *Energy Conversion and Management*, 78(0):862 – 871, 2014. ISSN 0196-8904. doi: http://dx.doi.org/10.1016/j.enconman.2013.08.065. URL `http://www.sciencedirect.com/science/article/pii/S0196890413005992`.

Arvind Tiwari and M.S. Sodha. Performance evaluation of hybrid pv/thermal wa-ter/air heating system: A parametric study. *Renewable Energy*, 31(15):2460 – 2474, 2006. ISSN 0960-1481. doi: http://dx.doi.org/10.1016/j.renene.2005.12.002. URL `http://www.sciencedirect.com/science/article/pii/S0960148105003575`.

Arvind Tiwari and M.S. Sodha. Parametric study of various configura-tions of hybrid pv/thermal air collector: Experimental validation of theoret-ical model. *Solar Energy Materials and Solar Cells*, 91(1):17 – 28, 2007. ISSN 0927-0248. doi: http://dx.doi.org/10.1016/j.solmat.2006.06.061. URL `http://www.sciencedirect.com/science/article/pii/S0927024806003448`.

U.N. Montreal protocol on substances that deplete the ozone layer, 1987. URL `ozone.unep.org`.

U.N. Kyoto protocol to the united nations framework convention on climate change, 1997. URL `unfccc.int`.

John C. Ward and George O.G. Löf. Long-term (18 years) performance of a residential solar heating system. *Solar Energy*, 18(4):301 – 308, 1976. ISSN 0038-092X. doi: http://dx.doi.org/10.1016/0038-092X(76)90057-8. URL `http://www.sciencedirect.com/science/article/pii/0038092X76900578`.

J. H. Watmuff, W. W. S. Charters, and D. Proctor. Solar and wind induced external coefficients - solar collectors. *Cooperation Mediterraneenne pour l'Energie Solaire, Revue Internationale d'Heliotechnique*, 2:56, 1977.

M. Wolf. *Solar Energy Handbook*, chapter Photovoltaic Solar Energy Conversion Systems. McGraw-Hill, New York, 1981.

T. S. Wurster and M. B. Schubert. Mismloss loss in photovoltaic systems. *Solar Energy*, 105: 505–511, 2014.

Yoshihiro Yamamoto. Pricing electricity from residential photovoltaic systems: A compari-son of feed-in tariffs, net metering, and net purchase and sale. *Solar Energy*, 86(9):2678 – 2685, 2012. ISSN 0038-092X. doi: http://dx.doi.org/10.1016/j.solener.2012.06.001. URL `http://www.sciencedirect.com/science/article/pii/S0038092X12002125`.

H.A. Zondag. Flat-plate pv-thermal collectors and systems: A re-view. *Renewable and Sustainable Energy Reviews*, 12(4):891 – 959, 2008. ISSN 1364-0321. doi: http://dx.doi.org/10.1016/j.rser.2005.12.012. URL `http://www.sciencedirect.com/science/article/pii/S1364032107000020`.

Appendix A

Additional theoretical and experimental results for summer

This work has been focused on heating season and the perfomance of the PV array and the heat pump for that function. However, the author consideres that the proposed cell temperature and PV production predicting model is robust and precise enough also during warmest days of the year. Thus it is claimed to be a valid model for the four seasons of the year.

In this appendix the cell temperature predicting model is validated for PV/T modules in a warm spring day and a hot summer day. In addition, the PV production predicting section of the model is tested with the spring day, as the system was kept in maximum production mode along that day. Finally, a previously published work about the cooling application of this PV system is reproduced.

A.1   Additional cell temperature validation

A.1.1   May 12$^{\text{th}}$ 2014

During this clear spring day, no clouds blocked the solar radiation and the outdoor dry bulb temperature oscillated between 12.8 °C and 31.1 °C (fig. A.1). This day, the thermal behavour of a PV/T module with no electrical production was tested. For this purpose, the front surface temperature of an open circuit module was measured, which was disconnected from the array.

Figure A.2 shows the measured surface temperature, which reached a maximum value of 60.3 °C, and the predicted temperature for the same surface by the developed heat transfer model. As it is shown on the figure, both lines overlap along the line, with a deviation shorter than the model uncertainty and measurement accuracy. On the other hand, as it has been explained, the hotter layer would be the silicon cells, which temperature is plotted with a red line, reaching a maximum of 62.4 °C.
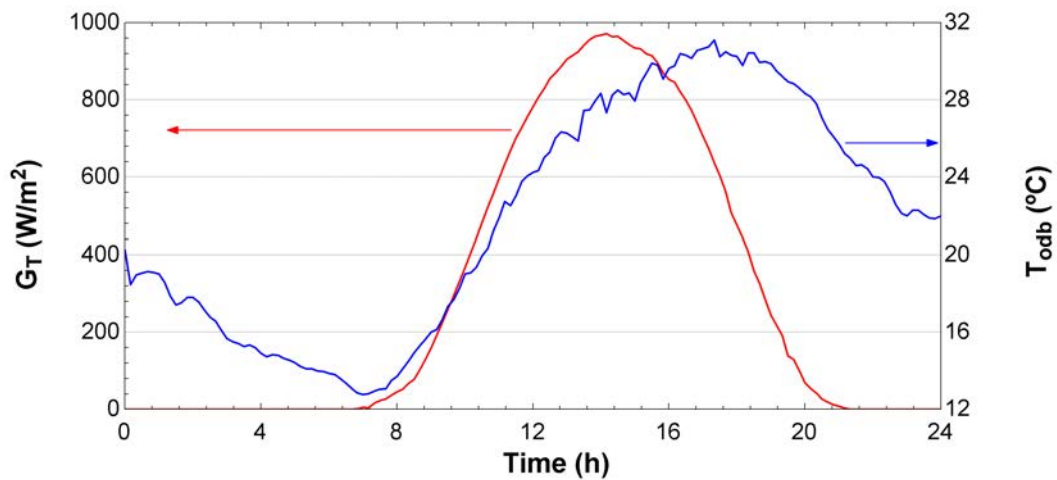
Figure A.1: Solar radiation and outdoor dry bulb temperature (12/05/2014).
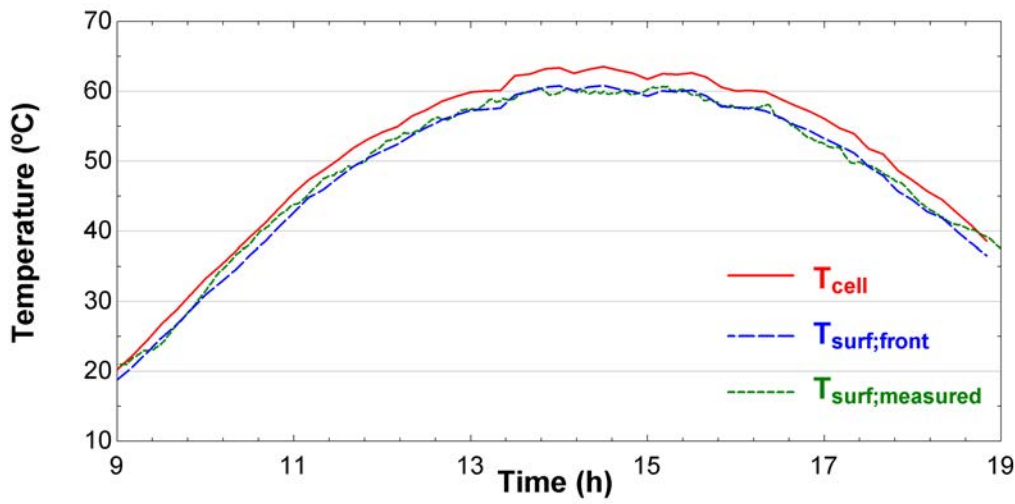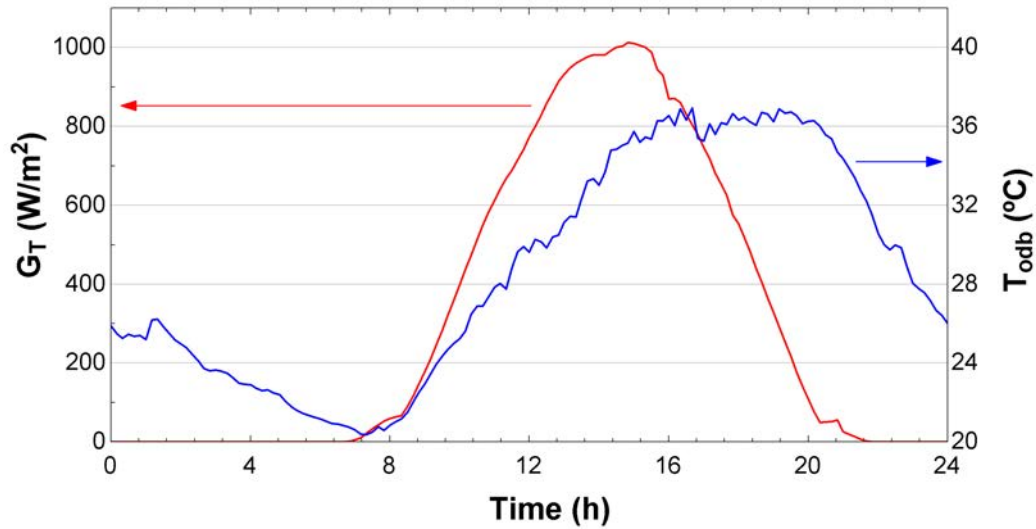

Figure A.2: Predicted and measured layers' temperatures (12/05/2014).

A.1.2   July 17th 2014

This day was typical hot and clear summer day at Madrid's region. The minimum outdoor dry bulb temperature just before sunshine was 20.5 °C, reaching a maximum value of 36.9 °C (fig. A.3). This day, all 16 PV/T modules were connected to charge the batteries and to feed the heat pump in its building cooling operation mode. The electrical production of the array, which was adapted to batteries' charge state, is plotted on figure A.4. Therefore, the cell temperature would be lower than the open circuit case.

Figure A.5 shows the measured surface temperature, which reached a maximum value of 66.7 °C, and the predicted temperature for the same surface by the developed heat transfer model. Both lines overlap each other, specially during the central hours of the day, when higher temperatures

are reached. Consequently, the predicted cell temperature is plotted in red, where the maximum temperature was 68.4 °C.

Figure A.3: Solar radiation and outdoor dry bulb temperature (17/07/2014).
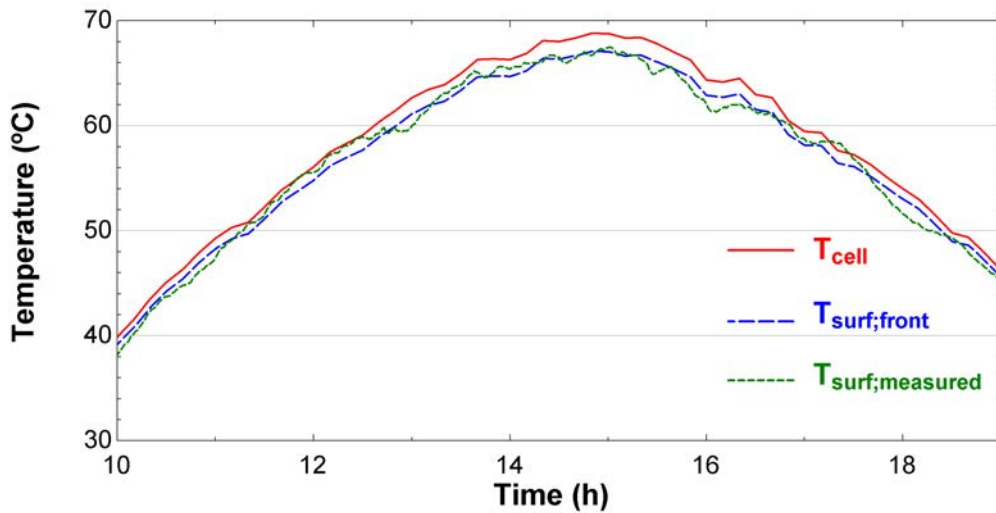
Figure A.5: Predicted and measured layers' temperatures (17/07/2014).
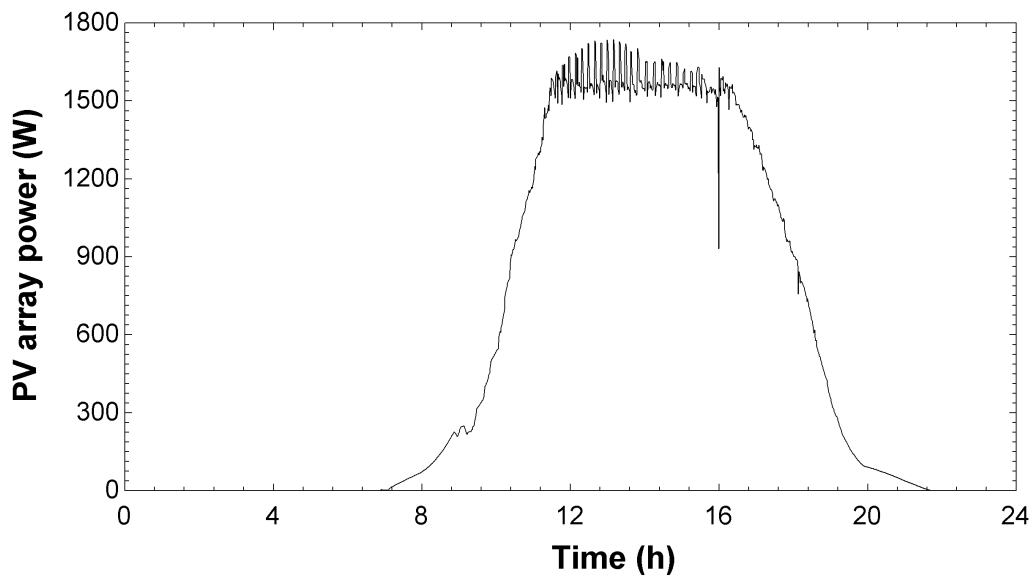
Figure A.4: PV array's electrical production (17/07/2014).

A.2 Additional PV production model validation

May 12$^{\text{th}}$ 2014, is used now as a PV production model's test.

A.2.1 Experimental result

During this clear day, 10 PV/T modules were connected to the controller. In order to maximize the production and to keep the controller on *MPPT* mode, a load of diverse resistances was connected to the batteries, $\dot{W}_{batt}$, trying to adapt the consumption to the PV production, as it is shown on figure A.6. The total electricity extracted from the batteries for this purpose was 10.31 kWh.

Along the day, the intercepted solar energy by array's useful surface (11.7 m^2) was 84.43 kWh and array's whole electrical production was 10.69 kWh. As it has been mentioned, these modules' nominal power is 180W, but during this day the maximum array output was 1465.8W (146.58 kW per module).
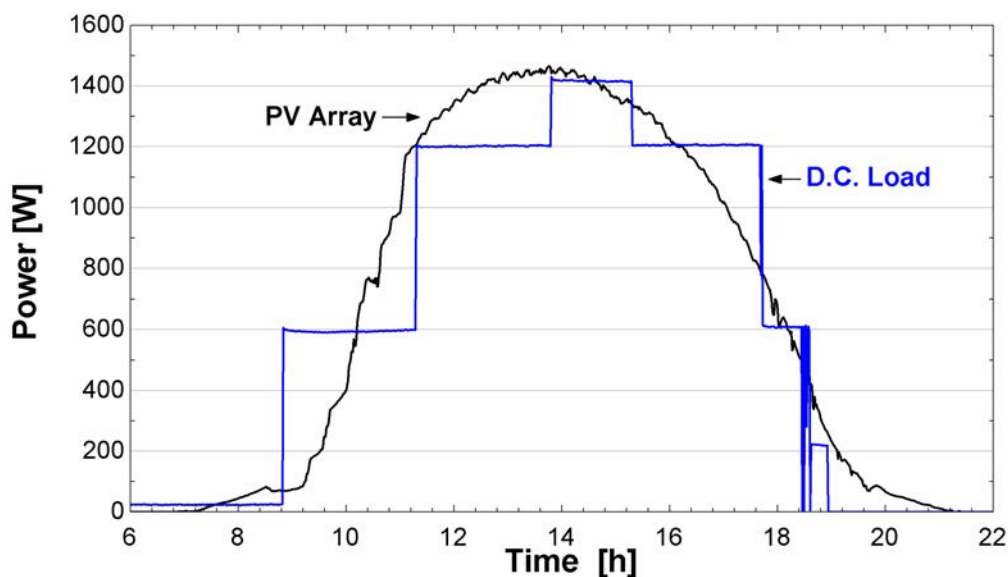
Figure A.6: PV array's output and consumption from the batteries (12/05/2014).

A.2.2 Simulation result

For the given meteorological conditions, photovoltaic prediction model is run. The simulated PV efficiency and production are plotted on figures A.7 and A.8, respectively. The daily simulated electrical production would be 11.29 kWh.
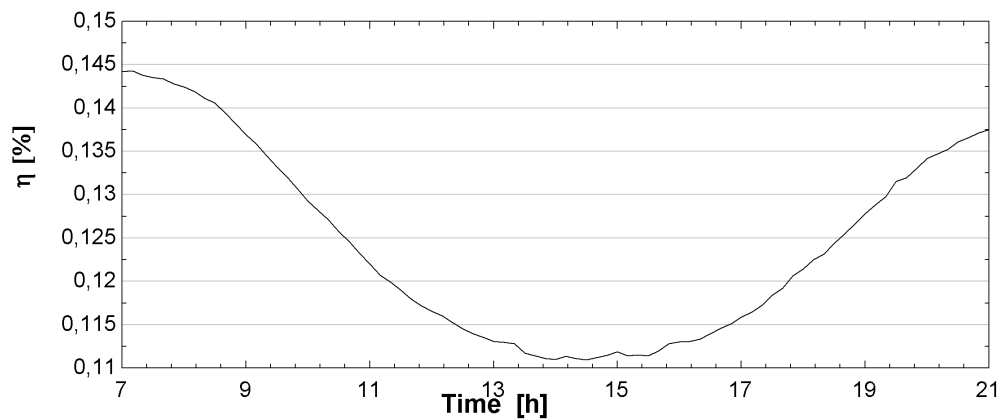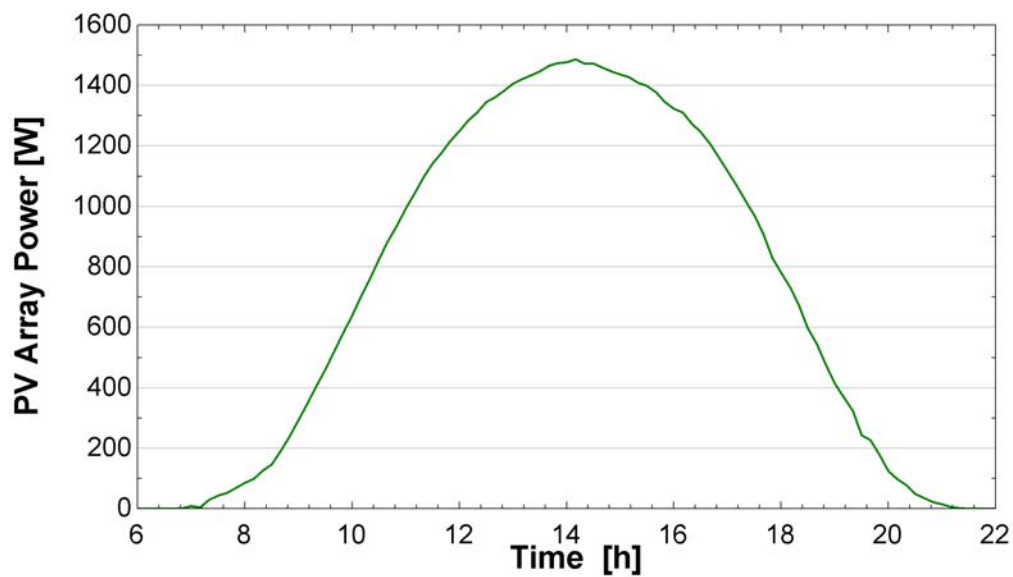
Figure A.7: Photovoltaic efficiency (12/05/2014).

Figure A.8: Simulated PV array production (12/05/2014).

A.3 Thermographic analysis of the heat transfer model

As a supplementary validation of the developed heat transfer model, on July 15th 2015 the temperature distribution was measured using infrared thermography and the usual PT100 sensors. The test was carried out during a heat wave that summer, when the minimum and maximum outdoor dry bulb temperatures were 21.9 °C and 40.4 °C, respectively (fig. A.9). That day, 14PV/T modules were connected operating continuosly in MPPT mode, as they were feeding the heat-pump in cooling mode, producing a maximum output of 1586.2 W (fig. A.10).
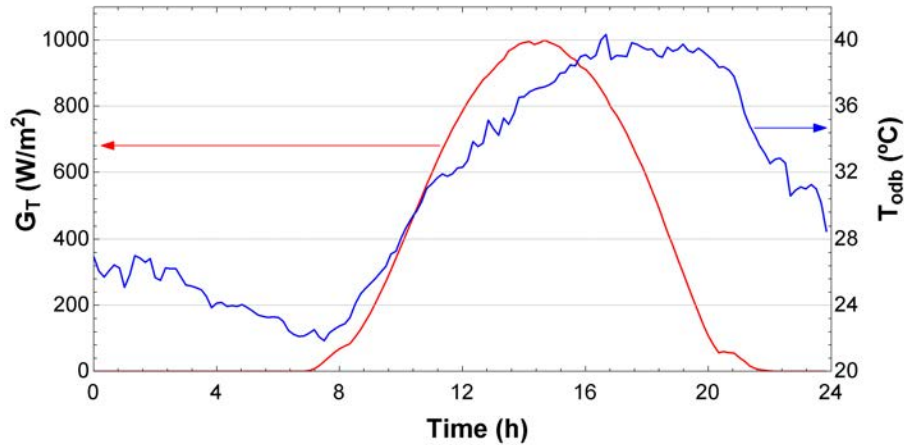
Figure A.9: Solar radiation and outdoor dry bulb temperature (15/07/2015).
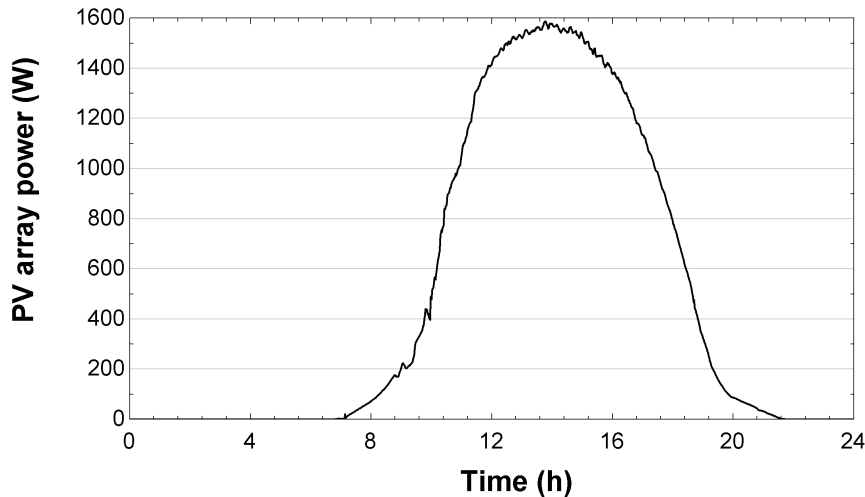
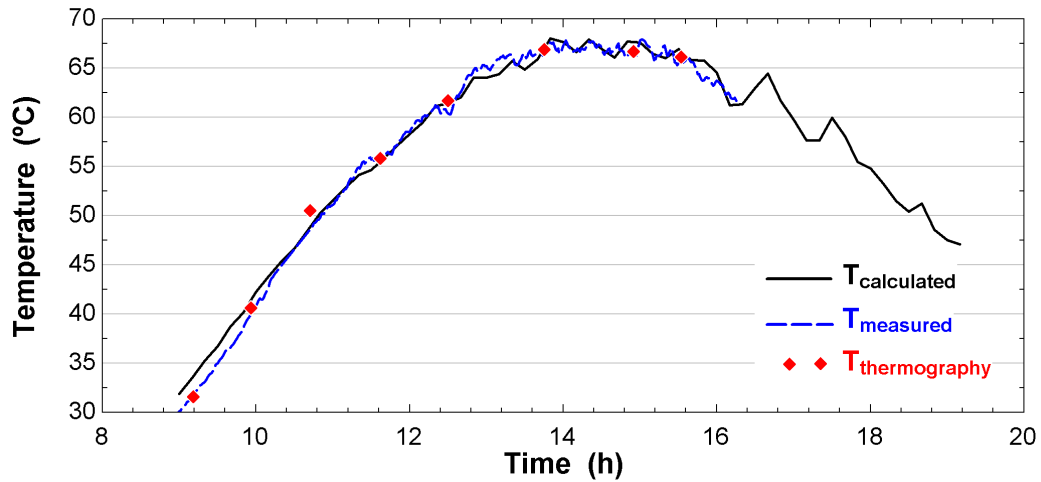Figure A.10: PV array's electrical production (15/07/2015).

Figure A.11: Predicted and measured temperature (15/07/2015).

Based on meteorological data and the produced PV electricity, the heat tranfer model was run predicting a maximum temperature of 67.9 °C at 14.33 hours. Figure A.11 shows the measured temperature at a PV/T module's back surface and the one predicted through the thermal model. Both lines match within instrumental and model's uncertainty. On the other hand, the same surface was photographed with an infrared thermography camera at eigh moments of the day (red points on fig. A.11). The thermographic pictures are shown on figures A.12, A.13, A.14 and A.15, were the temperature evolution and distribution can be observed.
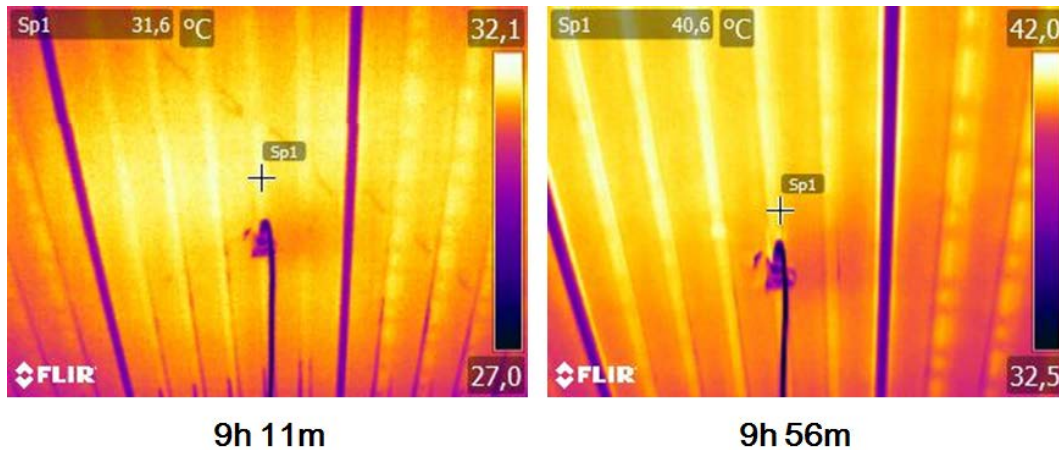

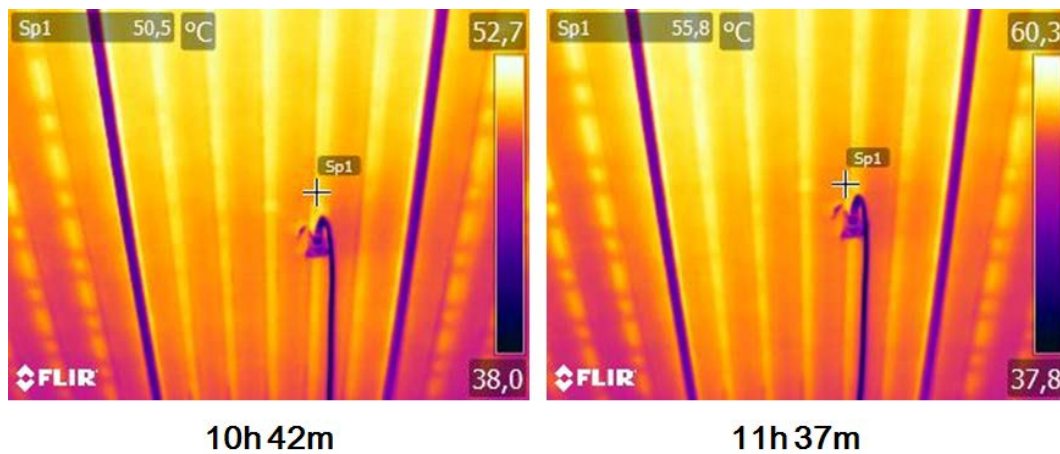Figure A.12: Thermograms of the PV/T back (points 1 and 2).

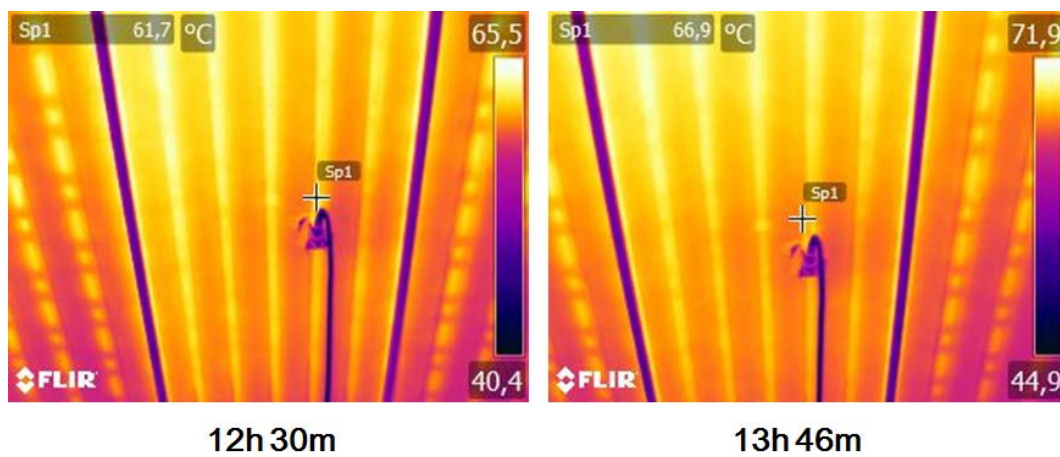Figure A.13: Thermograms of the PV/T back (points 3 and 4).

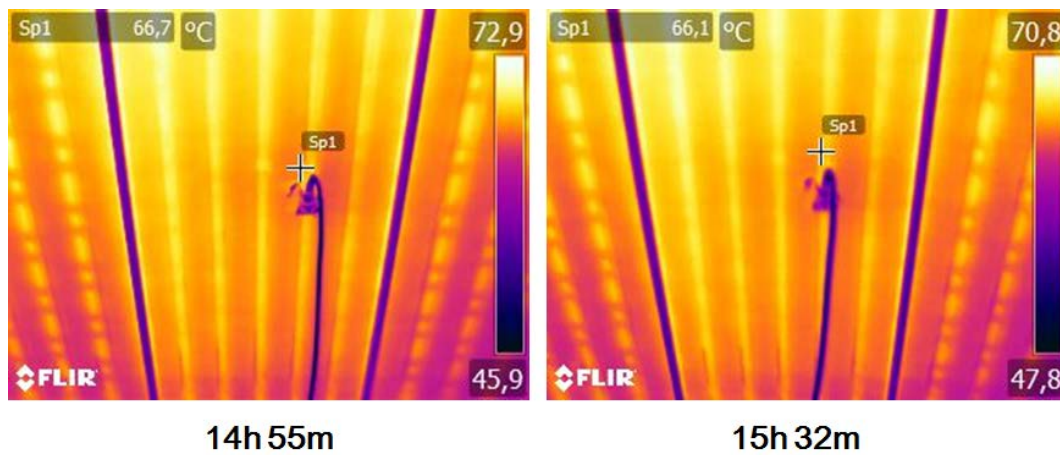Figure A.14: Thermograms of the PV/T back (points 5 and 6).

Figure A.15: Thermograms of the PV/T back (points 7 and 8).

A.4 Heat pump for radiant cooled floor: experimental results

As it has been mentioned on the state-of-the-art, the author has tested the PV system for feeding the heat pump also in reverse mode during summer [Izquierdo, de Agustin, and Martin, 2013]. Although this system's cooling application is out of scope of this dissertation, the cited paper is reproduced on the following pages as complementary work, to show the experimental perfomance of the cooled floor PV system. Additional papers about the PV cooling system's perfomance will be published in the future.